JAERI-Tech
2000-016

ROSA/LSTF EXPERIMENT REPORT FOR RUN SB-CL-24 REPEATED CORE HEATUP PHENOMENA DURING 0.5% COLD LEG BREAK LOCA

March 2000

Mitsuhiro SUZUKI and Yoshinari ANODA

日本原子力研究所
Japan Atomic Energy Research Institute

本レポートは，日本原子力研究所が不定期に公刊している研究報告書です。
入手の問合わせは，日本原子力研究所研究情報部研究情報課（〒319－1195 茨城県那珂郡東海村）あて，お申し越しください。なお，このほかに財団法人原子力弘済会資料センター（〒319－1195 茨城県那珂郡東海村日本原子力研究所内）で複写による実費頒布をおこなっております。

This report is issued irregularly.
Inquiries about availability of the reports should be addressed to Research Information Division, Department of Intellectual Resources, Japan Atomic Energy Research Institute, Tokai-mura, Naka-gun, Ibaraki-ken 〒319－1195, Japan.

編集兼発行　日本原子力研究所

JAERI-Tech 2000-016

ROSA/LSTF Experiment Report for RUN SB-CL-24
Repeated Core Heatup Phenomena during 0.5% Cold Leg Break LOCA

Mitsuhiro SUZUKI and Yoshinari ANODA

Department of Reactor Safety Research
Nuclear Safety Research Center
Tokai Research Establishment
Japan Atomic Eergy Research Institute
Tokai-mura, Naka-gun, Ibaraki-ken

(Received February 1, 2000)

A small break loss-of-coolant accident (SBLOCA) in a Westinghouse-type four-loop PWR was simulated in an experiment (SB-CL-24) conducted at the Large-Scale Test Facility (LSTF) with an intention to study repeated core heatup during a long-term cooldown process. The experiment was conducted on February 28, 1990 with specified test conditions including failure assumptions both on the high pressure injection (HPI) and the auxiliary feedwater systems, and the intentional secondary system depressurization as an operator action. The secondary depressurization contributed to promote the primary depressurization and the actuation of accumulator injection system (AIS). A temporary core heatup was observed in each of three loopseal clearing (LSC) processes. A significant core heatup occurred in the following boil-off process after loss of the secondary coolant mass and the AIS termination due to increase of the primary pressure. By additional opening of the pressurizer PORV and safety valves, the primary pressure rapidly decreased to result in the low pressure injection (LPI) which cooled the heated core.
This report summarizes results of the experiment (SB-CL-24) in addition to typical responses of some accident indication systems including the core exit thermocouples (CETs) and the water level meters in the primary system.

Keywords: Accident Indication System, Cold Leg Break, Experiment Report, Inadequate Core Cooling, Loopseal Clearing, LSTF, ROSA Program, SBLOCA, Secondary Depressurization Action

ＲＯＳＡ／ＬＳＴＦ実験報告（ＳＢ-ＣＬ-２４実験）
０．５％低温側配管破断ＬＯＣＡ時における炉心過熱事象の繰り返し発生

日本原子力研究所東海研究所安全性試験研究センター原子炉安全工学部
鈴木光弘・安濃田良成

(2000年２月１日受理)

大型非定常実験装置（ＬＳＴＦ）において、ウエスチングハウス社型４ループＰＷＲを対象とする小破断冷却材喪失事故（ＳＢＬＯＣＡ）模擬実験（ＳＢ－ＣＬ－２４）を実施し、長時間の冷却過程における炉心過熱事象が繰り返し生じる可能性について検討した。本実験は１９９０年２月２８日に実施され、実験条件として高圧注入系（ＨＰＩ）と補助給水系の不作動を仮定し、運転員による２次系減圧操作を行うこととした。

２次系減圧は１次系の減圧を促進し、蓄圧注入系（ＡＩＳ）の作動を早めた。一時的な炉心過熱が３回のループシール排除（ＬＳＣ）過程それぞれで生じた。その後のボイルオフ過程では、２次系保有水喪失により１次系圧力が上昇開始し、蓄圧注入系が注水停止して顕著な炉心過熱状態が生じた。加圧器逃し弁及び安全弁を開く追加操作により１次系圧力は急速に低下し、低圧注入系（ＬＰＩ）が作動開始し、過熱炉心を冷却した。

本報はＳＢ-ＣＬ-２４実験結果をまとめたものであり、併せて炉心出口温度計や１次系各種水位計を含む事故検出計装系の特性も示した。

東海研究所：〒 319-1195 茨城県那珂郡東海村白方白根 2-4

Contents

目　　次

List of Tables

List of Figures

ROSA/LSTF Acronyms and Abbrebiations

ACC.....Accumulator Tank Connected to Loop A
ACH.....Accumulator Tank Connected to Loop B
ADS.....Automatic Depressurization System
AIS.....Accumulator Injection System
AOV.....Air Operated Valve
BU.....Break Unit
CET.....Core Exit Thermocouple
CL-A, CL-B.....Cold Leg A, Cold Leg B
CP.....Conduction Probe
DAS.....Data Acquisition System
DEGB.....Double-Ended Guillotine Break
DNB.....Departure from Nucleate Boiling
DP.....Differential Pressure
ECCS.....Emergency Core Cooling System
EL.....Elevation above Core Bottom
HL-A, HL-B.....Hot Leg A, Hot Leg B
HPI.....High Pressure Injection System
HX.....Heat Exchanger
ICC.....Inadequate Core Cooling
JAERI.....Japan Atomic Energy Research Institute
LL.....Liquid Level
LOCA.....Loss-of-Coolant Accident
LPI.....Low Pressure Injection System
LS-A, LS-B.....Loop Seal A, Loop Seal B
LSC.....Loopseal Clearing
LSTF.....Large-Scale Test Facility
MSIV.....Main Steam Isolation Valve
PORV.....Power-operated Relief Valve
PV.....Pressure Vessel
PWR.....Pressurized Water Reactor
PZR.....Pressurizer
ROSA.....Rig-of-Safety Assessment
RV.....Relief Valve
RVLIS.....Reactor Vessel Level Indication System

SBLOCA.....Small Break Loss-of-Coolant Accident
SG-A, SG-B.....Steam Generator A, Steam Generator B
SMM.....Subcooled Margin Monitor
ST.....Suppression Tank
SV.....Safety Valve
TC.....Thermocouple
W-PWR.....Westinghouse-type PWR

This is a blank page.

1. Introduction

A small break loss-of-coolant accident (SBLOCA) experiment, SB-CL-24, was conducted on February 28, 1990 at the Large-Scale Test Facility (LSTF) [1-3] of Japan Atomic Energy Research Institute (JAERI). The experiment simulated 0.5% colg leg SBLOCA in a Westinghouse-type pressurized water reactor (W-PWR) and assumed failures on the high pressure injection (HPI) and the auxiliary feedwater systems. Two points were intended to clarify, i.e., (a) effects of secondary depressiurization action on core cooling, and (b) a possibility of repeated core heatups during a long-term cooldown process. In addition to these, the experiment results were investigated to clarify typical responses of accident indication systems including the core exit thermocouples (CETs) and some water level meters during inadequate core cooling (ICC) conditions.

1.1 Background

The secondary depressurization action is considered to be one of the important accident management measures to lead a PWR SBLOCA toward a cold stable condition when the HPI is unavailable. In the previous cold leg SBLOCA experiments [4, 5] with the manual HPI actuation, two types of core heatup behavior occured during the long transient, i.e., one was caused by the temporary liquid level decrease in the core during a loopseal clearing (LSC) period, and the other one was caused by a significant mass loss in the boil-off process which was terminated after the HPI actuation. The effects of secondary depressurization action on these core heatups are intended to clarify in this experiment.

A transient process toward and during the core heatup is to be accurately indicated by using the accident indication systems. In this experiment, characteristics are clarified for the CETs, the temperature measurements in the upper plenum and the hot legs, and the water level indication systems in the primary coolant system.

1.2 Objectives

The primary objectives of the experiment are to provide data for assessment of thermal-hydraulic safety analysis computer codes, and to study core cooling conditions during the long SBLOCA transient initiated by the 0.5% cold leg break followed by the HPI failure and the secondary depressurization action.

The objective of this report is to provide a summary of the overall thermal-hydraulic

behaviors and typical findings observed in Experiment SB-CL-24 in addition to descriptions on the facility and the test boundary conditions. The experiment results for the previous ROSA/LSTF experiments have been reported in References [4] through [11].

2. Facility Description

2.1 System Components

The LSTF was designed to simulate thermal-hydraulic phenomena peculiar to SBLOCAs and operational transients in PWRs. It features prototypical component elevation differences, large loop piping diameters, simulated system controls, prototypical primary pressures, simulated Emergency Core Cooling Systems (ECCS) and sufficient electric core power to simulate the core power decay except for a short time after scram as shown in Reference [1]. It has a 1/48 volume scale to a typical four-loop W-PWR with thermal power output of 3423 MW. These major design charactristics of the LSTF experiment are shown in Table 2.1-1 in comparison with those of the reference PWR. Figure 2.1.1 shows the LSTF configuration compared with that of the four-loop PWR.

Major difference between the LSTF and the reference PWR mainly exists in cross-sectional configuration of each component, i.e., the LSTF hot leg diameter is approximately 28% of the PWR, and the LSTF upper plenum diameter is approximately 14% of the PWR. These effects on the three-dimensional fluid behaviors in the LSTF components should be carefully studied in addition to the effects of relatively large metal stored heat and environmental heat loss compared to the reference PWR.

Figures 2.1.2, 2.1.3 and 2.1.4 show a general view of the total LSTF system, a cross-sectional view of the PV and that of the steam generator (SG), respectively. The primary coolant system consists of the PV with the simulated fuel rod assembly and the internals, a short-sized pressurizer (PZR), two primary loops with a SG and a coolant pump in each one, a break unit (BU) connected to the break flow storage tank (ST), three types of the ECCSs which consist of a high pressure injection (HPI) system, an accumulator injection system (AIS) for each loop (ACC for loop A and ACH for loop B) and a low pressure injection (LPI) system, and other miscellaneous systems. The secondary system includes each SG secondary side, steam and feedwater systems and a relief valve (RV) line. The SG U-tubes have the same height and inner diameter in each of 141 tubes in comparison with those of the reference PWR.

The following modifications[2] were made on the previous LSTF system with the first core assembly which was used until August, 1988. They include (a) the segmental differential pressure (DP) measurement in the core region, (b) the overall DP measurement in the upper head region, (c) improvement of the steam generator (SG) outlet plena to better sim-

ulate the primary volume distribution.

A cross-section of the core is shown in Fig. 2.1.5. The electric heater rods with the same diameter and heated length to the reference PWR are arranged in twenty-four bundles with 7×7 array except for peripheral regions. Total numbers of the heater rods and the non-heating tie rods are 1008 and 96, respectively. Four tie rods in one bundle simulate the control rods. Eight DP measurement tubes and dummy rods are arranged in the peripheral region. The core thermal characteristic conditions are shown in Table 2.1-2. Figure 2.1.6 shows an axial power distribution of a high power rods (bundle No. 13 through 20) with an axial peaking factor of 1.4945. Nine steps of the axial power distribution model a cosine curve around the core center. Other heater rods have similar axial power profiles. A steep radial power profile of "case 3" has a radial peaking factor of 1.51 for the high power bundles, 1.00 for the middle power bundles (bundle No. 21 through 24) and 0.66 for the peripheral low power bundles (bundle No. 1 through 12), respectively as shown in Fig. 2.1.7.

2.2 Instrumentation and Data Processing

2.2.1 Measurement Items

There are two types of data or measurements of interest in the ROSA-IV/LSTF experiments, i.e., directly measured quantities and derived quantities. The direct measurements include temperature, pressure and DP. The derived quantities result from the combination of two or more direct measurements, for example, fluid density, mass flow rate and water level.

Table 2.2-1 lists the various types of measurements recorded for this LSTF system. Some of the items listed are direct measurements, while others require post-test processing. The table also includes the general location of the measurements. All the measurement signals are sent to the data acquisition system (DAS), converted to digital form and recorded on magnetic disks. Major instrumentation locations are shown in Appendix A.

Nine thermocouples were axially embedded at each power step of one heater rod to measure transient thermal responses of the core. The axial thermocouple locations are designated like as Position 1 (bottom of core; EL 0.15 m), Position 5 (middle height; EL 1.86 m) and Position 9 (top of core; EL 3.61 m). In this experiment, SB-CL-24, the heater rod surface temperatures were not only recorded by the data loggers but also monitored during the experiment to detect core heatup initiation. This core heatup detection was used

to actuate the LPI system through the PORV onening action.

The following instrumentations are used to find ICC conditions, i.e., twenty CETs[12] located on the upper core plate to detect the core heatup, six thermocouples in the upper plenum and ten thermocouples in each hot leg to also detect the core heatup, and the DP measurements and conduction probes (CPs) for water level indication in the upper plenum, core and primary loops. These level measurements are used as the reactor vessel level indication system (RVLIS) and also used to estimate a total primary mass inventory with additional measurements of the primary loop fluid densities. The hot leg thermocouples are also utilized as subcooled margine monitors (SMM) by refering the saturated temperature.

2.2.2 Data Reduction and Qualification

An outline of the LSTF data reduction process is shown in Fig. 2.2.1. The instrument signals recorded on the data loggers, YEWCOM 7000 and FACOM S-3000, are converted from volts into engineering units using the appropriate conversion equations. Those instruments employing DP cells, such as flowmeters and liquid level meters, require fluid density to be calculated from local conditions. In general, fluid density is determined from a steam table lookup using a single local pressure and temperature.

After the data has been converted into engineering units, some data channels are corrected. For example, the readings from DP transducers are corrected to compensate for the effect of pressure. The corrections are based on instrument readings that were obtained at low and high system pressure, with zero DP across the instrument. Also, the readings from gamma-densitometers are corrected, if necessary, based on data taken during the heatup procedure.

The corrected data are then manually qualified, that is, each data channel is reviewed and placed into one of the following categories.

Good: The data have been reviewed manually and are believed to lie within the stated span and uncertainty values during the test.

Qualitative: In general, these data can be used for trend only. The absolute magnitude cannot be verified and uncertainty is unkown. This normally results from lack of calibration.

All the available experiment data which consist of the "Good" and "Qualitative" data are shown in Table 2.2-2. This table excludes data of other categories of "Bad" which should not be used because of a failure in the measurement channel, and "Unused" which should not be used because the sensor was not connected or installed in the environment to be measured or perhaps the region was not included.

Table 2.1-1 Major design characteristics of the LSTF and four-loop PWR

Item	(Unit)	LSTF	PWR	Ratio
Pressure	(MPa)	16	16	1 / 1
Temperature	(K)	598	598	1 / 1
Number of Fuel Rods		1008	50952	1 / 50.55
Core Height	(m)	3.66	3.66	1 / 1
Primary Fluid Volume (V)	(m^3)	7.83	347	1 / 44.3
Pressure Vessel Fluid Volume	(m^3)	2.67	131.7	1 / 49.4
Thermal Core Power (P)	(MW)	10	3423	1 / 342
(P/V)	(MW/m^3)	1.28	9.9	1 / 7.7
Core Inlet Flow Rate	(kg/s)	48.8	16700	1 / 342
Downcomer Gap	(m)	0.053	0.260	1 / 4.91
Number of Primary Loops		2	4	1 / 2
Hot Leg Diameter (D)	(m)	0.207	0.737	1 / 3.56
Hot Leg Length (L)	(m)	3.69	6.99	1 / 1.89
($L/\sqrt{D}$)	($m^{1/2}$)	8.15	8.15	1 / 1
$\pi D^2L/4$	(m^3)	0.124	2.98	1 / 24
Hot Leg Top Elevation*	(m)	EL 5.606	EL 5.606	1 / 1
Loopseal Bottom Elevation*	(m)	EL 1.701	EL (1.7)	1 / 1
Pressurizer Fluid Volume	(m^3)	1.147	51	1 / 44.5
Pressurizer Height	(m)	4.187	15.5	1 / 3.7
Number of SG		2	4	1 / 2
One SG Vessel Fluid Volume	(m^3)	7.0	163.1	1 / 23
Number of U-tubes per One SG		141	3382	1 / 24
U-tube Inner Diameter	(mm)	19.6	19.6	1 / 1
Average U-tube Length	(m)	20.2	20.2	1 / 1

* Elevation above core bottom (EL 0.0 m)

Table 2.1-2 Major core characteristics

Item	LSTF	PWR	Ratio
Number of Rod Bundles	24	193	
Bundle Size	7 x 7 (square)	17 x 17	
	40 rods (semi-crescent)		
Total Number of Rods	1,104	55,777	(1/50.52)
Heater Rods	1,008	50,952	(1/50.55)
Non-Heating Rods	96	4,825	(1/50.26)
Rod Diameter (mm)			
Heater Rod	9.5	9.5	1/1
Non-Heating Rod	12.24	12.24	1/1
Rod pitch (mm)	12.6	12.6	1/1
Effective Heated Length (m)	3.66	3.66	1/1
Output Power (MWth)	10.0	3,423	1/342.3
Peaking Factor	1.495	1.495	1/1
Cladding Thickness (mm)	1.0	0.57	1.754/1
Cladding Material	Inconel	Zr-4	
Number of Spacers in Core	9	9	1/1
Core Barrel			
Inner Diameter (mm)	514	3,759	1/7.313
Outer Diameter (mm)	534	3,875	1/7.255
Thickness (mm)	10	57.5	1/5.75
Core Volume (m^3)	0.4069	17.5	1/43.01
Flow Area (m^2)			
Core (at spacer)	0.06418	3.70	1/57.65
Core (below spacer)	0.1134	4.75	1/41.89
Grid (or Lower nozzle)	0.06425	2.988	1/46.51
End Box (or Upper Nozzle)	0.08720	4.187	1/48.02

Table 2.2-1 Summary of measurement types and locations

Instrument/Measurement	Symbol	Pressure Vessel	Primary System	Steam Generators	Pressurizer	Secondary System	Surpression Tank and Break Units	Other	Total
Fluid Temperature	TE	191	60	246	17	15	17	97	643
Wall Temperature	TW	485	50	92	16		4	9	656
Differential Temperature	DT	112	24	70	2				208
Conductance Probe	CP	143	20	20	4		1		188
Conductance Probe with TC	CPT		10	224					234
Flow Rate	F	2	4	12	3	8	4	25	58
Pitot-tube Velocimeter	PIT		3						3
Liquid Level	L	1		8	1	1	4	4	19
Pressure	P	3	10	2	8	5	10	4	42
Differential Pressure	DP	24	62	22	9		6	2	125
Gamma Densitometer(1 Beam)	GD_1		3	1	3				7
Gamma Densitometer(3 Beam)	GD_3		6	1			3		10
Drag Disk Flow Meter	DD		26		6		4		36
Video Probe	VP	2	6						8
Rotation Speed	RE		2						2
Pump oscillation	VE		2						2
Pump Torque	TQ		2						2
Power	WE	11	8	16	4			4	43
Total		974	298	714	73	29	53	145	2286

Table 2.2-2 List of available measurements for experiment SB-CL-24

SEQ NO	FUNC ID.		TAG NAME	OUTPUT RANGE LO	HI	UNIT	UNCERTAINTY ABS.	REL.(%)
6	TE	6	TE020C-HLA	2.700+2	7.200+2	K	3.307+0	7.350-1
7	TE	7	TE020D-HLA	2.700+2	7.200+2	K	3.307+0	7.350-1
8	TE	8	TE030C-HLA	2.700+2	7.200+2	K	3.307+0	7.350-1
9	TE	9	TE030D-HLA	2.700+2	7.200+2	K	3.307+0	7.350-1
15	TE	15	TE050C-LSA	2.700+2	7.200+2	K	3.307+0	7.350-1
16	TE	16	TE070C-CLA	2.700+2	7.200+2	K	3.307+0	7.350-1
17	TE	17	TE070D-CLA	2.700+2	7.200+2	K	3.307+0	7.350-1
18	TE	18	TE080C-CLA	2.700+2	7.200+2	K	3.307+0	7.350-1
19	TE	19	TE080D-CLA	2.700+2	7.200+2	K	3.307+0	7.350-1
25	TE	25	TE100-HLA	2.700+2	7.200+2	K	3.307+0	7.350-1
31	TE	31	TE160C-HLB	2.700+2	7.200+2	K	3.307+0	7.350-1
32	TE	32	TE160D-HLB	2.700+2	7.200+2	K	3.307+0	7.350-1
33	TE	33	TE170C-HLB	2.700+2	7.200+2	K	3.307+0	7.350-1
34	TE	34	TE170D-HLB	2.700+2	7.200+2	K	3.307+0	7.350-1
35	TE	35	TE180A-HLB	2.700+2	7.200+2	K	3.307+0	7.350-1
36	TE	36	TE180B-HLB	2.700+2	7.200+2	K	3.307+0	7.350-1
37	TE	37	TE180C-HLB	2.700+2	7.200+2	K	3.307+0	7.350-1
38	TE	38	TE180D-HLB	2.700+2	7.200+2	K	3.307+0	7.350-1
39	TE	39	TE180E-HLB	2.700+2	7.200+2	K	3.307+0	7.350-1
40	TE	40	TE190C-LSB	2.700+2	7.200+2	K	3.307+0	7.350-1
41	TE	41	TE210C-CLB	2.700+2	7.200+2	K	3.307+0	7.350-1
42	TE	42	TE210D-CLB	2.700+2	7.200+2	K	3.307+0	7.350-1
43	TE	43	TE220C-CLB	2.700+2	7.200+2	K	3.307+0	7.350-1
44	TE	44	TE220D-CLB	2.700+2	7.200+2	K	3.307+0	7.350-1
45	TE	45	TE230A-CLB	2.700+2	7.200+2	K	3.307+0	7.350-1
46	TE	46	TE230B-CLB	2.700+2	7.200+2	K	3.307+0	7.350-1
47	TE	47	TE230C-CLB	2.700+2	7.200+2	K	3.307+0	7.350-1
48	TE	48	TE230D-CLB	2.700+2	7.200+2	K	3.307+0	7.350-1
49	TE	49	TE230E-CLB	2.700+2	7.200+2	K	3.307+0	7.350-1
50	TE	50	TE240-HLB	2.700+2	7.200+2	K	3.307+0	7.350-1
51	TE	51	TE270C-PR	2.700+2	7.200+2	K	3.307+0	7.350-1
52	TE	52	TE280C-PR	2.700+2	7.200+2	K	3.307+0	7.350-1
53	TE	53	TE290-PR	2.700+2	7.200+2	K	3.307+0	7.350-1
54	TE	54	TE300-PR	2.700+2	7.200+2	K	3.307+0	7.350-1
55	TE	55	TE430-SGA	2.700+2	6.700+2	K	3.108+0	7.770-1
56	TE	56	TE440-SGA	2.700+2	6.700+2	K	3.108+0	7.770-1
57	TE	57	TE450-SGA	2.700+2	6.700+2	K	3.108+0	7.770-1
59	TE	59	TE470-SGB	2.700+2	6.700+2	K	3.108+0	7.770-1
60	TE	60	TE480-SGB	2.700+2	6.700+2	K	3.108+0	7.770-1
61	TE	61	TE490-SGB	2.700+2	6.700+2	K	3.108+0	7.770-1
63	TE	63	TE510-SH	2.700+2	6.700+2	K	3.108+0	7.770-1
64	TE	64	TE520-JC	2.700+2	6.700+2	K	3.108+0	7.770-1
65	TE	65	TE530-JC	2.700+2	6.700+2	K	3.108+0	7.770-1
66	TE	66	TE540-JC	2.700+2	6.700+2	K	3.108+0	7.770-1
67	TE	67	TE550-JC	2.700+2	6.700+2	K	3.108+0	7.770-1
68	TE	68	TE431-SGA	2.700+2	6.700+2	K	3.108+0	7.770-1
69	TE	69	TE432-SGA	2.700+2	6.700+2	K	3.108+0	7.770-1
70	TE	70	TE433-SGA	2.700+2	6.700+2	K	3.108+0	7.770-1
71	TE	71	TE434-SGA	2.700+2	6.700+2	K	3.108+0	7.770-1
72	TE	72	TE471-SGB	2.700+2	6.700+2	K	3.108+0	7.770-1
73	TE	73	TE472-SGB	2.700+2	6.700+2	K	3.108+0	7.770-1
74	TE	74	TE473-SGB	2.700+2	6.700+2	K	3.108+0	7.770-1
75	TE	75	TE474-SGB	2.700+2	6.700+2	K	3.108+0	7.770-1
80	TE	80	TE580C-BU	2.700+2	7.200+2	K	3.307+0	7.350-1
81	TE	81	TE580D-BU	2.700+2	7.200+2	K	3.307+0	7.350-1
82	TE	82	TE590C-BU	2.700+2	7.200+2	K	3.307+0	7.350-1
83	TE	83	TE590D-BU	2.700+2	7.200+2	K	3.307+0	7.350-1
84	TE	84	TE600-ST	2.700+2	4.700+2	K	2.304+0	1.152+0
85	TE	85	TE610-ST	2.700+2	4.700+2	K	2.304+0	1.152+0
86	TE	86	TE620-ST	2.700+2	4.700+2	K	2.304+0	1.152+0
87	TE	87	TE630-ST	2.700+2	4.700+2	K	2.304+0	1.152+0
88	TE	88	TE640-ST	2.700+2	4.700+2	K	2.304+0	1.152+0
89	TE	89	TE650-ACC	2.700+2	4.700+2	K	2.304+0	1.152+0
90	TE	90	TE660-ACC	2.700+2	4.700+2	K	2.304+0	1.152+0
91	TE	91	TE670-ACC	2.700+2	4.700+2	K	2.304+0	1.152+0
93	TE	93	TE690-ACH	2.700+2	5.700+2	K	2.706+0	9.020-1
94	TE	94	TE700-ACH	2.700+2	5.700+2	K	2.706+0	9.020-1
96	TE	96	TE720-ACH	2.700+2	5.700+2	K	2.706+0	9.020-1
97	TE	97	TE730-HLA	2.700+2	6.700+2	K	3.108+0	7.770-1
98	TE	98	TE740-LSA	2.700+2	6.700+2	K	3.108+0	7.770-1
99	TE	99	TE750-CLA	2.700+2	6.700+2	K	3.108+0	7.770-1
100	TE	100	TE760-HLB	2.700+2	6.700+2	K	3.108+0	7.770-1
101	TE	101	TE770-LSB	2.700+2	6.700+2	K	3.108+0	7.770-1
102	TE	102	TE780-CLB	2.700+2	6.700+2	K	3.108+0	7.770-1
112	TE	112	TE880-RWST	2.700+2	3.700+2	K	1.902+0	1.902+0
113	TE	113	TE890-RWST	2.700+2	3.700+2	K	1.902+0	1.902+0
115	TE	115	TE-E066F-PV	2.700+2	9.700+2	K	4.312+0	6.160-1
116	TE	116	TE-W066F-PV	2.700+2	9.700+2	K	4.312+0	6.160-1
117	TE	117	TE-E075F-PV	2.700+2	9.700+2	K	4.312+0	6.160-1
118	TE	118	TE-W075F-PV	2.700+2	9.700+2	K	4.312+0	6.160-1
119	TE	119	TE-E081F-PV	2.700+2	9.700+2	K	4.312+0	6.160-1
120	TE	120	TE-W081F-PV	2.700+2	9.700+2	K	4.312+0	6.160-1
121	TE	121	TE-E080H-PV	2.700+2	9.700+2	K	4.312+0	6.160-1
122	TE	122	TE-W080H-PV	2.700+2	9.700+2	K	4.312+0	6.160-1
123	TE	123	TE-E049F-PV	2.700+2	9.700+2	K	4.312+0	6.160-1
124	TE	124	TE-W049F-PV	2.700+2	9.700+2	K	4.312+0	6.160-1
125	TE	125	TE-E055F-PV	2.700+2	9.700+2	K	4.312+0	6.160-1
126	TE	126	TE-W055F-PV	2.700+2	9.700+2	K	4.312+0	6.160-1
127	TE	127	TE-E060F-PV	2.700+2	9.700+2	K	4.312+0	6.160-1
128	TE	128	TE-W060F-PV	2.700+2	9.700+2	K	4.312+0	6.160-1

Table 2.2-2 List of available measurements for experiment SB-CL-24 (Cont'd, 1/21)

SEQ NO	FUNC ID.	TAG NAME	OUTPUT RANGE LO	HI	UNIT	UNCERTAINTY ABS.	REL.(%)
129	TE 129	TE-IN038-B09-UCP	2.700+2	9.700+2	K	4.312+0	6.160-1
130	TE 130	TE-IN038-B11-UCP	2.700+2	9.700+2	K	4.312+0	6.160-1
131	TE 131	TE-IN038-B01-UCP	2.700+2	9.700+2	K	4.312+0	6.160-1
132	TE 132	TE-IN038-B03-UCP	2.700+2	9.700+2	K	4.312+0	6.160-1
133	TE 133	TE-IN038-B05-UCP	2.700+2	9.700+2	K	4.312+0	6.160-1
134	TE 134	TE-IN038-B07-UCP	2.700+2	9.700+2	K	4.312+0	6.160-1
135	TE 135	TE-IN038-B21-UCP	2.700+2	9.700+2	K	4.312+0	6.160-1
136	TE 136	TE-IN038-B23-UCP	2.700+2	9.700+2	K	4.312+0	6.160-1
137	TE 137	TE-IN038-B02-UCP	2.700+2	9.700+2	K	4.312+0	6.160-1
138	TE 138	TE-IN038-B06-UCP	2.700+2	9.700+2	K	4.312+0	6.160-1
139	TE 139	TE-IN038-B14-UCP	2.700+2	9.700+2	K	4.312+0	6.160-1
140	TE 140	TE-IN038-B15-UCP	2.700+2	9.700+2	K	4.312+0	6.160-1
141	TE 141	TE-IN038-B18-UCP	2.700+2	9.700+2	K	4.312+0	6.160-1
142	TE 142	TE-IN038-B19-UCP	2.700+2	9.700+2	K	4.312+0	6.160-1
143	TE 143	TE-IN038-B10-UCP	2.700+2	9.700+2	K	4.312+0	6.160-1
144	TE 144	TE-IN038-B12-UCP	2.700+2	9.700+2	K	4.312+0	6.160-1
145	TE 145	TE-IN038-B04-UCP	2.700+2	9.700+2	K	4.312+0	6.160-1
146	TE 146	TE-IN038-B08-UCP	2.700+2	9.700+2	K	4.312+0	6.160-1
147	TE 147	TE-IN038-B22-UCP	2.700+2	9.700+2	K	4.312+0	6.160-1
148	TE 148	TE-IN038-B24-UCP	2.700+2	9.700+2	K	4.312+0	6.160-1
149	TE 149	TE-EX040-B09-UCP	2.700+2	9.700+2	K	4.312+0	6.160-1
150	TE 150	TE-EX040-B11-UCP	2.700+2	9.700+2	K	4.312+0	6.160-1
151	TE 151	TE-EX040-B01-UCP	2.700+2	9.700+2	K	4.312+0	6.160-1
152	TE 152	TE-EX040-B03-UCP	2.700+2	9.700+2	K	4.312+0	6.160-1
153	TE 153	TE-EX040-B05-UCP	2.700+2	9.700+2	K	4.312+0	6.160-1
154	TE 154	TE-EX040-B07-UCP	2.700+2	9.700+2	K	4.312+0	6.160-1
155	TE 155	TE-EX040-B21-UCP	2.700+2	9.700+2	K	4.312+0	6.160-1
156	TE 156	TE-EX040-B23-UCP	2.700+2	9.700+2	K	4.312+0	6.160-1
157	TE 157	TE-EX040-B02-UCP	2.700+2	9.700+2	K	4.312+0	6.160-1
158	TE 158	TE-EX040-B06-UCP	2.700+2	9.700+2	K	4.312+0	6.160-1
159	TE 159	TE-EX040-B14-UCP	2.700+2	9.700+2	K	4.312+0	6.160-1
160	TE 160	TE-EX040-B15-UCP	2.700+2	9.700+2	K	4.312+0	6.160-1
161	TE 161	TE-EX040-B18-UCP	2.700+2	9.700+2	K	4.312+0	6.160-1
162	TE 162	TE-EX040-B19-UCP	2.700+2	9.700+2	K	4.312+0	6.160-1
163	TE 163	TE-EX040-B10-UCP	2.700+2	9.700+2	K	4.312+0	6.160-1
164	TE 164	TE-EX040-B12-UCP	2.700+2	9.700+2	K	4.312+0	6.160-1
165	TE 165	TE-EX040-B04-UCP	2.700+2	9.700+2	K	4.312+0	6.160-1
166	TE 166	TE-EX040-B08-UCP	2.700+2	9.700+2	K	4.312+0	6.160-1
167	TE 167	TE-EX040-B22-UCP	2.700+2	9.700+2	K	4.312+0	6.160-1
168	TE 168	TE-EX040-B24-UCP	2.700+2	9.700+2	K	4.312+0	6.160-1
169	TE 169	TE-IN-002B02-LCPP	2.700+2	7.200+2	K	3.307+0	7.350-1
170	TE 170	TE-IN-002B03-LCPP	2.700+2	7.200+2	K	3.307+0	7.350-1
171	TE 171	TE-IN-002B06-LCPP	2.700+2	7.200+2	K	3.307+0	7.350-1
172	TE 172	TE-IN-002B07-LCPP	2.700+2	7.200+2	K	3.307+0	7.350-1
173	TE 173	TE-IN-002B09-LCPP	2.700+2	7.200+2	K	3.307+0	7.350-1
174	TE 174	TE-IN-002B11-LCPP	2.700+2	7.200+2	K	3.307+0	7.350-1
175	TE 175	TE-IN-002B14-LCPP	2.700+2	7.200+2	K	3.307+0	7.350-1
176	TE 176	TE-IN-002B16-LCPP	2.700+2	7.200+2	K	3.307+0	7.350-1
177	TE 177	TE-IN-002B18-LCPP	2.700+2	7.200+2	K	3.307+0	7.350-1
178	TE 178	TE-IN-002B20-LCPP	2.700+2	7.200+2	K	3.307+0	7.350-1
179	TE 179	TE-IN-002B21-LCPP	2.700+2	7.200+2	K	3.307+0	7.350-1
180	TE 180	TE-IN-002B23-LCPP	2.700+2	7.200+2	K	3.307+0	7.350-1
181	TE 181	TE-EX-000B02-LCPP	2.700+2	7.200+2	K	3.307+0	7.350-1
182	TE 182	TE-EX-000B03-LCPP	2.700+2	7.200+2	K	3.307+0	7.350-1
183	TE 183	TE-EX-000B06-LCPP	2.700+2	7.200+2	K	3.307+0	7.350-1
184	TE 184	TE-EX-000B07-LCPP	2.700+2	7.200+2	K	3.307+0	7.350-1
185	TE 185	TE-EX-000B09-LCPP	2.700+2	7.200+2	K	3.307+0	7.350-1
186	TE 186	TE-EX-000B11-LCPP	2.700+2	7.200+2	K	3.307+0	7.350-1
187	TE 187	TE-EX-000B14-LCPP	2.700+2	7.200+2	K	3.307+0	7.350-1
188	TE 188	TE-EX-000B16-LCPP	2.700+2	7.200+2	K	3.307+0	7.350-1
189	TE 189	TE-EX-000B18-LCPP	2.700+2	7.200+2	K	3.307+0	7.350-1
190	TE 190	TE-EX-000B20-LCPP	2.700+2	7.200+2	K	3.307+0	7.350-1
191	TE 191	TE-EX-000B21-LCPP	2.700+2	7.200+2	K	3.307+0	7.350-1
192	TE 192	TE-EX-000B23-LCPP	2.700+2	7.200+2	K	3.307+0	7.350-1
193	TE 193	TE-N000C-DC	2.700+2	7.200+2	K	3.307+0	7.350-1
194	TE 194	TE-S000C-DC	2.700+2	7.200+2	K	3.307+0	7.350-1
195	TE 195	TE-E000C-DC	2.700+2	7.200+2	K	3.307+0	7.350-1
196	TE 196	TE-W000C-DC	2.700+2	7.200+2	K	3.307+0	7.350-1
197	TE 197	TE-N018C-DC	2.700+2	7.200+2	K	3.307+0	7.350-1
198	TE 198	TE-S018C-DC	2.700+2	7.200+2	K	3.307+0	7.350-1
199	TE 199	TE-E018C-DC	2.700+2	7.200+2	K	3.307+0	7.350-1
200	TE 200	TE-W018C-DC	2.700+2	7.200+2	K	3.307+0	7.350-1
201	TE 201	TE-N036C-DC	2.700+2	7.200+2	K	3.307+0	7.350-1
202	TE 202	TE-S036C-DC	2.700+2	7.200+2	K	3.307+0	7.350-1
203	TE 203	TE-E036C-DC	2.700+2	7.200+2	K	3.307+0	7.350-1
204	TE 204	TE-W036C-DC	2.700+2	7.200+2	K	3.307+0	7.350-1
205	TE 205	TE-N060C-DC	2.700+2	7.200+2	K	3.307+0	7.350-1
206	TE 206	TE-S060C-DC	2.700+2	7.200+2	K	3.307+0	7.350-1
207	TE 207	TE-E060C-DC	2.700+2	7.200+2	K	3.307+0	7.350-1
208	TE 208	TE-W060C-DC	2.700+2	7.200+2	K	3.307+0	7.350-1
209	TE 209	TE-N055C-DC	2.700+2	7.200+2	K	3.307+0	7.350-1
210	TE 210	TE-S055C-DC	2.700+2	7.200+2	K	3.307+0	7.350-1
211	TE 211	TE-C-021-LP	2.700+2	7.200+2	K	3.307+0	7.350-1
212	TE 212	TE-C-018-LP	2.700+2	7.200+2	K	3.307+0	7.350-1
213	TE 213	TE-C-015-LP	2.700+2	7.200+2	K	3.307+0	7.350-1
214	TE 214	TE-C-012-LP	2.700+2	7.200+2	K	3.307+0	7.350-1
215	TE 215	TE-C-009-LP	2.700+2	7.200+2	K	3.307+0	7.350-1
216	TE 216	TE-C-006-LP	2.700+2	7.200+2	K	3.307+0	7.350-1
217	TE 217	TE-C-005-LP	2.700+2	7.200+2	K	3.307+0	7.350-1
218	TE 218	TE-C-003-LP	2.700+2	7.200+2	K	3.307+0	7.350-1

Table 2.2-2 List of available measurements for experiment SB-CL-24 (Cont'd, 2/21)

SEQ NO	FUNC ID.	TAG NAME	OUTPUT RANGE LO	HI	UNIT	UNCERTAINTY ABS.	REL.(%)	SEQ NO	FUNC ID.	TAG NAME	OUTPUT RANGE LO	HI	UNIT	UNCERTAINTY ABS.	REL.(%)
219	TE 219	TE-B18621	2.700+2	9.700+2	K	4.312+0	6.160-1	306	TE 306	TE-B20667	2.700+2	9.700+2	K	4.312+0	6.160-1
220	TE 220	TE-B18622	2.700+2	9.700+2	K	4.312+0	6.160-1	307	TE 307	TE-B20668	2.700+2	9.700+2	K	4.312+0	6.160-1
221	TE 221	TE-B18623	2.700+2	9.700+2	K	4.312+0	6.160-1	308	TE 308	TE-B20669	2.700+2	9.700+2	K	4.312+0	6.160-1
222	TE 222	TE-B18624	2.700+2	9.700+2	K	4.312+0	6.160-1	309	TE 309	TE-B22661	2.700+2	9.700+2	K	4.312+0	6.160-1
223	TE 223	TE-B18625	2.700+2	9.700+2	K	4.312+0	6.160-1	310	TE 310	TE-B22662	2.700+2	9.700+2	K	4.312+0	6.160-1
224	TE 224	TE-B18626	2.700+2	9.700+2	K	4.312+0	6.160-1	311	TE 311	TE-B22663	2.700+2	9.700+2	K	4.312+0	6.160-1
225	TE 225	TE-B18627	2.700+2	9.700+2	K	4.312+0	6.160-1	312	TE 312	TE-B22664	2.700+2	9.700+2	K	4.312+0	6.160-1
226	TE 226	TE-B18628	2.700+2	9.700+2	K	4.312+0	6.160-1	313	TE 313	TE-B22665	2.700+2	9.700+2	K	4.312+0	6.160-1
227	TE 227	TE-B18629	2.700+2	9.700+2	K	4.312+0	6.160-1	314	TE 314	TE-B22666	2.700+2	9.700+2	K	4.312+0	6.160-1
234	TE 234	TE-B14262	2.700+2	9.700+2	K	4.312+0	6.160-1	315	TE 315	TE-B22667	2.700+2	9.700+2	K	4.312+0	6.160-1
235	TE 235	TE-B14264	2.700+2	9.700+2	K	4.312+0	6.160-1	316	TE 316	TE-B22668	2.700+2	9.700+2	K	4.312+0	6.160-1
236	TE 236	TE-B14268	2.700+2	9.700+2	K	4.312+0	6.160-1	317	TE 317	TE-B22669	2.700+2	9.700+2	K	4.312+0	6.160-1
255	TE 255	TE-B09661	2.700+2	9.700+2	K	4.312+0	6.160-1	318	TE 318	TE-B24621	2.700+2	9.700+2	K	4.312+0	6.160-1
256	TE 256	TE-B09663	2.700+2	9.700+2	K	4.312+0	6.160-1	319	TE 319	TE-B24623	2.700+2	9.700+2	K	4.312+0	6.160-1
257	TE 257	TE-B09665	2.700+2	9.700+2	K	4.312+0	6.160-1	320	TE 320	TE-B24625	2.700+2	9.700+2	K	4.312+0	6.160-1
258	TE 258	TE-B09666	2.700+2	9.700+2	K	4.312+0	6.160-1	321	TE 321	TE-B24626	2.700+2	9.700+2	K	4.312+0	6.160-1
259	TE 259	TE-B09667	2.700+2	9.700+2	K	4.312+0	6.160-1	322	TE 322	TE-B24627	2.700+2	9.700+2	K	4.312+0	6.160-1
260	TE 260	TE-B09669	2.700+2	9.700+2	K	4.312+0	6.160-1	323	TE 323	TE-B24629	2.700+2	9.700+2	K	4.312+0	6.160-1
273	TE 273	TE-B14261	2.700+2	9.700+2	K	4.312+0	6.160-1	324	TE 324	TE-IN0641-SGA	2.700+2	7.200+2	K	3.307+0	7.350-1
274	TE 274	TE-B14263	2.700+2	9.700+2	K	4.312+0	6.160-1	325	TE 325	TE-IN0642-SGA	2.700+2	7.200+2	K	3.307+0	7.350-1
275	TE 275	TE-B14265	2.700+2	9.700+2	K	4.312+0	6.160-1	326	TE 326	TE-IN0643-SGA	2.700+2	7.200+2	K	3.307+0	7.350-1
276	TE 276	TE-B14266	2.700+2	9.700+2	K	4.312+0	6.160-1	330	TE 330	TE-IN0861-SGA	2.700+2	7.200+2	K	3.307+0	7.350-1
277	TE 277	TE-B14267	2.700+2	9.700+2	K	4.312+0	6.160-1	331	TE 331	TE-IN0862-SGA	2.700+2	7.200+2	K	3.307+0	7.350-1
278	TE 278	TE-B14269	2.700+2	9.700+2	K	4.312+0	6.160-1	332	TE 332	TE-IN0863-SGA	2.700+2	7.200+2	K	3.307+0	7.350-1
279	TE 279	TE-B15261	2.700+2	9.700+2	K	4.312+0	6.160-1	333	TE 333	TE-IN0864-SGA	2.700+2	7.200+2	K	3.307+0	7.350-1
280	TE 280	TE-B15263	2.700+2	9.700+2	K	4.312+0	6.160-1	334	TE 334	TE-IN0865-SGA	2.700+2	7.200+2	K	3.307+0	7.350-1
281	TE 281	TE-B15265	2.700+2	9.700+2	K	4.312+0	6.160-1	335	TE 335	TE-IN0866-SGA	2.700+2	7.200+2	K	3.307+0	7.350-1
282	TE 282	TE-B15266	2.700+2	9.700+2	K	4.312+0	6.160-1	336	TE 336	TE-EX0861-SGA	2.700+2	7.200+2	K	3.307+0	7.350-1
283	TE 283	TE-B15267	2.700+2	9.700+2	K	4.312+0	6.160-1	337	TE 337	TE-EX0862-SGA	2.700+2	7.200+2	K	3.307+0	7.350-1
284	TE 284	TE-B15269	2.700+2	9.700+2	K	4.312+0	6.160-1	338	TE 338	TE-EX0863-SGA	2.700+2	7.200+2	K	3.307+0	7.350-1
291	TE 291	TE-B15262	2.700+2	9.700+2	K	4.312+0	6.160-1	339	TE 339	TE-EX0864-SGA	2.700+2	7.200+2	K	3.307+0	7.350-1
292	TE 292	TE-B15264	2.700+2	9.700+2	K	4.312+0	6.160-1	340	TE 340	TE-EX0865-SGA	2.700+2	7.200+2	K	3.307+0	7.350-1
293	TE 293	TE-B15268	2.700+2	9.700+2	K	4.312+0	6.160-1	341	TE 341	TE-EX0866-SGA	2.700+2	7.200+2	K	3.307+0	7.350-1
294	TE 294	TE-B23221	2.700+2	9.700+2	K	4.312+0	6.160-1	342	TE 342	TE-IN0931-SGA	2.700+2	7.200+2	K	3.307+0	7.350-1
295	TE 295	TE-B23223	2.700+2	9.700+2	K	4.312+0	6.160-1	343	TE 343	TE-IN0932-SGA	2.700+2	7.200+2	K	3.307+0	7.350-1
296	TE 296	TE-B23225	2.700+2	9.700+2	K	4.312+0	6.160-1	344	TE 344	TE-IN0933-SGA	2.700+2	7.200+2	K	3.307+0	7.350-1
297	TE 297	TE-B23226	2.700+2	9.700+2	K	4.312+0	6.160-1	345	TE 345	TE-IN0934-SGA	2.700+2	7.200+2	K	3.307+0	7.350-1
298	TE 298	TE-B23227	2.700+2	9.700+2	K	4.312+0	6.160-1	346	TE 346	TE-IN0935-SGA	2.700+2	7.200+2	K	3.307+0	7.350-1
299	TE 299	TE-B23229	2.700+2	9.700+2	K	4.312+0	6.160-1	347	TE 347	TE-IN0936-SGA	2.700+2	7.200+2	K	3.307+0	7.350-1
300	TE 300	TE-B20661	2.700+2	9.700+2	K	4.312+0	6.160-1	348	TE 348	TE-IN0991-SGA	2.700+2	7.200+2	K	3.307+0	7.350-1
301	TE 301	TE-B20662	2.700+2	9.700+2	K	4.312+0	6.160-1	349	TE 349	TE-EX0991-SGA	2.700+2	7.200+2	K	3.307+0	7.350-1
302	TE 302	TE-B20663	2.700+2	9.700+2	K	4.312+0	6.160-1	350	TE 350	TE-IN0992-SGA	2.700+2	7.200+2	K	3.307+0	7.350-1
303	TE 303	TE-B20664	2.700+2	9.700+2	K	4.312+0	6.160-1	351	TE 351	TE-EX0992-SGA	2.700+2	7.200+2	K	3.307+0	7.350-1
304	TE 304	TE-B20665	2.700+2	9.700+2	K	4.312+0	6.160-1	352	TE 352	TE-IN0993-SGA	2.700+2	7.200+2	K	3.307+0	7.350-1
305	TE 305	TE-B20666	2.700+2	9.700+2	K	4.312+0	6.160-1	353	TE 353	TE-EX0993-SGA	2.700+2	7.200+2	K	3.307+0	7.350-1

Table 2.2-2 List of available measurements for experiment SB-CL-24 (Cont'd, 3/21)

SEQ NO	FUNC ID.	TAG NAME	OUTPUT RANGE LO	HI	UNIT	UNCERTAINTY ABS.	REL.(%)
354	TE 354	TE-IN0994-SGA	2.700+2	7.200+2	K	3.307+0	7.350-1
355	TE 355	TE-EX0994-SGA	2.700+2	7.200+2	K	3.307+0	7.350-1
356	TE 356	TE-IN0995-SGA	2.700+2	7.200+2	K	3.307+0	7.350-1
357	TE 357	TE-EX0995-SGA	2.700+2	7.200+2	K	3.307+0	7.350-1
358	TE 358	TE-IN0996-SGA	2.700+2	7.200+2	K	3.307+0	7.350-1
359	TE 359	TE-EX0996-SGA	2.700+2	7.200+2	K	3.307+0	7.350-1
360	TE 360	TE-IN1051-SGA	2.700+2	7.200+2	K	3.307+0	7.350-1
361	TE 361	TE-IN1052-SGA	2.700+2	7.200+2	K	3.307+0	7.350-1
362	TE 362	TE-IN1053-SGA	2.700+2	7.200+2	K	3.307+0	7.350-1
363	TE 363	TE-IN1054-SGA	2.700+2	7.200+2	K	3.307+0	7.350-1
364	TE 364	TE-IN1055-SGA	2.700+2	7.200+2	K	3.307+0	7.350-1
365	TE 365	TE-IN1056-SGA	2.700+2	7.200+2	K	3.307+0	7.350-1
366	TE 366	TE-IN1121-SGA	2.700+2	7.200+2	K	3.307+0	7.350-1
367	TE 367	TE-EX1121-SGA	2.700+2	7.200+2	K	3.307+0	7.350-1
368	TE 368	TE-IN1122-SGA	2.700+2	7.200+2	K	3.307+0	7.350-1
369	TE 369	TE-EX1122-SGA	2.700+2	7.200+2	K	3.307+0	7.350-1
370	TE 370	TE-IN1123-SGA	2.700+2	7.200+2	K	3.307+0	7.350-1
371	TE 371	TE-EX1123-SGA	2.700+2	7.200+2	K	3.307+0	7.350-1
372	TE 372	TE-IN1124-SGA	2.700+2	7.200+2	K	3.307+0	7.350-1
373	TE 373	TE-EX1124-SGA	2.700+2	7.200+2	K	3.307+0	7.350-1
374	TE 374	TE-IN1125-SGA	2.700+2	7.200+2	K	3.307+0	7.350-1
375	TE 375	TE-EX1125-SGA	2.700+2	7.200+2	K	3.307+0	7.350-1
376	TE 376	TE-IN1126-SGA	2.700+2	7.200+2	K	3.307+0	7.350-1
377	TE 377	TE-EX1126-SGA	2.700+2	7.200+2	K	3.307+0	7.350-1
378	TE 378	TE-IN1251-SGA	2.700+2	7.200+2	K	3.307+0	7.350-1
379	TE 379	TE-EX1251-SGA	2.700+2	7.200+2	K	3.307+0	7.350-1
380	TE 380	TE-IN1252-SGA	2.700+2	7.200+2	K	3.307+0	7.350-1
381	TE 381	TE-EX1252-SGA	2.700+2	7.200+2	K	3.307+0	7.350-1
382	TE 382	TE-IN1253-SGA	2.700+2	7.200+2	K	3.307+0	7.350-1
383	TE 383	TE-EX1253-SGA	2.700+2	7.200+2	K	3.307+0	7.350-1
384	TE 384	TE-IN1254-SGA	2.700+2	7.200+2	K	3.307+0	7.350-1
385	TE 385	TE-EX1254-SGA	2.700+2	7.200+2	K	3.307+0	7.350-1
386	TE 386	TE-IN1255-SGA	2.700+2	7.200+2	K	3.307+0	7.350-1
387	TE 387	TE-EX1255-SGA	2.700+2	7.200+2	K	3.307+0	7.350-1
388	TE 388	TE-IN1256-SGA	2.700+2	7.200+2	K	3.307+0	7.350-1
389	TE 389	TE-EX1256-SGA	2.700+2	7.200+2	K	3.307+0	7.350-1
390	TE 390	TE-IN1371-SGA	2.700+2	7.200+2	K	3.307+0	7.350-1
391	TE 391	TE-EX1371-SGA	2.700+2	7.200+2	K	3.307+0	7.350-1
392	TE 392	TE-IN1372-SGA	2.700+2	7.200+2	K	3.307+0	7.350-1
393	TE 393	TE-EX1372-SGA	2.700+2	7.200+2	K	3.307+0	7.350-1
394	TE 394	TE-IN1373-SGA	2.700+2	7.200+2	K	3.307+0	7.350-1
395	TE 395	TE-EX1373-SGA	2.700+2	7.200+2	K	3.307+0	7.350-1
396	TE 396	TE-IN1374-SGA	2.700+2	7.200+2	K	3.307+0	7.350-1
397	TE 397	TE-EX1374-SGA	2.700+2	7.200+2	K	3.307+0	7.350-1
398	TE 398	TE-IN1375-SGA	2.700+2	7.200+2	K	3.307+0	7.350-1
399	TE 399	TE-EX1375-SGA	2.700+2	7.200+2	K	3.307+0	7.350-1
400	TE 400	TE-IN1376-SGA	2.700+2	7.200+2	K	3.307+0	7.350-1
401	TE 401	TE-EX1376-SGA	2.700+2	7.200+2	K	3.307+0	7.350-1
402	TE 402	TE-IN1501-SGA	2.700+2	7.200+2	K	3.307+0	7.350-1
403	TE 403	TE-EX1501-SGA	2.700+2	7.200+2	K	3.307+0	7.350-1
404	TE 404	TE-IN1502-SGA	2.700+2	7.200+2	K	3.307+0	7.350-1
405	TE 405	TE-EX1502-SGA	2.700+2	7.200+2	K	3.307+0	7.350-1
406	TE 406	TE-IN1503-SGA	2.700+2	7.200+2	K	3.307+0	7.350-1
407	TE 407	TE-EX1503-SGA	2.700+2	7.200+2	K	3.307+0	7.350-1
408	TE 408	TE-IN1504-SGA	2.700+2	7.200+2	K	3.307+0	7.350-1
409	TE 409	TE-EX1504-SGA	2.700+2	7.200+2	K	3.307+0	7.350-1
410	TE 410	TE-IN1505-SGA	2.700+2	7.200+2	K	3.307+0	7.350-1
411	TE 411	TE-EX1505-SGA	2.700+2	7.200+2	K	3.307+0	7.350-1
412	TE 412	TE-IN1506-SGA	2.700+2	7.200+2	K	3.307+0	7.350-1
413	TE 413	TE-EX1506-SGA	2.700+2	7.200+2	K	3.307+0	7.350-1
414	TE 414	TE-IN1632-SGA	2.700+2	7.200+2	K	3.307+0	7.350-1
415	TE 415	TE-EX1632-SGA	2.700+2	7.200+2	K	3.307+0	7.350-1
416	TE 416	TE-IN1633-SGA	2.700+2	7.200+2	K	3.307+0	7.350-1
417	TE 417	TE-EX1633-SGA	2.700+2	7.200+2	K	3.307+0	7.350-1
418	TE 418	TE-IN1634-SGA	2.700+2	7.200+2	K	3.307+0	7.350-1
419	TE 419	TE-EX1634-SGA	2.700+2	7.200+2	K	3.307+0	7.350-1
420	TE 420	TE-IN1635-SGA	2.700+2	7.200+2	K	3.307+0	7.350-1
421	TE 421	TE-EX1635-SGA	2.700+2	7.200+2	K	3.307+0	7.350-1
422	TE 422	TE-IN1701-SGA	2.700+2	7.200+2	K	3.307+0	7.350-1
423	TE 423	TE-IN1706-SGA	2.700+2	7.200+2	K	3.307+0	7.350-1
424	TE 424	TE-IN1782-SGA	2.700+2	7.200+2	K	3.307+0	7.350-1
425	TE 425	TE-IN1785-SGA	2.700+2	7.200+2	K	3.307+0	7.350-1
426	TE 426	TE-IN1863-SGA	2.700+2	7.200+2	K	3.307+0	7.350-1
427	TE 427	TE-IN1864-SGA	2.700+2	7.200+2	K	3.307+0	7.350-1
428	TE 428	TE-223D-SGA	2.700+2	6.700+2	K	3.108+0	7.770-1
429	TE 429	TE-086C-SGA	2.700+2	6.700+2	K	3.108+0	7.770-1
430	TE 430	TE-099C-SGA	2.700+2	6.700+2	K	3.108+0	7.770-1
431	TE 431	TE-112C-SGA	2.700+2	6.700+2	K	3.108+0	7.770-1
432	TE 432	TE-125C-SGA	2.700+2	6.700+2	K	3.108+0	7.770-1
433	TE 433	TE-137C-SGA	2.700+2	6.700+2	K	3.108+0	7.770-1
434	TE 434	TE-150C-SGA	2.700+2	6.700+2	K	3.108+0	7.770-1
435	TE 435	TE-163C-SGA	2.700+2	6.700+2	K	3.108+0	7.770-1
436	TE 436	TE-178C-SGA	2.700+2	6.700+2	K	3.108+0	7.770-1
437	TE 437	TE-192F-SGA	2.700+2	6.700+2	K	3.108+0	7.770-1
438	TE 438	TE-208F-SGA	2.700+2	6.700+2	K	3.108+0	7.770-1
439	TE 439	TE-192C-SGA	2.700+2	6.700+2	K	3.108+0	7.770-1
440	TE 440	TE-208C-SGA	2.700+2	6.700+2	K	3.108+0	7.770-1
441	TE 441	TE-223C-SGA	2.700+2	6.700+2	K	3.108+0	7.770-1
442	TE 442	TE-245C-SGA	2.700+2	6.700+2	K	3.108+0	7.770-1
443	TE 443	TE-IN0641-SGB	2.700+2	7.200+2	K	3.307+0	7.350-1

Table 2.2-2 List of available measurements for experiment SB-CL-24 (Cont'd, 4/21)

SEQ NO	FUNC ID.	TAG NAME	OUTPUT RANGE LO	OUTPUT RANGE HI	UNIT	UNCERTAINTY ABS.	UNCERTAINTY REL.(%)	SEQ NO	FUNC ID.	TAG NAME	OUTPUT RANGE LO	OUTPUT RANGE HI	UNIT	UNCERTAINTY ABS.	UNCERTAINTY REL.(%)
444	TE 444	TE-IN0642-SGB	2.700+2	7.200+2	K	3.307+0	7.350-1	492	TE 492	TE-EX1124-SGB	2.700+2	7.200+2	K	3.307+0	7.350-1
445	TE 445	TE-IN0643-SGB	2.700+2	7.200+2	K	3.307+0	7.350-1	493	TE 493	TE-IN1125-SGB	2.700+2	7.200+2	K	3.307+0	7.350-1
449	TE 449	TE-IN0861-SGB	2.700+2	7.200+2	K	3.307+0	7.350-1	494	TE 494	TE-EX1125-SGB	2.700+2	7.200+2	K	3.307+0	7.350-1
450	TE 450	TE-IN0862-SGB	2.700+2	7.200+2	K	3.307+0	7.350-1	495	TE 495	TE-IN1126-SGB	2.700+2	7.200+2	K	3.307+0	7.350-1
451	TE 451	TE-IN0863-SGB	2.700+2	7.200+2	K	3.307+0	7.350-1	496	TE 496	TE-EX1126-SGB	2.700+2	7.200+2	K	3.307+0	7.350-1
452	TE 452	TE-IN0864-SGB	2.700+2	7.200+2	K	3.307+0	7.350-1	497	TE 497	TE-IN1251-SGB	2.700+2	7.200+2	K	3.307+0	7.350-1
453	TE 453	TE-IN0865-SGB	2.700+2	7.200+2	K	3.307+0	7.350-1	498	TE 498	TE-EX1251-SGB	2.700+2	7.200+2	K	3.307+0	7.350-1
454	TE 454	TE-IN0866-SGB	2.700+2	7.200+2	K	3.307+0	7.350-1	499	TE 499	TE-IN1252-SGB	2.700+2	7.200+2	K	3.307+0	7.350-1
455	TE 455	TE-EX0861-SGB	2.700+2	7.200+2	K	3.307+0	7.350-1	500	TE 500	TE-EX1252-SGB	2.700+2	7.200+2	K	3.307+0	7.350-1
456	TE 456	TE-EX0862-SGB	2.700+2	7.200+2	K	3.307+0	7.350-1	501	TE 501	TE-IN1253-SGB	2.700+2	7.200+2	K	3.307+0	7.350-1
457	TE 457	TE-EX0863-SGB	2.700+2	7.200+2	K	3.307+0	7.350-1	502	TE 502	TE-EX1253-SGB	2.700+2	7.200+2	K	3.307+0	7.350-1
458	TE 458	TE-EX0864-SGB	2.700+2	7.200+2	K	3.307+0	7.350-1	503	TE 503	TE-IN1254-SGB	2.700+2	7.200+2	K	3.307+0	7.350-1
459	TE 459	TE-EX0865-SGB	2.700+2	7.200+2	K	3.307+0	7.350-1	504	TE 504	TE-EX1254-SGB	2.700+2	7.200+2	K	3.307+0	7.350-1
460	TE 460	TE-EX0866-SGB	2.700+2	7.200+2	K	3.307+0	7.350-1	505	TE 505	TE-IN1255-SGB	2.700+2	7.200+2	K	3.307+0	7.350-1
461	TE 461	TE-IN0931-SGB	2.700+2	7.200+2	K	3.307+0	7.350-1	506	TE 506	TE-EX1255-SGB	2.700+2	7.200+2	K	3.307+0	7.350-1
462	TE 462	TE-IN0932-SGB	2.700+2	7.200+2	K	3.307+0	7.350-1	507	TE 507	TE-IN1256-SGB	2.700+2	7.200+2	K	3.307+0	7.350-1
463	TE 463	TE-IN0933-SGB	2.700+2	7.200+2	K	3.307+0	7.350-1	508	TE 508	TE-EX1256-SGB	2.700+2	7.200+2	K	3.307+0	7.350-1
464	TE 464	TE-IN0934-SGB	2.700+2	7.200+2	K	3.307+0	7.350-1	509	TE 509	TE-IN1371-SGB	2.700+2	7.200+2	K	3.307+0	7.350-1
465	TE 465	TE-IN0935-SGB	2.700+2	7.200+2	K	3.307+0	7.350-1	510	TE 510	TE-EX1371-SGB	2.700+2	7.200+2	K	3.307+0	7.350-1
466	TE 466	TE-IN0936-SGB	2.700+2	7.200+2	K	3.307+0	7.350-1	511	TE 511	TE-IN1372-SGB	2.700+2	7.200+2	K	3.307+0	7.350-1
467	TE 467	TE-IN0991-SGB	2.700+2	7.200+2	K	3.307+0	7.350-1	512	TE 512	TE-EX1372-SGB	2.700+2	7.200+2	K	3.307+0	7.350-1
468	TE 468	TE-EX0991-SGB	2.700+2	7.200+2	K	3.307+0	7.350-1	513	TE 513	TE-IN1373-SGB	2.700+2	7.200+2	K	3.307+0	7.350-1
469	TE 469	TE-IN0992-SGB	2.700+2	7.200+2	K	3.307+0	7.350-1	514	TE 514	TE-EX1373-SGB	2.700+2	7.200+2	K	3.307+0	7.350-1
470	TE 470	TE-EX0992-SGB	2.700+2	7.200+2	K	3.307+0	7.350-1	515	TE 515	TE-IN1374-SGB	2.700+2	7.200+2	K	3.307+0	7.350-1
471	TE 471	TE-IN0993-SGB	2.700+2	7.200+2	K	3.307+0	7.350-1	516	TE 516	TE-EX1374-SGB	2.700+2	7.200+2	K	3.307+0	7.350-1
472	TE 472	TE-EX0993-SGB	2.700+2	7.200+2	K	3.307+0	7.350-1	517	TE 517	TE-IN1375-SGB	2.700+2	7.200+2	K	3.307+0	7.350-1
473	TE 473	TE-IN0994-SGB	2.700+2	7.200+2	K	3.307+0	7.350-1	518	TE 518	TE-EX1375-SGB	2.700+2	7.200+2	K	3.307+0	7.350-1
474	TE 474	TE-EX0994-SGB	2.700+2	7.200+2	K	3.307+0	7.350-1	519	TE 519	TE-IN1376-SGB	2.700+2	7.200+2	K	3.307+0	7.350-1
475	TE 475	TE-IN0995-SGB	2.700+2	7.200+2	K	3.307+0	7.350-1	520	TE 520	TE-EX1376-SGB	2.700+2	7.200+2	K	3.307+0	7.350-1
476	TE 476	TE-EX0995-SGB	2.700+2	7.200+2	K	3.307+0	7.350-1	521	TE 521	TE-IN1501-SGB	2.700+2	7.200+2	K	3.307+0	7.350-1
477	TE 477	TE-IN0996-SGB	2.700+2	7.200+2	K	3.307+0	7.350-1	522	TE 522	TE-EX1501-SGB	2.700+2	7.200+2	K	3.307+0	7.350-1
478	TE 478	TE-EX0996-SGB	2.700+2	7.200+2	K	3.307+0	7.350-1	523	TE 523	TE-IN1502-SGB	2.700+2	7.200+2	K	3.307+0	7.350-1
479	TE 479	TE-IN1051-SGB	2.700+2	7.200+2	K	3.307+0	7.350-1	524	TE 524	TE-EX1502-SGB	2.700+2	7.200+2	K	3.307+0	7.350-1
480	TE 480	TE-IN1052-SGB	2.700+2	7.200+2	K	3.307+0	7.350-1	525	TE 525	TE-IN1503-SGB	2.700+2	7.200+2	K	3.307+0	7.350-1
481	TE 481	TE-IN1053-SGB	2.700+2	7.200+2	K	3.307+0	7.350-1	526	TE 526	TE-EX1503-SGB	2.700+2	7.200+2	K	3.307+0	7.350-1
482	TE 482	TE-IN1054-SGB	2.700+2	7.200+2	K	3.307+0	7.350-1	527	TE 527	TE-IN1504-SGB	2.700+2	7.200+2	K	3.307+0	7.350-1
483	TE 483	TE-IN1055-SGB	2.700+2	7.200+2	K	3.307+0	7.350-1	528	TE 528	TE-EX1504-SGB	2.700+2	7.200+2	K	3.307+0	7.350-1
484	TE 484	TE-IN1056-SGB	2.700+2	7.200+2	K	3.307+0	7.350-1	529	TE 529	TE-IN1505-SGB	2.700+2	7.200+2	K	3.307+0	7.350-1
485	TE 485	TE-IN1121-SGB	2.700+2	7.200+2	K	3.307+0	7.350-1	530	TE 530	TE-EX1505-SGB	2.700+2	7.200+2	K	3.307+0	7.350-1
486	TE 486	TE-EX1121-SGB	2.700+2	7.200+2	K	3.307+0	7.350-1	531	TE 531	TE-IN1506-SGB	2.700+2	7.200+2	K	3.307+0	7.350-1
487	TE 487	TE-IN1122-SGB	2.700+2	7.200+2	K	3.307+0	7.350-1	532	TE 532	TE-EX1506-SGB	2.700+2	7.200+2	K	3.307+0	7.350-1
488	TE 488	TE-EX1122-SGB	2.700+2	7.200+2	K	3.307+0	7.350-1	533	TE 533	TE-IN1632-SGB	2.700+2	7.200+2	K	3.307+0	7.350-1
489	TE 489	TE-IN1123-SGB	2.700+2	7.200+2	K	3.307+0	7.350-1	534	TE 534	TE-EX1632-SGB	2.700+2	7.200+2	K	3.307+0	7.350-1
490	TE 490	TE-EX1123-SGB	2.700+2	7.200+2	K	3.307+0	7.350-1	535	TE 535	TE-IN1633-SGB	2.700+2	7.200+2	K	3.307+0	7.350-1
491	TE 491	TE-IN1124-SGB	2.700+2	7.200+2	K	3.307+0	7.350-1	536	TE 536	TE-EX1633-SGB	2.700+2	7.200+2	K	3.307+0	7.350-1

Table 2.2-2 List of available measurements for experiment SB-CL-24 (Cont'd, 5/21)

SEQ NO	FUNC ID.	TAG NAME	OUTPUT RANGE LO	OUTPUT RANGE HI	UNIT	UNCERTAINTY ABS.	UNCERTAINTY REL.(%)
537	TE 537	TE-IN1634-SGB	2.700+2	7.200+2	K	3.307+0	7.350-1
538	TE 538	TE-EX1634-SGB	2.700+2	7.200+2	K	3.307+0	7.350-1
539	TE 539	TE-IN1635-SGB	2.700+2	7.200+2	K	3.307+0	7.350-1
540	TE 540	TE-EX1635-SGB	2.700+2	7.200+2	K	3.307+0	7.350-1
541	TE 541	TE-IN1701-SGB	2.700+2	7.200+2	K	3.307+0	7.350-1
542	TE 542	TE-IN1706-SGB	2.700+2	7.200+2	K	3.307+0	7.350-1
543	TE 543	TE-IN1782-SGB	2.700+2	7.200+2	K	3.307+0	7.350-1
544	TE 544	TE-IN1785-SGB	2.700+2	7.200+2	K	3.307+0	7.350-1
545	TE 545	TE-IN1863-SGB	2.700+2	7.200+2	K	3.307+0	7.350-1
546	TE 546	TE-IN1864-SGB	2.700+2	7.200+2	K	3.307+0	7.350-1
547	TE 547	TE-223D-SGB	2.700+2	6.700+2	K	3.108+0	7.770-1
548	TE 548	TE-086C-SGB	2.700+2	6.700+2	K	3.108+0	7.770-1
549	TE 549	TE-099C-SGB	2.700+2	6.700+2	K	3.108+0	7.770-1
550	TE 550	TE-112C-SGB	2.700+2	6.700+2	K	3.108+0	7.770-1
551	TE 551	TE-125C-SGB	2.700+2	6.700+2	K	3.108+0	7.770-1
552	TE 552	TE-137C-SGB	2.700+2	6.700+2	K	3.108+0	7.770-1
553	TE 553	TE-150C-SGB	2.700+2	6.700+2	K	3.108+0	7.770-1
554	TE 554	TE-163C-SGB	2.700+2	6.700+2	K	3.108+0	7.770-1
555	TE 555	TE-178C-SGB	2.700+2	6.700+2	K	3.108+0	7.770-1
556	TE 556	TE-192F-SGB	2.700+2	6.700+2	K	3.108+0	7.770-1
557	TE 557	TE-208F-SGB	2.700+2	6.700+2	K	3.108+0	7.770-1
558	TE 558	TE-192C-SGB	2.700+2	6.700+2	K	3.108+0	7.770-1
559	TE 559	TE-208C-SGB	2.700+2	6.700+2	K	3.108+0	7.770-1
560	TE 560	TE-223C-SGB	2.700+2	6.700+2	K	3.108+0	7.770-1
561	TE 561	TE-245C-SGB	2.700+2	6.700+2	K	3.108+0	7.770-1
562	TE 562	TE-211C-PR	2.700+2	7.200+2	K	3.307+0	7.350-1
563	TE 563	TE-194C-PR	2.700+2	7.200+2	K	3.307+0	7.350-1
564	TE 564	TE-177C-PR	2.700+2	7.200+2	K	3.307+0	7.350-1
596	TE 596	TE-177D-PR	2.700+2	7.200+2	K	3.307+0	7.350-1
597	TE 597	TE-181D-PR	2.700+2	7.200+2	K	3.307+0	7.350-1
598	TE 598	TE-185D-PR	2.700+2	7.200+2	K	3.307+0	7.350-1
599	TE 599	TE-189D-PR	2.700+2	7.200+2	K	3.307+0	7.350-1
600	TE 600	TE-192D-PR	2.700+2	7.200+2	K	3.307+0	7.350-1
601	TE 601	TE-196D-PR	2.700+2	7.200+2	K	3.307+0	7.350-1
602	TE 602	TE-200D-PR	2.700+2	7.200+2	K	3.307+0	7.350-1
603	TE 603	TE-204D-PR	2.700+2	7.200+2	K	3.307+0	7.350-1
604	TE 604	TE-207D-PR	2.700+2	7.200+2	K	3.307+0	7.350-1
605	TE 605	TE-211D-PR	2.700+2	7.200+2	K	3.307+0	7.350-1
606	TE 606	TE011A-HLA	2.700+2	7.200+2	K	3.307+0	7.350-1
607	TE 607	TE011B-HLA	2.700+2	7.200+2	K	3.307+0	7.350-1
608	TE 608	TE011C-HLA	2.700+2	7.200+2	K	3.307+0	7.350-1
609	TE 609	TE012C-HLA	2.700+2	7.200+2	K	3.307+0	7.350-1
610	TE 610	TE012D-HLA	2.700+2	7.200+2	K	3.307+0	7.350-1
613	TE 613	TE051C-LSA	2.700+2	7.200+2	K	3.307+0	7.350-1
614	TE 614	TE051D-LSA	2.700+2	7.200+2	K	3.307+0	7.350-1
615	TE 615	TE052-LSA	2.700+2	7.200+2	K	3.307+0	7.350-1
616	TE 616	TE071A-CLA	2.700+2	7.200+2	K	3.307+0	7.350-1
617	TE 617	TE071B-CLA	2.700+2	7.200+2	K	3.307+0	7.350-1
618	TE 618	TE071C-CLA	2.700+2	7.200+2	K	3.307+0	7.350-1
619	TE 619	TE072C-CLA	2.700+2	7.200+2	K	3.307+0	7.350-1
620	TE 620	TE072D-CLA	2.700+2	7.200+2	K	3.307+0	7.350-1
622	TE 622	TE151B-HLB	2.700+2	7.200+2	K	3.307+0	7.350-1
623	TE 623	TE151C-HLB	2.700+2	7.200+2	K	3.307+0	7.350-1
624	TE 624	TE152C-HLB	2.700+2	7.200+2	K	3.307+0	7.350-1
625	TE 625	TE152D-HLB	2.700+2	7.200+2	K	3.307+0	7.350-1
626	TE 626	TE191A-LSB	2.700+2	7.200+2	K	3.307+0	7.350-1
628	TE 628	TE191C-LSB	2.700+2	7.200+2	K	3.307+0	7.350-1
629	TE 629	TE191D-LSB	2.700+2	7.200+2	K	3.307+0	7.350-1
630	TE 630	TE192-LSB	2.700+2	7.200+2	K	3.307+0	7.350-1
631	TE 631	TE211A-CLB	2.700+2	7.200+2	K	3.307+0	7.350-1
634	TE 634	TE212C-CLB	2.700+2	7.200+2	K	3.307+0	7.350-1
635	TE 635	TE212D-CLB	2.700+2	7.200+2	K	3.307+0	7.350-1
636	TE 636	TE291C-PR	2.700+2	7.200+2	K	3.307+0	7.350-1
637	TE 637	TE291D-PR	2.700+2	7.200+2	K	3.307+0	7.350-1
638	TE 638	TE301C-PR	2.700+2	7.200+2	K	3.307+0	7.350-1
639	TE 639	TE301D-PR	2.700+2	7.200+2	K	3.307+0	7.350-1
640	TE 640	TE311C-PR	2.700+2	7.200+2	K	3.307+0	7.350-1
641	TE 641	TE311D-PR	2.700+2	7.200+2	K	3.307+0	7.350-1
645	TE 645	TE571D-BU	2.700+2	7.200+2	K	3.307+0	7.350-1
664	TE 664	TE-E-006-DC	2.700+2	7.200+2	K	3.307+0	7.350-1
665	TE 665	TE-W-006-DC	2.700+2	7.200+2	K	3.307+0	7.350-1
670	TE 670	TE-111A-CDP	2.700+2	7.200+2	K	3.307+0	7.350-1
671	TE 671	TE-111B-CDP	2.700+2	7.200+2	K	3.307+0	7.350-1
672	TE 672	TE-112A-CDP	2.700+2	7.200+2	K	3.307+0	7.350-1
673	TE 673	TE-112B-CDP	2.700+2	7.200+2	K	3.307+0	7.350-1
674	TE 674	TE-113A-CDP	2.700+2	7.200+2	K	3.307+0	7.350-1
675	TE 675	TE-113B-CDP	2.700+2	7.200+2	K	3.307+0	7.350-1
676	TE 676	TE-114A-CDP	2.700+2	7.200+2	K	3.307+0	7.350-1
677	TE 677	TE-114B-CDP	2.700+2	7.200+2	K	3.307+0	7.350-1
678	TE 678	TE-115A-CDP	2.700+2	7.200+2	K	3.307+0	7.350-1
679	TE 679	TE-115B-CDP	2.700+2	7.200+2	K	3.307+0	7.350-1
680	TE 680	TE-115C-CDP	2.700+2	7.200+2	K	3.307+0	7.350-1
681	TE 681	TE-116A-CDP	2.700+2	7.200+2	K	3.307+0	7.350-1
682	TE 682	TE-116B-CDP	2.700+2	7.200+2	K	3.307+0	7.350-1
683	TE 683	TE-116C-CDP	2.700+2	7.200+2	K	3.307+0	7.350-1
684	TE 684	TE-117A-CDP	2.700+2	7.200+2	K	3.307+0	7.350-1
685	TE 685	TE-117B-CDP	2.700+2	7.200+2	K	3.307+0	7.350-1
686	TE 686	TE-117C-CDP	2.700+2	7.200+2	K	3.307+0	7.350-1
687	TE 687	TE-118A-CDP	2.700+2	7.200+2	K	3.307+0	7.350-1
688	TE 688	TE-118B-CDP	2.700+2	7.200+2	K	3.307+0	7.350-1

Table 2.2-2 List of available measurements for experiment SB-CL-24 (Cont'd, 6/21)

SEQ NO	FUNC ID.	TAG NAME	OUTPUT RANGE LO	HI	UNIT	UNCERTAINTY ABS.	REL.(%)
689	TE 689	TE-118C-CDP	2.700+2	7.200+2	K	3.307+0	7.350-1
690	TE 690	TE-131-CDP	2.700+2	7.200+2	K	3.307+0	7.350-1
691	TE 691	TE-132-CDP	2.700+2	7.200+2	K	3.307+0	7.350-1
692	TE 692	TE-133-CDP	2.700+2	7.200+2	K	3.307+0	7.350-1
693	TE 693	TE-134-CDP	2.700+2	7.200+2	K	3.307+0	7.350-1
694	TE 694	TE-135-CDP	2.700+2	7.200+2	K	3.307+0	7.350-1
695	TE 695	TE-136-CDP	2.700+2	7.200+2	K	3.307+0	7.350-1
696	TE 696	TE-137-CDP	2.700+2	7.200+2	K	3.307+0	7.350-1
697	TE 697	TE-138-CDP	2.700+2	7.200+2	K	3.307+0	7.350-1
698	TE 698	TE-139-CDP	2.700+2	7.200+2	K	3.307+0	7.350-1
699	TE 699	TE-111E-CDP	2.700+2	7.200+2	K	3.307+0	7.350-1
700	TE 700	TE-112E-CDP	2.700+2	7.200+2	K	3.307+0	7.350-1
701	TE 701	TE-113E-CDP	2.700+2	7.200+2	K	3.307+0	7.350-1
702	TE 702	TE-114E-CDP	2.700+2	7.200+2	K	3.307+0	7.350-1
703	TE 703	TE-115E-CDP	2.700+2	7.200+2	K	3.307+0	7.350-1
704	TE 704	TE-116E-CDP	2.700+2	7.200+2	K	3.307+0	7.350-1
705	TE 705	TE-117E-CDP	2.700+2	7.200+2	K	3.307+0	7.350-1
706	TE 706	TE-118E-CDP	2.700+2	7.200+2	K	3.307+0	7.350-1
707	TE 707	TE-121E-UHDP	2.700+2	7.200+2	K	3.307+0	7.350-1
708	TE 708	TE-121A-UHDP	2.700+2	7.200+2	K	3.307+0	7.350-1
709	TE 709	TE-121B-UHDP	2.700+2	7.200+2	K	3.307+0	7.350-1
710	TE 710	TE-121C-UHDP	2.700+2	7.200+2	K	3.307+0	7.350-1
711	TE 711	TE-E071C-DC	2.700+2	7.200+2	K	3.307+0	7.350-1
712	TE 712	TE-W071C-DC	2.700+2	7.200+2	K	3.307+0	7.350-1
713	TE 713	TE-E067C-DC	2.700+2	7.200+2	K	3.307+0	7.350-1
714	TE 714	TE-W067C-DC	2.700+2	7.200+2	K	3.307+0	7.350-1
715	TE 715	TE-951-CS	2.700+2	7.200+2	K	3.307+0	7.350-1
716	TE 716	TE-952-CS	2.700+2	7.200+2	K	3.307+0	7.350-1
717	TE 717	TE-953-CS	2.700+2	7.200+2	K	3.307+0	7.350-1
718	TE 718	TE-B05221	2.700+2	9.700+2	K	4.312+0	6.160-1
719	TE 719	TE-B05223	2.700+2	9.700+2	K	4.312+0	6.160-1
720	TE 720	TE-B05225	2.700+2	9.700+2	K	4.312+0	6.160-1
721	TE 721	TE-B05226	2.700+2	9.700+2	K	4.312+0	6.160-1
722	TE 722	TE-B05227	2.700+2	9.700+2	K	4.312+0	6.160-1
723	TE 723	TE-B05229	2.700+2	9.700+2	K	4.312+0	6.160-1
724	TE 724	TE-B07221	2.700+2	9.700+2	K	4.312+0	6.160-1
725	TE 725	TE-B07223	2.700+2	9.700+2	K	4.312+0	6.160-1
726	TE 726	TE-B07225	2.700+2	9.700+2	K	4.312+0	6.160-1
727	TE 727	TE-B07226	2.700+2	9.700+2	K	4.312+0	6.160-1
728	TE 728	TE-B07227	2.700+2	9.700+2	K	4.312+0	6.160-1
729	TE 729	TE-B07229	2.700+2	9.700+2	K	4.312+0	6.160-1
730	TE 730	TE-EX0650-SGA	2.700+2	7.200+2	K	3.307+0	7.350-1
731	TE 731	TE-EX0680-SGA	2.700+2	7.200+2	K	3.307+0	7.350-1
732	TE 732	TE-EX0720-SGA	2.700+2	7.200+2	K	3.307+0	7.350-1
733	TE 733	TE-EX0650-SGB	2.700+2	7.200+2	K	3.307+0	7.350-1
734	TE 734	TE-EX0680-SGB	2.700+2	7.200+2	K	3.307+0	7.350-1
735	TE 735	TE-EX0720-SGB	2.700+2	7.200+2	K	3.307+0	7.350-1
751	DT 1	DTE020A-HLA	-1.500+2	1.500+2	K	1.665+0	5.550-1
752	DT 2	DTE020B-HLA	-1.500+2	1.500+2	K	1.665+0	5.550-1
753	DT 3	DTE030A-HLA	-1.500+2	1.500+2	K	1.665+0	5.550-1
754	DT 4	DTE030B-HLA	-1.500+2	1.500+2	K	1.665+0	5.550-1
755	DT 5	DTE050A-LSA	-1.500+2	1.500+2	K	1.665+0	5.550-1
756	DT 6	DTE050B-LSA	-1.500+2	1.500+2	K	1.665+0	5.550-1
757	DT 7	DTE060A-PCA	-1.500+2	1.500+2	K	1.665+0	5.550-1
758	DT 8	DTE070A-CLA	-1.500+2	1.500+2	K	1.665+0	5.550-1
759	DT 9	DTE070B-CLA	-1.500+2	1.500+2	K	1.665+0	5.550-1
760	DT 10	DTE080A-CLA	-1.500+2	1.500+2	K	1.665+0	5.550-1
761	DT 11	DTE080B-CLA	-1.500+2	1.500+2	K	1.665+0	5.550-1
762	DT 12	DTE100-HLA	-1.500+2	1.500+2	K	2.970+0	9.900-1
763	DT 13	DTE160A-HLB	-1.500+2	1.500+2	K	1.665+0	5.550-1
764	DT 14	DTE160B-HLB	-1.500+2	1.500+2	K	1.665+0	5.550-1
765	DT 15	DTE170A-HLB	-1.500+2	1.500+2	K	1.665+0	5.550-1
766	DT 16	DTE170B-HLB	-1.500+2	1.500+2	K	1.665+0	5.550-1
767	DT 17	DTE190A-LSB	-1.500+2	1.500+2	K	1.665+0	5.550-1
768	DT 18	DTE190B-LSB	-1.500+2	1.500+2	K	1.665+0	5.550-1
769	DT 19	DTE200A-PCB	-1.500+2	1.500+2	K	1.665+0	5.550-1
770	DT 20	DTE210A-CLB	-1.500+2	1.500+2	K	1.665+0	5.550-1
771	DT 21	DTE210B-CLB	-1.500+2	1.500+2	K	1.665+0	5.550-1
772	DT 22	DTE220A-CLB	-1.500+2	1.500+2	K	1.665+0	5.550-1
773	DT 23	DTE220B-CLB	-1.500+2	1.500+2	K	1.665+0	5.550-1
774	DT 24	DTE240-HLB	-1.500+2	1.500+2	K	2.970+0	9.900-1
775	DT 25	DTE270A-PR	-1.500+2	1.500+2	K	1.665+0	5.550-1
776	DT 26	DTE280A-PR	-1.500+2	1.500+2	K	1.665+0	5.550-1
777	DT 27	DTE-E-015A-PV	-1.500+2	1.500+2	K	1.665+0	5.550-1
778	DT 28	DTE-W-015A-PV	-1.500+2	1.500+2	K	1.665+0	5.550-1
779	DT 29	DTE-N000A-PV	-1.500+2	1.500+2	K	1.665+0	5.550-1
780	DT 30	DTE-S000A-PV	-1.500+2	1.500+2	K	1.665+0	5.550-1
781	DT 31	DTE-E000A-PV	-1.500+2	1.500+2	K	1.665+0	5.550-1
782	DT 32	DTE-W000A-PV	-1.500+2	1.500+2	K	1.665+0	5.550-1
783	DT 33	DTE-N018A-PV	-1.500+2	1.500+2	K	1.665+0	5.550-1
784	DT 34	DTE-S018A-PV	-1.500+2	1.500+2	K	1.665+0	5.550-1
785	DT 35	DTE-E018A-PV	-1.500+2	1.500+2	K	1.665+0	5.550-1
786	DT 36	DTE-W018A-PV	-1.500+2	1.500+2	K	1.665+0	5.550-1
787	DT 37	DTE-N036A-PV	-1.500+2	1.500+2	K	1.665+0	5.550-1
788	DT 38	DTE-S036A-PV	-1.500+2	1.500+2	K	1.665+0	5.550-1
789	DT 39	DTE-E036A-PV	-1.500+2	1.500+2	K	1.665+0	5.550-1
790	DT 40	DTE-W036A-PV	-1.500+2	1.500+2	K	1.665+0	5.550-1
791	DT 41	DTE-N060A-PV	-1.500+2	1.500+2	K	1.665+0	5.550-1
792	DT 42	DTE-S060A-PV	-1.500+2	1.500+2	K	1.665+0	5.550-1
793	DT 43	DTE-E060A-PV	-1.500+2	1.500+2	K	1.665+0	5.550-1

Table 2.2-2 List of available measurements for experiment SB-CL-24 (Cont'd, 7/21)

SEQ NO	FUNC ID.	TAG NAME	OUTPUT RANGE LO	OUTPUT RANGE HI	UNIT	UNCERTAINTY ABS.	UNCERTAINTY REL.(%)
794	DT 44	DTE-W060A-PV	-1.500+2	1.500+2	K	1.665+0	5.550-1
795	DT 45	DTE-E080A-PV	-1.500+2	1.500+2	K	1.665+0	5.550-1
796	DT 46	DTE-W080A-PV	-1.500+2	1.500+2	K	1.665+0	5.550-1
797	DT 47	DTE-N000B-PV	-1.500+2	1.500+2	K	1.665+0	5.550-1
798	DT 48	DTE-S000B-PV	-1.500+2	1.500+2	K	1.665+0	5.550-1
799	DT 49	DTE-E000B-PV	-1.500+2	1.500+2	K	1.665+0	5.550-1
800	DT 50	DTE-W000B-PV	-1.500+2	1.500+2	K	1.665+0	5.550-1
801	DT 51	DTE-N018B-PV	-1.500+2	1.500+2	K	1.665+0	5.550-1
802	DT 52	DTE-S018B-PV	-1.500+2	1.500+2	K	1.665+0	5.550-1
803	DT 53	DTE-E018B-PV	-1.500+2	1.500+2	K	1.665+0	5.550-1
804	DT 54	DTE-W018B-PV	-1.500+2	1.500+2	K	1.665+0	5.550-1
805	DT 55	DTE-N036B-PV	-1.500+2	1.500+2	K	1.665+0	5.550-1
806	DT 56	DTE-S036B-PV	-1.500+2	1.500+2	K	1.665+0	5.550-1
807	DT 57	DTE-E036B-PV	-1.500+2	1.500+2	K	1.665+0	5.550-1
808	DT 58	DTE-W036B-PV	-1.500+2	1.500+2	K	1.665+0	5.550-1
809	DT 59	DTE-N060B-PV	-1.500+2	1.500+2	K	1.665+0	5.550-1
810	DT 60	DTE-S060B-PV	-1.500+2	1.500+2	K	1.665+0	5.550-1
811	DT 61	DTE-E060B-PV	-1.500+2	1.500+2	K	1.665+0	5.550-1
812	DT 62	DTE-W060B-PV	-1.500+2	1.500+2	K	1.665+0	5.550-1
813	DT 63	DTE-N000C-PV	-1.500+2	1.500+2	K	1.665+0	5.550-1
814	DT 64	DTE-S000C-PV	-1.500+2	1.500+2	K	1.665+0	5.550-1
815	DT 65	DTE-E000C-PV	-1.500+2	1.500+2	K	1.665+0	5.550-1
816	DT 66	DTE-W000C-PV	-1.500+2	1.500+2	K	1.665+0	5.550-1
817	DT 67	DTE-N018C-PV	-1.500+2	1.500+2	K	1.665+0	5.550-1
818	DT 68	DTE-S018C-PV	-1.500+2	1.500+2	K	1.665+0	5.550-1
819	DT 69	DTE-E018C-PV	-1.500+2	1.500+2	K	1.665+0	5.550-1
820	DT 70	DTE-W018C-PV	-1.500+2	1.500+2	K	1.665+0	5.550-1
821	DT 71	DTE-N036C-PV	-1.500+2	1.500+2	K	1.665+0	5.550-1
822	DT 72	DTE-S036C-PV	-1.500+2	1.500+2	K	1.665+0	5.550-1
823	DT 73	DTE-E036C-PV	-1.500+2	1.500+2	K	1.665+0	5.550-1
824	DT 74	DTE-W036C-PV	-1.500+2	1.500+2	K	1.665+0	5.550-1
825	DT 75	DTE-N060C-PV	-1.500+2	1.500+2	K	1.665+0	5.550-1
826	DT 76	DTE-S060C-PV	-1.500+2	1.500+2	K	1.665+0	5.550-1
827	DT 77	DTE-E060C-PV	-1.500+2	1.500+2	K	1.665+0	5.550-1
828	DT 78	DTE-W060C-PV	-1.500+2	1.500+2	K	1.665+0	5.550-1
829	DT 79	DTE-N000E-PV	-1.500+2	1.500+2	K	1.665+0	5.550-1
830	DT 80	DTE-S000E-PV	-1.500+2	1.500+2	K	1.665+0	5.550-1
831	DT 81	DTE-E000E-PV	-1.500+2	1.500+2	K	1.665+0	5.550-1
832	DT 82	DTE-W000E-PV	-1.500+2	1.500+2	K	1.665+0	5.550-1
833	DT 83	DTE-N010E-PV	-1.500+2	1.500+2	K	1.665+0	5.550-1
834	DT 84	DTE-S010E-PV	-1.500+2	1.500+2	K	1.665+0	5.550-1
835	DT 85	DTE-E010E-PV	-1.500+2	1.500+2	K	1.665+0	5.550-1
836	DT 86	DTE-W010E-PV	-1.500+2	1.500+2	K	1.665+0	5.550-1
837	DT 87	DTE-N018E-PV	-1.500+2	1.500+2	K	1.665+0	5.550-1
838	DT 88	DTE-S018E-PV	-1.500+2	1.500+2	K	1.665+0	5.550-1
839	DT 89	DTE-E018E-PV	-1.500+2	1.500+2	K	1.665+0	5.550-1
840	DT 90	DTE-W018E-PV	-1.500+2	1.500+2	K	1.665+0	5.550-1
841	DT 91	DTE-N026E-PV	-1.500+2	1.500+2	K	1.665+0	5.550-1
842	DT 92	DTE-S026E-PV	-1.500+2	1.500+2	K	1.665+0	5.550-1
843	DT 93	DTE-E026E-PV	-1.500+2	1.500+2	K	1.665+0	5.550-1
844	DT 94	DTE-W026E-PV	-1.500+2	1.500+2	K	1.665+0	5.550-1
845	DT 95	DTE-N036E-PV	-1.500+2	1.500+2	K	1.665+0	5.550-1
846	DT 96	DTE-S036E-PV	-1.500+2	1.500+2	K	1.665+0	5.550-1
847	DT 97	DTE-E036E-PV	-1.500+2	1.500+2	K	1.665+0	5.550-1
848	DT 98	DTE-W036E-PV	-1.500+2	1.500+2	K	1.665+0	5.550-1
849	DT 99	DTE-N049E-PV	-1.500+2	1.500+2	K	1.665+0	5.550-1
850	DT 100	DTE-S049E-PV	-1.500+2	1.500+2	K	1.665+0	5.550-1
851	DT 101	DTE-E049E-PV	-1.500+2	1.500+2	K	1.665+0	5.550-1
852	DT 102	DTE-W049E-PV	-1.500+2	1.500+2	K	1.665+0	5.550-1
853	DT 103	DTE-N060E-PV	-1.500+2	1.500+2	K	1.665+0	5.550-1
854	DT 104	DTE-S060E-PV	-1.500+2	1.500+2	K	1.665+0	5.550-1
855	DT 105	DTE-E060E-PV	-1.500+2	1.500+2	K	1.665+0	5.550-1
856	DT 106	DTE-W060E-PV	-1.500+2	1.500+2	K	1.665+0	5.550-1
857	DT 107	DTE-040-B09-UCP	-1.500+2	1.500+2	K	1.665+0	5.550-1
858	DT 108	DTE-040-B11-UCP	-1.500+2	1.500+2	K	1.665+0	5.550-1
859	DT 109	DTE-040-B01-UCP	-1.500+2	1.500+2	K	1.665+0	5.550-1
860	DT 110	DTE-040-B03-UCP	-1.500+2	1.500+2	K	1.665+0	5.550-1
861	DT 111	DTE-040-B05-UCP	-1.500+2	1.500+2	K	1.665+0	5.550-1
862	DT 112	DTE-040-B07-UCP	-1.500+2	1.500+2	K	1.665+0	5.550-1
863	DT 113	DTE-040-B21-UCP	-1.500+2	1.500+2	K	1.665+0	5.550-1
864	DT 114	DTE-040-B23-UCP	-1.500+2	1.500+2	K	1.665+0	5.550-1
865	DT 115	DTE-040-B02-UCP	-1.500+2	1.500+2	K	1.665+0	5.550-1
866	DT 116	DTE-040-B15-UCP	-1.500+2	1.500+2	K	1.665+0	5.550-1
867	DT 117	DTE-040-B06-UCP	-1.500+2	1.500+2	K	1.665+0	5.550-1
868	DT 118	DTE-040-B14-UCP	-1.500+2	1.500+2	K	1.665+0	5.550-1
869	DT 119	DTE-040-B18-UCP	-1.500+2	1.500+2	K	1.665+0	5.550-1
870	DT 120	DTE-040-B19-UCP	-1.500+2	1.500+2	K	1.665+0	5.550-1
871	DT 121	DTE-040-B10-UCP	-1.500+2	1.500+2	K	1.665+0	5.550-1
872	DT 122	DTE-040-B12-UCP	-1.500+2	1.500+2	K	1.665+0	5.550-1
873	DT 123	DTE-040-B04-UCP	-1.500+2	1.500+2	K	1.665+0	5.550-1
874	DT 124	DTE-040-B08-UCP	-1.500+2	1.500+2	K	1.665+0	5.550-1
875	DT 125	DTE-040-B22-UCP	-1.500+2	1.500+2	K	1.665+0	5.550-1
876	DT 126	DTE-040-B24-UCP	-1.500+2	1.500+2	K	1.665+0	5.550-1
877	DT 127	DTE-000-B02-LCP	-4.000+1	4.000+1	K	1.664+0	2.080+0
878	DT 128	DTE-000-B03-LCP	-4.000+1	4.000+1	K	1.664+0	2.080+0
879	DT 129	DTE-000-B06-LCP	-4.000+1	4.000+1	K	1.664+0	2.080+0
880	DT 130	DTE-000-B07-LCP	-4.000+1	4.000+1	K	1.664+0	2.080+0
881	DT 131	DTE-000-B09-LCP	-4.000+1	4.000+1	K	1.664+0	2.080+0
882	DT 132	DTE-000-B11-LCP	-4.000+1	4.000+1	K	1.664+0	2.080+0
883	DT 133	DTE-000-B14-LCP	-4.000+1	4.000+1	K	1.664+0	2.080+0

Table 2.2-2 List of available measurements for experiment SB-CL-24 (Cont'd, 8/21)

SEQ NO	FUNC ID.	TAG NAME	OUTPUT RANGE LO	HI	UNIT	UNCERTAINTY ABS.	REL.(%)
884	DT 134	DTE-000-B16-LCP	-4.000+1	4.000+1	K	1.664+0	2.080+0
885	DT 135	DTE-000-B18-LCP	-4.000+1	4.000+1	K	1.664+0	2.080+0
886	DT 136	DTE-000-B20-LCP	-4.000+1	4.000+1	K	1.664+0	2.080+0
887	DT 137	DTE-000-B21-LCP	-4.000+1	4.000+1	K	1.664+0	2.080+0
888	DT 138	DTE-000-B23-LCP	-4.000+1	4.000+1	K	1.664+0	2.080+0
889	DT 139	DTE-086A-SGA	-4.000+1	4.000+1	K	1.664+0	2.080+0
890	DT 140	DTE-137A-SGA	-4.000+1	4.000+1	K	1.664+0	2.080+0
891	DT 141	DTE-178A-SGA	-4.000+1	4.000+1	K	1.664+0	2.080+0
892	DT 142	DTE-223A-SGA	-4.000+1	4.000+1	K	1.664+0	2.080+0
893	DT 143	DTE-IN0861-SGA	-1.000+2	1.000+2	K	1.664+0	8.320-1
894	DT 144	DTE-EX0861-SGA	-1.000+2	1.000+2	K	1.664+0	8.320-1
895	DT 145	DTE-IN0862-SGA	-1.000+2	1.000+2	K	1.664+0	8.320-1
896	DT 146	DTE-EX0862-SGA	-1.000+2	1.000+2	K	1.664+0	8.320-1
897	DT 147	DTE-IN0863-SGA	-1.000+2	1.000+2	K	1.664+0	8.320-1
898	DT 148	DTE-EX0863-SGA	-1.000+2	1.000+2	K	1.664+0	8.320-1
899	DT 149	DTE-IN0991-SGA	-1.000+2	1.000+2	K	1.664+0	8.320-1
900	DT 150	DTE-EX0991-SGA	-1.000+2	1.000+2	K	1.664+0	8.320-1
901	DT 151	DTE-IN0992-SGA	-1.000+2	1.000+2	K	1.664+0	8.320-1
902	DT 152	DTE-EX0992-SGA	-1.000+2	1.000+2	K	1.664+0	8.320-1
903	DT 153	DTE-IN0993-SGA	-1.000+2	1.000+2	K	1.664+0	8.320-1
904	DT 154	DTE-EX0993-SGA	-1.000+2	1.000+2	K	1.664+0	8.320-1
905	DT 155	DTE-IN1121-SGA	-1.000+2	1.000+2	K	1.664+0	8.320-1
906	DT 156	DTE-EX1121-SGA	-1.000+2	1.000+2	K	1.664+0	8.320-1
907	DT 157	DTE-IN1122-SGA	-1.000+2	1.000+2	K	1.664+0	8.320-1
908	DT 158	DTE-EX1122-SGA	-1.000+2	1.000+2	K	1.664+0	8.320-1
909	DT 159	DTE-IN1123-SGA	-1.000+2	1.000+2	K	1.664+0	8.320-1
910	DT 160	DTE-EX1123-SGA	-1.000+2	1.000+2	K	1.664+0	8.320-1
911	DT 161	DTE-IN1371-SGA	-1.000+2	1.000+2	K	1.664+0	8.320-1
912	DT 162	DTE-EX1371-SGA	-1.000+2	1.000+2	K	1.664+0	8.320-1
913	DT 163	DTE-IN1372-SGA	-1.000+2	1.000+2	K	1.664+0	8.320-1
914	DT 164	DTE-EX1372-SGA	-1.000+2	1.000+2	K	1.664+0	8.320-1
915	DT 165	DTE-IN1373-SGA	-1.000+2	1.000+2	K	1.664+0	8.320-1
916	DT 166	DTE-EX1373-SGA	-1.000+2	1.000+2	K	1.664+0	8.320-1
917	DT 167	DTE-IN1632-SGA	-1.000+2	1.000+2	K	1.664+0	8.320-1
918	DT 168	DTE-EX1632-SGA	-1.000+2	1.000+2	K	1.664+0	8.320-1
919	DT 169	DTE-IN1633-SGA	-1.000+2	1.000+2	K	1.664+0	8.320-1
920	DT 170	DTE-EX1633-SGA	-1.000+2	1.000+2	K	1.664+0	8.320-1
921	DT 171	DTE-IN1701-SGA	-1.000+2	1.000+2	K	1.664+0	8.320-1
922	DT 172	DTE-IN1782-SGA	-1.000+2	1.000+2	K	1.664+0	8.320-1
923	DT 173	DTE-IN1863-SGA	-1.000+2	1.000+2	K	1.664+0	8.320-1
924	DT 174	DTE-086A-SGB	-4.000+1	4.000+1	K	1.664+0	2.080+0
925	DT 175	DTE-137A-SGB	-4.000+1	4.000+1	K	1.664+0	2.080+0
926	DT 176	DTE-178A-SGB	-4.000+1	4.000+1	K	1.664+0	2.080+0
927	DT 177	DTE-223A-SGB	-4.000+1	4.000+1	K	1.664+0	2.080+0
928	DT 178	DTE-IN0861-SGB	-1.000+2	1.000+2	K	1.664+0	8.320-1
929	DT 179	DTE-EX0861-SGB	-1.000+2	1.000+2	K	1.664+0	8.320-1
930	DT 180	DTE-IN0862-SGB	-1.000+2	1.000+2	K	1.664+0	8.320-1
931	DT 181	DTE-EX0862-SGB	-1.000+2	1.000+2	K	1.664+0	8.320-1
932	DT 182	DTE-IN0863-SGB	-1.000+2	1.000+2	K	1.664+0	8.320-1
933	DT 183	DTE-EX0863-SGB	-1.000+2	1.000+2	K	1.664+0	8.320-1
934	DT 184	DTE-IN0991-SGB	-1.000+2	1.000+2	K	1.664+0	8.320-1
935	DT 185	DTE-EX0991-SGB	-1.000+2	1.000+2	K	1.664+0	8.320-1
936	DT 186	DTE-IN0992-SGB	-1.000+2	1.000+2	K	1.664+0	8.320-1
937	DT 187	DTE-EX0992-SGB	-1.000+2	1.000+2	K	1.664+0	8.320-1
938	DT 188	DTE-IN0993-SGB	-1.000+2	1.000+2	K	1.664+0	8.320-1
939	DT 189	DTE-EX0993-SGB	-1.000+2	1.000+2	K	1.664+0	8.320-1
940	DT 190	DTE-IN1121-SGB	-1.000+2	1.000+2	K	1.664+0	8.320-1
941	DT 191	DTE-EX1121-SGB	-1.000+2	1.000+2	K	1.664+0	8.320-1
942	DT 192	DTE-IN1122-SGB	-1.000+2	1.000+2	K	1.664+0	8.320-1
943	DT 193	DTE-EX1122-SGB	-1.000+2	1.000+2	K	1.664+0	8.320-1
944	DT 194	DTE-IN1123-SGB	-1.000+2	1.000+2	K	1.664+0	8.320-1
945	DT 195	DTE-EX1123-SGB	-1.000+2	1.000+2	K	1.664+0	8.320-1
946	DT 196	DTE-IN1371-SGB	-1.000+2	1.000+2	K	1.664+0	8.320-1
947	DT 197	DTE-EX1371-SGB	-1.000+2	1.000+2	K	1.664+0	8.320-1
948	DT 198	DTE-IN1372-SGB	-1.000+2	1.000+2	K	1.664+0	8.320-1
949	DT 199	DTE-EX1372-SGB	-1.000+2	1.000+2	K	1.664+0	8.320-1
950	DT 200	DTE-IN1373-SGB	-1.000+2	1.000+2	K	1.664+0	8.320-1
951	DT 201	DTE-EX1373-SGB	-1.000+2	1.000+2	K	1.664+0	8.320-1
952	DT 202	DTE-IN1632-SGB	-1.000+2	1.000+2	K	1.664+0	8.320-1
953	DT 203	DTE-EX1632-SGB	-1.000+2	1.000+2	K	1.664+0	8.320-1
954	DT 204	DTE-IN1633-SGB	-1.000+2	1.000+2	K	1.664+0	8.320-1
955	DT 205	DTE-EX1633-SGB	-1.000+2	1.000+2	K	1.664+0	8.320-1
956	DT 206	DTE-IN1701-SGB	-1.000+2	1.000+2	K	1.664+0	8.320-1
957	DT 207	DTE-IN1782-SGB	-1.000+2	1.000+2	K	1.664+0	8.320-1
958	DT 208	DTE-IN1863-SGB	-1.000+2	1.000+2	K	1.664+0	8.320-1
1051	TW 1	TWE020B-HLA	2.700+2	7.200+2	K	3.307+0	7.350-1
1052	TW 2	TWE030B-HLA	2.700+2	7.200+2	K	3.307+0	7.350-1
1053	TW 3	TWE050B-LSA	2.700+2	7.200+2	K	3.307+0	7.350-1
1054	TW 4	TWE060B-PCA	2.700+2	7.200+2	K	3.307+0	7.350-1
1055	TW 5	TWE070B-CLA	2.700+2	7.200+2	K	3.307+0	7.350-1
1056	TW 6	TWE080B-CLA	2.700+2	7.200+2	K	3.307+0	7.350-1
1057	TW 7	TWE160B-HLB	2.700+2	7.200+2	K	3.307+0	7.350-1
1058	TW 8	TWE170B-HLB	2.700+2	7.200+2	K	3.307+0	7.350-1
1059	TW 9	TWE190B-LSB	2.700+2	7.200+2	K	3.307+0	7.350-1
1060	TW 10	TWE200B-PCB	2.700+2	7.200+2	K	3.307+0	7.350-1
1061	TW 11	TWE210B-CLB	2.700+2	7.200+2	K	3.307+0	7.350-1
1062	TW 12	TWE220B-CLB	2.700+2	7.200+2	K	3.307+0	7.350-1
1063	TW 13	TWE280B-PR	2.700+2	7.200+2	K	3.307+0	7.350-1
1064	TW 14	TWE431A-SGA	2.700+2	6.700+2	K	3.108+0	7.770-1
1065	TW 15	TWE432A-SGA	2.700+2	6.700+2	K	3.108+0	7.770-1

Table 2.2-2 List of available measurements for experiment SB-CL-24 (Cont'd, 9/21)

SEQ NO	FUNC ID.	TAG NAME	OUTPUT RANGE LO	HI	UNIT	UNCERTAINTY ABS.	REL.(%)
1066	TW 16	TWE433A-SGA	2.700+2	6.700+2	K	3.108+0	7.770-1
1067	TW 17	TWE434A-SGA	2.700+2	6.700+2	K	3.108+0	7.770-1
1068	TW 18	TWE471A-SGB	2.700+2	6.700+2	K	3.108+0	7.770-1
1069	TW 19	TWE472A-SGB	2.700+2	6.700+2	K	3.108+0	7.770-1
1070	TW 20	TWE473A-SGB	2.700+2	6.700+2	K	3.108+0	7.770-1
1071	TW 21	TWE474A-SGB	2.700+2	6.700+2	K	3.108+0	7.770-1
1072	TW 22	TWE-E-015B-PV	2.700+2	7.200+2	K	3.307+0	7.350-1
1073	TW 23	TWE-W-015B-PV	2.700+2	7.200+2	K	3.307+0	7.350-1
1074	TW 24	TWE-N000B-PV	2.700+2	7.200+2	K	3.307+0	7.350-1
1075	TW 25	TWE-S000B-PV	2.700+2	7.200+2	K	3.307+0	7.350-1
1076	TW 26	TWE-E000B-PV	2.700+2	7.200+2	K	3.307+0	7.350-1
1077	TW 27	TWE-W000B-PV	2.700+2	7.200+2	K	3.307+0	7.350-1
1078	TW 28	TWE-N018B-PV	2.700+2	7.200+2	K	3.307+0	7.350-1
1079	TW 29	TWE-S018B-PV	2.700+2	7.200+2	K	3.307+0	7.350-1
1080	TW 30	TWE-E018B-PV	2.700+2	7.200+2	K	3.307+0	7.350-1
1081	TW 31	TWE-W018B-PV	2.700+2	7.200+2	K	3.307+0	7.350-1
1082	TW 32	TWE-N036B-PV	2.700+2	7.200+2	K	3.307+0	7.350-1
1083	TW 33	TWE-S036B-PV	2.700+2	7.200+2	K	3.307+0	7.350-1
1084	TW 34	TWE-E036B-PV	2.700+2	7.200+2	K	3.307+0	7.350-1
1085	TW 35	TWE-W036B-PV	2.700+2	7.200+2	K	3.307+0	7.350-1
1086	TW 36	TWE-N060B-PV	2.700+2	7.200+2	K	3.307+0	7.350-1
1087	TW 37	TWE-S060B-PV	2.700+2	7.200+2	K	3.307+0	7.350-1
1088	TW 38	TWE-E060B-PV	2.700+2	7.200+2	K	3.307+0	7.350-1
1089	TW 39	TWE-W060B-PV	2.700+2	7.200+2	K	3.307+0	7.350-1
1090	TW 40	TWE-E080B-PV	2.700+2	7.200+2	K	3.307+0	7.350-1
1091	TW 41	TWE-W080B-PV	2.700+2	7.200+2	K	3.307+0	7.350-1
1092	TW 42	TWE-N000D-CB	2.700+2	9.700+2	K	4.312+0	6.160-1
1093	TW 43	TWE-S000D-CB	2.700+2	9.700+2	K	4.312+0	6.160-1
1094	TW 44	TWE-E000D-CB	2.700+2	9.700+2	K	4.312+0	6.160-1
1095	TW 45	TWE-W000D-CB	2.700+2	9.700+2	K	4.312+0	6.160-1
1096	TW 46	TWE-N010D-CB	2.700+2	9.700+2	K	4.312+0	6.160-1
1097	TW 47	TWE-S010D-CB	2.700+2	9.700+2	K	4.312+0	6.160-1
1098	TW 48	TWE-E010D-CB	2.700+2	9.700+2	K	4.312+0	6.160-1
1099	TW 49	TWE-W010D-CB	2.700+2	9.700+2	K	4.312+0	6.160-1
1100	TW 50	TWE-N018D-CB	2.700+2	9.700+2	K	4.312+0	6.160-1
1101	TW 51	TWE-S018D-CB	2.700+2	9.700+2	K	4.312+0	6.160-1
1102	TW 52	TWE-E018D-CB	2.700+2	9.700+2	K	4.312+0	6.160-1
1103	TW 53	TWE-W018D-CB	2.700+2	9.700+2	K	4.312+0	6.160-1
1104	TW 54	TWE-N026D-CB	2.700+2	9.700+2	K	4.312+0	6.160-1
1105	TW 55	TWE-S026D-CB	2.700+2	9.700+2	K	4.312+0	6.160-1
1106	TW 56	TWE-E026D-CB	2.700+2	9.700+2	K	4.312+0	6.160-1
1107	TW 57	TWE-W026D-CB	2.700+2	9.700+2	K	4.312+0	6.160-1
1108	TW 58	TWE-N036D-CB	2.700+2	9.700+2	K	4.312+0	6.160-1
1109	TW 59	TWE-S036D-CB	2.700+2	9.700+2	K	4.312+0	6.160-1
1110	TW 60	TWE-E036D-CB	2.700+2	9.700+2	K	4.312+0	6.160-1
1111	TW 61	TWE-W036D-CB	2.700+2	9.700+2	K	4.312+0	6.160-1
1112	TW 62	TWE-N049D-CB	2.700+2	9.700+2	K	4.312+0	6.160-1
1113	TW 63	TWE-S049D-CB	2.700+2	9.700+2	K	4.312+0	6.160-1
1114	TW 64	TWE-E049D-CB	2.700+2	9.700+2	K	4.312+0	6.160-1
1115	TW 65	TWE-W049D-CB	2.700+2	9.700+2	K	4.312+0	6.160-1
1116	TW 66	TWE-N060D-CB	2.700+2	9.700+2	K	4.312+0	6.160-1
1117	TW 67	TWE-S060D-CB	2.700+2	9.700+2	K	4.312+0	6.160-1
1118	TW 68	TWE-E060D-CB	2.700+2	9.700+2	K	4.312+0	6.160-1
1119	TW 69	TWE-W060D-CB	2.700+2	9.700+2	K	4.312+0	6.160-1
1120	TW 70	TWE-N000E-CB	2.700+2	9.700+2	K	4.312+0	6.160-1
1121	TW 71	TWE-S000E-CB	2.700+2	9.700+2	K	4.312+0	6.160-1
1122	TW 72	TWE-E000E-CB	2.700+2	9.700+2	K	4.312+0	6.160-1
1123	TW 73	TWE-W000E-CB	2.700+2	9.700+2	K	4.312+0	6.160-1
1124	TW 74	TWE-N010E-CB	2.700+2	9.700+2	K	4.312+0	6.160-1
1125	TW 75	TWE-S010E-CB	2.700+2	9.700+2	K	4.312+0	6.160-1
1126	TW 76	TWE-E010E-CB	2.700+2	9.700+2	K	4.312+0	6.160-1
1127	TW 77	TWE-W010E-CB	2.700+2	9.700+2	K	4.312+0	6.160-1
1128	TW 78	TWE-N018E-CB	2.700+2	9.700+2	K	4.312+0	6.160-1
1129	TW 79	TWE-S018E-CB	2.700+2	9.700+2	K	4.312+0	6.160-1
1130	TW 80	TWE-E018E-CB	2.700+2	9.700+2	K	4.312+0	6.160-1
1131	TW 81	TWE-W018E-CB	2.700+2	9.700+2	K	4.312+0	6.160-1
1132	TW 82	TWE-N026E-CB	2.700+2	9.700+2	K	4.312+0	6.160-1
1133	TW 83	TWE-S026E-CB	2.700+2	9.700+2	K	4.312+0	6.160-1
1134	TW 84	TWE-E026E-CB	2.700+2	9.700+2	K	4.312+0	6.160-1
1135	TW 85	TWE-W026E-CB	2.700+2	9.700+2	K	4.312+0	6.160-1
1136	TW 86	TWE-N036E-CB	2.700+2	9.700+2	K	4.312+0	6.160-1
1137	TW 87	TWE-S036E-CB	2.700+2	9.700+2	K	4.312+0	6.160-1
1138	TW 88	TWE-E036E-CB	2.700+2	9.700+2	K	4.312+0	6.160-1
1139	TW 89	TWE-W036E-CB	2.700+2	9.700+2	K	4.312+0	6.160-1
1140	TW 90	TWE-N049E-CB	2.700+2	9.700+2	K	4.312+0	6.160-1
1141	TW 91	TWE-S049E-CB	2.700+2	9.700+2	K	4.312+0	6.160-1
1142	TW 92	TWE-E049E-CB	2.700+2	9.700+2	K	4.312+0	6.160-1
1143	TW 93	TWE-W049E-CB	2.700+2	9.700+2	K	4.312+0	6.160-1
1144	TW 94	TWE-N060E-CB	2.700+2	9.700+2	K	4.312+0	6.160-1
1145	TW 95	TWE-S060E-CB	2.700+2	9.700+2	K	4.312+0	6.160-1
1146	TW 96	TWE-E060E-CB	2.700+2	9.700+2	K	4.312+0	6.160-1
1147	TW 97	TWE-W060E-CB	2.700+2	9.700+2	K	4.312+0	6.160-1
1148	TW 98	TWE-IN038B02-UCPP	2.700+2	9.700+2	K	4.312+0	6.160-1
1149	TW 99	TWE-IN038B04-UCPP	2.700+2	9.700+2	K	4.312+0	6.160-1
1150	TW 100	TWE-IN038B06-UCPP	2.700+2	9.700+2	K	4.312+0	6.160-1
1151	TW 101	TWE-IN038B08-UCPP	2.700+2	9.700+2	K	4.312+0	6.160-1
1152	TW 102	TWE-IN038B21-UCPP	2.700+2	9.700+2	K	4.312+0	6.160-1
1153	TW 103	TWE-EX040B02-UCPP	2.700+2	9.700+2	K	4.312+0	6.160-1
1154	TW 104	TWE-EX040B04-UCPP	2.700+2	9.700+2	K	4.312+0	6.160-1
1155	TW 105	TWE-EX040B06-UCPP	2.700+2	9.700+2	K	4.312+0	6.160-1

Table 2.2-2 List of available measurements for experiment SB-CL-24 (Cont'd, 10/21)

SEQ NO	FUNC ID.	TAG NAME	OUTPUT RANGE LO	HI	UNIT	UNCERTAINTY ABS.	REL.(%)
1156	TW 106	TWE-EX040B08-UCPP	2.700+2	9.700+2	K	4.312+0	6.160-1
1157	TW 107	TWE-EX040B21-UCPP	2.700+2	9.700+2	K	4.312+0	6.160-1
1158	TW 108	TWE-063-B09-UCSP	2.700+2	9.700+2	K	4.312+0	6.160-1
1159	TW 109	TWE-065-B09-UCSP	2.700+2	9.700+2	K	4.312+0	6.160-1
1160	TW 110	TWE-E047G-UP	2.700+2	9.700+2	K	4.312+0	6.160-1
1161	TW 111	TWE-W047G-UP	2.700+2	9.700+2	K	4.312+0	6.160-1
1162	TW 112	TWE-E056G-UP	2.700+2	9.700+2	K	4.312+0	6.160-1
1163	TW 113	TWE-W056G-UP	2.700+2	9.700+2	K	4.312+0	6.160-1
1164	TW 114	TWE-080G-UH	2.700+2	9.700+2	K	4.312+0	6.160-1
1165	TW 115	TWE-B01342	2.700+2	1.470+3	K	6.324+0	5.270-1
1166	TW 116	TWE-B01344	2.700+2	1.470+3	K	6.324+0	5.270-1
1167	TW 117	TWE-B01345	2.700+2	1.470+3	K	6.324+0	5.270-1
1168	TW 118	TWE-B01346	2.700+2	1.470+3	K	6.324+0	5.270-1
1169	TW 119	TWE-B01347	2.700+2	1.470+3	K	6.324+0	5.270-1
1170	TW 120	TWE-B01348	2.700+2	1.470+3	K	6.324+0	5.270-1
1171	TW 121	TWE-B20431	2.700+2	1.470+3	K	6.324+0	5.270-1
1172	TW 122	TWE-B20433	2.700+2	1.470+3	K	6.324+0	5.270-1
1173	TW 123	TWE-B20435	2.700+2	1.470+3	K	6.324+0	5.270-1
1174	TW 124	TWE-B20436	2.700+2	1.470+3	K	6.324+0	5.270-1
1175	TW 125	TWE-B20438	2.700+2	1.470+3	K	6.324+0	5.270-1
1176	TW 126	TWE-B20439	2.700+2	1.470+3	K	6.324+0	5.270-1
1177	TW 127	TWE-B02241	2.700+2	1.470+3	K	6.324+0	5.270-1
1178	TW 128	TWE-B02242	2.700+2	1.470+3	K	6.324+0	5.270-1
1179	TW 129	TWE-B02244	2.700+2	1.470+3	K	6.324+0	5.270-1
1180	TW 130	TWE-B02245	2.700+2	1.470+3	K	6.324+0	5.270-1
1181	TW 131	TWE-B02247	2.700+2	1.470+3	K	6.324+0	5.270-1
1182	TW 132	TWE-B02249	2.700+2	1.470+3	K	6.324+0	5.270-1
1183	TW 133	TWE-B02341	2.700+2	1.470+3	K	6.324+0	5.270-1
1184	TW 134	TWE-B02343	2.700+2	1.470+3	K	6.324+0	5.270-1
1185	TW 135	TWE-B02345	2.700+2	1.470+3	K	6.324+0	5.270-1
1186	TW 136	TWE-B02346	2.700+2	1.470+3	K	6.324+0	5.270-1
1187	TW 137	TWE-B02348	2.700+2	1.470+3	K	6.324+0	5.270-1
1188	TW 138	TWE-B02349	2.700+2	1.470+3	K	6.324+0	5.270-1
1195	TW 145	TWE-B03421	2.700+2	1.470+3	K	6.324+0	5.270-1
1196	TW 146	TWE-B03422	2.700+2	1.470+3	K	6.324+0	5.270-1
1197	TW 147	TWE-B03424	2.700+2	1.470+3	K	6.324+0	5.270-1
1198	TW 148	TWE-B03425	2.700+2	1.470+3	K	6.324+0	5.270-1
1199	TW 149	TWE-B03427	2.700+2	1.470+3	K	6.324+0	5.270-1
1200	TW 150	TWE-B03429	2.700+2	1.470+3	K	6.324+0	5.270-1
1201	TW 151	TWE-B03431	2.700+2	1.470+3	K	6.324+0	5.270-1
1202	TW 152	TWE-B03433	2.700+2	1.470+3	K	6.324+0	5.270-1
1203	TW 153	TWE-B03435	2.700+2	1.470+3	K	6.324+0	5.270-1
1204	TW 154	TWE-B03436	2.700+2	1.470+3	K	6.324+0	5.270-1
1205	TW 155	TWE-B03438	2.700+2	1.470+3	K	6.324+0	5.270-1
1206	TW 156	TWE-B03439	2.700+2	1.470+3	K	6.324+0	5.270-1
1213	TW 163	TWE-B04432	2.700+2	1.470+3	K	6.324+0	5.270-1
1214	TW 164	TWE-B04434	2.700+2	1.470+3	K	6.324+0	5.270-1
1215	TW 165	TWE-B04435	2.700+2	1.470+3	K	6.324+0	5.270-1
1216	TW 166	TWE-B04436	2.700+2	1.470+3	K	6.324+0	5.270-1
1217	TW 167	TWE-B04437	2.700+2	1.470+3	K	6.324+0	5.270-1
1218	TW 168	TWE-B04438	2.700+2	1.470+3	K	6.324+0	5.270-1
1219	TW 169	TWE-B05342	2.700+2	1.470+3	K	6.324+0	5.270-1
1220	TW 170	TWE-B05344	2.700+2	1.470+3	K	6.324+0	5.270-1
1221	TW 171	TWE-B05345	2.700+2	1.470+3	K	6.324+0	5.270-1
1222	TW 172	TWE-B05346	2.700+2	1.470+3	K	6.324+0	5.270-1
1223	TW 173	TWE-B05347	2.700+2	1.470+3	K	6.324+0	5.270-1
1224	TW 174	TWE-B05348	2.700+2	1.470+3	K	6.324+0	5.270-1
1231	TW 181	TWE-B06241	2.700+2	1.470+3	K	6.324+0	5.270-1
1232	TW 182	TWE-B06242	2.700+2	1.470+3	K	6.324+0	5.270-1
1233	TW 183	TWE-B06244	2.700+2	1.470+3	K	6.324+0	5.270-1
1234	TW 184	TWE-B06245	2.700+2	1.470+3	K	6.324+0	5.270-1
1235	TW 185	TWE-B06247	2.700+2	1.470+3	K	6.324+0	5.270-1
1236	TW 186	TWE-B06249	2.700+2	1.470+3	K	6.324+0	5.270-1
1237	TW 187	TWE-B06341	2.700+2	1.470+3	K	6.324+0	5.270-1
1238	TW 188	TWE-B06343	2.700+2	1.470+3	K	6.324+0	5.270-1
1239	TW 189	TWE-B06345	2.700+2	1.470+3	K	6.324+0	5.270-1
1240	TW 190	TWE-B06346	2.700+2	1.470+3	K	6.324+0	5.270-1
1241	TW 191	TWE-B06348	2.700+2	1.470+3	K	6.324+0	5.270-1
1242	TW 192	TWE-B06349	2.700+2	1.470+3	K	6.324+0	5.270-1
1249	TW 199	TWE-B07421	2.700+2	1.470+3	K	6.444+0	5.370-1
1250	TW 200	TWE-B07422	2.700+2	1.470+3	K	6.324+0	5.270-1
1251	TW 201	TWE-B07424	2.700+2	1.470+3	K	6.324+0	5.270-1
1252	TW 202	TWE-B07425	2.700+2	1.470+3	K	6.324+0	5.270-1
1253	TW 203	TWE-B07427	2.700+2	1.470+3	K	6.324+0	5.270-1
1254	TW 204	TWE-B07429	2.700+2	1.470+3	K	6.324+0	5.270-1
1255	TW 205	TWE-B07431	2.700+2	1.470+3	K	6.324+0	5.270-1
1256	TW 206	TWE-B07433	2.700+2	1.470+3	K	6.324+0	5.270-1
1257	TW 207	TWE-B07435	2.700+2	1.470+3	K	6.324+0	5.270-1
1258	TW 208	TWE-B07436	2.700+2	1.470+3	K	6.324+0	5.270-1
1259	TW 209	TWE-B07438	2.700+2	1.470+3	K	6.324+0	5.270-1
1260	TW 210	TWE-B07439	2.700+2	1.470+3	K	6.324+0	5.270-1
1267	TW 217	TWE-B08222	2.700+2	9.700+2	K	4.312+0	6.160-1
1268	TW 218	TWE-B08224	2.700+2	9.700+2	K	4.312+0	6.160-1
1269	TW 219	TWE-B08225	2.700+2	9.700+2	K	4.312+0	6.160-1
1270	TW 220	TWE-B08226	2.700+2	9.700+2	K	4.312+0	6.160-1
1271	TW 221	TWE-B08227	2.700+2	9.700+2	K	4.312+0	6.160-1
1272	TW 222	TWE-B08228	2.700+2	9.700+2	K	4.312+0	6.160-1
1273	TW 223	TWE-B08432	2.700+2	1.470+3	K	6.324+0	5.270-1
1274	TW 224	TWE-B08434	2.700+2	1.470+3	K	6.324+0	5.270-1
1275	TW 225	TWE-B08435	2.700+2	1.470+3	K	6.324+0	5.270-1

Table 2.2-2 List of available measurements for experiment SB-CL-24 (Cont'd, 11/21)

SEQ NO	FUNC ID.	TAG NAME	OUTPUT RANGE LO	HI	UNIT	UNCERTAINTY ABS.	REL.(%)
1276	TW 226	TWE-B08436	2.700+2	1.470+3	K	6.324+0	5.270-1
1277	TW 227	TWE-B08437	2.700+2	1.470+3	K	6.324+0	5.270-1
1278	TW 228	TWE-B08438	2.700+2	1.470+3	K	6.324+0	5.270-1
1279	TW 229	TWE-B09442	2.700+2	1.470+3	K	6.324+0	5.270-1
1280	TW 230	TWE-B09444	2.700+2	1.470+3	K	6.324+0	5.270-1
1281	TW 231	TWE-B09445	2.700+2	1.470+3	K	6.324+0	5.270-1
1282	TW 232	TWE-B09446	2.700+2	1.470+3	K	6.324+0	5.270-1
1283	TW 233	TWE-B09447	2.700+2	1.470+3	K	6.324+0	5.270-1
1284	TW 234	TWE-B09448	2.700+2	1.470+3	K	6.324+0	5.270-1
1285	TW 235	TWE-B10441	2.700+2	1.470+3	K	6.324+0	5.270-1
1286	TW 236	TWE-B10442	2.700+2	1.470+3	K	6.324+0	5.270-1
1287	TW 237	TWE-B10444	2.700+2	1.470+3	K	6.324+0	5.270-1
1288	TW 238	TWE-B10445	2.700+2	1.470+3	K	6.324+0	5.270-1
1289	TW 239	TWE-B10447	2.700+2	1.470+3	K	6.324+0	5.270-1
1290	TW 240	TWE-B10449	2.700+2	1.470+3	K	6.324+0	5.270-1
1291	TW 241	TWE-B10451	2.700+2	1.470+3	K	6.324+0	5.270-1
1292	TW 242	TWE-B10453	2.700+2	1.470+3	K	6.324+0	5.270-1
1293	TW 243	TWE-B10455	2.700+2	1.470+3	K	6.324+0	5.270-1
1294	TW 244	TWE-B10456	2.700+2	1.470+3	K	6.324+0	5.270-1
1295	TW 245	TWE-B10458	2.700+2	1.470+3	K	6.324+0	5.270-1
1296	TW 246	TWE-B10459	2.700+2	1.470+3	K	6.324+0	5.270-1
1297	TW 247	TWE-B11442	2.700+2	1.470+3	K	6.324+0	5.270-1
1298	TW 248	TWE-B11444	2.700+2	1.470+3	K	6.324+0	5.270-1
1299	TW 249	TWE-B11445	2.700+2	1.470+3	K	6.324+0	5.270-1
1300	TW 250	TWE-B11446	2.700+2	1.470+3	K	6.324+0	5.270-1
1301	TW 251	TWE-B11447	2.700+2	1.470+3	K	6.324+0	5.270-1
1302	TW 252	TWE-B11448	2.700+2	1.470+3	K	6.324+0	5.270-1
1303	TW 253	TWE-B11172	2.700+2	1.470+3	K	6.324+0	5.270-1
1304	TW 254	TWE-B11174	2.700+2	1.470+3	K	6.324+0	5.270-1
1305	TW 255	TWE-B11175	2.700+2	1.470+3	K	6.324+0	5.270-1
1306	TW 256	TWE-B11176	2.700+2	1.470+3	K	6.324+0	5.270-1
1307	TW 257	TWE-B11177	2.700+2	1.470+3	K	6.324+0	5.270-1
1308	TW 258	TWE-B11178	2.700+2	1.470+3	K	6.324+0	5.270-1
1309	TW 259	TWE-B12262	2.700+2	9.700+2	K	4.312+0	6.160-1
1310	TW 260	TWE-B12264	2.700+2	9.700+2	K	4.312+0	6.160-1
1311	TW 261	TWE-B12265	2.700+2	9.700+2	K	4.312+0	6.160-1
1312	TW 262	TWE-B12266	2.700+2	9.700+2	K	4.312+0	6.160-1
1313	TW 263	TWE-B12267	2.700+2	9.700+2	K	4.312+0	6.160-1
1314	TW 264	TWE-B12268	2.700+2	9.700+2	K	4.312+0	6.160-1
1315	TW 265	TWE-B12441	2.700+2	1.470+3	K	6.324+0	5.270-1
1316	TW 266	TWE-B12442	2.700+2	1.470+3	K	6.324+0	5.270-1
1317	TW 267	TWE-B12444	2.700+2	1.470+3	K	6.324+0	5.270-1
1318	TW 268	TWE-B12445	2.700+2	1.470+3	K	6.324+0	5.270-1
1319	TW 269	TWE-B12447	2.700+2	1.470+3	K	6.324+0	5.270-1
1320	TW 270	TWE-B12449	2.700+2	1.470+3	K	6.324+0	5.270-1
1321	TW 271	TWE-B12431	2.700+2	1.470+3	K	6.324+0	5.270-1
1322	TW 272	TWE-B12433	2.700+2	1.470+3	K	6.324+0	5.270-1
1323	TW 273	TWE-B12435	2.700+2	1.470+3	K	6.324+0	5.270-1
1324	TW 274	TWE-B12436	2.700+2	1.470+3	K	6.324+0	5.270-1
1325	TW 275	TWE-B12438	2.700+2	1.470+3	K	6.324+0	5.270-1
1326	TW 276	TWE-B12439	2.700+2	1.470+3	K	6.324+0	5.270-1
1327	TW 277	TWE-B13662	2.700+2	9.700+2	K	4.312+0	6.160-1
1328	TW 278	TWE-B13664	2.700+2	9.700+2	K	4.312+0	6.160-1
1329	TW 279	TWE-B13665	2.700+2	9.700+2	K	4.312+0	6.160-1
1330	TW 280	TWE-B13666	2.700+2	9.700+2	K	4.312+0	6.160-1
1331	TW 281	TWE-B13667	2.700+2	9.700+2	K	4.312+0	6.160-1
1332	TW 282	TWE-B13668	2.700+2	9.700+2	K	4.312+0	6.160-1
1333	TW 283	TWE-B13442	2.700+2	1.470+3	K	6.324+0	5.270-1
1334	TW 284	TWE-B13444	2.700+2	1.470+3	K	6.324+0	5.270-1
1335	TW 285	TWE-B13445	2.700+2	1.470+3	K	6.324+0	5.270-1
1336	TW 286	TWE-B13446	2.700+2	1.470+3	K	6.324+0	5.270-1
1337	TW 287	TWE-B13447	2.700+2	1.470+3	K	6.324+0	5.270-1
1338	TW 288	TWE-B13448	2.700+2	1.470+3	K	6.324+0	5.270-1
1339	TW 289	TWE-B14541	2.700+2	1.470+3	K	6.324+0	5.270-1
1340	TW 290	TWE-B14542	2.700+2	1.470+3	K	6.324+0	5.270-1
1341	TW 291	TWE-B14544	2.700+2	1.470+3	K	6.324+0	5.270-1
1342	TW 292	TWE-B14545	2.700+2	1.470+3	K	6.324+0	5.270-1
1343	TW 293	TWE-B14547	2.700+2	1.470+3	K	6.324+0	5.270-1
1344	TW 294	TWE-B14549	2.700+2	1.470+3	K	6.324+0	5.270-1
1345	TW 295	TWE-B14441	2.700+2	1.470+3	K	6.324+0	5.270-1
1346	TW 296	TWE-B14443	2.700+2	1.470+3	K	6.324+0	5.270-1
1347	TW 297	TWE-B14445	2.700+2	1.470+3	K	6.324+0	5.270-1
1348	TW 298	TWE-B14446	2.700+2	1.470+3	K	6.324+0	5.270-1
1349	TW 299	TWE-B14448	2.700+2	1.470+3	K	6.324+0	5.270-1
1350	TW 300	TWE-B14449	2.700+2	1.470+3	K	6.324+0	5.270-1
1351	TW 301	TWE-B14172	2.700+2	1.470+3	K	6.324+0	5.270-1
1352	TW 302	TWE-B14174	2.700+2	1.470+3	K	6.324+0	5.270-1
1353	TW 303	TWE-B14175	2.700+2	1.470+3	K	6.324+0	5.270-1
1354	TW 304	TWE-B14176	2.700+2	1.470+3	K	6.324+0	5.270-1
1355	TW 305	TWE-B14177	2.700+2	1.470+3	K	6.324+0	5.270-1
1356	TW 306	TWE-B14178	2.700+2	1.470+3	K	6.324+0	5.270-1
1357	TW 307	TWE-B15441	2.700+2	1.470+3	K	6.324+0	5.270-1
1358	TW 308	TWE-B15442	2.700+2	1.470+3	K	6.324+0	5.270-1
1359	TW 309	TWE-B15444	2.700+2	1.470+3	K	6.324+0	5.270-1
1360	TW 310	TWE-B15445	2.700+2	1.470+3	K	6.324+0	5.270-1
1361	TW 311	TWE-B15447	2.700+2	1.470+3	K	6.324+0	5.270-1
1362	TW 312	TWE-B15449	2.700+2	1.470+3	K	6.324+0	5.270-1
1363	TW 313	TWE-B15451	2.700+2	1.470+3	K	6.324+0	5.270-1
1364	TW 314	TWE-B15453	2.700+2	1.470+3	K	6.324+0	5.270-1
1365	TW 315	TWE-B15455	2.700+2	1.470+3	K	6.324+0	5.270-1

Table 2.2-2 List of available measurements for experiment SB-CL-24 (Cont'd, 12/21)

SEQ NO	FUNC ID.	TAG NAME	OUTPUT RANGE LO	HI	UNIT	UNCERTAINTY ABS.	REL.(%)	SEQ NO	FUNC ID.	TAG NAME	OUTPUT RANGE LO	HI	UNIT	UNCERTAINTY ABS.	REL.(%)
1366	TW 316	TWE-B15456	2.700+2	1.470+3	K	6.324+0	5.270-1	1411	TW 361	TWE-B19451	2.700+2	1.470+3	K	6.324+0	5.270-1
1367	TW 317	TWE-B15458	2.700+2	1.470+3	K	6.324+0	5.270-1	1412	TW 362	TWE-B19452	2.700+2	1.470+3	K	6.324+0	5.270-1
1368	TW 318	TWE-B15459	2.700+2	1.470+3	K	6.324+0	5.270-1	1413	TW 363	TWE-B19454	2.700+2	1.470+3	K	6.324+0	5.270-1
1369	TW 319	TWE-B15172	2.700+2	1.470+3	K	6.324+0	5.270-1	1414	TW 364	TWE-B19455	2.700+2	1.470+3	K	6.324+0	5.270-1
1370	TW 320	TWE-B15174	2.700+2	1.470+3	K	6.324+0	5.270-1	1415	TW 365	TWE-B19457	2.700+2	1.470+3	K	6.324+0	5.270-1
1371	TW 321	TWE-B15175	2.700+2	1.470+3	K	6.324+0	5.270-1	1416	TW 366	TWE-B19459	2.700+2	1.470+3	K	6.324+0	5.270-1
1372	TW 322	TWE-B15176	2.700+2	1.470+3	K	6.324+0	5.270-1	1417	TW 367	TWE-B19441	2.700+2	1.470+3	K	6.324+0	5.270-1
1373	TW 323	TWE-B15177	2.700+2	1.470+3	K	6.324+0	5.270-1	1418	TW 368	TWE-B19443	2.700+2	1.470+3	K	6.324+0	5.270-1
1374	TW 324	TWE-B15178	2.700+2	1.470+3	K	6.324+0	5.270-1	1419	TW 369	TWE-B19445	2.700+2	1.470+3	K	6.324+0	5.270-1
1375	TW 325	TWE-B16442	2.700+2	1.470+3	K	6.324+0	5.270-1	1420	TW 370	TWE-B19446	2.700+2	1.470+3	K	6.324+0	5.270-1
1376	TW 326	TWE-B16444	2.700+2	1.470+3	K	6.324+0	5.270-1	1421	TW 371	TWE-B19448	2.700+2	1.470+3	K	6.324+0	5.270-1
1377	TW 327	TWE-B16445	2.700+2	1.470+3	K	6.324+0	5.270-1	1422	TW 372	TWE-B19449	2.700+2	1.470+3	K	6.324+0	5.270-1
1378	TW 328	TWE-B16446	2.700+2	1.470+3	K	6.324+0	5.270-1	1423	TW 373	TWE-B20441	2.700+2	1.470+3	K	6.324+0	5.270-1
1379	TW 329	TWE-B16447	2.700+2	1.470+3	K	6.324+0	5.270-1	1424	TW 374	TWE-B20442	2.700+2	1.470+3	K	6.324+0	5.270-1
1380	TW 330	TWE-B16448	2.700+2	1.470+3	K	6.324+0	5.270-1	1425	TW 375	TWE-B20444	2.700+2	1.470+3	K	6.324+0	5.270-1
1381	TW 331	TWE-B16172	2.700+2	1.470+3	K	6.324+0	5.270-1	1426	TW 376	TWE-B20445	2.700+2	1.470+3	K	6.324+0	5.270-1
1382	TW 332	TWE-B16174	2.700+2	1.470+3	K	6.324+0	5.270-1	1427	TW 377	TWE-B20447	2.700+2	1.470+3	K	6.324+0	5.270-1
1383	TW 333	TWE-B16175	2.700+2	1.470+3	K	6.324+0	5.270-1	1428	TW 378	TWE-B20449	2.700+2	1.470+3	K	6.324+0	5.270-1
1384	TW 334	TWE-B16176	2.700+2	1.470+3	K	6.324+0	5.270-1	1429	TW 379	TWE-B21441	2.700+2	1.470+3	K	6.324+0	5.270-1
1385	TW 335	TWE-B16177	2.700+2	1.470+3	K	6.324+0	5.270-1	1430	TW 380	TWE-B21442	2.700+2	1.470+3	K	6.324+0	5.270-1
1386	TW 336	TWE-B16178	2.700+2	1.470+3	K	6.324+0	5.270-1	1431	TW 381	TWE-B21444	2.700+2	1.470+3	K	6.324+0	5.270-1
1387	TW 337	TWE-B17442	2.700+2	1.470+3	K	6.324+0	5.270-1	1432	TW 382	TWE-B21445	2.700+2	1.470+3	K	6.324+0	5.270-1
1388	TW 338	TWE-B17444	2.700+2	1.470+3	K	6.324+0	5.270-1	1433	TW 383	TWE-B21447	2.700+2	1.470+3	K	6.324+0	5.270-1
1389	TW 339	TWE-B17445	2.700+2	1.470+3	K	6.324+0	5.270-1	1434	TW 384	TWE-B21449	2.700+2	1.470+3	K	6.324+0	5.270-1
1390	TW 340	TWE-B17446	2.700+2	1.470+3	K	6.324+0	5.270-1	1435	TW 385	TWE-B21541	2.700+2	1.470+3	K	6.324+0	5.270-1
1391	TW 341	TWE-B17447	2.700+2	1.470+3	K	6.324+0	5.270-1	1436	TW 386	TWE-B21543	2.700+2	1.470+3	K	6.324+0	5.270-1
1392	TW 342	TWE-B17448	2.700+2	1.470+3	K	6.324+0	5.270-1	1437	TW 387	TWE-B21545	2.700+2	1.470+3	K	6.324+0	5.270-1
1393	TW 343	TWE-B17172	2.700+2	1.470+3	K	6.324+0	5.270-1	1438	TW 388	TWE-B21546	2.700+2	1.470+3	K	6.324+0	5.270-1
1394	TW 344	TWE-B17174	2.700+2	1.470+3	K	6.324+0	5.270-1	1439	TW 389	TWE-B21548	2.700+2	1.470+3	K	6.324+0	5.270-1
1395	TW 345	TWE-B17175	2.700+2	1.470+3	K	6.324+0	5.270-1	1440	TW 390	TWE-B21549	2.700+2	1.470+3	K	6.324+0	5.270-1
1396	TW 346	TWE-B17176	2.700+2	1.470+3	K	6.324+0	5.270-1	1441	TW 391	TWE-B21662	2.700+2	9.700+2	K	4.312+0	6.160-1
1397	TW 347	TWE-B17177	2.700+2	1.470+3	K	6.324+0	5.270-1	1442	TW 392	TWE-B21664	2.700+2	9.700+2	K	4.312+0	6.160-1
1398	TW 348	TWE-B17178	2.700+2	1.470+3	K	6.324+0	5.270-1	1443	TW 393	TWE-B21665	2.700+2	9.700+2	K	4.312+0	6.160-1
1399	TW 349	TWE-B18341	2.700+2	1.470+3	K	6.324+0	5.270-1	1444	TW 394	TWE-B21666	2.700+2	9.700+2	K	4.312+0	6.160-1
1400	TW 350	TWE-B18342	2.700+2	1.470+3	K	6.324+0	5.270-1	1445	TW 395	TWE-B21667	2.700+2	9.700+2	K	4.312+0	6.160-1
1401	TW 351	TWE-B18344	2.700+2	1.470+3	K	6.324+0	5.270-1	1446	TW 396	TWE-B21668	2.700+2	9.700+2	K	4.312+0	6.160-1
1402	TW 352	TWE-B18345	2.700+2	1.470+3	K	6.324+0	5.270-1	1447	TW 397	TWE-B21112	2.700+2	1.470+3	K	6.324+0	5.270-1
1403	TW 353	TWE-B18347	2.700+2	1.470+3	K	6.324+0	5.270-1	1448	TW 398	TWE-B21114	2.700+2	1.470+3	K	6.324+0	5.270-1
1404	TW 354	TWE-B18349	2.700+2	1.470+3	K	6.324+0	5.270-1	1449	TW 399	TWE-B21115	2.700+2	1.470+3	K	6.324+0	5.270-1
1405	TW 355	TWE-B18441	2.700+2	1.470+3	K	6.324+0	5.270-1	1450	TW 400	TWE-B21116	2.700+2	1.470+3	K	6.324+0	5.270-1
1406	TW 356	TWE-B18443	2.700+2	1.470+3	K	6.324+0	5.270-1	1451	TW 401	TWE-B21117	2.700+2	1.470+3	K	6.324+0	5.270-1
1407	TW 357	TWE-B18445	2.700+2	1.470+3	K	6.324+0	5.270-1	1452	TW 402	TWE-B21118	2.700+2	1.470+3	K	6.324+0	5.270-1
1408	TW 358	TWE-B18446	2.700+2	1.470+3	K	6.324+0	5.270-1	1453	TW 403	TWE-B22541	2.700+2	1.470+3	K	6.324+0	5.270-1
1409	TW 359	TWE-B18448	2.700+2	1.470+3	K	6.324+0	5.270-1	1454	TW 404	TWE-B22542	2.700+2	1.470+3	K	6.324+0	5.270-1
1410	TW 360	TWE-B18449	2.700+2	1.470+3	K	6.324+0	5.270-1	1455	TW 405	TWE-B22544	2.700+2	1.470+3	K	6.324+0	5.270-1

Table 2.2-2 List of available measurements for experiment SB-CL-24 (Cont'd, 13/21)

SEQ NO	FUNC ID.	TAG NAME	OUTPUT RANGE LO	OUTPUT RANGE HI	UNIT	UNCERTAINTY ABS.	UNCERTAINTY REL.(%)
1456	TW 406	TWE-B22545	2.700+2	1.470+3	K	6.324+0	5.270-1
1457	TW 407	TWE-B22547	2.700+2	1.470+3	K	6.324+0	5.270-1
1458	TW 408	TWE-B22549	2.700+2	1.470+3	K	6.324+0	5.270-1
1459	TW 409	TWE-B22441	2.700+2	1.470+3	K	6.324+0	5.270-1
1460	TW 410	TWE-B22443	2.700+2	1.470+3	K	6.324+0	5.270-1
1461	TW 411	TWE-B22445	2.700+2	1.470+3	K	6.324+0	5.270-1
1462	TW 412	TWE-B22446	2.700+2	1.470+3	K	6.324+0	5.270-1
1463	TW 413	TWE-B22448	2.700+2	1.470+3	K	6.324+0	5.270-1
1464	TW 414	TWE-B22449	2.700+2	1.470+3	K	6.324+0	5.270-1
1465	TW 415	TWE-B22172	2.700+2	1.470+3	K	6.324+0	5.270-1
1466	TW 416	TWE-B22174	2.700+2	1.470+3	K	6.324+0	5.270-1
1467	TW 417	TWE-B22175	2.700+2	1.470+3	K	6.324+0	5.270-1
1468	TW 418	TWE-B22176	2.700+2	1.470+3	K	6.324+0	5.270-1
1469	TW 419	TWE-B22177	2.700+2	1.470+3	K	6.324+0	5.270-1
1470	TW 420	TWE-B22178	2.700+2	1.470+3	K	6.324+0	5.270-1
1471	TW 421	TWE-B23441	2.700+2	1.470+3	K	6.324+0	5.270-1
1472	TW 422	TWE-B23442	2.700+2	1.470+3	K	6.324+0	5.270-1
1473	TW 423	TWE-B23444	2.700+2	1.470+3	K	6.324+0	5.270-1
1474	TW 424	TWE-B23445	2.700+2	1.470+3	K	6.324+0	5.270-1
1475	TW 425	TWE-B23447	2.700+2	1.470+3	K	6.324+0	5.270-1
1476	TW 426	TWE-B23449	2.700+2	1.470+3	K	6.324+0	5.270-1
1477	TW 427	TWE-B23451	2.700+2	1.470+3	K	6.324+0	5.270-1
1478	TW 428	TWE-B23453	2.700+2	1.470+3	K	6.324+0	5.270-1
1479	TW 429	TWE-B23455	2.700+2	1.470+3	K	6.324+0	5.270-1
1480	TW 430	TWE-B23456	2.700+2	1.470+3	K	6.324+0	5.270-1
1481	TW 431	TWE-B23458	2.700+2	1.470+3	K	6.324+0	5.270-1
1482	TW 432	TWE-B23459	2.700+2	1.470+3	K	6.324+0	5.270-1
1483	TW 433	TWE-B20112	2.700+2	1.470+3	K	6.324+0	5.270-1
1484	TW 434	TWE-B20114	2.700+2	1.470+3	K	6.324+0	5.270-1
1485	TW 435	TWE-B20115	2.700+2	1.470+3	K	6.324+0	5.270-1
1486	TW 436	TWE-B20116	2.700+2	1.470+3	K	6.324+0	5.270-1
1487	TW 437	TWE-B20117	2.700+2	1.470+3	K	6.324+0	5.270-1
1488	TW 438	TWE-B20118	2.700+2	1.470+3	K	6.324+0	5.270-1
1489	TW 439	TWE-B24341	2.700+2	1.470+3	K	6.324+0	5.270-1
1490	TW 440	TWE-B24342	2.700+2	1.470+3	K	6.324+0	5.270-1
1491	TW 441	TWE-B24344	2.700+2	1.470+3	K	6.324+0	5.270-1
1492	TW 442	TWE-B24345	2.700+2	1.470+3	K	6.324+0	5.270-1
1493	TW 443	TWE-B24347	2.700+2	1.470+3	K	6.324+0	5.270-1
1494	TW 444	TWE-B24349	2.700+2	1.470+3	K	6.324+0	5.270-1
1495	TW 445	TWE-B24441	2.700+2	1.470+3	K	6.324+0	5.270-1
1496	TW 446	TWE-B24443	2.700+2	1.470+3	K	6.324+0	5.270-1
1497	TW 447	TWE-B24445	2.700+2	1.470+3	K	6.324+0	5.270-1
1498	TW 448	TWE-B24446	2.700+2	1.470+3	K	6.324+0	5.270-1
1499	TW 449	TWE-B24448	2.700+2	1.470+3	K	6.324+0	5.270-1
1500	TW 450	TWE-B24449	2.700+2	1.470+3	K	6.324+0	5.270-1
1501	TW 451	TWE-B24712	2.700+2	1.470+3	K	6.324+0	5.270-1
1502	TW 452	TWE-B24714	2.700+2	1.470+3	K	6.324+0	5.270-1
1503	TW 453	TWE-B24715	2.700+2	1.470+3	K	6.324+0	5.270-1
1504	TW 454	TWE-B24716	2.700+2	1.470+3	K	6.324+0	5.270-1
1505	TW 455	TWE-B24717	2.700+2	1.470+3	K	6.324+0	5.270-1
1506	TW 456	TWE-B24718	2.700+2	1.470+3	K	6.324+0	5.270-1
1507	TW 457	TWE-IN0641-SGA	2.700+2	7.200+2	K	3.307+0	7.350-1
1508	TW 458	TWE-IN0642-SGA	2.700+2	7.200+2	K	3.307+0	7.350-1
1509	TW 459	TWE-IN0643-SGA	2.700+2	7.200+2	K	3.307+0	7.350-1
1513	TW 463	TWE-086B-SGA	2.700+2	6.700+2	K	3.108+0	7.770-1
1514	TW 464	TWE-137B-SGA	2.700+2	6.700+2	K	3.108+0	7.770-1
1515	TW 465	TWE-178B-SGA	2.700+2	6.700+2	K	3.108+0	7.770-1
1516	TW 466	TWE-223B-SGA	2.700+2	6.700+2	K	3.108+0	7.770-1
1517	TW 467	TWE-IN0861-SGA	2.700+2	7.200+2	K	3.307+0	7.350-1
1518	TW 468	TWE-EX0861-SGA	2.700+2	7.200+2	K	3.307+0	7.350-1
1519	TW 469	TWE-IN0862-SGA	2.700+2	7.200+2	K	3.307+0	7.350-1
1520	TW 470	TWE-EX0862-SGA	2.700+2	7.200+2	K	3.307+0	7.350-1
1521	TW 471	TWE-IN0863-SGA	2.700+2	7.200+2	K	3.307+0	7.350-1
1522	TW 472	TWE-EX0863-SGA	2.700+2	7.200+2	K	3.307+0	7.350-1
1523	TW 473	TWE-IN0991-SGA	2.700+2	7.200+2	K	3.307+0	7.350-1
1524	TW 474	TWE-EX0991-SGA	2.700+2	7.200+2	K	3.307+0	7.350-1
1525	TW 475	TWE-IN0992-SGA	2.700+2	7.200+2	K	3.307+0	7.350-1
1526	TW 476	TWE-EX0992-SGA	2.700+2	7.200+2	K	3.307+0	7.350-1
1527	TW 477	TWE-IN0993-SGA	2.700+2	7.200+2	K	3.307+0	7.350-1
1528	TW 478	TWE-EX0993-SGA	2.700+2	7.200+2	K	3.307+0	7.350-1
1529	TW 479	TWE-IN1121-SGA	2.700+2	7.200+2	K	3.307+0	7.350-1
1530	TW 480	TWE-EX1121-SGA	2.700+2	7.200+2	K	3.307+0	7.350-1
1531	TW 481	TWE-IN1122-SGA	2.700+2	7.200+2	K	3.307+0	7.350-1
1532	TW 482	TWE-EX1122-SGA	2.700+2	7.200+2	K	3.307+0	7.350-1
1533	TW 483	TWE-IN1123-SGA	2.700+2	7.200+2	K	3.307+0	7.350-1
1534	TW 484	TWE-EX1123-SGA	2.700+2	7.200+2	K	3.307+0	7.350-1
1535	TW 485	TWE-IN1371-SGA	2.700+2	7.200+2	K	3.307+0	7.350-1
1536	TW 486	TWE-EX1371-SGA	2.700+2	7.200+2	K	3.307+0	7.350-1
1537	TW 487	TWE-IN1372-SGA	2.700+2	7.200+2	K	3.307+0	7.350-1
1538	TW 488	TWE-EX1372-SGA	2.700+2	7.200+2	K	3.307+0	7.350-1
1539	TW 489	TWE-IN1373-SGA	2.700+2	7.200+2	K	3.307+0	7.350-1
1540	TW 490	TWE-EX1373-SGA	2.700+2	7.200+2	K	3.307+0	7.350-1
1541	TW 491	TWE-IN1632-SGA	2.700+2	7.200+2	K	3.307+0	7.350-1
1542	TW 492	TWE-EX1632-SGA	2.700+2	7.200+2	K	3.307+0	7.350-1
1543	TW 493	TWE-IN1633-SGA	2.700+2	7.200+2	K	3.307+0	7.350-1
1544	TW 494	TWE-EX1633-SGA	2.700+2	7.200+2	K	3.307+0	7.350-1
1545	TW 495	TWE-IN1701-SGA	2.700+2	7.200+2	K	3.307+0	7.350-1
1546	TW 496	TWE-IN1782-SGA	2.700+2	7.200+2	K	3.307+0	7.350-1
1547	TW 497	TWE-IN1863-SGA	2.700+2	7.200+2	K	3.307+0	7.350-1
1548	TW 498	TWE-IN0641-SGB	2.700+2	7.200+2	K	3.307+0	7.350-1

Table 2.2-2 List of available measurements for experiment SB-CL-24 (Cont'd, 14/21)

SEQ NO	FUNC ID.	TAG NAME	OUTPUT RANGE LO	HI	UNIT	UNCERTAINTY ABS.	REL.(%)	SEQ NO	FUNC ID.	TAG NAME	OUTPUT RANGE LO	HI	UNIT	UNCERTAINTY ABS.	REL.(%)
1549	TW 499	TWE-IN0642-SGB	2.700+2	7.200+2	K	3.307+0	7.350-1	1641	TW 591	TWE-112D-CDP	2.700+2	9.700+2	K	4.312+0	6.160-1
1550	TW 500	TWE-IN0643-SGB	2.700+2	7.200+2	K	3.307+0	7.350-1	1642	TW 592	TWE-113D-CDP	2.700+2	9.700+2	K	4.312+0	6.160-1
1554	TW 504	TWE-086B-SGB	2.700+2	6.700+2	K	3.108+0	7.770-1	1643	TW 593	TWE-114D-CDP	2.700+2	9.700+2	K	4.312+0	6.160-1
1555	TW 505	TWE-137B-SGB	2.700+2	6.700+2	K	3.108+0	7.770-1	1644	TW 594	TWE-115D-CDP	2.700+2	9.700+2	K	4.312+0	6.160-1
1556	TW 506	TWE-178B-SGB	2.700+2	6.700+2	K	3.108+0	7.770-1	1645	TW 595	TWE-116D-CDP	2.700+2	9.700+2	K	4.312+0	6.160-1
1557	TW 507	TWE-223B-SGB	2.700+2	6.700+2	K	3.108+0	7.770-1	1646	TW 596	TWE-117D-CDP	2.700+2	9.700+2	K	4.312+0	6.160-1
1558	TW 508	TWE-IN0861-SGB	2.700+2	7.200+2	K	3.307+0	7.350-1	1647	TW 597	TWE-118D-CDP	2.700+2	9.700+2	K	4.312+0	6.160-1
1559	TW 509	TWE-EX0861-SGB	2.700+2	7.200+2	K	3.307+0	7.350-1	1648	TW 598	TWE-121D-UHDP	2.700+2	9.700+2	K	4.312+0	6.160-1
1560	TW 510	TWE-IN0862-SGB	2.700+2	7.200+2	K	3.307+0	7.350-1	1649	TW 599	TWE-B02552	2.700+2	1.470+3	K	6.324+0	5.270-1
1561	TW 511	TWE-EX0862-SGB	2.700+2	7.200+2	K	3.307+0	7.350-1	1650	TW 600	TWE-B02554	2.700+2	1.470+3	K	6.324+0	5.270-1
1562	TW 512	TWE-IN0863-SGB	2.700+2	7.200+2	K	3.307+0	7.350-1	1651	TW 601	TWE-B02555	2.700+2	1.470+3	K	6.324+0	5.270-1
1563	TW 513	TWE-EX0863-SGB	2.700+2	7.200+2	K	3.307+0	7.350-1	1652	TW 602	TWE-B02556	2.700+2	1.470+3	K	6.324+0	5.270-1
1564	TW 514	TWE-IN0991-SGB	2.700+2	7.200+2	K	3.307+0	7.350-1	1653	TW 603	TWE-B02557	2.700+2	1.470+3	K	6.324+0	5.270-1
1565	TW 515	TWE-EX0991-SGB	2.700+2	7.200+2	K	3.307+0	7.350-1	1654	TW 604	TWE-B02558	2.700+2	1.470+3	K	6.324+0	5.270-1
1566	TW 516	TWE-IN0992-SGB	2.700+2	7.200+2	K	3.307+0	7.350-1	1655	TW 605	TWE-B03552	2.700+2	1.470+3	K	6.324+0	5.270-1
1567	TW 517	TWE-EX0992-SGB	2.700+2	7.200+2	K	3.307+0	7.350-1	1656	TW 606	TWE-B03554	2.700+2	1.470+3	K	6.324+0	5.270-1
1568	TW 518	TWE-IN0993-SGB	2.700+2	7.200+2	K	3.307+0	7.350-1	1657	TW 607	TWE-B03555	2.700+2	1.470+3	K	6.324+0	5.270-1
1569	TW 519	TWE-EX0993-SGB	2.700+2	7.200+2	K	3.307+0	7.350-1	1658	TW 608	TWE-B03556	2.700+2	1.470+3	K	6.324+0	5.270-1
1570	TW 520	TWE-IN1121-SGB	2.700+2	7.200+2	K	3.307+0	7.350-1	1659	TW 609	TWE-B03557	2.700+2	1.470+3	K	6.324+0	5.270-1
1571	TW 521	TWE-EX1121-SGB	2.700+2	7.200+2	K	3.307+0	7.350-1	1660	TW 610	TWE-B03558	2.700+2	1.470+3	K	6.324+0	5.270-1
1572	TW 522	TWE-IN1122-SGB	2.700+2	7.200+2	K	3.307+0	7.350-1	1661	TW 611	TWE-B05112	2.700+2	1.470+3	K	6.324+0	5.270-1
1573	TW 523	TWE-EX1122-SGB	2.700+2	7.200+2	K	3.307+0	7.350-1	1662	TW 612	TWE-B05114	2.700+2	1.470+3	K	6.324+0	5.270-1
1574	TW 524	TWE-IN1123-SGB	2.700+2	7.200+2	K	3.307+0	7.350-1	1663	TW 613	TWE-B05115	2.700+2	1.470+3	K	6.324+0	5.270-1
1575	TW 525	TWE-EX1123-SGB	2.700+2	7.200+2	K	3.307+0	7.350-1	1664	TW 614	TWE-B05116	2.700+2	1.470+3	K	6.324+0	5.270-1
1576	TW 526	TWE-IN1371-SGB	2.700+2	7.200+2	K	3.307+0	7.350-1	1665	TW 615	TWE-B05117	2.700+2	1.470+3	K	6.324+0	5.270-1
1577	TW 527	TWE-EX1371-SGB	2.700+2	7.200+2	K	3.307+0	7.350-1	1666	TW 616	TWE-B05118	2.700+2	1.470+3	K	6.324+0	5.270-1
1578	TW 528	TWE-IN1372-SGB	2.700+2	7.200+2	K	3.307+0	7.350-1	1667	TW 617	TWE-B06552	2.700+2	1.470+3	K	6.324+0	5.270-1
1579	TW 529	TWE-EX1372-SGB	2.700+2	7.200+2	K	3.307+0	7.350-1	1668	TW 618	TWE-B06554	2.700+2	1.470+3	K	6.324+0	5.270-1
1580	TW 530	TWE-IN1373-SGB	2.700+2	7.200+2	K	3.307+0	7.350-1	1669	TW 619	TWE-B06555	2.700+2	1.470+3	K	6.324+0	5.270-1
1581	TW 531	TWE-EX1373-SGB	2.700+2	7.200+2	K	3.307+0	7.350-1	1670	TW 620	TWE-B06556	2.700+2	1.470+3	K	6.324+0	5.270-1
1582	TW 532	TWE-IN1632-SGB	2.700+2	7.200+2	K	3.307+0	7.350-1	1671	TW 621	TWE-B06557	2.700+2	1.470+3	K	6.324+0	5.270-1
1583	TW 533	TWE-EX1632-SGB	2.700+2	7.200+2	K	3.307+0	7.350-1	1672	TW 622	TWE-B06558	2.700+2	1.470+3	K	6.324+0	5.270-1
1584	TW 534	TWE-IN1633-SGB	2.700+2	7.200+2	K	3.307+0	7.350-1	1673	TW 623	TWE-B07552	2.700+2	1.470+3	K	6.324+0	5.270-1
1585	TW 535	TWE-EX1633-SGB	2.700+2	7.200+2	K	3.307+0	7.350-1	1674	TW 624	TWE-B07554	2.700+2	1.470+3	K	6.324+0	5.270-1
1586	TW 536	TWE-IN1701-SGB	2.700+2	7.200+2	K	3.307+0	7.350-1	1675	TW 625	TWE-B07555	2.700+2	1.470+3	K	6.324+0	5.270-1
1587	TW 537	TWE-IN1782-SGB	2.700+2	7.200+2	K	3.307+0	7.350-1	1676	TW 626	TWE-B07556	2.700+2	1.470+3	K	6.324+0	5.270-1
1588	TW 538	TWE-IN1863-SGB	2.700+2	7.200+2	K	3.307+0	7.350-1	1677	TW 627	TWE-B07557	2.700+2	1.470+3	K	6.324+0	5.270-1
1589	TW 539	TWE-211A-PR	2.700+2	7.200+2	K	3.307+0	7.350-1	1678	TW 628	TWE-B07558	2.700+2	1.470+3	K	6.324+0	5.270-1
1590	TW 540	TWE-211B-PR	2.700+2	7.200+2	K	3.307+0	7.350-1	1679	TW 629	TWE-B01221	2.700+2	9.700+2	K	4.312+0	6.160-1
1591	TW 541	TWE-194A-PR	2.700+2	7.200+2	K	3.307+0	7.350-1	1680	TW 630	TWE-B01223	2.700+2	9.700+2	K	4.312+0	6.160-1
1592	TW 542	TWE-194B-PR	2.700+2	7.200+2	K	3.307+0	7.350-1	1681	TW 631	TWE-B01225	2.700+2	9.700+2	K	4.312+0	6.160-1
1593	TW 543	TWE-177A-PR	2.700+2	7.200+2	K	3.307+0	7.350-1	1682	TW 632	TWE-B01226	2.700+2	9.700+2	K	4.312+0	6.160-1
1594	TW 544	TWE-177B-PR	2.700+2	7.200+2	K	3.307+0	7.350-1	1683	TW 633	TWE-B01227	2.700+2	9.700+2	K	4.312+0	6.160-1
1595	TW 545	TWE270A-PR	2.700+2	7.200+2	K	3.307+0	7.350-1	1684	TW 634	TWE-B01229	2.700+2	9.700+2	K	4.312+0	6.160-1
1640	TW 590	TWE-111D-CDP	2.700+2	9.700+2	K	4.312+0	6.160-1	1685	TW 635	TWE-B04221	2.700+2	9.700+2	K	4.312+0	6.160-1

Table 2.2-2 List of available measurements for experiment SB-CL-24 (Cont'd, 15/21)

SEQ NO	FUNC ID.	TAG NAME	OUTPUT RANGE LO	HI	UNIT	UNCERTAINTY ABS.	REL.(%)
1686	TW 636	TWE-B04223	2.700+2	9.700+2	K	4.312+0	6.160-1
1687	TW 637	TWE-B04225	2.700+2	9.700+2	K	4.312+0	6.160-1
1688	TW 638	TWE-B04226	2.700+2	9.700+2	K	4.312+0	6.160-1
1689	TW 639	TWE-B04227	2.700+2	9.700+2	K	4.312+0	6.160-1
1690	TW 640	TWE-B04229	2.700+2	9.700+2	K	4.312+0	6.160-1
1691	TW 641	TWE-B10621	2.700+2	9.700+2	K	4.312+0	6.160-1
1692	TW 642	TWE-B10623	2.700+2	9.700+2	K	4.312+0	6.160-1
1693	TW 643	TWE-B10625	2.700+2	9.700+2	K	4.312+0	6.160-1
1694	TW 644	TWE-B10626	2.700+2	9.700+2	K	4.312+0	6.160-1
1695	TW 645	TWE-B10627	2.700+2	9.700+2	K	4.312+0	6.160-1
1696	TW 646	TWE-B10629	2.700+2	9.700+2	K	4.312+0	6.160-1
1697	TW 647	TWE-B11221	2.700+2	9.700+2	K	4.312+0	6.160-1
1698	TW 648	TWE-B11223	2.700+2	9.700+2	K	4.312+0	6.160-1
1699	TW 649	TWE-B11225	2.700+2	9.700+2	K	4.312+0	6.160-1
1700	TW 650	TWE-B11226	2.700+2	9.700+2	K	4.312+0	6.160-1
1701	TW 651	TWE-B11227	2.700+2	9.700+2	K	4.312+0	6.160-1
1702	TW 652	TWE-B11229	2.700+2	9.700+2	K	4.312+0	6.160-1
1703	TW 653	TWE-B16221	2.700+2	9.700+2	K	4.312+0	6.160-1
1704	TW 654	TWE-B16223	2.700+2	9.700+2	K	4.312+0	6.160-1
1705	TW 655	TWE-B16225	2.700+2	9.700+2	K	4.312+0	6.160-1
1706	TW 656	TWE-B16226	2.700+2	9.700+2	K	4.312+0	6.160-1
1707	TW 657	TWE-B16227	2.700+2	9.700+2	K	4.312+0	6.160-1
1708	TW 658	TWE-B16229	2.700+2	9.700+2	K	4.312+0	6.160-1
1731	FE 1	FE010-HLA	0.000+0	4.000-1	kg/s	6.680-3	1.670+0
1732	FE 2	FE020A-LSA	0.000+0	9.000+1	kg/s	1.071+0	1.190+0
1733	FE 3	FE020B-LSA	0.000+0	1.581+1	kg/s	1.736-1	1.098+0
1734	FE 4	FE150-HLB	0.000+0	4.000-1	kg/s	6.680-3	1.670+0
1735	FE 5	FE160A-LSB	0.000+0	9.000+1	kg/s	1.071+0	1.190+0
1736	FE 6	FE160B-LSB	0.000+0	1.581+1	kg/s	1.736-1	1.098+0
1737	FE 7	FE270-PR	0.000+0	1.000+0	kg/s	1.190-2	1.190+0
1740	FE 10	FE290-PR	0.000+0	3.000+0	kg/s	5.010-2	1.670+0
1741	FE 11	FE300-PR	0.000+0	6.000+0	kg/s	1.002-1	1.670+0
1743	FE 13	FE430-SGA	0.000+0	4.000+0	kg/s	6.452-2	1.613+0
1744	FE 14	FE431-SGA	0.000+0	7.000+0	kg/s	1.129-1	1.613+0
1745	FE 15	FE432-SGA	0.000+0	7.000+0	kg/s	1.129-1	1.613+0
1746	FE 16	FE433-SGA	0.000+0	7.000+0	kg/s	1.129-1	1.613+0
1747	FE 17	FE434-SGA	0.000+0	7.000+0	kg/s	1.129-1	1.613+0
1748	FE 18	FE440-SGA	0.000+0	5.000+0	kg/s	1.141-1	2.283+0
1749	FE 19	FE450-SGA	0.000+0	4.000+0	kg/s	9.132-2	2.283+0
1751	FE 21	FE470-SGB	0.000+0	4.000+0	kg/s	6.680-2	1.670+0
1752	FE 22	FE471-SGB	0.000+0	7.000+0	kg/s	1.169-1	1.670+0
1753	FE 23	FE472-SGB	0.000+0	7.000+0	kg/s	1.169-1	1.670+0
1754	FE 24	FE473-SGB	0.000+0	7.000+0	kg/s	1.169-1	1.670+0
1755	FE 25	FE474-SGB	0.000+0	7.000+0	kg/s	1.169-1	1.670+0
1756	FE 26	FE480-SGB	0.000+0	5.000+0	kg/s	1.161-1	2.323+0
1757	FE 27	FE490-SGB	0.000+0	4.000+0	kg/s	9.292-2	2.323+0
1759	FE 29	FE510-SH	0.000+0	1.000+1	kg/s	2.283-1	2.283+0
1767	FE 37	FE650-ACC	0.000+0	1.500+1	kg/s	3.485-1	2.323+0
1770	FE 40	FE680-ACH	0.000+0	1.000+1	kg/s	2.323-1	2.323+0
1778	FE 48	FE820-PL	0.000+0	1.500+1	kg/s	3.485-1	2.323+0
1779	FE 49	FE830-PL	0.000+0	1.500+1	kg/s	3.485-1	2.323+0
1780	FE 50	FE840-PL	0.000+0	1.500+1	kg/s	3.485-1	2.323+0
1792	FE 62	FE010B-HLA	0.000+0	4.000-1	kg/s	6.452-3	1.613+0
1793	FE 63	FE150B-HLB	0.000+0	4.000-1	kg/s	6.452-3	1.613+0
1795	FE 65	FE440B-SGA	0.000+0	1.000+0	kg/s	2.278-2	2.278+0
1796	FE 66	FE451-SGA	0.000+0	2.000+1	kg/s	4.566-1	2.283+0
1797	FE 67	FE480B-SGB	0.000+0	1.000+0	kg/s	2.278-2	2.278+0
1798	FE 68	FE491-SGB	0.000+0	2.000+1	kg/s	4.566-1	2.283+0
1808	FE 78	FE820B-PL	0.000+0	5.000+0	kg/s	1.139-1	2.278+0
1809	FE 79	FE830B-PL	0.000+0	5.000+0	kg/s	1.139-1	2.278+0
1810	FE 80	FE840B-PL	0.000+0	3.000+0	kg/s	6.834-2	2.278+0
1813	FE 83	FE960-CS	0.000+0	2.000+0	kg/s	3.212-2	1.606+0
1882	PE 2	PE581-BU	0.000+0	2.000+1	MPa	1.078-1	5.390-1
1883	PE 3	PE010-SGA	0.000+0	2.000+1	MPa	1.078-1	5.390-1
1884	PE 4	PE020-LSA	0.000+0	2.000+1	MPa	1.078-1	5.390-1
1885	PE 5	PE030-CLA	0.000+0	2.000+1	MPa	1.078-1	5.390-1
1886	PE 6	PE150-SGB	0.000+0	2.000+1	MPa	1.078-1	5.390-1
1887	PE 7	PE160-LSB	0.000+0	2.000+1	MPa	1.078-1	5.390-1
1888	PE 8	PE170-CLB	0.000+0	2.000+1	MPa	1.078-1	5.390-1
1889	PE 9	PE290-PV	0.000+0	2.000+1	MPa	1.078-1	5.390-1
1890	PE 10	PE280A-PV	0.000+0	2.000+1	MPa	1.078-1	5.390-1
1891	PE 11	PE280B-PV	0.000+0	5.000+0	MPa	2.695-2	5.390-1
1892	PE 12	PE270-PV	0.000+0	2.000+1	MPa	1.078-1	5.390-1
1893	PE 13	PE300A-PR	0.000+0	2.000+1	MPa	1.078-1	5.390-1
1894	PE 14	PE300B-PR	0.000+0	5.000+0	MPa	2.695-2	5.390-1
1895	PE 15	PE310-PR	0.000+0	2.000+1	MPa	1.078-1	5.390-1
1896	PE 16	PE320-PR	0.000+0	2.000+1	MPa	1.078-1	5.390-1
1897	PE 17	PE330-PR	0.000+0	2.000+1	MPa	1.078-1	5.390-1
1898	PE 18	PE340-PR	0.000+0	2.000+1	MPa	1.078-1	5.390-1
1899	PE 19	PE430-SGA	0.000+0	1.000+1	MPa	5.390-2	5.390-1
1900	PE 20	PE440-SGA	0.000+0	1.000+1	MPa	5.390-2	5.390-1
1901	PE 21	PE450-SGB	0.000+0	1.000+1	MPa	5.390-2	5.390-1
1902	PE 22	PE460-SGB	0.000+0	1.000+1	MPa	5.390-2	5.390-1
1903	PE 23	PE470-SH	0.000+0	1.000+1	MPa	5.390-2	5.390-1
1904	PE 24	PE480-JC	0.000+0	1.000+1	MPa	5.390-2	5.390-1
1905	PE 25	PE610-ST	0.000+0	1.000+0	MPa	3.200-3	3.200-1
1908	PE 28	PE580-BU	0.000+0	2.000+1	MPa	1.078-1	5.390-1
1909	PE 29	PE590-BU	0.000+0	2.000+1	MPa	1.078-1	5.390-1
1910	PE 30	PE600-ST	0.000+0	2.000+0	MPa	6.400-3	3.200-1
1911	PE 31	PE650-ACC	0.000+0	1.000+1	MPa	5.390-2	5.390-1

Table 2.2-2 List of available measurements for experiment SB-CL-24 (Cont'd, 16/21)

SEQ NO	FUNC ID.	TAG NAME	OUTPUT RANGE LO	HI	UNIT	UNCERTAINTY ABS.	REL.(%)
1912	PE 32	PE660-ACH	0.000+0	1.000+1	MPa	5.390-2	5.390-1
1915	PE 35	PE011-HLA	0.000+0	2.000+1	MPa	1.078-1	5.390-1
1916	PE 36	PE071-CLA	0.000+0	2.000+1	MPa	1.078-1	5.390-1
1917	PE 37	PE151-HLB	0.000+0	2.000+1	MPa	1.078-1	5.390-1
1918	PE 38	PE211-CLB	0.000+0	2.000+1	MPa	1.078-1	5.390-1
1919	PE 39	PE291-PR	0.000+0	2.000+1	MPa	1.118-1	5.590-1
1920	PE 40	PE301-PR	0.000+0	2.000+1	MPa	1.118-1	5.590-1
1921	PE 41	PE311-PR	0.000+0	2.000+1	MPa	1.118-1	5.590-1
1924	PE 44	PE591-BU	0.000+0	2.000+1	MPa	1.118-1	5.590-1
1981	MI 1	RE010-PCA	0.000+0	7.000+1	Hz	3.836-1	5.480-1
1982	MI 2	RE150-PCB	0.000+0	7.000+1	Hz	3.836-1	5.480-1
1983	MI 3	OPE270-PR	0.000+0	1.000+2	%	5.390-1	5.390-1
1985	MI 5	OPE430-SGA	0.000+0	1.000+2	%	5.390-1	5.390-1
1986	MI 6	OPE470-SGB	0.000+0	1.000+2	%	5.390-1	5.390-1
1988	MI 8	OPE510-SH	0.000+0	1.000+2	%	5.390-1	5.390-1
1989	MI 9	OPE820-PL	0.000+0	1.000+2	%	5.390-1	5.390-1
1991	MI 11	VBE010-PCA	0.000+0	2.000+2	um	1.001+1	5.005+0
1992	MI 12	VBE150-PCB	0.000+0	2.000+2	um	1.001+1	5.005+0
1993	MI 13	TQE010-PCA	0.000+0	1.000+2	Nm	1.601+0	1.601+0
1995	MI 15	AE010-PCA	0.000+0	1.500+2	A	1.554+0	1.036+0
1996	MI 16	AE150-PCB	0.000+0	1.500+2	A	1.554+0	1.036+0
1997	MI 17	WE270A-T	0.000+0	1.600+1	MW	7.024-2	4.390-1
1998	MI 18	WE270B-M	0.000+0	2.000+0	MW	8.780-3	4.390-1
1999	MI 19	WE270C-M1	0.000+0	4.000+0	MW	1.756-2	4.390-1
2000	MI 20	WE270D-M2	0.000+0	4.000+0	MW	1.756-2	4.390-1
2001	MI 21	WE270E-L1	0.000+0	2.000+0	MW	8.780-3	4.390-1
2002	MI 22	WE270F-L2	0.000+0	2.000+0	MW	8.780-3	4.390-1
2003	MI 23	WE270G-L3	0.000+0	2.000+0	MW	8.780-3	4.390-1
2004	MI 24	WE280A-PR	0.000+0	1.000+1	kW	1.503-1	1.503+0
2005	MI 25	WE280B-PR	0.000+0	1.500+2	kW	2.254+0	1.503+0
2006	MI 26	WE010-PCA	0.000+0	3.000+1	kW	4.509-1	1.503+0
2007	MI 27	WE150-PCB	0.000+0	3.000+1	kW	4.509-1	1.503+0
2009	MI 29	WE020-HLA	0.000+0	5.000+0	kW	7.555-2	1.511+0
2010	MI 30	WE030-LSA	0.000+0	7.500+0	kW	1.133-1	1.511+0
2011	MI 31	WE040-CLA	0.000+0	2.000+0	kW	3.022-2	1.511+0
2012	MI 32	WE160-HLB	0.000+0	5.000+0	kW	7.555-2	1.511+0
2013	MI 33	WE170-LSB	0.000+0	7.500+0	kW	1.133-1	1.511+0
2014	MI 34	WE180-CLB	0.000+0	2.000+0	kW	3.022-2	1.511+0
2015	MI 35	WE271A-PV	0.000+0	1.500+1	kW	2.266-1	1.511+0
2016	MI 36	WE271B-PV	0.000+0	1.500+1	kW	2.266-1	1.511+0
2017	MI 37	WE271C-PV	0.000+0	1.500+1	kW	2.266-1	1.511+0
2018	MI 38	WE271D-PV	0.000+0	1.500+1	kW	2.266-1	1.511+0
2019	MI 39	WE430A-SGA	0.000+0	4.000+0	kW	6.044-2	1.511+0
2020	MI 40	WE430B-SGA	0.000+0	4.000+0	kW	6.044-2	1.511+0
2021	MI 41	WE430C-SGA	0.000+0	4.000+0	kW	6.044-2	1.511+0
2022	MI 42	WE430D-SGA	0.000+0	4.000+0	kW	6.044-2	1.511+0
2023	MI 43	WE440A-SGA	0.000+0	2.000+0	kW	3.022-2	1.511+0
2024	MI 44	WE440B-SGA	0.000+0	2.000+0	kW	3.022-2	1.511+0
2025	MI 45	WE440C-SGA	0.000+0	2.000+0	kW	3.022-2	1.511+0
2026	MI 46	WE440D-SGA	0.000+0	2.000+0	kW	3.022-2	1.511+0
2027	MI 47	WE290-PR	0.000+0	4.000+0	kW	6.044-2	1.511+0
2028	MI 48	WE300-PR	0.000+0	7.500+0	kW	1.133-1	1.511+0
2029	MI 49	WE450A-SGB	0.000+0	4.000+0	kW	6.044-2	1.511+0
2030	MI 50	WE450B-SGB	0.000+0	4.000+0	kW	6.044-2	1.511+0
2031	MI 51	WE450C-SGB	0.000+0	4.000+0	kW	6.044-2	1.511+0
2032	MI 52	WE450D-SGB	0.000+0	4.000+0	kW	6.044-2	1.511+0
2033	MI 53	WE460A-SGB	0.000+0	2.000+0	kW	3.022-2	1.511+0
2034	MI 54	WE460B-SGB	0.000+0	2.000+0	kW	3.022-2	1.511+0
2035	MI 55	WE460C-SGB	0.000+0	2.000+0	kW	3.022-2	1.511+0
2036	MI 56	WE460D-SGB	0.000+0	2.000+0	kW	3.022-2	1.511+0
2037	MI 57	WE650A-ACC	0.000+0	1.000+1	kW	1.511-1	1.511+0
2040	MI 60	WE660B-ACH	0.000+0	1.500+1	kW	2.266-1	1.511+0
2181	LE 1	LE270-PV	0.000+0	1.100+1	m	3.520-2	3.200-1
2182	LE 2	LE280-PR	0.000+0	5.000+0	m	2.695-2	5.390-1
2183	LE 3	LE430-SGA	0.000+0	1.700+1	m	5.440-2	3.200-1
2184	LE 4	LE440-SGA	0.000+0	6.000+0	m	1.920-2	3.200-1
2185	LE 5	LE441-SGA	0.000+0	1.100+1	m	3.520-2	3.200-1
2186	LE 6	LE450-SGB	0.000+0	1.700+1	m	5.440-2	3.200-1
2187	LE 7	LE460-SGB	0.000+0	6.000+0	m	1.920-2	3.200-1
2188	LE 8	LE461-SGB	0.000+0	1.100+1	m	3.520-2	3.200-1
2189	LE 9	LE470-JC	0.000+0	5.500+0	m	1.760-2	3.200-1
2190	LE 10	LE560-ST	0.000+0	1.200+1	m	3.840-2	3.200-1
2191	LE 11	LE570-ST	0.000+0	4.000+0	m	1.280-2	3.200-1
2192	LE 12	LE580-ST	0.000+0	4.000+0	m	1.280-2	3.200-1
2193	LE 13	LE590-ST	0.000+0	4.000+0	m	1.280-2	3.200-1
2194	LE 14	LE650-ACC	0.000+0	5.000+0	m	2.695-2	5.390-1
2195	LE 15	LE660-ACH	0.000+0	5.000+0	m	2.695-2	5.390-1
2197	LE 17	LE830-RWST	0.000+0	1.000+1	m	3.200-2	3.200-1
2198	LE 18	LE442-SGA	0.000+0	1.200+1	m	3.840-2	3.200-1
2199	LE 19	LE462-SGB	0.000+0	1.200+1	m	3.840-2	3.200-1
2200	LE 20	DLE270-PV	0.000+0	1.075+2	kPa	3.806-1	3.540-1
2201	LE 21	DLE280-PR	0.000+0	3.909+1	kPa	2.185-1	5.590-1
2202	LE 22	DLE430-SGA	0.000+0	1.662+2	kPa	5.882-1	3.540-1
2203	LE 23	DLE440-SGA	0.000+0	5.864+1	kPa	2.076-1	3.540-1
2204	LE 24	DLE441-SGA	0.000+0	1.075+2	kPa	3.806-1	3.540-1
2205	LE 25	DLE442-SGA	0.000+0	1.106+2	kPa	3.916-1	3.540-1
2206	LE 26	DLE450-SGB	0.000+0	1.662+2	kPa	5.882-1	3.540-1
2207	LE 27	DLE460-SGB	0.000+0	5.864+1	kPa	2.076-1	3.540-1
2208	LE 28	DLE461-SGB	0.000+0	1.075+2	kPa	3.806-1	3.540-1
2209	LE 29	DLE462-SGB	0.000+0	1.106+2	kPa	3.916-1	3.540-1

Table 2.2-2 List of available measurements for experiment SB-CL-24 (Cont'd, 17/21)

SEQ NO	FUNC ID.	TAG NAME	OUTPUT RANGE LO	OUTPUT RANGE HI	UNIT	UNCERTAINTY ABS.	UNCERTAINTY REL.(%)
2210	LE 30	DLE470-JC	0.000+0	5.375+1	kPa	1.903-1	3.540-1
2211	LE 31	DLE560-ST	0.000+0	1.173+2	kPa	4.152-1	3.540-1
2212	LE 32	DLE570-ST	0.000+0	3.909+1	kPa	1.384-1	3.540-1
2213	LE 33	DLE580-ST	0.000+0	3.909+1	kPa	1.384-1	3.540-1
2214	LE 34	DLE590-ST	0.000+0	3.909+1	kPa	1.384-1	3.540-1
2215	LE 35	DLE650-ACC	0.000+0	4.887+1	kPa	2.732-1	5.590-1
2216	LE 36	DLE660-ACH	0.000+0	4.887+1	kPa	2.732-1	5.590-1
2218	LE 38	DLE830-RWST	0.000+0	9.807+1	kPa	3.472-1	3.540-1
2251	DP 1	DPE010-HLA	-4.000+1	4.000+1	kPa	4.472-1	5.590-1
2252	DP 2	DPE020-HLA	-4.000+1	4.000+1	kPa	4.472-1	5.590-1
2254	DP 4	DPE040-HLA	-4.000+1	4.000+1	kPa	4.472-1	5.590-1
2255	DP 5	DPE050A-SGA	-1.500+2	5.000+1	kPa	1.118+0	5.590-1
2256	DP 6	DPE050B-SGA	-1.500+2	5.000+1	kPa	1.118+0	5.590-1
2257	DP 7	DPE050C-SGA	-1.500+2	5.000+1	kPa	1.118+0	5.590-1
2258	DP 8	DPE050D-SGA	-1.500+2	5.000+1	kPa	1.118+0	5.590-1
2259	DP 9	DPE050E-SGA	-1.500+2	5.000+1	kPa	1.118+0	5.590-1
2260	DP 10	DPE050F-SGA	-1.500+2	5.000+1	kPa	1.118+0	5.590-1
2261	DP 11	DPE060A-SGA	-1.500+2	5.000+1	kPa	1.118+0	5.590-1
2262	DP 12	DPE060B-SGA	-1.500+2	5.000+1	kPa	1.118+0	5.590-1
2263	DP 13	DPE060C-SGA	-1.500+2	5.000+1	kPa	7.080-1	3.540-1
2264	DP 14	DPE060D-SGA	-1.500+2	5.000+1	kPa	1.118+0	5.590-1
2265	DP 15	DPE060E-SGA	-1.500+2	5.000+1	kPa	1.118+0	5.590-1
2266	DP 16	DPE060F-SGA	-1.500+2	5.000+1	kPa	1.118+0	5.590-1
2267	DP 17	DPE070-LSA	-8.000+1	8.000+1	kPa	8.944-1	5.590-1
2268	DP 18	DPE080-LSA	-5.000+1	5.000+1	kPa	5.590-1	5.590-1
2269	DP 19	DPE090-PCA	-5.000+1	5.000+1	kPa	5.590-1	5.590-1
2270	DP 20	DPE100-CLA	-2.000+2	2.000+2	kPa	2.236+0	5.590-1
2271	DP 21	DPE110-CLA	-5.000+1	5.000+1	kPa	5.590-1	5.590-1
2272	DP 22	DPE120-CLA	-5.000+1	5.000+1	kPa	5.590-1	5.590-1
2273	DP 23	DPE130-CLA	-5.000+1	5.000+1	kPa	5.590-1	5.590-1
2274	DP 24	DPE140-HLA	-3.000+1	3.000+1	kPa	3.354-1	5.590-1
2275	DP 25	DPE150-HLB	-3.000+1	3.000+1	kPa	3.354-1	5.590-1
2276	DP 26	DPE160-HLB	-3.000+1	3.000+1	kPa	3.354-1	5.590-1
2277	DP 27	DPE170-HLB	-3.000+1	3.000+1	kPa	3.354-1	5.590-1
2278	DP 28	DPE180-HLB	-3.000+1	3.000+1	kPa	3.354-1	5.590-1
2279	DP 29	DPE190A-SGB	-1.500+2	5.000+1	kPa	1.118+0	5.590-1
2280	DP 30	DPE190B-SGB	-1.500+2	5.000+1	kPa	1.118+0	5.590-1
2281	DP 31	DPE190C-SGB	-1.500+2	5.000+1	kPa	1.118+0	5.590-1
2282	DP 32	DPE190D-SGB	-1.500+2	5.000+1	kPa	1.118+0	5.590-1
2283	DP 33	DPE190E-SGB	-1.500+2	5.000+1	kPa	1.118+0	5.590-1
2284	DP 34	DPE190F-SGB	-1.500+2	5.000+1	kPa	1.118+0	5.590-1
2285	DP 35	DPE200A-SGB	-1.500+2	5.000+1	kPa	1.118+0	5.590-1
2286	DP 36	DPE200B-SGB	-1.500+2	5.000+1	kPa	1.118+0	5.590-1
2287	DP 37	DPE200C-SGB	-1.500+2	5.000+1	kPa	1.118+0	5.590-1
2288	DP 38	DPE200D-SGB	-1.500+2	5.000+1	kPa	1.118+0	5.590-1
2289	DP 39	DPE200E-SGB	-1.500+2	5.000+1	kPa	1.118+0	5.590-1
2290	DP 40	DPE200F-SGB	-1.500+2	5.000+1	kPa	1.118+0	5.590-1
2291	DP 41	DPE210-LSB	-8.000+1	8.000+1	kPa	8.944-1	5.590-1
2292	DP 42	DPE220-LSB	-5.000+1	5.000+1	kPa	5.590-1	5.590-1
2293	DP 43	DPE230-PCB	-5.000+1	5.000+1	kPa	5.590-1	5.590-1
2294	DP 44	DPE240-CLB	-2.000+1	2.000+1	kPa	2.236-1	5.590-1
2295	DP 45	DPE250-CLB	-2.000+1	2.000+1	kPa	2.236-1	5.590-1
2296	DP 46	DPE260-CLB	-2.000+1	2.000+1	kPa	2.236-1	5.590-1
2297	DP 47	DPE270-PV	-1.000+2	4.000+2	kPa	2.795+0	5.590-1
2298	DP 48	DPE280-PV	-5.000+1	1.000+2	kPa	8.385-1	5.590-1
2299	DP 49	DPE290-PV	-5.000+1	1.000+2	kPa	8.385-1	5.590-1
2300	DP 50	DPE300-PV	-5.000+1	1.000+2	kPa	8.385-1	5.590-1
2301	DP 51	DPE320-PV	-5.000+1	1.000+2	kPa	8.385-1	5.590-1
2302	DP 52	DPE330-PV	-5.000+1	1.000+2	kPa	8.385-1	5.590-1
2303	DP 53	DPE310-PV	-1.000+2	1.000+2	kPa	1.118+0	5.590-1
2304	DP 54	DPE350A-PV	-1.000+2	1.000+2	kPa	1.118+0	5.590-1
2305	DP 55	DPE350B-PV	-1.000+2	1.000+2	kPa	1.118+0	5.590-1
2306	DP 56	DPE360-PV	-1.000+2	3.000+2	kPa	2.236+0	5.590-1
2307	DP 57	DPE370-PV	-5.000+1	1.500+2	kPa	1.118+0	5.590-1
2308	DP 58	DPE380-PV	-5.000+1	1.500+2	kPa	1.118+0	5.590-1
2312	DP 62	DPE332-PV	-1.000+2	1.000+2	kPa	1.118+0	5.590-1
2313	DP 63	DPE331-PV	-1.000+2	1.000+2	kPa	1.118+0	5.590-1
2317	DP 67	DPE580A-BU	0.000+0	1.000+2	kPa	5.590-1	5.590-1
2318	DP 68	DPE580B-BU	0.000+0	5.000+0	kPa	1.600-2	3.200-1
2319	DP 69	DPE590-BU	0.000+0	5.000+2	kPa	2.795+0	5.590-1
2320	DP 70	DPE030B-HLA	-3.000+2	3.000+2	kPa	3.354+0	5.590-1
2321	DP 71	DPE072-LSA	0.000+0	4.500+1	kPa	2.515-1	5.590-1
2322	DP 72	DPE073-LSA	-1.000+1	1.000+1	kPa	1.118-1	5.590-1
2323	DP 73	DPE074-LSA	-1.000+1	1.000+1	kPa	1.118-1	5.590-1
2324	DP 74	DPE075-LSA	-1.000+1	1.000+1	kPa	1.118-1	5.590-1
2325	DP 75	DPE076-LSA	0.000+0	3.000+1	kPa	1.677-1	5.590-1
2326	DP 76	DPE212-LSB	0.000+0	4.500+1	kPa	2.515-1	5.590-1
2327	DP 77	DPE213-LSB	-1.000+1	1.000+1	kPa	1.118-1	5.590-1
2328	DP 78	DPE214-LSB	-1.000+1	1.000+1	kPa	1.118-1	5.590-1
2329	DP 79	DPE215-LSB	-1.000+1	1.000+1	kPa	1.118-1	5.590-1
2330	DP 80	DPE216-LSB	0.000+0	3.000+1	kPa	1.677-1	5.590-1
2331	DP 81	DPE430-SGA	-3.000+1	0.000+0	kPa	1.677-1	5.590-1
2332	DP 82	DPE431-SGA	-3.000+1	0.000+0	kPa	1.677-1	5.590-1
2333	DP 83	DPE432-SGA	-3.000+1	0.000+0	kPa	1.677-1	5.590-1
2334	DP 84	DPE433-SGA	-3.000+1	0.000+0	kPa	1.677-1	5.590-1
2335	DP 85	DPE434-SGA	-3.000+1	0.000+0	kPa	1.677-1	5.590-1
2336	DP 86	DPE435-SGA	-3.000+1	0.000+0	kPa	1.677-1	5.590-1
2337	DP 87	DPE436-SGA	-3.000+1	0.000+0	kPa	1.677-1	5.590-1
2338	DP 88	DPE437-SGA	-3.000+1	0.000+0	kPa	1.677-1	5.590-1
2339	DP 89	DPE438-SGA	-3.000+1	0.000+0	kPa	1.677-1	5.590-1

Table 2.2-2 List of available measurements for experiment SB-CL-24 (Cont'd, 18/21)

SEQ NO	FUNC ID.	TAG NAME	OUTPUT RANGE LO	HI	UNIT	UNCERTAINTY ABS.	REL.(%)
2340	DP 90	DPE439-SGA	-3.000+1	0.000+0	kPa	1.677-1	5.590-1
2341	DP 91	DPE440-SGA	-4.000+1	0.000+0	kPa	2.236-1	5.590-1
2342	DP 92	DPE450-SGB	-3.000+1	0.000+0	kPa	1.677-1	5.590-1
2343	DP 93	DPE451-SGB	-3.000+1	0.000+0	kPa	1.677-1	5.590-1
2344	DP 94	DPE452-SGB	-3.000+1	0.000+0	kPa	1.677-1	5.590-1
2345	DP 95	DPE453-SGB	-3.000+1	0.000+0	kPa	1.677-1	5.590-1
2346	DP 96	DPE454-SGB	-3.000+1	0.000+0	kPa	1.677-1	5.590-1
2347	DP 97	DPE455-SGB	-3.000+1	0.000+0	kPa	1.677-1	5.590-1
2348	DP 98	DPE456-SGB	-3.000+1	0.000+0	kPa	1.677-1	5.590-1
2349	DP 99	DPE457-SGB	-3.000+1	0.000+0	kPa	1.677-1	5.590-1
2350	DP 100	DPE458-SGB	-3.000+1	0.000+0	kPa	1.677-1	5.590-1
2351	DP 101	DPE459-SGB	-3.000+1	0.000+0	kPa	1.677-1	5.590-1
2352	DP 102	DPE460-SGB	-4.000+1	0.000+0	kPa	2.236-1	5.590-1
2353	DP 103	DPE011-HLA	-1.000+1	1.000+1	kPa	6.410-2	3.205-1
2354	DP 104	DPE071-CLA	-1.000+1	1.000+1	kPa	6.410-2	3.205-1
2355	DP 105	DPE151-HLB	-1.000+1	1.000+1	kPa	6.410-2	3.205-1
2356	DP 106	DPE211-CLB	-1.000+1	1.000+1	kPa	6.410-2	3.205-1
2358	DP 108	DPE591-BU	-1.000+2	1.000+2	kPa	1.118+0	5.590-1
2359	DP 109	DPE041-PR	0.000+0	6.118+0	kPa	1.958-2	3.200-1
2360	DP 110	DPE042-PR	0.000+0	7.340+0	kPa	2.349-2	3.200-1
2361	DP 111	DPE043-PR	0.000+0	3.670+0	kPa	1.174-2	3.200-1
2362	DP 112	DPE044-PR	0.000+0	3.670+0	kPa	1.174-2	3.200-1
2363	DP 113	DPE045-PR	0.000+0	1.101+1	kPa	3.524-2	3.200-1
2364	DP 114	DPE046-PR	0.000+0	7.342+0	kPa	2.349-2	3.200-1
2365	DP 115	DPE101-PR	-2.000+2	2.000+2	kPa	1.280+0	3.200-1
2366	DP 116	DPE055A-SGA	-3.000+1	3.000+1	kPa	1.920-1	3.200-1
2367	DP 117	DPE055B-SGA	-3.000+0	3.000+0	kPa	1.920-2	3.200-1
2368	DP 118	DPE195A-SGB	-3.000+1	3.000+1	kPa	1.920-1	3.200-1
2369	DP 119	DPE195B-SGB	-3.000+0	3.000+0	kPa	1.920-2	3.200-1
2370	DP 120	DPE056-SGA	-4.000+1	4.000+1	kPa	2.560-1	3.200-1
2371	DP 121	DPE057-SGA	-1.000+0	1.000+0	MPa	6.400-3	3.200-1
2372	DP 122	DPE196-SGB	-4.000+1	4.000+1	kPa	2.560-1	3.200-1
2373	DP 123	DPE197-SGB	-1.000+0	1.000+0	MPa	6.400-3	3.200-1
2374	DP 124	DPE301-PV	-5.000+0	1.000+1	kPa	4.245-2	2.830-1
2375	DP 125	DPE302-PV	-5.000+0	5.000+0	kPa	2.830-2	2.830-1
2376	DP 126	DPE303-PV	-5.000+0	5.000+0	kPa	2.830-2	2.830-1
2377	DP 127	DPE304-PV	-5.000+0	5.000+0	kPa	2.830-2	2.830-1
2378	DP 128	DPE305-PV	-5.000+0	5.000+0	kPa	2.830-2	2.830-1
2379	DP 129	DPE306-PV	-5.000+0	5.000+0	kPa	2.830-2	2.830-1
2380	DP 130	DPE307-PV	-5.000+0	5.000+0	kPa	2.830-2	2.830-1
2381	DP 131	DPE308-PV	-5.000+0	5.000+0	kPa	2.830-2	2.830-1
2382	DP 132	DPE309-PV	-3.000+1	0.000+0	kPa	8.490-2	2.830-1
2383	DP 133	DPE333-PV	-3.500+1	0.000+0	kPa	9.905-2	2.830-1
2613	CP 3	CPE-E000C-DC	0.000+0	1.000+2	%	3.000-1	3.000-1
2617	CP 7	CPE-E024C-DC	0.000+0	1.000+2	%	3.000-1	3.000-1
2618	CP 8	CPE-E031C-DC	0.000+0	1.000+2	%	3.000-1	3.000-1
2620	CP 10	CPE-E043C-DC	0.000+0	1.000+2	%	3.000-1	3.000-1
2621	CP 11	CPE-E049C-DC	0.000+0	1.000+2	%	3.000-1	3.000-1
2622	CP 12	CPE-E055C-DC	0.000+0	1.000+2	%	3.000-1	3.000-1
2623	CP 13	CPE-E061C-DC	0.000+0	1.000+2	%	3.000-1	3.000-1
2626	CP 16	CPE-W066F-UH	0.000+0	1.000+2	%	3.000-1	3.000-1
2627	CP 17	CPE-E069F-UH	0.000+0	1.000+2	%	3.000-1	3.000-1
2628	CP 18	CPE-W069F-UH	0.000+0	1.000+2	%	3.000-1	3.000-1
2629	CP 19	CPE-E072F-UH	0.000+0	1.000+2	%	3.000-1	3.000-1
2632	CP 22	CPE-W075F-UH	0.000+0	1.000+2	%	3.000-1	3.000-1
2633	CP 23	CPE-E078F-UH	0.000+0	1.000+2	%	3.000-1	3.000-1
2634	CP 24	CPE-W078F-UH	0.000+0	1.000+2	%	3.000-1	3.000-1
2636	CP 26	CPE-W081F-UH	0.000+0	1.000+2	%	3.000-1	3.000-1
2637	CP 27	CPE-E066H-GT	0.000+0	1.000+2	%	3.000-1	3.000-1
2638	CP 28	CPE-W066H-GT	0.000+0	1.000+2	%	3.000-1	3.000-1
2639	CP 29	CPE-E072H-GT	0.000+0	1.000+2	%	3.000-1	3.000-1
2640	CP 30	CPE-W072H-GT	0.000+0	1.000+2	%	3.000-1	3.000-1
2641	CP 31	CPE-E078H-GT	0.000+0	1.000+2	%	3.000-1	3.000-1
2642	CP 32	CPE-W078H-GT	0.000+0	1.000+2	%	3.000-1	3.000-1
2643	CP 33	CPE-E043H-GT	0.000+0	1.000+2	%	3.000-1	3.000-1
2644	CP 34	CPE-W043H-GT	0.000+0	1.000+2	%	3.000-1	3.000-1
2645	CP 35	CPE-E044H-GT	0.000+0	1.000+2	%	3.000-1	3.000-1
2646	CP 36	CPE-W044H-GT	0.000+0	1.000+2	%	3.000-1	3.000-1
2647	CP 37	CPE-E048H-GT	0.000+0	1.000+2	%	3.000-1	3.000-1
2648	CP 38	CPE-W048H-GT	0.000+0	1.000+2	%	3.000-1	3.000-1
2649	CP 39	CPE-E054H-GT	0.000+0	1.000+2	%	3.000-1	3.000-1
2650	CP 40	CPE-W054H-GT	0.000+0	1.000+2	%	3.000-1	3.000-1
2651	CP 41	CPE-E060H-GT	0.000+0	1.000+2	%	3.000-1	3.000-1
2652	CP 42	CPE-W060H-GT	0.000+0	1.000+2	%	3.000-1	3.000-1
2653	CP 43	CPE-E042-UP	0.000+0	1.000+2	%	3.000-1	3.000-1
2654	CP 44	CPE-W042-UP	0.000+0	1.000+2	%	3.000-1	3.000-1
2655	CP 45	CPE-E043-UP	0.000+0	1.000+2	%	3.000-1	3.000-1
2656	CP 46	CPE-W043-UP	0.000+0	1.000+2	%	3.000-1	3.000-1
2657	CP 47	CPE-E044-UP	0.000+0	1.000+2	%	3.000-1	3.000-1
2658	CP 48	CPE-W044-UP	0.000+0	1.000+2	%	3.000-1	3.000-1
2659	CP 49	CPE-E048-UP	0.000+0	1.000+2	%	3.000-1	3.000-1
2660	CP 50	CPE-W048-UP	0.000+0	1.000+2	%	3.000-1	3.000-1
2661	CP 51	CPE-E051-UP	0.000+0	1.000+2	%	3.000-1	3.000-1
2662	CP 52	CPE-W051-UP	0.000+0	1.000+2	%	3.000-1	3.000-1
2663	CP 53	CPE-E054-UP	0.000+0	1.000+2	%	3.000-1	3.000-1
2664	CP 54	CPE-W054-UP	0.000+0	1.000+2	%	3.000-1	3.000-1
2665	CP 55	CPE-E057-UP	0.000+0	1.000+2	%	3.000-1	3.000-1
2666	CP 56	CPE-W057-UP	0.000+0	1.000+2	%	3.000-1	3.000-1
2667	CP 57	CPE-E060-UP	0.000+0	1.000+2	%	3.000-1	3.000-1
2668	CP 58	CPE-W060-UP	0.000+0	1.000+2	%	3.000-1	3.000-1

Table 2.2-2 List of available measurements for experiment SB-CL-24 (Cont'd, 19/21)

SEQ NO	FUNC ID.	TAG NAME	OUTPUT RANGE LO	HI	UNIT	UNCERTAINTY ABS.	REL.(%)
2669	CP 59	CPE-C-021-LP	0.000+0	1.000+2	%	3.000-1	3.000-1
2670	CP 60	CPE-C-018-LP	0.000+0	1.000+2	%	3.000-1	3.000-1
2671	CP 61	CPE-C-015-LP	0.000+0	1.000+2	%	3.000-1	3.000-1
2672	CP 62	CPE-C-012-LP	0.000+0	1.000+2	%	3.000-1	3.000-1
2673	CP 63	CPE-C-009-LP	0.000+0	1.000+2	%	3.000-1	3.000-1
2674	CP 64	CPE-C-006-LP	0.000+0	1.000+2	%	3.000-1	3.000-1
2675	CP 65	CPE-C-005-LP	0.000+0	1.000+2	%	3.000-1	3.000-1
2676	CP 66	CPE-C-003-LP	0.000+0	1.000+2	%	3.000-1	3.000-1
2677	CP 67	CPE-C-002-LP	0.000+0	1.000+2	%	3.000-1	3.000-1
2687	CP 77	CPE-B15661	0.000+0	1.000+2	%	3.000-1	3.000-1
2691	CP 81	CPE-B15665	0.000+0	1.000+2	%	3.000-1	3.000-1
2692	CP 82	CPE-B15666	0.000+0	1.000+2	%	3.000-1	3.000-1
2693	CP 83	CPE-B15667	0.000+0	1.000+2	%	3.000-1	3.000-1
2705	CP 95	CPE-B20621	0.000+0	1.000+2	%	3.000-1	3.000-1
2708	CP 98	CPE-B20624	0.000+0	1.000+2	%	3.000-1	3.000-1
2709	CP 99	CPE-B20625	0.000+0	1.000+2	%	3.000-1	3.000-1
2710	CP 100	CPE-B20626	0.000+0	1.000+2	%	3.000-1	3.000-1
2711	CP 101	CPE-B20627	0.000+0	1.000+2	%	3.000-1	3.000-1
2712	CP 102	CPE-B20628	0.000+0	1.000+2	%	3.000-1	3.000-1
2713	CP 103	CPE-B20629	0.000+0	1.000+2	%	3.000-1	3.000-1
2714	CP 104	CPE-B22621	0.000+0	1.000+2	%	3.000-1	3.000-1
2715	CP 105	CPE-B22622	0.000+0	1.000+2	%	3.000-1	3.000-1
2717	CP 107	CPE-B22624	0.000+0	1.000+2	%	3.000-1	3.000-1
2718	CP 108	CPE-B22625	0.000+0	1.000+2	%	3.000-1	3.000-1
2719	CP 109	CPE-B22626	0.000+0	1.000+2	%	3.000-1	3.000-1
2720	CP 110	CPE-B22627	0.000+0	1.000+2	%	3.000-1	3.000-1
2721	CP 111	CPE-B22628	0.000+0	1.000+2	%	3.000-1	3.000-1
2722	CP 112	CPE-B22629	0.000+0	1.000+2	%	3.000-1	3.000-1
2724	CP 114	CPE-207-PR	0.000+0	1.000+2	%	3.000-1	3.000-1
2725	CP 115	CPE-204-PR	0.000+0	1.000+2	%	3.000-1	3.000-1
2726	CP 116	CPE-200-PR	0.000+0	1.000+2	%	3.000-1	3.000-1
2727	CP 117	CPE-196-PR	0.000+0	1.000+2	%	3.000-1	3.000-1
2729	CP 119	CPE-189-PR	0.000+0	1.000+2	%	3.000-1	3.000-1
2731	CP 121	CPE-181-PR	0.000+0	1.000+2	%	3.000-1	3.000-1
2733	CP 123	CPE-086C-SGA	0.000+0	1.000+2	%	3.000-1	3.000-1
2735	CP 125	CPE-112C-SGA	0.000+0	1.000+2	%	3.000-1	3.000-1
2736	CP 126	CPE-125C-SGA	0.000+0	1.000+2	%	3.000-1	3.000-1
2737	CP 127	CPE-137C-SGA	0.000+0	1.000+2	%	3.000-1	3.000-1
2738	CP 128	CPE-150C-SGA	0.000+0	1.000+2	%	3.000-1	3.000-1
2739	CP 129	CPE-163C-SGA	0.000+0	1.000+2	%	3.000-1	3.000-1
2740	CP 130	CPE-178C-SGA	0.000+0	1.000+2	%	3.000-1	3.000-1
2743	CP 133	CPE-192C-SGA	0.000+0	1.000+2	%	3.000-1	3.000-1
2744	CP 134	CPE-208C-SGA	0.000+0	1.000+2	%	3.000-1	3.000-1
2745	CP 135	CPE-223C-SGA	0.000+0	1.000+2	%	3.000-1	3.000-1
2746	CP 136	CPE-245C-SGA	0.000+0	1.000+2	%	3.000-1	3.000-1
2770	CP 160	CPE-EX0993-SGA	0.000+0	1.000+2	%	3.000-1	3.000-1
2797	CP 187	CPE-IN1252-SGA	0.000+0	1.000+2	%	3.000-1	3.000-1
2800	CP 190	CPE-EX1253-SGA	0.000+0	1.000+2	%	3.000-1	3.000-1
2803	CP 193	CPE-IN1255-SGA	0.000+0	1.000+2	%	3.000-1	3.000-1
2836	CP 226	CPE-EX1634-SGA	0.000+0	1.000+2	%	3.000-1	3.000-1
2845	CP 235	CPE-086C-SGB	0.000+0	1.000+2	%	3.000-1	3.000-1
2849	CP 239	CPE-137C-SGB	0.000+0	1.000+2	%	3.000-1	3.000-1
2850	CP 240	CPE-150C-SGB	0.000+0	1.000+2	%	3.000-1	3.000-1
2851	CP 241	CPE-163C-SGB	0.000+0	1.000+2	%	3.000-1	3.000-1
2852	CP 242	CPE-178C-SGB	0.000+0	1.000+2	%	3.000-1	3.000-1
2854	CP 244	CPE-208F-SGB	0.000+0	1.000+2	%	3.000-1	3.000-1
2855	CP 245	CPE-192C-SGB	0.000+0	1.000+2	%	3.000-1	3.000-1
2856	CP 246	CPE-208C-SGB	0.000+0	1.000+2	%	3.000-1	3.000-1
2859	CP 249	CPE-IN0861-SGB	0.000+0	1.000+2	%	3.000-1	3.000-1
2863	CP 253	CPE-IN0863-SGB	0.000+0	1.000+2	%	3.000-1	3.000-1
2881	CP 271	CPE-IN0993-SGB	0.000+0	1.000+2	%	3.000-1	3.000-1
2885	CP 275	CPE-IN0995-SGB	0.000+0	1.000+2	%	3.000-1	3.000-1
2891	CP 281	CPE-IN1053-SGB	0.000+0	1.000+2	%	3.000-1	3.000-1
2893	CP 283	CPE-IN1055-SGB	0.000+0	1.000+2	%	3.000-1	3.000-1
2925	CP 315	CPE-IN1374-SGB	0.000+0	1.000+2	%	3.000-1	3.000-1
2947	CP 337	CPE-IN1634-SGB	0.000+0	1.000+2	%	3.000-1	3.000-1
2956	CP 346	CPE-IN1864-SGB	0.000+0	1.000+2	%	3.000-1	3.000-1
2977	CP 367	CPE-180A-HLB	0.000+0	1.000+2	%	3.000-1	3.000-1
2978	CP 368	CPE-180B-HLB	0.000+0	1.000+2	%	3.000-1	3.000-1
2979	CP 369	CPE-180C-HLB	0.000+0	1.000+2	%	3.000-1	3.000-1
2980	CP 370	CPE-180D-HLB	0.000+0	1.000+2	%	3.000-1	3.000-1
2981	CP 371	CPE-180E-HLB	0.000+0	1.000+2	%	3.000-1	3.000-1
2982	CP 372	CPE-230A-CLB	0.000+0	1.000+2	%	3.000-1	3.000-1
2983	CP 373	CPE-230B-CLB	0.000+0	1.000+2	%	3.000-1	3.000-1
2984	CP 374	CPE-230C-CLB	0.000+0	1.000+2	%	3.000-1	3.000-1
2985	CP 375	CPE-230D-CLB	0.000+0	1.000+2	%	3.000-1	3.000-1
2986	CP 376	CPE-230E-CLB	0.000+0	1.000+2	%	3.000-1	3.000-1
2988	CP 378	CPE051A-LSA	0.000+0	1.000+2	%	3.350-1	3.350-1
2989	CP 379	CPE051B-LSA	0.000+0	1.000+2	%	3.350-1	3.350-1
2992	CP 382	CPE051E-LSA	0.000+0	1.000+2	%	3.350-1	3.350-1
2993	CP 383	CPE051F-LSA	0.000+0	1.000+2	%	3.350-1	3.350-1
2994	CP 384	CPE051G-LSA	0.000+0	1.000+2	%	3.350-1	3.350-1
2995	CP 385	CPE051H-LSA	0.000+0	1.000+2	%	3.350-1	3.350-1
2996	CP 386	CPE051I-LSA	0.000+0	1.000+2	%	3.350-1	3.350-1
2997	CP 387	CPE051J-LSA	0.000+0	1.000+2	%	3.350-1	3.350-1
2998	CP 388	CPE191A-LSB	0.000+0	1.000+2	%	3.350-1	3.350-1
2999	CP 389	CPE191B-LSB	0.000+0	1.000+2	%	3.350-1	3.350-1
3000	CP 390	CPE191C-LSB	0.000+0	1.000+2	%	3.350-1	3.350-1
3001	CP 391	CPE191D-LSB	0.000+0	1.000+2	%	3.350-1	3.350-1
3003	CP 393	CPE191F-LSB	0.000+0	1.000+2	%	3.350-1	3.350-1

Table 2.2-2 List of available measurements for experiment SB-CL-24 (Cont'd, 20/21)

SEQ NO	FUNC ID.	TAG NAME	OUTPUT RANGE LO	OUTPUT RANGE HI	UNIT	UNCERTAINTY ABS.	UNCERTAINTY REL.(%)
3004	CP 394	CPE191G-LSB	0.000+0	1.000+2	%	3.350-1	3.350-1
3005	CP 395	CPE191H-LSB	0.000+0	1.000+2	%	3.350-1	3.350-1
3006	CP 396	CPE191I-LSB	0.000+0	1.000+2	%	3.350-1	3.350-1
3007	CP 397	CPE191J-LSB	0.000+0	1.000+2	%	3.350-1	3.350-1
3019	CP 409	CP-VALVE-Y	0.000+0	1.000+2	%	3.000-1	3.000-1
3020	CP 410	CP-VALVE-S	0.000+0	1.000+2	%	0.000+0	0.000+0
3021	CP 411	CPE-W057C-DC	0.000+0	1.000+2	%	3.350-1	3.350-1
3022	CP 412	CPE-W067C-DC	0.000+0	1.000+2	%	3.350-1	3.350-1
3023	CP 413	CPE-W071C-DC	0.000+0	1.000+2	%	3.350-1	3.350-1
3024	CP 414	CPE-E071C-DC	0.000+0	1.000+2	%	3.350-1	3.350-1
3025	CP 415	CPE-B23661	0.000+0	1.000+2	%	3.350-1	3.350-1
3026	CP 416	CPE-B23662	0.000+0	1.000+2	%	3.350-1	3.350-1
3027	CP 417	CPE-B23663	0.000+0	1.000+2	%	3.350-1	3.350-1
3028	CP 418	CPE-B23664	0.000+0	1.000+2	%	3.350-1	3.350-1
3030	CP 420	CPE-B23666	0.000+0	1.000+2	%	3.350-1	3.350-1
3031	CP 421	CPE-B23667	0.000+0	1.000+2	%	3.350-1	3.350-1
3032	CP 422	CPE-B23668	0.000+0	1.000+2	%	3.350-1	3.350-1
3033	CP 423	CPE-B23669	0.000+0	1.000+2	%	3.350-1	3.350-1
3034	CP 424	CPE-B01001	0.000+0	1.000+2	%	3.350-1	3.350-1
3035	CP 425	CPE-B01002	0.000+0	1.000+2	%	3.350-1	3.350-1
3036	CP 426	CPE-B01003	0.000+0	1.000+2	%	3.350-1	3.350-1
3037	CP 427	CPE-B01004	0.000+0	1.000+2	%	3.350-1	3.350-1
3038	CP 428	CPE-B01005	0.000+0	1.000+2	%	3.350-1	3.350-1
3039	CP 429	CPE-B01006	0.000+0	1.000+2	%	3.350-1	3.350-1
3040	CP 430	CPE-B01007	0.000+0	1.000+2	%	3.350-1	3.350-1
3041	CP 431	CPE-B01008	0.000+0	1.000+2	%	3.350-1	3.350-1
3042	CP 432	CPE-B01009	0.000+0	1.000+2	%	3.350-1	3.350-1
3043	CP 433	CPE-B05001	0.000+0	1.000+2	%	3.350-1	3.350-1
3044	CP 434	CPE-B05002	0.000+0	1.000+2	%	3.350-1	3.350-1
3045	CP 435	CPE-B05003	0.000+0	1.000+2	%	3.350-1	3.350-1
3046	CP 436	CPE-B05004	0.000+0	1.000+2	%	3.350-1	3.350-1
3047	CP 437	CPE-B05005	0.000+0	1.000+2	%	3.350-1	3.350-1
3048	CP 438	CPE-B05006	0.000+0	1.000+2	%	3.350-1	3.350-1
3049	CP 439	CPE-B05007	0.000+0	1.000+2	%	3.350-1	3.350-1
3050	CP 440	CPE-B05008	0.000+0	1.000+2	%	3.350-1	3.350-1
3051	CP 441	CPE-B05009	0.000+0	1.000+2	%	3.350-1	3.350-1
3052	CP 442	CPE-B07001	0.000+0	1.000+2	%	3.000-1	3.000-1
3053	CP 443	CPE-B07002	0.000+0	1.000+2	%	3.000-1	3.000-1
3054	CP 444	CPE-B07003	0.000+0	1.000+2	%	3.000-1	3.000-1
3055	CP 445	CPE-B07004	0.000+0	1.000+2	%	3.000-1	3.000-1
3056	CP 446	CPE-B07005	0.000+0	1.000+2	%	3.000-1	3.000-1
3057	CP 447	CPE-B07006	0.000+0	1.000+2	%	3.000-1	3.000-1
3058	CP 448	CPE-B07007	0.000+0	1.000+2	%	3.000-1	3.000-1
3059	CP 449	CPE-B07008	0.000+0	1.000+2	%	3.000-1	3.000-1
3060	CP 450	CPE-B07009	0.000+0	1.000+2	%	3.000-1	3.000-1
991	CP 451	CPE-B03001	0.000+0	1.000+2	%	3.000-1	3.000-1
992	CP 452	CPE-B03002	0.000+0	1.000+2	%	3.000-1	3.000-1
993	CP 453	CPE-B03003	0.000+0	1.000+2	%	3.000-1	3.000-1
994	CP 454	CPE-B03004	0.000+0	1.000+2	%	3.000-1	3.000-1
995	CP 455	CPE-B03005	0.000+0	1.000+2	%	3.000-1	3.000-1
996	CP 456	CPE-B03006	0.000+0	1.000+2	%	3.000-1	3.000-1
997	CP 457	CPE-B03007	0.000+0	1.000+2	%	3.000-1	3.000-1
998	CP 458	CPE-B03008	0.000+0	1.000+2	%	3.000-1	3.000-1
999	CP 459	CPE-B03009	0.000+0	1.000+2	%	3.000-1	3.000-1
1000	CP 460	CPE-IN0630-SGA	0.000+0	1.000+2	%	3.350-1	3.350-1
1001	CP 461	CPE-IN0650-SGA	0.000+0	1.000+2	%	3.350-1	3.350-1
1002	CP 462	CPE-IN0680-SGA	0.000+0	1.000+2	%	3.350-1	3.350-1
1003	CP 463	CPE-IN0720-SGA	0.000+0	1.000+2	%	3.350-1	3.350-1
1004	CP 464	CPE-IN0760-SGA	0.000+0	1.000+2	%	3.350-1	3.350-1
1005	CP 465	CPE-EX0630-SGA	0.000+0	1.000+2	%	3.350-1	3.350-1
1006	CP 466	CPE-EX0650-SGA	0.000+0	1.000+2	%	3.350-1	3.350-1
1007	CP 467	CPE-EX0680-SGA	0.000+0	1.000+2	%	3.350-1	3.350-1
1009	CP 469	CPE-EX0760-SGA	0.000+0	1.000+2	%	3.350-1	3.350-1
1010	CP 470	CPE-IN0630-SGB	0.000+0	1.000+2	%	3.350-1	3.350-1
1011	CP 471	CPE-IN0650-SGB	0.000+0	1.000+2	%	3.350-1	3.350-1
1012	CP 472	CPE-IN0680-SGB	0.000+0	1.000+2	%	3.350-1	3.350-1
1013	CP 473	CPE-IN0720-SGB	0.000+0	1.000+2	%	3.350-1	3.350-1
1015	CP 475	CPE-EX0630-SGB	0.000+0	1.000+2	%	3.350-1	3.350-1
1016	CP 476	CPE-EX0650-SGB	0.000+0	1.000+2	%	3.350-1	3.350-1
1017	CP 477	CPE-EX0680-SGB	0.000+0	1.000+2	%	3.350-1	3.350-1
1018	CP 478	CPE-EX0720-SGB	0.000+0	1.000+2	%	3.350-1	3.350-1
1019	CP 479	CPE-EX0760-SGB	0.000+0	1.000+2	%	3.350-1	3.350-1
3191	RC 31	DE011A-HLA-EU	0.000+0	1.000+3	kg/m3	2.700+1	2.700+0
3192	RC 32	DE011B-HLA-EU	0.000+0	1.000+3	kg/m3	2.000+1	2.000+0
3193	RC 33	DE011C-HLA-EU	0.000+0	1.000+3	kg/m3	2.200+1	2.200+0
3195	RC 35	DE151B-HLB-EU	0.000+0	1.000+3	kg/m3	2.000+1	2.000+0
3196	RC 36	DE151C-HLB-EU	0.000+0	1.000+3	kg/m3	2.200+1	2.200+0
3197	RC 37	DE071A-CLA-EU	0.000+0	1.000+3	kg/m3	5.000+1	5.000+0
3198	RC 38	DE071B-CLA-EU	0.000+0	1.000+3	kg/m3	5.000+1	5.000+0
3199	RC 39	DE071C-CLA-EU	0.000+0	1.000+3	kg/m3	5.000+1	5.000+0
3200	RC 40	DE211A-CLB-EU	0.000+0	1.000+3	kg/m3	5.000+1	5.000+0
3201	RC 41	DE211B-CLB-EU	0.000+0	1.000+3	kg/m3	5.000+1	5.000+0
3202	RC 42	DE211C-CLB-EU	0.000+0	1.000+3	kg/m3	5.000+1	5.000+0
3206	RC 46	FRE-011-HLA	-1.210+2	1.210+2	kg/s	5.490+0	2.270+0
3207	RC 47	DAE-011-HLA	0.000+0	1.000+3	kg/m3	4.170+1	4.170+0
3210	RC 50	FRE-071-CLA	-1.210+2	1.210+2	kg/s	2.171+1	8.970+0
3211	RC 51	FRE-211-CLB	-1.210+2	1.210+2	kg/s	2.171+1	8.970+0
3212	RC 52	DAE-071-CLA	0.000+0	1.000+3	kg/m3	8.930+1	8.930+0
3213	RC 53	DAE-211-CLB	0.000+0	1.000+3	kg/m3	8.930+1	8.930+0
3216	RC 56	DE051A-LSA-EU	0.000+0	1.000+3	kg/m3	5.000+1	5.000+0

Table 2.2-2 List of available measurements for experiment SB-CL-24 (Cont'd, 21/21)

SEQ NO	FUNC ID.	TAG NAME	OUTPUT RANGE LO	OUTPUT RANGE HI	UNIT	UNCERTAINTY ABS.	UNCERTAINTY REL.(%)
3217	RC 57	DE051B-LSA-EU	0.000+0	1.000+3	kg/m3	5.000+1	5.000+0
3218	RC 58	DE051C-LSA-EU	0.000+0	1.000+3	kg/m3	5.000+1	5.000+0
3219	RC 59	DE191A-LSB-EU	0.000+0	1.000+3	kg/m3	5.000+1	5.000+0
3220	RC 60	DE191B-LSB-EU	0.000+0	1.000+3	kg/m3	5.000+1	5.000+0
3221	RC 61	DE191C-LSB-EU	0.000+0	1.000+3	kg/m3	5.000+1	5.000+0
3222	RC 62	DE052-LSA-EU	0.000+0	1.000+3	kg/m3	5.000+1	5.000+0
3223	RC 63	DE192-LSB-EU	0.000+0	1.000+3	kg/m3	5.000+1	5.000+0
3224	RC 64	DE281-PR-EU	0.000+0	1.000+3	kg/m3	5.000+1	5.000+0
3225	RC 65	DE291-PR-EU	0.000+0	1.000+3	kg/m3	5.000+1	5.000+0
3228	RC 68	DE431-SGA-EU	0.000+0	1.000+3	kg/m3	5.000+1	5.000+0
3229	RC 69	DE471-SGB-EU	0.000+0	1.000+3	kg/m3	5.500+1	5.500+0
3233	RC 73	DE591A-BU-EU	0.000+0	1.000+1	kg/m3	1.000+0	1.000+1
3234	RC 74	DE591B-BU-EU	0.000+0	1.000+1	kg/m3	1.000+0	1.000+1
3235	RC 75	DE591C-BU-EU	0.000+0	1.000+1	kg/m3	7.200+0	7.200-1
3236	RC 76	MFE061A-LSA-EU	0.000+0	1.239+4	kg/ms2	0.000+0	0.000+0
3237	RC 77	MFE061B-LSA-EU	0.000+0	1.239+4	kg/ms2	0.000+0	0.000+0
3238	RC 78	MFE201A-LSB-EU	0.000+0	1.239+4	kg/ms2	0.000+0	0.000+0
3239	RC 79	MFE201B-LSB-EU	0.000+0	1.239+4	kg/ms2	0.000+0	0.000+0
3246	RC 86	MFE591A-BU-EU	0.000+0	1.239+4	kg/ms2	0.000+0	0.000+0
3067	RC 107	FRE590-ST	0.000+0	1.000+1	kg/s	2.600+2	1.000+0
3068	RC 108	FRE675-ACH	-1.300+4	1.300+4	kg/s	2.600+2	1.000+0
3069	RC 109	FRE655-ACC	-1.300+4	1.300+4	kg/s	2.600+2	1.000+0
3070	RC 110	FRE-051-LSA	-1.300+4	1.300+4	kg/s	2.600+2	1.000+0
3071	RC 111	FRE-191-LSB	-1.300+4	1.300+4	kg/s	2.600+2	1.000+0
3072	RC 112	DAE-051-LSA	0.000+0	1.000+3	kg/m3	0.000+0	0.000+0
3073	RC 113	DAE-191-LSB	0.000+0	1.000+3	kg/m3	0.000+0	0.000+0
3074	RC 114	FRE-061-LSA	-1.300+4	1.300+4	kg/s	2.600+2	1.000+0
3075	RC 115	FRE-201-LSB	-1.300+4	1.300+4	kg/s	2.600+2	1.000+0
3078	RC 118	FRE-591A-BU	-1.300+4	1.300+4	kg/s	2.600+2	1.000+0
3080	RC 120	DAE-051-LSA-TY	0.000+0	1.000+3	kg/m3	5.000+1	5.000+0
3081	RC 121	DAE-191-LSB-TY	0.000+0	1.000+3	kg/m3	5.000+1	5.000+0
3084	RC 124	DAE-591A-BU	0.000+0	1.000+3	kg/m3	0.000+0	0.000+0
3085	RC 125	DAE-591B-BU	0.000+0	1.000+3	kg/m3	0.000+0	0.000+0
3092	RC 132	DE591-AVG	-1.210+2	1.210+2	kg/m3	0.000+0	0.000+0
3093	RC 133	TWE-PCT	0.000+0	0.000+0	K	0.000+0	0.000+0
3095	RC 135	FE591A-AVG	-1.210+2	1.210+2	kg/s	0.000+0	0.000+0

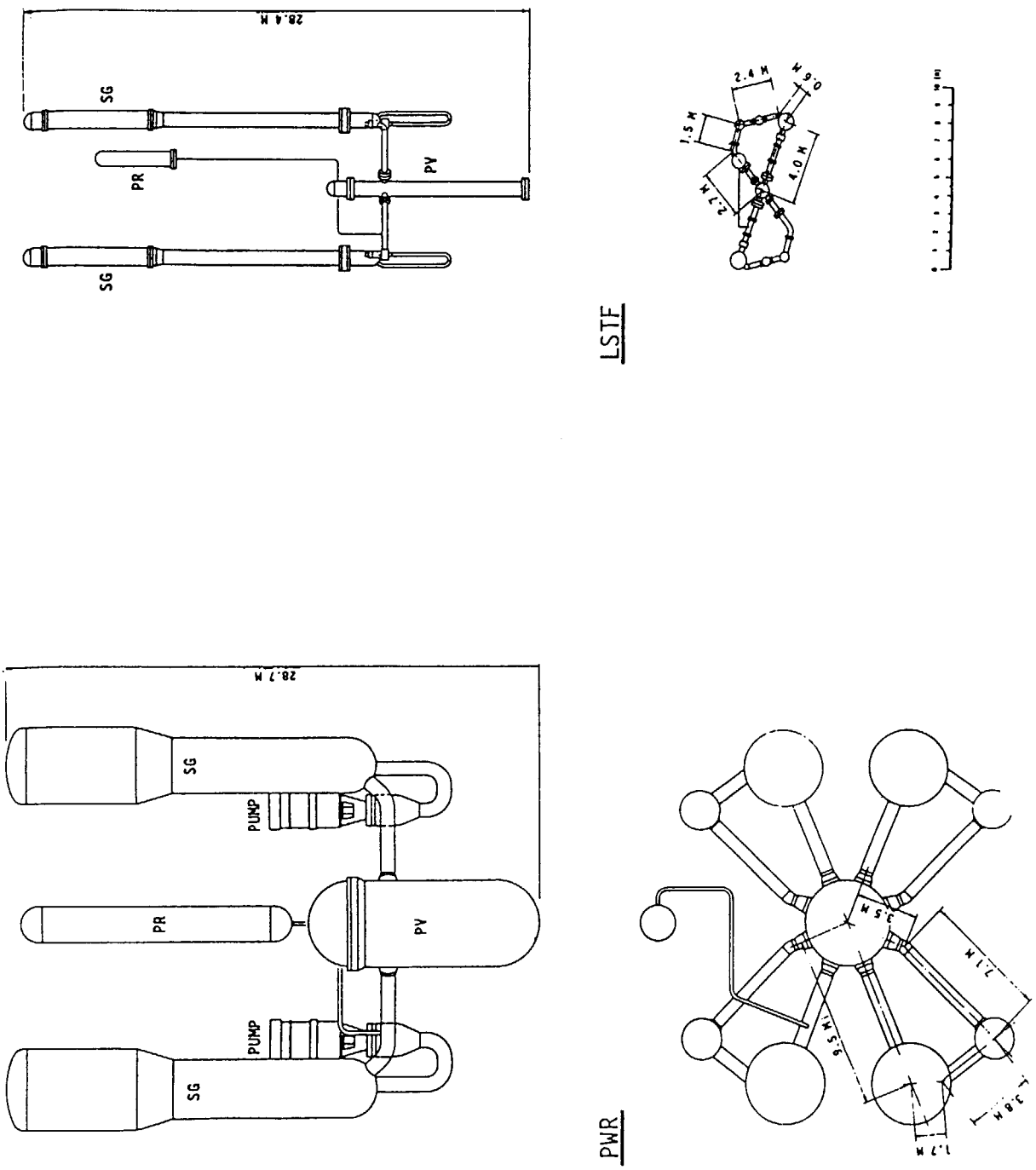

Fig. 2.1.1 Comparison of LSTF and four-loop PWR

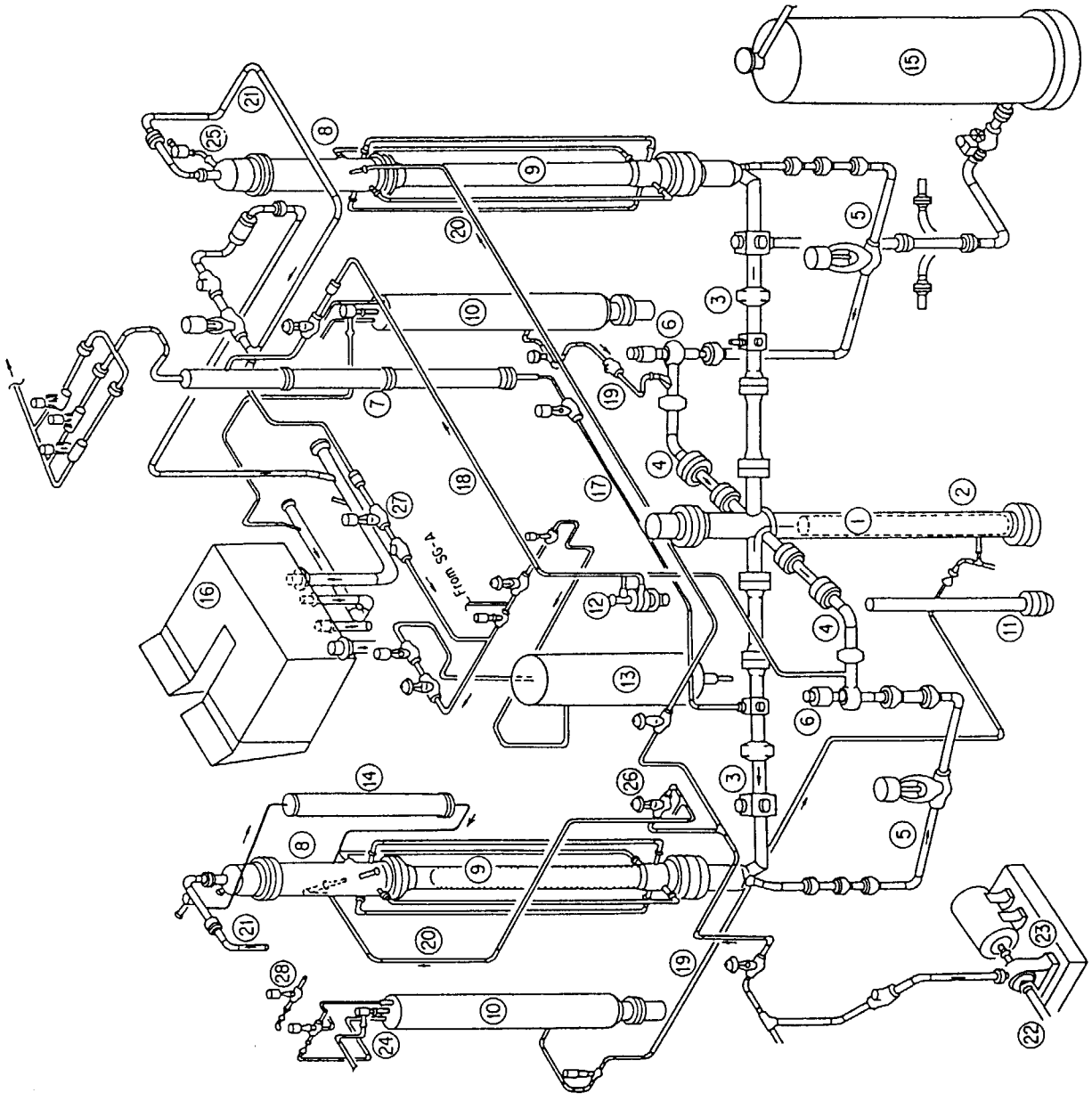

Fig. 2.1.2 General view of total LSTF system

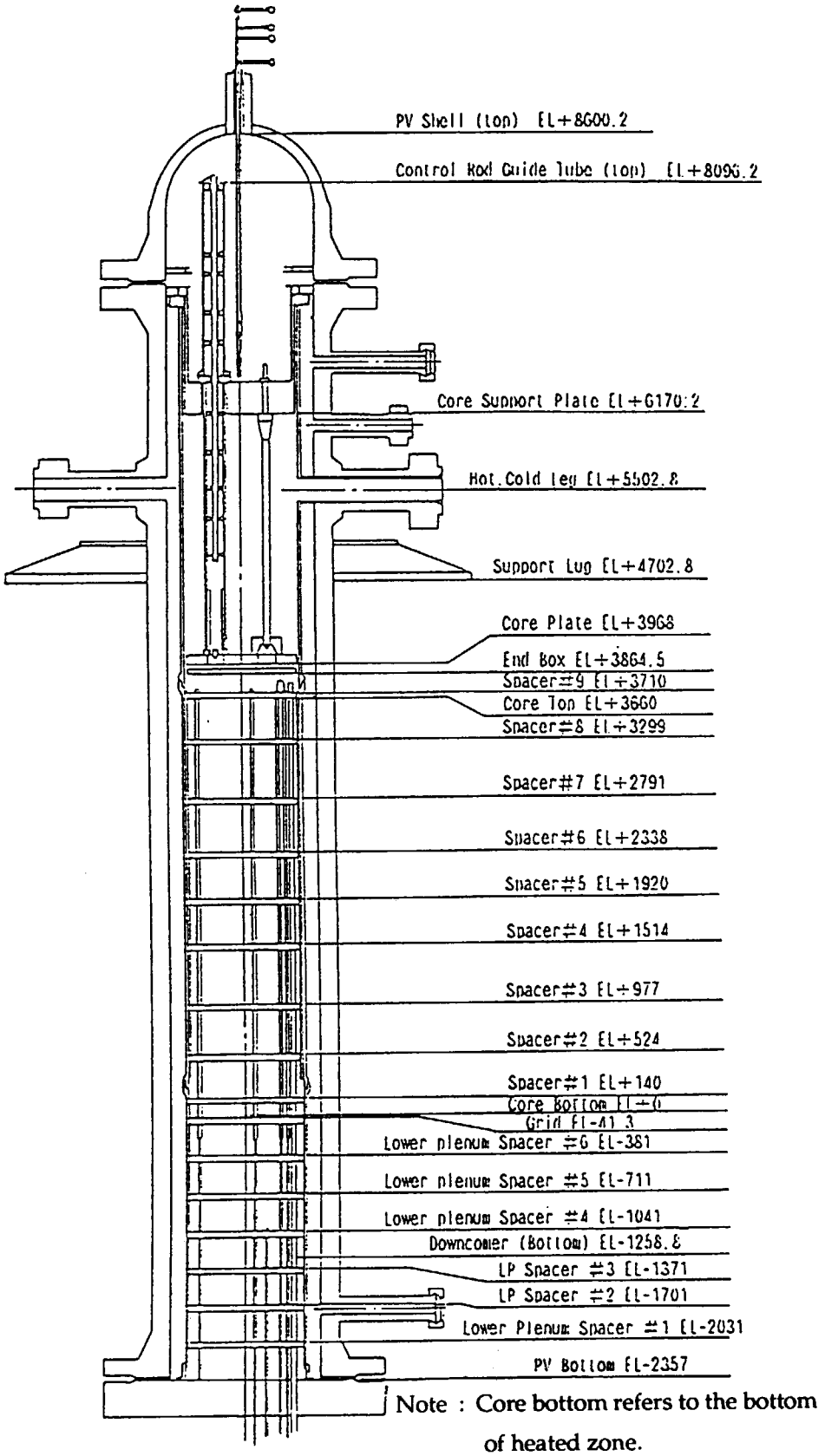

Fig. 2.1.3 Pressure vessel and internal assembly

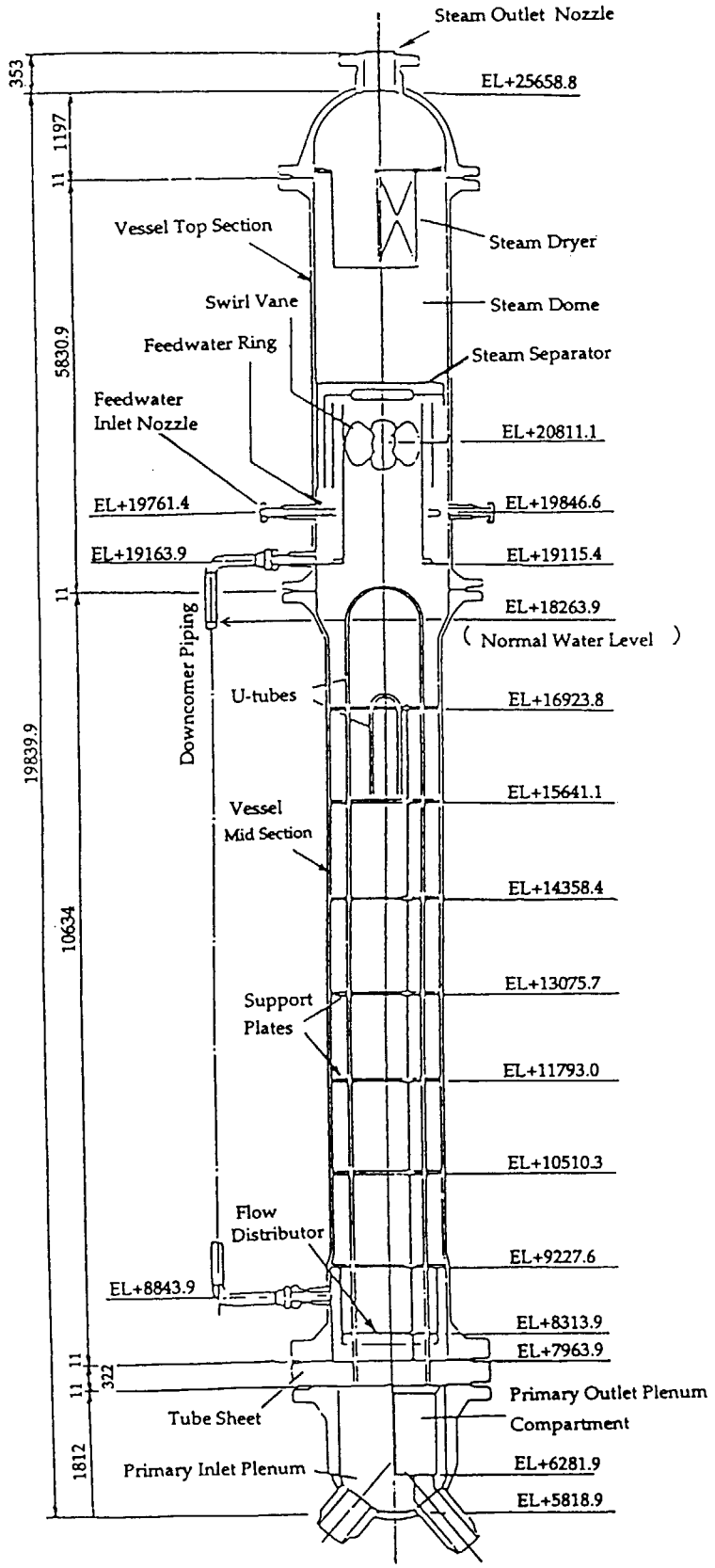

Fig. 2.1.4 Primary and secondary sides at steam generators (SG-A and SG-B)

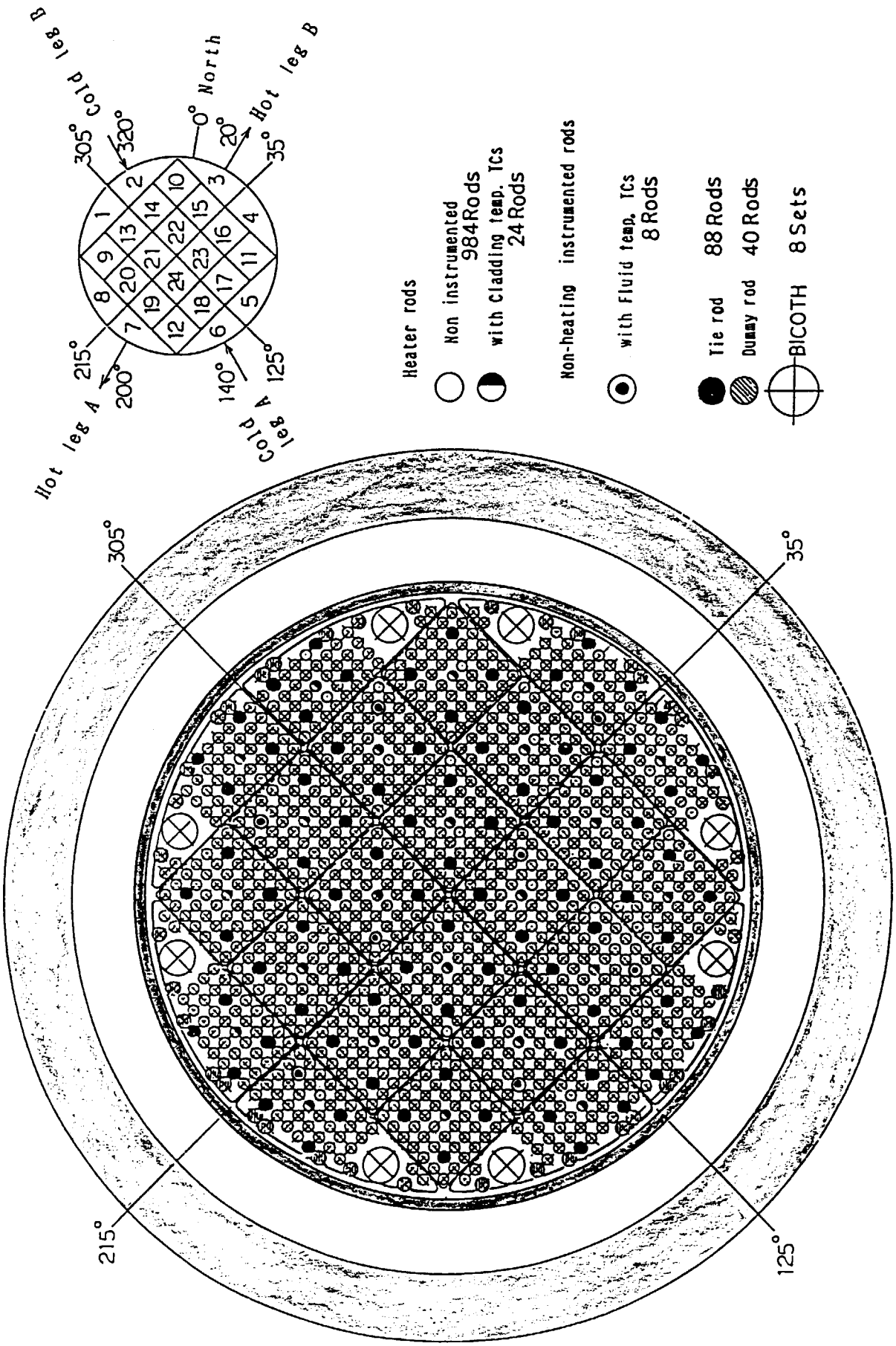

Fig. 2.1.5 Cross-section of core heater rod assembly

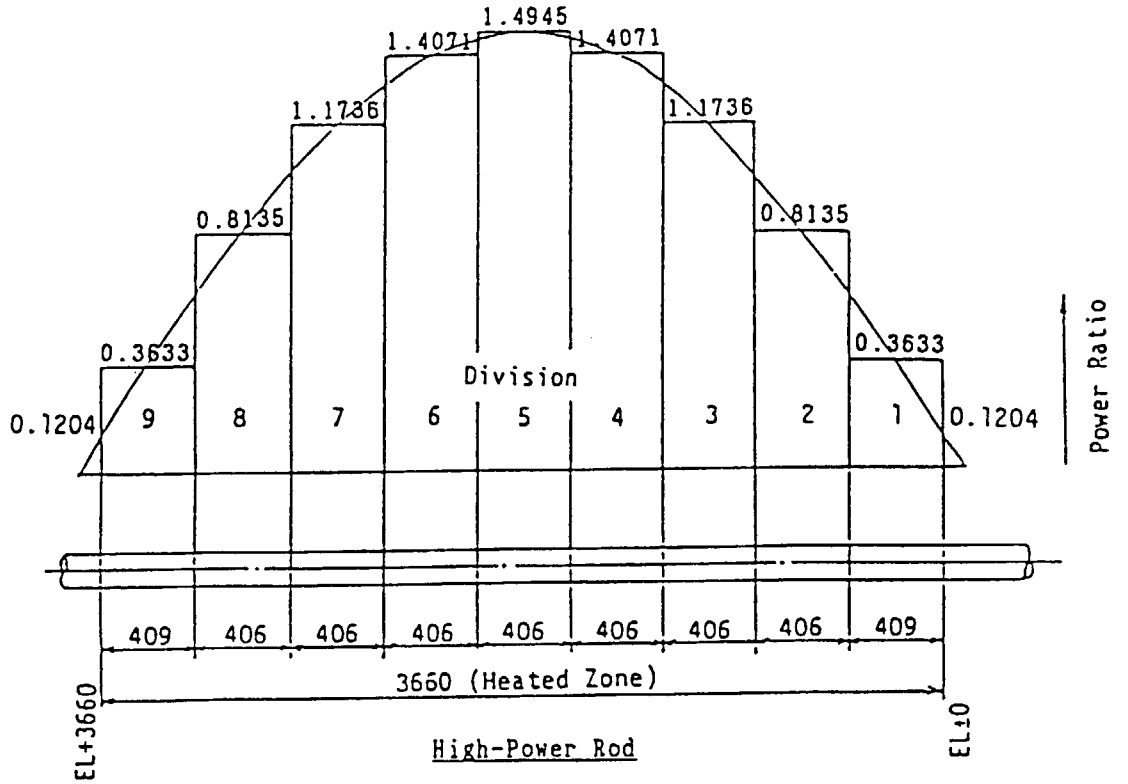

Fig. 2.1.6 Axial power distribution for high-power rod

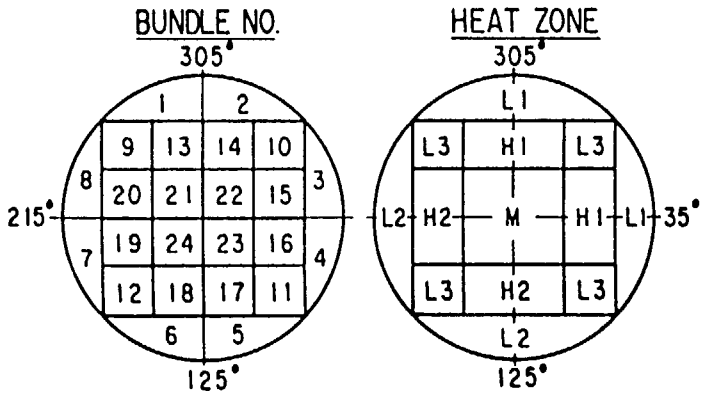

HEAT ZONE		MAX. HEATER OUTPUT (DESIGN VALUE)
LOW	L1, L3	11.0kW/ROD x468ROD= 5.148 MW
HIGH	H1 H2	16.6kW/ROD x360ROD= 5.976 MW
MEAN	M	11.0kW/ROD x180 ROD= 1.980 MW
TOTAL		1008 ROD 13.104 MW

HEAT ZONE	PIECE	CASE 3	
		PEAK FACTOR	HEATER OUTPUT
L 1	144	0.66	9.69kW/ROD ×0.66×144 =921kW
L 2	144		9.69kW/ROD ×0.66×144 =921kW
L 3	180		9.69kW/ROD ×0.66×180 =1151kW
H 1	180	1.51	9.69kW/ROD ×1.51×180 =2634kW
H 2	180		9.69kW/ROD ×1.51×180 =2634kW
M	180	1.00	9.69kW/ROD ×1.00×180 =1744kW
TOTAL	1008	10.005MW	

Fig. 2.1.7 Radial core power distribution in Experiment SB-CL-24

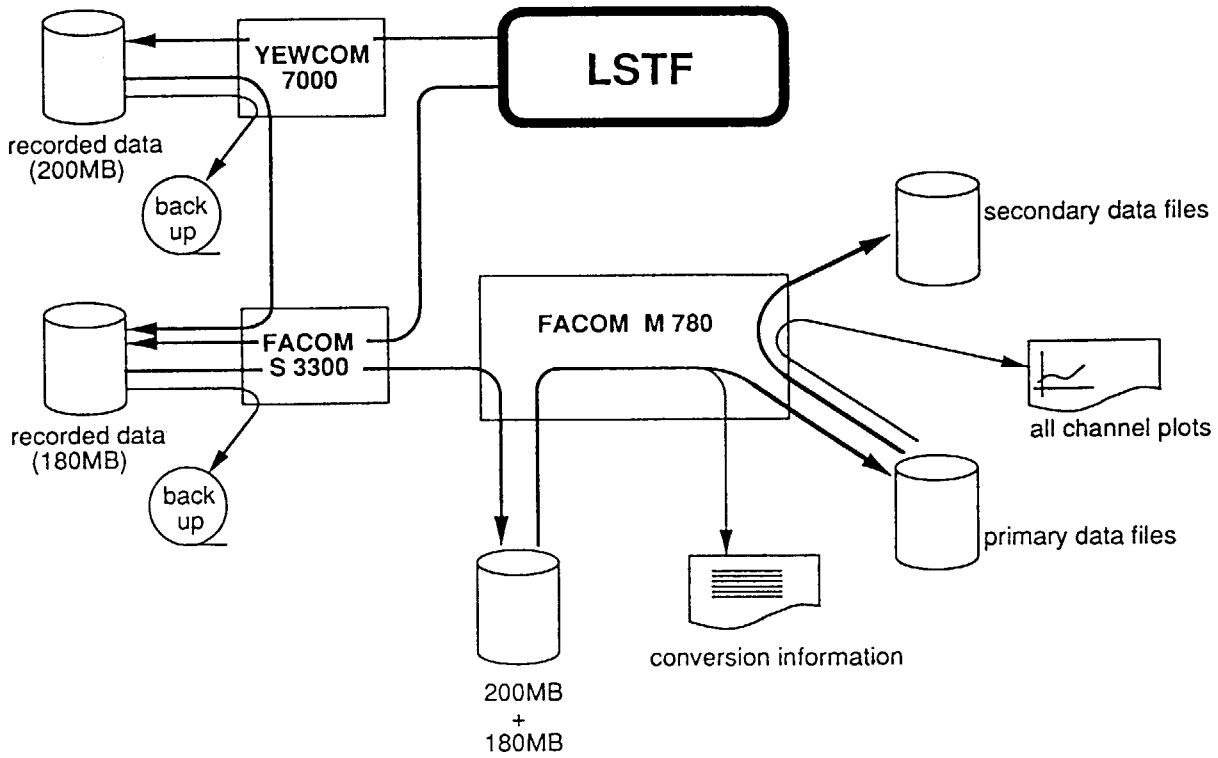

Fig. 2. 2. 1 Outline of data reduction process

3. Test Procedures and Boundary Conditions

3.1 Test Preparation Procedure

The system was necessarily drained prior to the test preparation procedures, so any instrument calibration normally done under voided conditions was also performed at that time. All of the DP transducers were zero checked while voided. The next action was to fill and vent the air from the primary system. This was done in several steps. First, the system was filled with demineralized water up to the bottom of the loops. The system was then vented using three vacuum pumps connected to the top of the pressurizer and to the outlet plenum of each SG. The vacuum pumps were operated until the air space pressure reached 735 mm Hg below atmospheric pressure.

Next, the remaining air was purged by injecting steam into the system gas spaces. The steam was generated in an accumulator tank in loop A (ACH) using an electric heater installed in that tank and was injected into the outlet plenum of both SGs and into the pump discharge side of both cold legs. The vacuum pumps were operated continuously during the steam injection process. This purging process was continued until well after the primary system gas phase temperatures had reached the vapor saturation temperature.

The system was next filled with water and pressurized. Under the pressurized condition, the primary coolant pumps were operated repeatedly at full capacity to ultimately transport any remaining air bubbles to the pressurizer where the air could be vented.

Then, after these steps were completed, the system was depressurized and drained slightly to lower the liquid level in the pressurizer. The amount of air remaining in the system was then measured by pressurizing the system by injecting air into the pressurizer air space and measuring the decrease in pressurizer liquid level in response to this pressure increase. This decrease in liquid level is thus an indication of air remaining in the primary system at a room temperature condition. In the preparation process of experiment SB-CL-24, this water level dropped by 21 cm (corresponding to a volume of $\Delta V = 0.0594\ m^3$) when the pressurizer was pressurized from a condition of P1=0.06 MPa to a higher pressure condition of P2=0.75 MPa. Thus, the residual airvolume (ΔVr) was estimated as,

$$\Delta Vr = \Delta V \times P2/(P2-P1) \times (0.06/0.1013) = 0.0383\ m^3$$

at the room temperature and atmospheric pressure condition (P=0.1013 MPa).

With the primary system satisfactorily filled and clear of air, the gamma densitometers and the conduction probes were again calibrated. Zero adjustments on the DP transducers checked under full conditions were completed. The system was then pressurized in steps to five different elevated pressures. The system was held for four minutes at each level to check the instrument drift. A check of all thermocouple outputs was made to verify that each was reading at a room temperature.

Most of the above procedures were performed during the two weeks preceding the experiment. On the day the experiment was performed, zero data was recorded from all the drag disks. During the heat-up period, output from the gamma densitometers was recorded at six different times to provide calibration data.

The primary and secondary systems were maintained at the full initial conditions for approximately 65 minutes before the start of Experiment SB-CL-24. Immediately before the test initiation, the three-way valves connecting the sense lines of certain DP transducers were opened for two minutes. Following the decision to terminate the experiment, the three way valves were again opened for two minutes. These data are used for post-test correction. A quiescent measure of liquid inventory was conducted after the test termination at the zero core power condition. The data recording was initiated at 290 s prior to the break signal and terminated at 8300 s.

3.2 Boundary and Initial Conditions

Major boundary conditions for the primary and secondary components are shown below in addition to the initial experiment conditions. The control logic used in this experiment is shown in Table 3.2-1.

(1) Failure Assumptions

The Experiment SB-CL-24 assumed no actuation of both HPI and auxiliary feedwater systems in a case of 0.5% cold leg break LOCA. The primary mass recovery was expected only by the accumulators (ACH and ACC) and the low pressure injection system (LPI). In order to actuate these injection systems, an intentional primary depressurization was planned.

(2) Break Unit

The break was initiated in the B-loop cold leg by quickly opening the air operated valve (AOV 300) located at downstream of the break unit (BU) as shown in Fig. 3.2.1. The break direction was horizontal and the break orifice had an inner diameter of 7.2 mm as shown in Fig. 3.2.2. The break orifice and the instruments including the three-beam gammadensi-

tometer and thermocouples were set in BU as shown in Fig. 3.2.3. The break flow was finally lead to the ST and its flow rate was reduced from the ST mass increasing rate. Air was injected into the BU downstream line to mitigate effects of condensation-induced pressure spikes.

(3) Core Power

The core power was regulated by the test sequence controller, CENTUM, to simulate the post-scram core power decay as shown in Table 3.2-2. The decay curve used in this test, designated the "JAERI" power curve[2], was developed by considering the fission product decay power, the actinide decay power and the delayed neutron effects with conservative assumptions. Since the maximum electric core power available in the LSTF is limited to 10 MW, i.e., 14% of the 1/48 scaled PWR rated power, the "JAERI" power curve maintains the LSTF core power at the initial value of 10MW, until the scaled PWR core decay power drops to 10 MW, at 29 s after the scram signal actuation. After this time, the electric core power was regulated to follow the scaled PWR core power decay. Figure 3.2.4 (a) shows the core power curves during the test period of SB-CL-24.

An additional core power control is usually programmed to protect the heater rods from overheating in a case of core heatup, i.e., the core power decreases to 75% at the maximum heater rod temperature of 908 K, 50% at 918K, 25% at 919 K and finally 0% at 923K, respectively. In this experiment, the final step to 0% power was remodeled to 10% power to study the succeeding thermal-hydraulic behaviors in the core as shown in Fig. 3.2.4 (b)and the 10% power was finally tripped to 0% at 7822 s.

(4) Pump Coastdown

The coastdown of the primary coolant pumps was controlled by CENTUM accoding to a programmed characteristics as shown in Table 3.2-3 and Fig. 3.2.5. The initial pump speed is generally maintained at a certain low level so that the primary coolant temperature increase across the core can meet the rated PWR conditions under the limited core power condition (14% of the 1/48 scaled PWR thermal output). After the break initiation, the pump speeds were quickly increased to 1500 rpm (rotation per minute). These pump coastdown characteristics are common in the LSTF SBLOCA experiments to better simulate the PWR transient responses of the primary pressure and temperatures after the scram trip. The primary pump power was finally terminated at 250 s after the pump coastdown initiation.

(5) Pressurizer Heaters and Trace Heaters

The LSTF pressurizer heaters consist of simulated proportional and backup heaters with

the maximum power of 7.5 kW and 112.5 kW, respectively. The proportional heater power is automatically controlled so that the primary pressure can be kept constant as long as the water level is higher than the heater assembly. The base heater is used to compensate the environmental heat loss from the primary system as long as the pressurizer liquid level is higher than 2.3 m. In addition to these, trace heater powers were supplied to the surge and spray lines. In this test, a sum of these powers was 33.8 kW in the ini tial state as shown in Fig. 3.2.6. The trace heaters at the surge and spray lines were tripped off at the test initiation while the proportional and base heaters were tripped off at 70 and 77 s, respectively, by the low pressurizer water level signal.

Many regions of the LSTF primary and secondary systems are equipped with trace heaters intended to compensate for environmental heat losses. In this test, all the trace heater powers were tripped off after the break initiation except for those attached to the accumulator lines. A total trace heater power in each region is listed in Table 3.2-4.

(6) ECCS Injection

As shown in the failure assumptions, both the AIS and LPI systems were available in this experiment. These ECCS injection flows were led to each cold leg through each injection line. The AIS injection started when the primary pressure decreased below each tank pressure (see Table 3.2-4). The nitrogen gas injection from the accumulator tanks to the primary system was prevented by closing the air operated valves at their injection lines when their tank water levels reached each low setpoint. The injection flow rates to the CL-A and the CL-B were expected to be in a ratio of 3 : 1 by selecting the orifices in their injection lines. An actual LPI flow rate ratio between the CL-A and the CL-B, however, was not the same as 3 : 1 due to a result of inadequate flow path resistances between them.

(7) Opening of SG Relief Valves, Pressurizer PORVs and Safety Valves

The secondary depressurization in both SGs was planned to initiate at 600 s by repeatedly opening the RVs according to a programmed SG pressure control logic so that the secondary temperature decreased on a speed of 100 K in one hour. This operation was continued untill the test was terminated. The orifices used to limit the SG steam flows at the valves of RV and SV had diameters of 19.4 and 26.6 mm, respectively as shown in Fig. 3.2.7.

The pressurizer PORV and the SVs were planned to open when the core heatup was detected. The orifices to limit the pressurizer steam discharge flows had diameters of 6.83 mm for the PORV and 14.5 mm for the SV, respectively (see Fig. 3.2.7). In this experiment, the

PORV and the pressurizer SV were opened by operators at 6568 and 6610 s, respectively. The discharged steam mass through these pressurizer valves was not measured in this experiment but was estimated from the mass balance in the primary system (refer Section 4.3.1).

(8) Control Logic

As shown in Table 3.2-1, the break signal and the trace heater power trips were actuated at time zero. Immediately after the break signal, the primary pumps were powered to speedup.

The scram and the safety injection (SI) signals were generated when the pressurizer pressure decreased to setpoints of 12.97 and 12.27 MPa, respectively. The scram signal tripped to initiate the primary pump coastdown, core power decay and isolation of two SGs by closing their steam and feedwater lines. The SG-RV was automatically controlled to maintain the secondary pressure between 8.03 and 7.82 MPa in the first 600 s. At the time of 600 s, the SG pressure control was changed according to a programmed logic so that the secondary depressurization action was simulated. The LPI was actuated by the SI signal and it started to injection when the primary pressure decreased to 1.29 MPa.

(9) Initial Test Conditions

The measured initial test conditions almost agreed with the specified conditions within each measurement accuracy as shown in Table 3.2-4. The primary and secondary pressures, the hot leg temperatures, the fluid temperature increase across the core simulated the rated PWR conditions at full power. As the LSTF core power was approximately 14% of the 1/48 scaled PWR core power, the LSTF initial core flow rate was lowered to achieve the same enthalpy distribution in the rated PWR primary conditions.

The SG secondary sides were almost in saturated conditions except for the lower region which the subcooled downcomer flows entered. The steam and feedwater flow rates were controlled to constantly maintain the secondary pressure and the water level in each SG. The initial SG collapsed water level of 10.2 m allowed to recirculate the secondary fluid between the boiling section and the downcomer region and this recirculation flow ratio (a total recirculation flow rate devided by a steam flow rate) was approximately 6.1 for each SG.

Downcomer to hot leg leak lines were prepared to simulate a leak flow of 0.049 kg/s in one loop. The total trace heater power for the primary system was 83.7 kW and that for the two SG secondary systems was 26.7 kW, respectively.

Table 3.2-1 Control logic for experiment SB-CL-24

Event	Cause	Delay
Break and Trace Heaters Power Off	Time = 0.0 s	
Pressurizer Heater Power Off	$L_{PZR} \leq 1.0$ m	
Scram Signal	$P_{PZR} \leq 12.97$ MPa	
SI Signal	$P_{PZR} \leq 12.27$ MPa	
Core Power Tripped to Decay Curve	Scram Signal	
Core Power Control on Decay Curve	75 % for Rod Temp. ≧ 908 K 50 % for Rod Temp. ≧ 918 K 25 % for Rod Temp. ≧ 919 K 0 % for Rod Temp. ≧ 923 K	
Primary Pumps Speed-up Primary Pumps Tripped	Break Signal Scram Signal	
Turbine Trip	Scram Signal	
Feedwater Valve Closed	Scram Signal	
SG PORV Setpoint to Open SG PORV Setpoint to Close	$P_{SG} \geq 8.03$ MPa $P_{SG} \leq 7.82$ MPa	
Pressurizer PORV Open	Operator Action (*)	
SG Safety Valve Open	Time = 600.0 s	
High Pressure Injection System	Failure	
Low Pressure Injection System	SI Signal	17 s
Auxiliary Feedwater System	Failure	

* Detection of Core heatup initiation by super-heated rod temperatures.

Table 3.2-2 Specified core power decay curve after the scram

Time (s)	Power (MW)	Time (s)	Power (MW)	Time (s)	Power (MW)	Time (s)	Power (MW)
0	10.000	60	7.344	800	1.488	10020	0.784
1	10.000	80	6.128	1000	1.424	19980	0.592
5	10.000	100	5.200	1500	1.280	60000	0.464
10	10.000	150	3.632	2000	1.200	100020	0.368
20	10.000	200	2.848	4000	0.992		
29	10.000	400	1.776	6000	0.848		
40	8.912	600	1.568	7980	0.784		

Table 3.2-3 Specified primary pump coastdown curve after the scram

Time (s)	Pump Speed Ratio	Time (s)	Pump Speed Ratio	Time (s)	Pump Speed Ratio
0	1.000	30	0.280	80	0.125
2	0.850	40	0.220	90	0.110
5	0.730	50	0.185	100	0.100
10	0.540	60	0.160	250	0.000
20	0.370	70	0.140		

The pump speed ratio is normarized by the maximun pump speed of 1500 rpm.
A time delay of 16.2 s is assumed after the scram.

Table 3.2-4 Initial conditions in experiment SB-CL-24

Region and Items	(Unit)	Specified	Measured (Accuracy*1)
Pressure Vessel:			
Core Power	(MW)	10.0	10.0*2 (± 0.07)
Primary Loops (A-Loop / B-Loop)			
Hot leg temperature	(K)	598.1	598.7 / 598.5 (± 2.75)
Cold leg temperature	(K)	562.4	563.8 / 564.0 (± 2.75)
Mass flow rate per loop	(kg/s)	24.3	24.8 / 24.3 (± 1.25)
Downcomer-to-hot leg bypass	(kg/s)	0.049	0.054 / 0.046 (± 0.01)
Pressurizer:			
Pressure	(MPa)	15.52	15.4 (± 0.108)
Water level above bottom	(m)	2.7	2.71 (± 0.013)
Steam generators (A-Loop / B-Loop)			
Pressure	(MPa)	7.3	7.38 / 7.38 (± 0.054)
Water level	(m)	10.3	10.2 / 10.2 (± 0.38)
Main feedwater flow rate	(kg/s)	2.74	2.74 / 2.70 (± 0.05)
Main feedwater temperature	(K)	(497)	495.9/495.8 (± 2.63)
Accumulators (ACC to CLA / ACH to CLB)			
Flow Distribution Ratio (A:B)		3 : 1	3 : 1
Injection Pressure	(MPa)	4.51 / 4.51	4.56 / 4.54 (± 0.054)
Water Temperature	(K)	320 / 320	319.8/321.2 (± 2.3/2.4)
Water Level above Bottom	(m)	5.76 / 6.43	3.64/4.36 (±0.12/0.15)
Low Pressure Injection System			
Flow Distribution Ratio (A:B)		3 : 1	3 : 1
Actuation Pressure	(MPa)	1.29	1.20 (± 0.064)
Water Temperature	(K)	310	312 (± 2.63)
Trace Heater Power before Break			
Pressurizer and Surge Line	(kW)		33.8 (± 0.59)
Pressure Vessel	(kW)		35.0 (± 0.04)
A-Loop	(kW)		7.5 (± 0.014)
B-Loop	(kW)		7.4 (± 0.014)
SG-A System	(kW)		13.4 (± 0.02)
SG-B System	(kW)		13.3 (± 0.02)
ACC	(kW)		0.0*3
ACH	(kW)		0.0*3

*1 Reference [1]
*2 Actual power supplied to the core, which is 1 % lower than the MI 17 data. The data of MI 17 includes an electric loss (1 % of 10 MW) at vessel outside.
*3 The trace heater powers for ACC and ACH were initially 0.0 kW and became a maximum power of 6.8 kW for ACC and 3.0 kW for ACH, respectively during the injection periods.

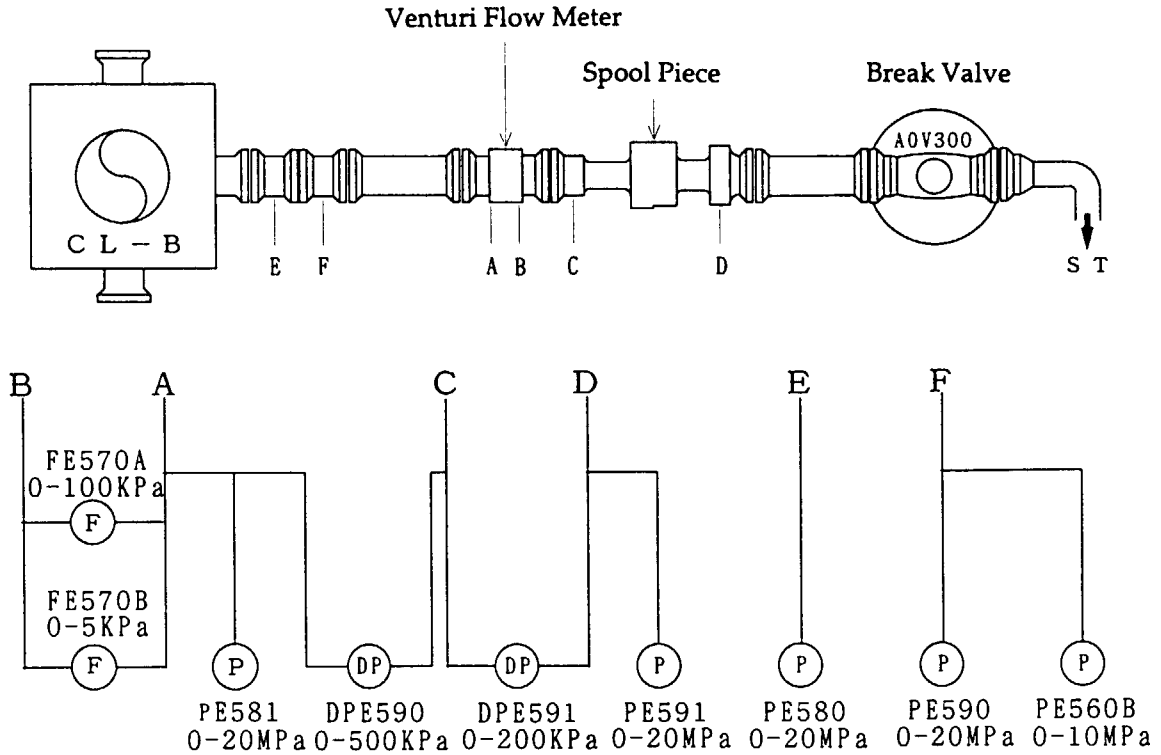

Fig. 3. 2. 1 Configuration of break unit

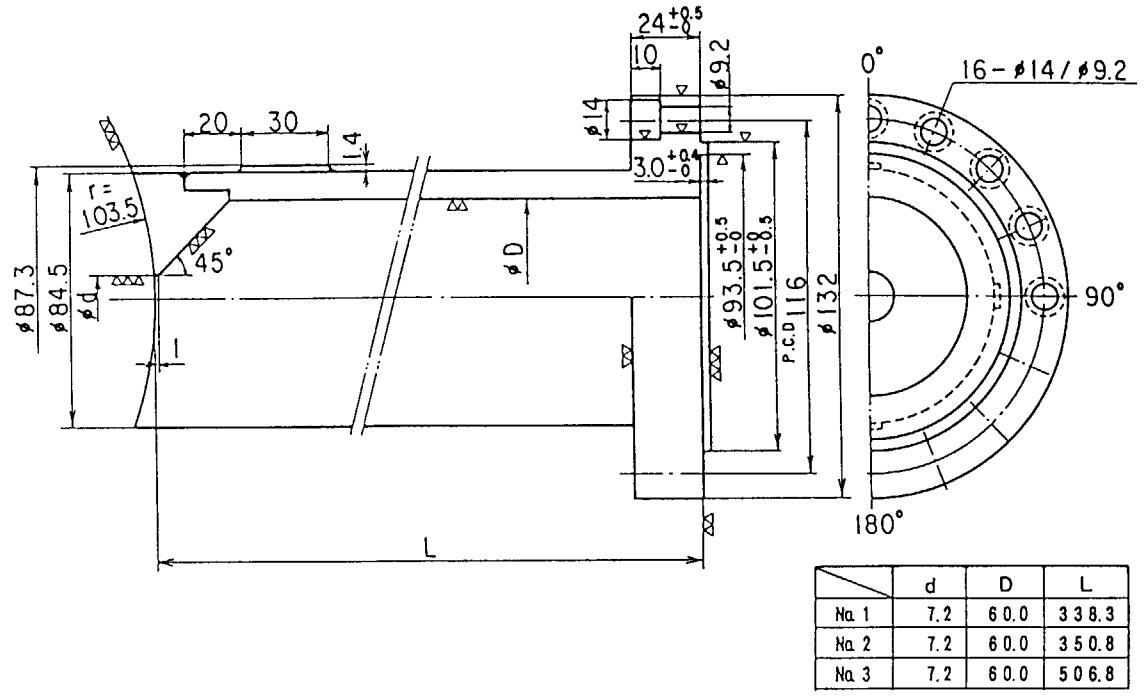

	d	D	L
No. 1	7.2	60.0	338.3
No. 2	7.2	60.0	350.8
No. 3	7.2	60.0	506.8

Fig. 3. 2. 2 Geometry of break orifice

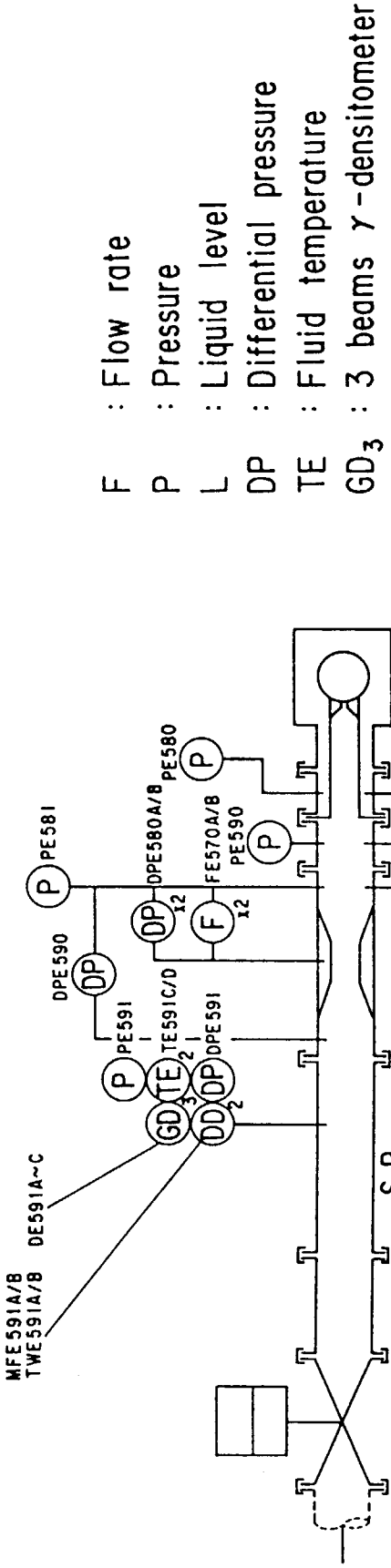

Fig. 3.2.3 Instrumentation in break unit

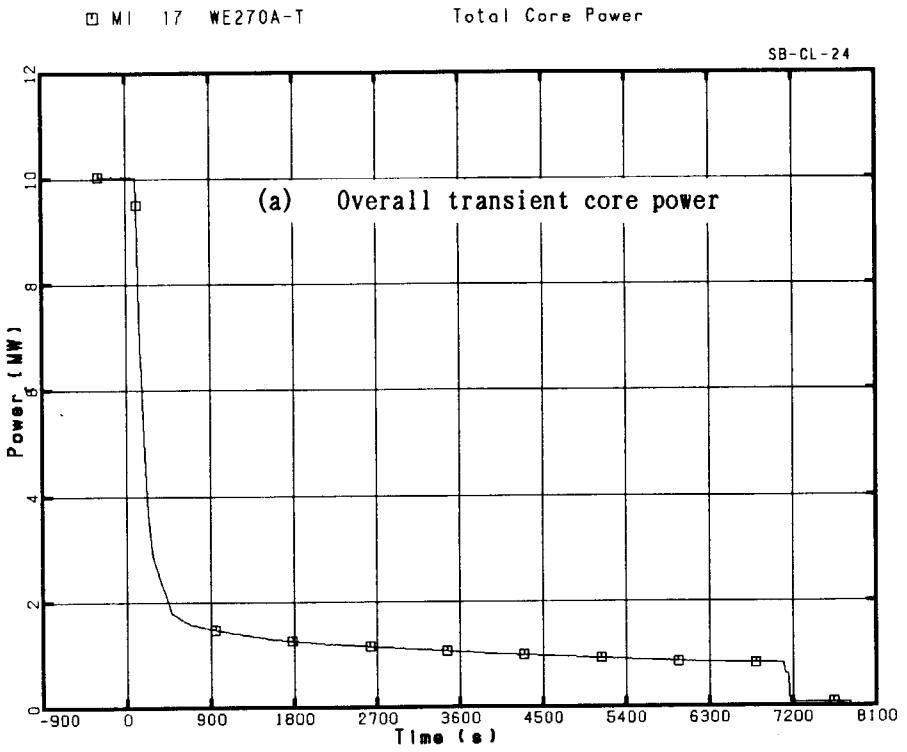

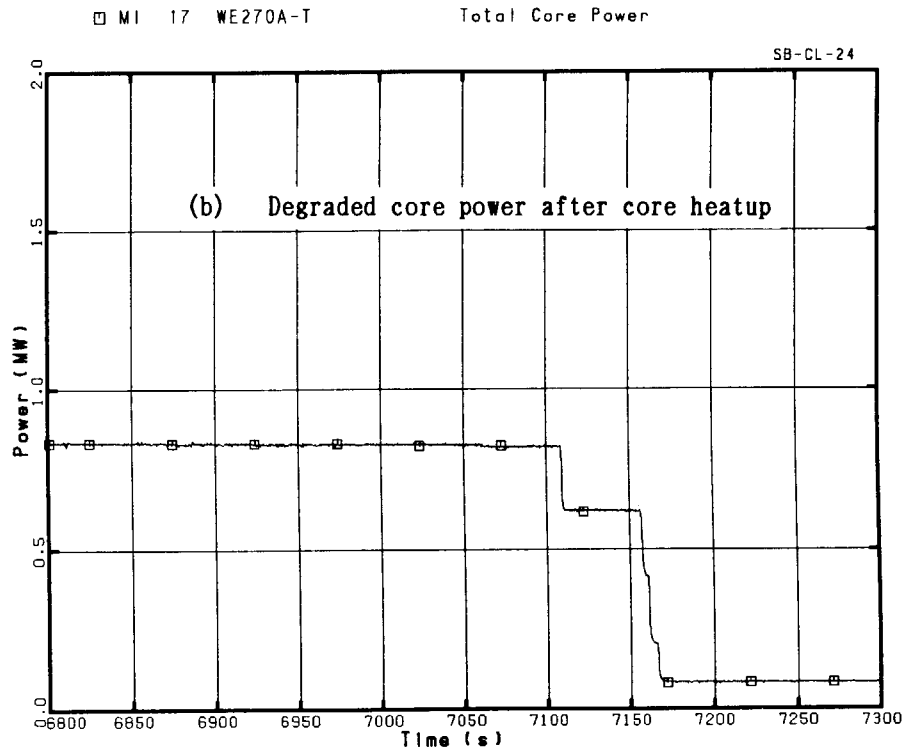

Fig. 3.2.4 Core power curve in experiment SB-CL-24

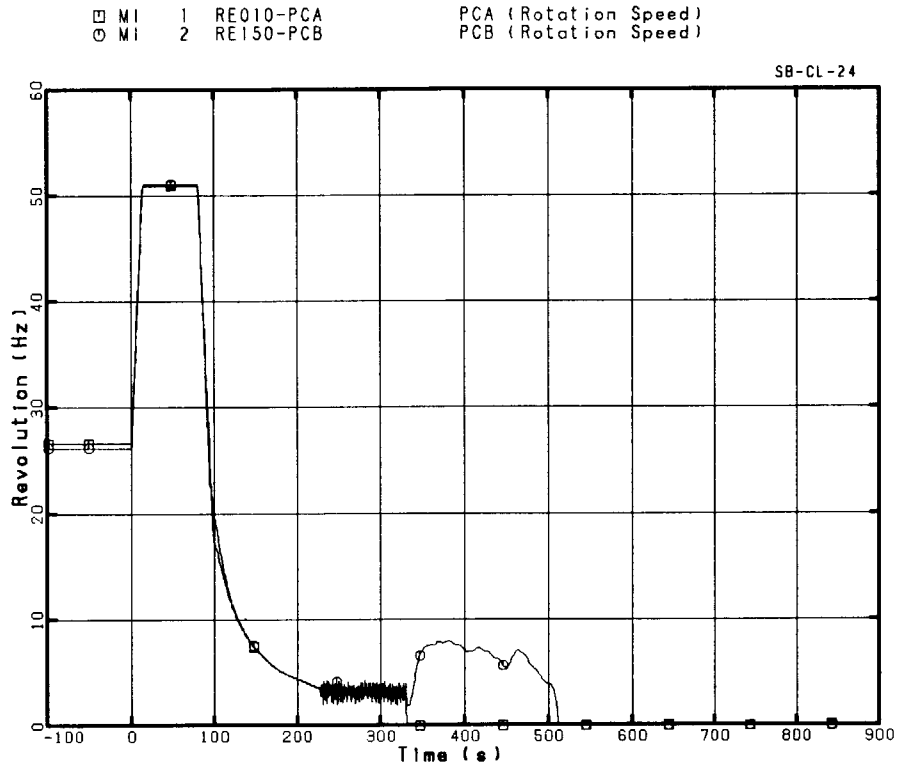

Fig. 3. 2. 5 Primary coolant pump speeds

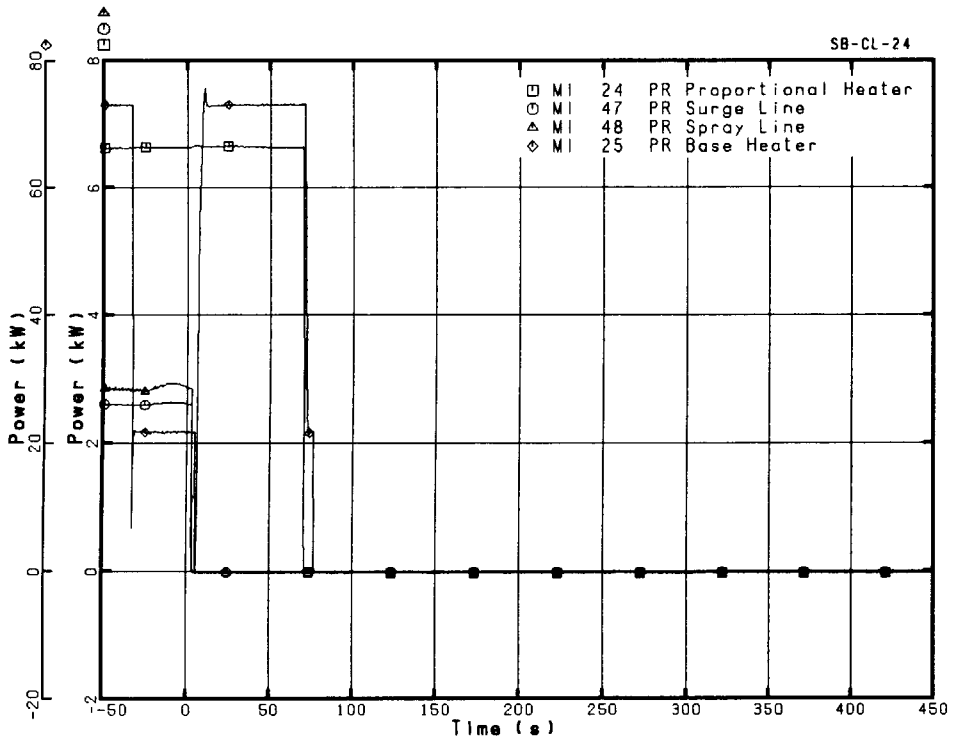

Fig. 3. 2. 6 Pressurizer heater powers in Experiment SB-CL-24

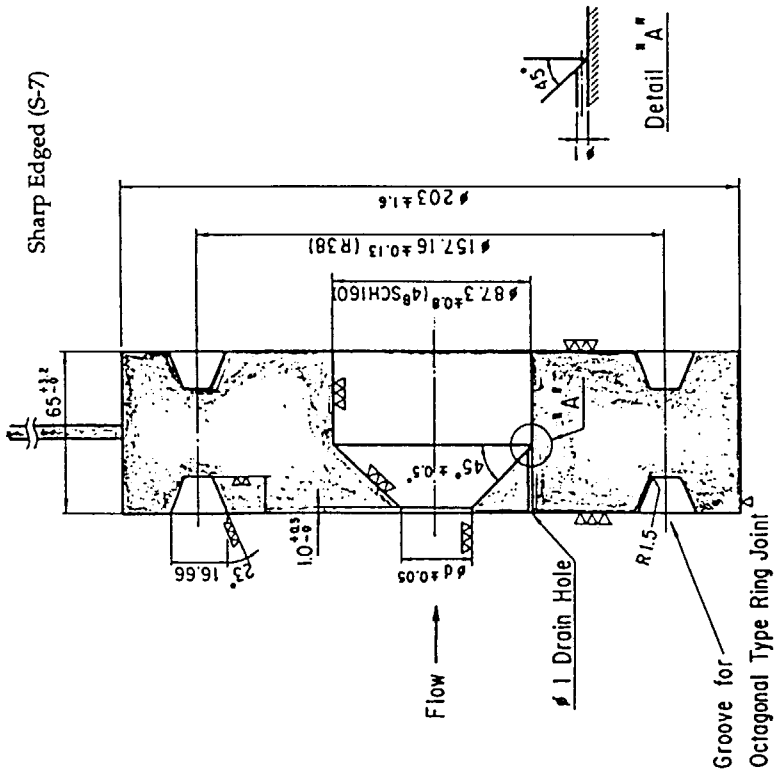

orifices for pressurizer PORV and SV

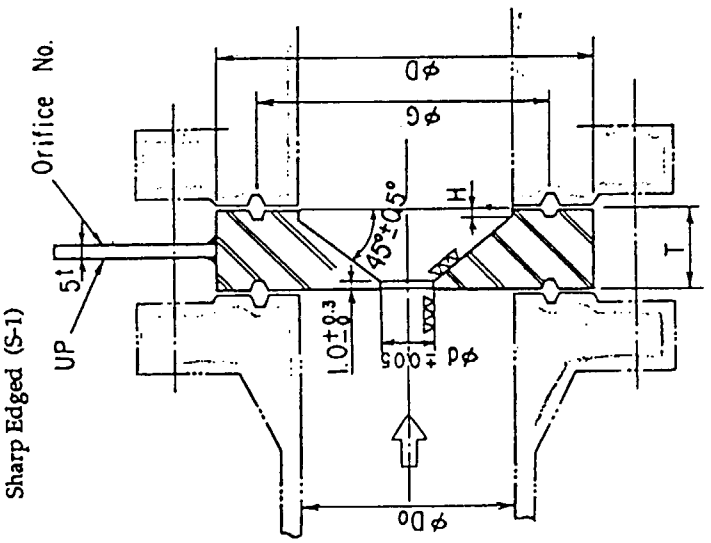

orifices for SG-RVs

Fig. 3. 2. 7 Geometry of orifices for SG-RVs, pressurizer PORV and SV

4. Test Results of Experiment SB-CL-24

The experiment SB-CL-24 was conducted on February 28, 1990 with the specified boundary and initial conditions shown in the previous chapter. Described in this chapter are experiment results on the general thermal-hydraulic behaviors in the 0.5% SBLOCA phenomena associated with the secondary depressurization action, and the repeated core heatup phenomena which were observed in three LSC processes and in the following boil-off process (Sections 4.1 through 4.3). In addition to these, typical responses of the accident indication systems including the CETs and the water level meters are described in Sections 4.2 and 4.3, respectively. An energy balance at both SGs and steam condensation in the SG U-tubes are described in Section 4.4.

4.1 General Thermal-hydraulic Behavior

This experiment is characterized by four typical phases, i.e., ① an initial SBLOCA transient after the break initiated (0 - 600 s), ② a long cooldown transient initiated by the secondary depressurization action, including the core heatup phenomena repeated twice in the LSC processes and the intermittent accumulator injection (600 - 4163 s), ③ a primary pressurization phase caused by loss of the secondary heat sinks, including the third LSC and initiation of the boil-off core heatup (4163 - 6568 s), and ④ a rapid depressurization phase initiated by the pressurizer PORV opening to lead the LPI injection (6568 s - end). These are described in the subsections of 4.1.1 through 4.1.4.

Events and actions in this experiment are listed in Table 4.1-1. The four typical phases and the major events are briefly indicated in the pressure responses, the break flow and the discharged mass, the reduced collapsed water levels in PV, and the typical heater rod temperatures (see Figs. 4.1.1 through 4.1.4). The core power decay was simulated until 7109 s and thereafter a degraded power was supplied to protect the heater rod from overheat. Even after the break valve was closed at the test end (7844 s), the data acquisition continued until 8300 s. The measurement uncertainties for the experiment data are included in the measurement list of Table 2.2-2.

4.1.1 Core Cooling during Initial Transient (0 - 600 s)

(1) Break Initiation and Scram Trip Signal

Experiment SB-CL-24 was initiated by opening the BU air-operated valve (AOV-300) in the

cold leg B (CL-B) and the primary coolant pumps were immediately powered to speed up to the specified speed. The mass discharge from the break caused the pressurizer level decrease and the primary pressure decrease (see Fig. 4.1.5). The proportional and base heaters in the pressurizer were tripped off by the low level signal between 70 and 77 s. When the primary pressure decreased to 12.97 MPa at 75 s, the scram signal was generated, which tripped to start the primary pumps coastdown (80 s), isolation of the SG steam and feedwater lines (78 to 81 s), and initiation of the core decay power control. The primary coolant started to boil at the core top region at 91 s resulting in increases both in the pressurizer water level and the primary pressure. The core power started to decrease at 110 s from the initial 10MW (see Fig. 3.2.4 (a)).

The pressurizer water level started to decrease again at 125 s due to the significantly decreased core power in addition to the continued mass discharge from the break unit. The pressurizer water level finally decreased below the level range at 216 s and thereafter no recovery was observed during the test.

(2) Responses in SG Secondary System in Initial Phase

After the SGs were isolated, the energy transferred from the primary side to the secondary side raised the secondary pressures to the RV cyclic opening level at 116 s in SG-A and at 126 s in SG-B, respectively. Thereafter, the secondary pressures were maintained within the setpoint pressures (8.03 to 7.82 MPa) until the secondary depressurization action started at 600 s. Representative responses of the steam discharge flow and the pressure at SG-A are shown in Fig. 4.1.6. As the core power decreased with time, the RV closure time lengths became longer and the RV open time length became shorter.

(3) Primary Coolant Flow and Core Cooling Condition in Initial Phase

The primary coolant flows shown in Fig. 4.1.7 were controlled by the primary pump speeds (refer Fig. 3.2.5) until the pumps stopped at 332 s in loop A and at 513 s in loop B, respectively. After the primary pumps stopped, natural circulation flow continued in each loop for several hundreds seconds as long as the SG U-tubes were filled with water.

The coolant temperatures in the core are shown in Fig. 4.1.8 in comparison with the pressurizer temperatures which showed saturated conditions as long as the water remained in the pressurizer until 216 s. The upper core fluid temperatures rapidly decreased as the primary loop flows increased after the break, and they turned to increase when the loop flows started to decrease at 80 s. It is shown that the upper core fluid temperatures at Pos. 9 and Pos. 8 reached a saturated condition at 91 and 95 s, respectively suggesting steam generation in these regions. The steam generation was confirmed by the abrupt de-

creases in the upper core DP data. The middle and lower core fluid tended to saturated conditions as the primary loop flows became stagnant but the bottom core fluid (Pos. 1) remained in a subcooled condition until 600 s.

(4) Void Formation and Mixture Level Responses in Hot Primary Regions

After the top core fluid started boiling, two-phase fluid or a water level was observed in the following primary regions, i.e., the upper plenum (95 s), the HL-A top region (111s, see Fig. 4.1.9), the HL-B top region (116 s) and the upper head (180 s). The hot leg collapsed water levels were kept higher than 0.12 m for the initial 600 s. It is clear that steam generated in the core was continuously transported to the SG U-tubes through these steam spaces above the hot leg water levels. On the other hand, the cold leg fluid remained in subcooled conditions for the initial 600 s as shown in Fig. 4.1.10.

The mixture levels in the PV upper regions were also detected by the conduction probes (CPs, refer Appendix-A) as shown in Figs. 4.1.11 through 4.1.14. Figure 4.1.11 shows data of seven CPs located between bottom (EL 4.157 m) and top (EL 6.038 m) of the upper plenum. The thick broken lines in the figure mean a range of mixture level trajectory. It is shown that the decreased upper plenum mixture level stayed for a long time at a level correponding to the hot leg upper part. Figure 4.1.12 shows that a mixture level in the upper head stayed at a level below the bypass nozzle top (EL 7.381 m). Similarly, the upper downcomer mixture level (see Fig. 4.1.13) started to decrease at 286 s and reached the cold leg top after 600 s. The downcomer CP data (CP 12, EL 5.490 m) near the cold leg center line showed significant fluctuations because the mixture level stayed close to this CP level. Figure 4.1.14 shows a rapid mixture level decrease in the control rod guide tube (CRGT) after 235 s and also shows a constant mixture level below the CP 37 level (EL 4.768 m) after 300 s.

Collapsed water levels in the SG U-tubes were detected in six instrumented tubes at both SGs by measuring DPs as shown in Figs. 4.1.15 through 4.1.18. These data included frictional pressure losses which became negligibly small after the primary pumps stopped. These DP data started to rapidly decrease between 320 and 475 s indicating steam generation or a water level formation in the U-tubes, and the DP data decreased with cyclic fluctuations controlled by the secondary cyclic RV opening. These level decrease behaviors in U-tubes were different each other. These figures indicate that the U-tube collapsed water levels in the inlet sides were higher than those in the outlet sides. This is a result of the pressure balance in the primary system, i.e., a steam flow from the core to the SG resulted in a less total water head in the hot primary region (core, upper plenum, hot legs and SG inlet plena) compared to that in the cold primary region in-

cluding cold legs, loopseal regions and SG outlet plena.

The primary coolant flows (see Fig. 4.1.7) continued for a while after the U-tube fluid started boiling and the two-phase circulation flows became almost stagnant at 673 s in loop-A and at 682 s in loop-B, respectively when all U-tube inlet-side DP data decreased lower than 50 kPa. The primary coolant flows transported the core power to the secondary sides during the initial 600 s, and the core was well cooled by these coolant flows.

4.1.2 Long Cooldown Transient Promoted by Secondary Depressurization (600 - 4163 s)

The secondary depressurization actions were initiated at 600 s (at the primary pressure of 8.15 MPa) by simultaneously opening the RVs of both SGs, and thereafter the primary system cool down was promoted by these actions in addition to the continuing break flow. The AIS (ACC and ACH) started at approximately 4.5 MPa with significantly oscillated injection flow rates, which were a result of the primary pressure oscillation, and the AIS injections were interrupted in a short time after the first LSC. The core was well cooled during this phase (600 to 4163 s) except for two short times prior to the first and second LSCs, in which the upper core region partially showed temporary heatups. The primary cooldown by the secondary depressurization actions was almost terminated when the SG secondary water levels reached 0.4 m above the bottom at 4163 s.

(1) Secondary Depressurization Action

The secondary pressures were lowered by changing the RV open/close setpoints to achieve a temperature descending rate of 100 K/h. The primary pressure followed the secondary pressures as shown in Fig. 4.1.1. Figure 4.1.19 shows DPs between the primary and secondary systems (DP between the inlet plenum top and the secondary side bottom at each SG). These data in the initial 390 s are not qualified. It is shown that these DPs oscillated in a positive domain accoding to the RV cyclic opening at each SG, and their mean values were almost constant in a time period from 600 s to the first LSC (2831 s) indicating effective depressurization actions on the primary cooldown.

During the secondary depressurization action, the collapsed water levels in the U-tubes (refer Figs. 4.1.15 through 4.1.18) continued to decrease and the U-tube primary sides were finally filled with steam at 927 s in the SG-A outlet sides, 1200 s in the SG-B outlet sides, 1244 s in the SG-A inlet sides and 2127 s in the SG-B inlet sides, respectively. It is shown in the U-tube DP data that the collapsed water levels in the outlet sides decreased earlier than in the inlet sides at each SG. After the water levels diminished in the U-tube outlet sides, the inlet side DP data showed simultaneous oscilla-

tions with similar amplitudes among the six instrumented tubes. On the other hand, larger water masses remained for a longer time in the SG-B U-tube inlet sides than in the SG-A U-tube inlet sides. Even after the U-tube water levels completely diminished, the secondary depressurization was effective as long as a part of the U-tubes was covered by the secondary water level (see Fig. 4. 1. 20).

After the first LSC occurrence at 2831 s, the DP data between the primary and secondary systems temporarily showed negative values. This DP decrease was due to two reasons, i. e., one is a faster depressurization in the primary system, which was caused by the steam discharge through the break unit, and another one is a rapid steam condensation in the cold legs in which the temporarily increased AIS water mass directly contacted with steam.

Then the DPs between the primary and secondary systems recovered and started to gradually increase until the second LSC occurred at 4009 s. These gradual DP increases mean lowered heat transfer from the primary to secondary systems as a result of the secondary water level decrease in two SGs. After the CL-B AIS injection was terminated at 3537 s, steam condensation in the CL-B was not significant after the second LSC. Then the DP data between the primary and secondary systems started to increase faster than the previous period. Although the RV cyclic opening was continued at two SGs, the primary system pressure finally started to increase at 4163 s (refer Fig. 4. 1. 1) when the SG secondary water levels were at approximately 0. 4 m. Both secondary water levels reached the bottom at approximately 5067 s (see Fig. 4. 4. 4).

(2) Phase Separation in Cold Legs

After the secondary depressurization action started, a steam phase appeared in the upper region of cold legs (Beam A) at 635-638 s (see Fig. 4. 1. 10). The CL-B fluid density at beam B which crossed the pipe wall at the center line level, showed decrease at 753 s indicating an initiation of two-phase flow discharge through the break nozzle. The break flow rate (see Fig. 4. 1. 2) significantly decreased after this time. Thereafter, the cold leg steam region gradually expanded until the AIS actuation at 2110 s, which rapidly increased the cold leg fluid density as shown in Fig. 4. 1. 10.

On the other hand, the hot leg collapsed water level was detected only in the pipe top region between 246 and 2110 s and it was kept higher than the cold leg collapsed water level. It is also shown in these figures that the RV cyclic opening in two SGs significantly affected the fluid density data or collapsed water levels in both hot and cold legs with the same oscilating period.

(3) AIS Injection into Cold Legs

Figures 4.1.21 and 4.1.22 show the injection flow rate, the tank water level and the pressure in the injection line of the loop A accumulator (ACC) and the loop B accumulator (ACH), respectively. The injection flow rate (RC 109 or RC 108) was derived from the mass inventory data in each accumulator tank. Both accumulators started to injection at 2110 s. It is shown in these figures that the ACC and ACH flow rates significantly oscillated accoding to the cyclic primary pressure change. A ratio between the ACC and ACH flow rates was approximately 3 : 1, as specified. It should be noted that the AIS injection flow rates became almost zero whenever the oscillating primary pressure became the highest in each cyclic period.

It should be also noted that these AIS injection rates temporarily increased immediately after the first LSC (2831 s) because of the rapidly decreased primary pressure. After this temporary increase, the AIS injections stopped in a short time (2886 to 3026 s) due to the slightly increased primary pressure as shown in the figures. The temporary increase of the ACC injection flow was observed again after the second LSC at 4009 s.

The AIS injection continued until the water level decreased to each low setpoint and the ACH and ACC injections stopped at 3537 s and 4086 s, respectively. A total amount of the ACH water injected into the CL-B was 553.1 kg and that of ACC water into the CL-A was 1675.6 kg, respectively. These masses are just in a ratio of 3 : 1 between the CL-A and the CL-B. A sum of these injected masses was 2228.7 kg which is equivallent to 41% of the initial primary mass inventory of 5401 kg (refer Section 4.3.1).

(4) Mixture Level and Mass Distribution in Primary System

During the second phase (600 - 4163 s), the primary coolant discharge from the break and the injected AIS water controlled the remained primary fluid mass. Two phase break flow changed again to a water phase flow after the AIS actuated. Thereafter, the break flow repeated a steam discharge and a water-phase discharge according to the LSC and loopseal reformation processes of the first and second LSCs. The primary mass distribution and the core cooling conditions during the second phase are described below. The repeated LSC phenomena related to the primary mass distribution are precisely described in Section 4.3.

Five CPs were vertically installed in both inlet and outlet plena at each SG in order to detect mixture levels but some of the CP measurements were failed. The measured CP data showed cyclic oscillations accoding to the primary pressure changes. Figures 4.1.23 and

4.1.24 show mixture levels detected by the CPs between the SG-A outlet plenum and the loopseal-A bottom, and those in the SG-A inlet plenum, respectively, from the test start to 2700 s. The mixture level in the SG-A outlet plenum started to decrease from the top (CP 469, EL 7.582 m) just after the collapsed water levels in the U-tube outlet sides became zero at 927 s, and it reached the outlet plenum lower part (CP 466, EL 6.482 m) at approximately 1200 s. Similarly the mixture level in the SG-A inlet plenum started to decrease from the top (CP 464, EL 7.582 m) after the water levels in the U-tube inlet sides became zero at 1244 s, and it reached the plenum bottom (CP 460, EL 6.332m) at approximately 1700 s. Figure 4.1.24 includes the DP data measured between the top and bottom of the SG-A inlet plenum, which represented a collapsed water level in the plenum, and a good correspondence was confirmed between the collapsed water level decrease and the CP data mixture level responses in the SG-A inlet plenum.

Figures 4.1.25 and 4.1.26 show similar mixture level responses between the SG-B outlet plenum and loopseal-B bottom, and in the SG-B inlet plenum, respectively. The SG-B outlet plenum mixture level started to decrease at the upper part (CP 478, EL 7.182 m) after the collapsed levels in U-tube outlet sides became zero at approximately 1200 s, and reached the plenum bottom (CP.475, EL 6.332 m) at approximately 2100s. The SG-B inlet plenum mixture level decreased after the U-tube collapsed water level became zero at 2127 s. The DP data in the SG-B inlet plenum showed a good correspondence with the CP data mixture level decrease like as in the SG-A inlet plenum. The decrease of SG-B inlet plenum mixture level started after the AIS initiation at 2110 s.

It is shown in these figures that the mixture level in the SG outlet plenum started to decrease earlier by more than 300 s compared to that in the inlet plenum for both SGs. On the other hand, the SG-B inlet plenum mixture level was kept higher than that in the SG-A inlet plenum for a long time (approximately 900 s) as a result of larger pressure difference from the SG-B to the CL-B break location compared with a DP across the SG-A. These asymmetrical U-tube fluid behaviors between the intact and broken loops are common for the cold leg break experiments.

Figures 4.1.27 through 4.1.30 show the CP data mixture levels measured in the SG plena between 2400 and 5400 s (following the experiment data in Figs.4.1.23 through 4.1.26). It is shown in these figures that no mixture level was detected in the outlet plena of both SGs and SG-A inlet plenum during the first and second LSC processes. Only the SG-B inlet plenum was temporarily filled with two-phase fluid after the first and second LSC occurred. On the other hand, the mixture levels in both loopseal downflow-sides showed decreases before each LSC time and recoveries after each LSC time. The level recovery in

the loopseal-A occurred immediately after each LSC, while that in the loopseal-B occurred with certain time delay from the LSC time and in smaller heights compared with the loopseal-A level behaviors. The delayed level recovery and the smaller level height in the loopseal-B was due to a larger steam flow from the SG-B to the CL-B break location after each LSC occurrence compared with fluid conditions in the loop-A. The larger SG-B steam flows also caused the mixture level increase after each LSC only in the SG-B inlet plenum.

Figures 4.1.31 and 4.1.32 show fluid densities measured between 2400 and 5400 s in the HL-A and CL-B, respectively. The HL-A density data show a temporary level recovery after the first or second LSC occurred. The hot leg top region (Beam A) was not covered by a mixture level even after the LSCs. The HL-B fluid density data showed similar behaviors but slightly higher values compared with those in the HL-A. Figure 4.1.32 showed an almost water-filled condition in the CL-B before each LSC time and a rapid change to a steam condition just after each LSC. It is also shown in this figure that the CL-B was no more completely filled with water after termination of the AIS injection (4086 s).

(5) Core Cooling Conditions during Repeated LSC processes

A typical mass distribution in the primary system after the second LSC (4160 s, just before the primary pressurization start) is illustrated in Fig.4.1.33. Namely, mixture levels were observed in upper regions of the hot legs, the SG-B inlet plenum, the upper plenum, the upper downcomer and the loopseal-A region. On the other hand, both cold legs, the loopseal-B region, the SG-A plena and the U-tubes at two SGs were almost filled with steam. At this time, steam generated in the core mainly passed the SG-B toward the CL-B break. The core was completely covered by a mixture level after the second LSC time. The remained primary coolant mass of 1906 kg (35.3% of the initial mass) in Fig.4.1.33 was slightly lower than a value estimated from the primary mass balance (see Section 4.3.1).

Figure 4.1.34 shows the collapsed water levels in the upper plenum and the core between 2400 and 5400 s. The collapsed water level in the upper plenum was kept constant at approximately 1 m above its bottom elevation (EL 4.06 m) except for the level decreasing periods prior to each LSC. The constant collapsed level in the upper plenum corresponded to the hot leg levels which were kept in the top region. It is shown that the upper plenum collapsed water level started to decrease for the first time from this 1 m level at approximately 2442 s (earlier than the first LSC occurrence by 389 s), and reached zero level at approximately 2700 s. This level recovered immediately after the first LSC. In the second LSC process, this level started to decrease again at 3415 s (594 s prior to the LSC) and became zero at 3845 s. It rapidly recovered after the second LSC.

On the other hand, the core collapsed water level was kept almost constant at approximately 2.8 m above the bottom (EL 0.0 m) before the primary pressurization start except for short time decreases to approximately 2.0 m at the first and second LSCs. When the core was covered with a mixture level with the collapsed level data of 2.8 m, an average void fraction in the core was estimated as approximately 0.3. When the core collapsed water level decreased to the minimum level of 2.0 m, a part of the upper core showed a temporary heatup as shown below.

Figures 4.1.35 and 4.1.36 show the regional DP data with the fluid temperatures in the upper half core, and the representative heater rod surface temperatures (B-18 high power rod), respectively, between 2400 and 5400 s. It is shown in these figures that DP data in the upper core region decreased to minimum values with significant oscillations. The heater rod temperature showed temporary increases at Pos.8 just before the first and second LSCs and rewetted after the LSCs.

4.1.3 Primary Pressurization and Boil-off Core Heatup (4163 - 6568 s)

As the secondary water levels decreased to the SG bottom, the primary depressurization stopped and the primary pressure started to increased at 4163 s. The primary coolant decrease was promoted. Then the core was twice heated up in this third phase, i.e., one in the third LSC process and the other one in a boil-off process. This primary pressurization continued until the operator actions started to open the pressurizer PORV (6568 s) and the SV (6610 s) for promotion of the LPI actuation.

(1) Degraded Heat Sinks at Two SGs and Primary System Pressurization

The primary system started to pressurize at 4163 s (refer Figs.4.1.1 and 4.1.19) when the collapsed water levels in the SG secondary sides became lower than 0.4 m above the bottom as mentioned previously. This means that a sum of the primary-to-secondary heat transfer rates, the energy discharge through the break and a system environmental heat loss became lower than the core decay power (approximately 1 MW at 4163 s). The degraded heat sink at two SGs is a major reason of the primary pressurization (see Section 4.4.4). Thus, the secondary depressurization actions at two SGs became ineffective after 4163 s.

The degraded heat removal at two SGs also resulted in decreases of the primary pressure oscillations. The primary pressurization resulted in slight decreases in the core void fraction (refer Figs.4.1.34 and 4.1.35) and in slight increases in the fluid density in the hot legs.

(2) Primary Mass Decrease and the Third LSC Occurrence

During the third phase (4163 - 6568 s), the primary mass inventory decreased from 36.8 to 24.4% of the initial primary mass (estimated as 5401 kg, see Section 4.3.1). The responses of mixture and collapsed water levels in the primary system during the third LSC process are described below.

After the second LSC occurred at 4009 s, the loopseal-B and the CL-B regions were filled with steam except for their bottom parts in which water remained in small amounts. The CL-B water level started to increase at 4579 s (see fluid density data in Fig. 4.1.32) and the loopseal-B water level (Fig. 4.1.29) increased from approximately 4870 s. Thereafter, a manometric pressure balance in the primary system caused again the temporary water level decrease in the core and the resulting core heatup as shown in Figs. 4.1.34 through 4.1.36. This third core heatup was terminated by the third LSC occurrence at 5122 s. After the third LSC, the loopseal-A region was filled again with water while the loopseal-B region was no more filled with water until the LPI actuation (7371 s).

It is shown in Fig. 4.1.36 that the increased rod temperatures during the third LSC process was higher than those during the first and second LSC processes. The better core cooling conditions in the first two LSC processes than the third one can be ascribed to (a) an effect of fall-back condensed water from the two SGs, and (b) higher mixture level swelling in the upper core region in the primary depressurization process, while the effects became small in the later pressurization phase. The minimum collapsed water level of 2.0 m in the core during the third LSC (5122 s) caused a core heatup between Pos. 9 through Pos. 7, and the core mixture level decreased to a minimum level just above Pos. 6 elevation (EL 2.236 m). The highest heater rod temperature during the third LSC process was 543 K (super-heated by 36 K) at Pos. 8.

(3) Significant Core Heatup during Boil-off Process

The upper plenum mixture level started to decrease again after a short time from the third LSC. Figures 4.1.37 and 4.1.38 show the mixture levels between 5100 and 8100 s detected by the CP data in the upper plenum and the core (from CP 441 at Pos. 9 to CP 436 at Pos. 4), respectively. After the upper plenum mixture level became zero, the core mixture level started to decrease and reached the half core elevation (CP 437 at Pos. 5, EL 1.830 m) before the time of PORV opening (6568 s).

The mass loss in the core resulted in significant core heatup. Figure 4.1.39 shows representative heater rod temperatures (high power rods in bundle 18) at nine different

vertical elevations between 5100 and 8100 s. Figures 4.1.40, 4.1.41 and 4.1.42 show the core top (Pos.9) heater rod temperatures in the peripheral region (low power rods), the intermediate region (high power rods) and the central region (middle power rods), respectively. The heater rod temperatures in the peripheral bundles at Pos.7 are shown in Fig.4.1.43 to compare the heatup distribution in the horizontal domain between two elevations at Pos.9 and Pos.7. In addition, heatup and quench behaviors of all heater rods with instrumentation were compared with both responses of the collapsed water level (DP measurement between EL -0.035 and 3.945 m) and the mixture level trajectory in the core as shown in Fig.4.1.44. The collapsed level (DP measurement between 4.060 and 6.135 m) and the mixture level trajectory in the upper plenum are also shown in this figure.

The following are derived as the boil-off core heatup behaviors.

(a) The upper half core started heatup from the top (Pos.9 at 5929 s) to middle core (Pos.5 at 6536 s) during the boil-off process. The heatup initiation times in the bundles close to the hot leg sides were significantly delayed from those in the other bundles. Thus, the heatup initiation times distributed from 5929 to 6619 s at the core top (Pos.9), from 6070 to 6589 s at Pos.8, from 6180 to 6477 s at Pos.7 and from 6327 to 6396 s at Pos.6, respectively. As the SG secondary temperatures continuously decreased in the boil-off process, condensed steam in the SG U-tubes fell back to the core through the hot legs. This fall back water is a reason of the delayed heatups observed in peripheral bundles close to the hot leg sides. It is shown that the rod heatup speed depended on both the rod power density and the local distribution of fall-back water.

(b) When the core was covered with mixture level after the third LSC, an average void fraction in the whole core was estimated from the collapsed level data (Fig.4.1.44) as 20% at 5400 s, and a regional void fraction in the upper core was estimated from each DP data (see Fig.4.1.35) as 30% at the top (EL 3.251 to 3.945 m), 37% (EL 2.845 to 3.251 m), 33% (EL 2.439 to 2.845 m), 26% (EL 2.033 to 2.439 m) and 22% at the middle (EL1.628 to 2.033 m), respectively. Similarly, an average void fraction in the upper plenum was estimated from the mixture and collapsed levels as 16%. Thus the upper core void fraction was approximately two times higher than that in the upper plenum. This higher void fraction and a narrower cross-sectional flow area in the core compared with those in the upper plenum resulted in faster mixture level decrease in the core than in the upper plenum as shown in Fig.4.1.44.

(c) A rod heatup front, i.e., a trajectory of the first heatup time at each core height, agreed well with the core mixture level detected by the CP data during the boil-off core heatup period as shown in Fig.4.1.44. On the other hand, a trajectory of the de-

layed heatup points at Pos. 9 through Pos. 7 did not agree with the mixture level responses.

(d) Measurements of a mixture level and a collapsed water level in the upper plenum are valuable to predict the forthcoming core heatup, and those in the core are valuable to directly detect the core heatup.

4.1.4 Primary Depressurization Action to Lead LPI Injection (6568 s to end)

In this experiment, intentional actions to open the PORV and SV at the pressurizer were adopted after detecting the core heatup by the heater rod temperature measurements. By these actions, the primary system was rapidly depressrized and the LPI injection was promoted to cool down the heated core as shown below.

(1) Primary Depressurization and Accompanied Mass Loss

The primary depressurization was conducted by operator actions in two steps, i.e., first to open the PORV (orifice diameter of 6.83 mm) at 6568 s and secondly to open the SV (orifice diameter of 14.5 mm) at 6610 s. By these actions, the primary pressure started to decrease from 3.75 MPa at 6568 s, and reached the LPI actuation pressure (1.20 MPa) at 7371 s. In addition to these actions, the secondary RV cyclic opening was continued with long time intervals as shown also in Fig. 4.1.45.

On the other hand, the primary coolant further decreased by the opening of PORV and SV in addition to the break flow. Figures 4.1.46 and 4.1.47 compare the primary mass distribution maps at two times just after the pressurizer SV open (6620 s) and just before the LPI initiation (7366.2 s), respectively. It is found that the primary mass decreased by 400 kg (from 23 to 16 % of the initial mass) between these two times. The decreased mass of 400 kg consisted of 308 kg (77%) discharged through the PORV and SV, and 92 kg (23%) discharged through the break unit.

(2) A Temporary Core Cooling and Limited Core Power before LPI Actuation

Figure 4.1.38 shows a temporary mixture level swell in the core after the PORV and SV openings and Figs. 4.1.39, 4.1.43 and 4.1.44 show that a part of the heated core was temporarily cooled by this mixture level swell. Namely, the heated core at Pos. 5 (EL 1.830 m) and Pos. 6 (EL 2.236 m) were temporarily quenched and that at Pos. 7 (EL 2.642 m) showed a slight temperature decrease during this level swell period. On the other hand, the mixture level swell did not cool the core top region (Pos. 9) but caused further temperature excursions due to the hot steam arrival from the lower region with the higher temperatures.

As the mixture level swelling became almost diminished, the rewetted core at Pos. 6 showed again a temperature excursion and the upper core was heated further. When the maximum heater rod temperature reached a setpoint temperature of 908 K at 7109 s, the core power was controlled to a 75% value of the normal core decay power in order to suppress the temperature excursion. As the core heatup lasted, the core power was further decreased step by step as shown in Fig. 3. 2. 4 (b) and finally reached a 10% power at 7166 s. The maximum heater rod temperature was detected as 921 K at 7167 s in the high power bundle (Pos. 8 of rod(4, 4) in No. 18 bundle) after the core power was reduced to 10% decay power. The middle height of the core (Pos. 5) started to heatup again at approximately 7320 s.

(3) Primary Mass Recovery and Final Core Quench after LPI Actuation

The LPI system started to inject water into cold legs at 7371 s as shown in Fig. 4. 1. 48. An actual ratio of the injection flow rates between CL-A and CL-B was not 3 : 1, but the CL-A flow rate was dominant as shown in the figure. This was due to an inadequate flow resistance ratio between the two injection paths. Despite the inadequate flow distribution between the cold legs, the injected water rapidly filled the PV region as shown in Fig. 4. 1. 44. The heated core was finally quenched by the LPI water until 7675 s.

In this core reflooding process after the LPI actuation, a core quench front which was determined by the heater rod quench times at various elevations, agreed well with the mixture level transient detected by the CP data as shown in Fig. 4. 1. 44. After the core was finally quenched, the core power supply was terminated at 7822 s and the break valve was closed at 7844 s to terminate the test.

4. 2 Detection of Core Heatup by Temperature Measurements

In this experiment, the primary depressurization action to open the PORV was initiated after the core heatup was detected by thermocouples (T/Cs) embedded on the heater rods. In a practical use to detect a core heatup at an actual PWR, the core exit thermocouples (CETs) are installed at the core exit instead of the fuel rod temperature measurements. In addition to these, the fluid temperature measurements in the hot legs can be also available. The temperature responses of the heater rods in this experiment are related to those of the CETs, the hot leg temperatures and the upper plenum temperatures during both the repeated LSCs and the boil-off core heatup processes as shown in the following sections.

4.2.1 Core Heatup Distribution during Repeated LSC Processes

The heater rod surface temperatures were measured in this experiment by 30 T/Cs at the core top (Pos. 9), 38 T/Cs at Pos. 8, 38 T/Cs at Pos. 7, 38 T/Cs at Pos. 6 and 53 T/Cs at the middle height of core (Pos. 5). The non-heated rod surface temperatures were also measured by 5 T/Cs at Pos. 9, 4 T/Cs at Pos. 8, 9 T/Cs at Pos. 7, 9 T/Cs at Pos. 6 and 9 T/Cs at Pos. 5. Nine rod bundles among the twenty four bundles have no T/Cs at Pos. 9, while all bundles have one or more T/Cs in the horizontal domains at Pos. 8 through Pos. 5. An uncertainty of these temperature measurements is ± 6.3 K.

All these temperature responses during the repeated LSC processes were investigated and heatup or non-heatup bundles were grouped into five with respect to an increased value (ΔT) of rod temperature above the saturation temperature as shown in Fig. 4.2.1. Namely, the five groups are; (a) a bundle with the most highly heated rod at $\Delta T \geqq 50$ K is shown by a solid circle around each bundle number, (c) a bundle with a minor rod heatup at $\Delta T \leqq 13$ K (two times of the measurement uncertainty) is shown only by its number, (b) a bundle with an intermediate rod heatup between (a) and (c) is shown in a broken line circle, (d) a bundle with non-heatup rod is shaded by horizontal lines and (e) a bundle with no T/C is shown by a vacant box which exist only at Pos. 9. A hemicircle or a half-shaded bundle means a mixed condition of two behaviors among these heatup types.

The following are derived from the core heatup behaviors during the repeated LSCs.

(a) All instrumented bundles at the core top (Pos. 9) showed no heatup in the first and second LSC processes (except for an insignificant heatup at No. 18 bundle in the second LSC) under the primary depressurization phase. On the other hand, a half number of the instrumented bundles at the core top showed a slight heatup in the third LSC process (primary pressurization phase) but the bundles located near the hot leg directions (shown by arrows toward outside at 20° and 200° in Fig. 4.2.1) showed no heatup. The highest value of ΔT at the core top was approximately 50 K in the No. 18 bundle. The better core cooling conditions in the first and second LSC processes than those in the third LSC process can be ascribed to a higher mixture level swell in the core which was promoted in the primary depressurization process.

(b) At the Pos. 8 elevation, a part (20 to 40 %) of the bundles showed a slight heatup with the highest value of $\Delta T \leqq 26$ K during the first two LSC processes. On the other hand, most of the bundles showed heatup including higher rises of 78 K $\geqq \Delta T \geqq$ 65 K in seven high-power bundles (No. 13 through No. 20 except for No. 15). Three bundles close to the HL-B direction (with arrow at 20°) showed no heatup, and six bundles included

both heatup and non-heatup rods in the third LSC process.

(c) At the Pos. 7 elevation, a slight heatup ($\Delta T \leqq 16$ K) was observed in the first LSC process among 16 heatup bundles, and an insignificant heatup was observed in five bundles during the second LSC process. On the other hand, most of the rod bundles showed significant heatups including temperature rises of $\Delta T \leqq 68$ K at the high-power bundles in the third LSC process, but five bundles at the HL-B side and three bundles at the HL-A side included no heatup rods indicating a better cooling condition in these hot leg side bundles.

(d) Thus, the better cooling conditions in the hot leg side bundles was commonly observed in three LSC processes, and the higher heatups were mainly observed in the high-power bundles. This heatup distribution in the horizontal domain was due to the fall-back condensed water from the SG primary sides under the continued secondary depressurization actions at two SGs.

4.2.2 No Heatup Detection by CETs and HL Temperatures during Repeated LSCs

Twenty CETs measured fluid temperatures at the exit of upper core plate (EL 4.044 m). As the upper plenum collapsed water level completely diminished in each LSC process (refer Fig. 4.1.34), the CETs were repeatedly uncovered by water level for a short time in each process. The measured CET data, however, showed no temperature increase above the saturation temperature during the repeated LSC processes as shown below.

All the CETs showed only a saturation temperature between 2400 and 5400 s as shown in Fig. 4.2.2. It is easy to understand that the CETs did not detect the core heatup during the first and second LSC processes since the heater rods at the core top (Pos. 9) showed no heatup in these periods. In the third LSC process, however, the CETs detected no heatup despite a half number of rod bundles showed heatup at Position 9 as shown in Fig. 4.2.1. Thus, the CETs did not give any core heatup information during all the repeated LSC processes.

The similar CET responses during a LSC process had been observed in some ROSA/LSTF experiments like as a 0.5% cold leg break experiment (SB-CL-15) [12] with an SG-B secondary depressurization action. Major reasons of these CET responses were as follows. First, some amount of condensed water continuously fell on the upper core plate from the hot legs and the CETs were much affected by this water temperature. Secondly, super-heated steam rizing up from the heatup bundles mixed in the mixing zone (below the upper core plate) with saturated steam rizing from the cooled bundles or with falling water through the upper core plate, and the super-heated steam was not detected at the CET locations.

In a case of LSC phenomena at an actual PWR plant, however, these experimental results of the limited CET responses can not be directly applied without any analysis or further experimental results based on an improved scaling concept for the upper plenum configuration. Namely, the LSTF upper plenum has the same height, an approximately 1/7 scaled inner diameter and the higher elevation of the hot leg bottom cpmpared with the reference PWR. These limit a three-dimensional steam flow from the heated core and thus limit the CET characteristics to detect the core heatups in the ROSA/LSTF system.

The temporary core heatup during the LSC processes was not detected by the hot leg temperature measurements as shown in Fig. 4. 2. 3. The hot leg temperatures were measured at two locations in each loop, i.e., one is the PV side and the other one is the SG side. The measured data show almost saturated temperature between 2400 and 5400 s except for superheated temperatures detected at the top part in the HL-A SG-side (TE 8), which was a result of superheated steam flowed out of the pressurizer surge line. Therefore, the HL-A SG-side temperature (TE 8) detected super-heated temperature with no relation to the LSC occurrence. Concludingly, the hot leg temperature measurements also did not give core heatup information during the repeated LSC processes.

4. 2. 3 Detection of Core Heatup by CETs in Boil-off Process

In this section, the core heatup initiation times during the boil-off process are precisely analyzed in each horizontal domain of the upper core region and those at the CETs, and the CET temperature rises are related to the rod temperature increases on a view point of core heatup detection by CETs. Each CET location in the horizontal domain corresponds to one bundle among the twenty bundles and no CET corresponds to four bundles (No. 13, 16, 17 and 20).

(1) Delayed Detection of Core Heatup Initiation

First, all the CET responses between 5100 and 8100 s are shown in Figs. 4. 2. 4 and 4. 2. 5. The boil-off core heatup period and the saturated temperature are shown in the figures. It is found that the CET temperature responses reflected the heater rod temperature responses (refer Figs. 4. 1. 40 through 4. 1. 42) with certain time delays, and that they showed wide distribution between the earliest and the latest responses. The earlist CET temperature increase above the saturation temperature was detected at 6280 s (351 s after the core heatup start) and the latest increase was detected at 6614 s (46 s after the PORV opened). The CETs finally showed saturation temperature when the core heatup was finally terminated at 7675 s.

The heatup initiation times of the CETs are compared with those of the heater rods at Pos. 9 through Pos. 7 in Fig. 4. 2. 6 which indicates a horizontal distribution of the heatup initiation times. In order to analyze the horizontal distribution, the twenty four rod bundles were grouped into six according to their locations; i. e., two peripheral groups (group 6 at the HL-sides and group 5 far from the HLs), an intermediate corner group (group 4), two groups with high power bundles in the intermediate region (group 3 near the HL-sides and group 2 far from the HLs) and a central region (group 1). Each group includes four rod bundles and the four bundles are distinguished each other by a marked circle. For the bundles with two T/Cs, an average value is shown in the figure with a time period bar indicating their heatup initiation times.

The distribution of temperature rise initiation times among the twenty CETs is clearly shown in Fig. 4. 2. 6 in comparison with the core heatup initiation behaviors.

(a) The CET heatups started earlier at the locations far from the HL-sides (groups 5 and 2) compared with the locations at HL-sides (groups 6 and 3), and the CET heatups at the central core region (group 1) were earlier than those in the peripheral regions (groups 4 through 6). It is shown that the CETs above five bundles near the hot leg sides (No. 7, 8, 12, 15 and 19) started to increase after the PORV opened at 6568 s, which forced the superheated steam in the upper core to flow into the upper plenum. These indicate that the CETs near the hot leg sides were significantly affected by the fall-back water from both SGs and that, on the contrary, the CETs in the central core region were less affected by the fall-back water.

(b) These local cooling effects were more significant among the heater rod temperatures at the core top region (Pos. 9). The earliest heatup started at 5929 s in the No. 18 bundle, and heater rods both in the central core (group 1) and regions far from the hot leg sides (groups 2 and 5) showed earlier heatup initiation. On the other hand, heater rods in bundles near the hot leg sides (No. 3, 7 and 15) showed later heatup. The latest heatup initiation at the core top region was 6619 s in bundle No. 7. Therefore, a period between the earliest and the latest heatup times at the core top was 690 s which was more than two times as long as the CET temperature rise distribution.

(c) The heatup distribution in the core at Pos. 8 was slightly shortened compared to that at Pos. 9, and more than half of all bundles showed simultaneous heatup initiation when the mixture level passed the Pos. 8 elevation (EL 3. 048 m). The local cooling effect of fall-back water was also observed in several bundles close to the hot legs.

(d) The core heatups at Pos. 7 started almost uniformly except for three bundles near the hot leg sides. The simulatneous heatups started when the mixture level passed Pos. 7

elevation (EL 2.642 m). Thus, the core heatup behaviors during the boil-off process were controlled by two factors, i.e., one is the core mixture level decrease which caused an uniform heatup in the horizontal domain, and the other one is the fall-back water which caused a local cooling in the hot leg side bundles (with an axial cooling region of approximately one third of the active core length).

Then, a correspondence between heatup initiation times at the CETs and the heater rods at Pos.9 or Pos.8 is shown below. Namely, a heatup initiation time of one CET (t_{CET}) is compared with that of a heater rod at Pos.9 (t_{HR9}) of the same bundle in Fig.4.2.7 (a), and the former is similarly compared with that of a Pos.8 heater rod (t_{HR8}) in Fig.4.2.7 (b). These figures indicate vertical correspondences between the upper core heatups and the CET temperature responses, namely time delays of core heatup detection, during the boil-off process. Figure 4.2.7 (a) shows these correspondences among fourteen bundles and Fig.4.2.7 (b) shows those in twenty bundles. The following are derived from these figures.

(a) The CET delay times for the core top heatup detection widely distributed between - 64 s (bundle 3) and 624 s (bundle 2) and an average delay time among the fourteen delay times was 308 s. A negative value of the detection delay time in bundle 3 means a relatively earlier CET heatup initiation than the delayed rod temperature increase in the hot leg side bundle 3, which was caused by transversely uprising steam flow from the heated bundles. The CET at bundle 7 showed also negative time delay. Most of the detection delay times (including the central four bundles) were between 200 and 400 s from the core top heatup initiations.

(b) The CET delay times for the Pos.8 heatup detection distributed between - 125 s at bundle 3 and 540 s at bundles 8 and 19, and an average delay time among the twenty bundles was 300 s. The CETs in central core region detected the core heatup at Pos.8 with a relatively shorter time delay less than 214 s. On the other hand, the CETs in peripheral bundles (No.1, 2, 4, 8, 10 and 12) showed longer delay times than the average delay time at Pos.8.

(c) Consequently, it is shown that the core heatup detection times by the CET temperature measurements widely distributed around an average delay time of approximately 300 s in this experiment. It is also shown that the CETs in the central core region detected the core heatups with rather shorter delay times.

(2) Super-heated Temperatures at CETs and Core Top Region

Next, the CET temperatures increased above the saturation temperature ($DT = T - T_{SAT}$) are compared with the heater rod temperature rises at Pos.9. All the temperature data of

DT at the CETs and heater rods (Pos. 9) were statistically processed to derive an average value of DT(Average), a maximum value of DT(Maximum) and a minimum value of DT(Minimum) at each time.

Figure 4.2.8 shows these super-heated temperatures obtained from the twenty CETs (refer Figs. 4.2.4 and 4.2.5). It is shown that DT(Average) started to gradually increase at 6280 s, increased faster after the PORV opened, temporarily decreased after 7000 s, reached a maximum value of 173 K at 7585 s and finally returned to zero (within a measurement accuracy of ± 6.3 K) at 7680 s. DT(Maximum) showed similar responses but significantly higher values (less than 125 K) compared to the responses of DT(Average), and reached a maximum value of 301 K at 7620 s. DT(Minimum) showed a later increase, a temporary rewetting after 7000 s and an earlier quench in addition to lower values (less than 119 K) compared to the responses of DT(Average). Thus, all the CET data distributed around the DT(Average) data within a range of ± 125 K except for a quench period after 7560 s.

Figures 4.2.9 through 4.2.12 show the super-heated temperature data for the heater rods at Pos. 9. Figure 4.2.9 was derived from ten heater rod temperatures in eight high power bundles, Fig. 4.2.10 was from twenty heater rod temperatures in other low power bundles, Fig. 4.2.11 was from five non-heated rods (four low power bundles and a high-power bundle) and Fig. 4.2.12 shows a total of all these rod data. The following are derived from the sedata analyses.

(a) The high power rods showed a similar response of temperature increase and all data were included within a narrow range between - 97 and + 70 K around the DT(Average). DT(Average) started to increase at 5929 s, increased faster after the PORV open, showed a maximum value of approximately 428 K for 415 s from 7165 s, and finally returned to zero at 7680 s.

(b) The other heater rods showed lower temperature responses with wider distribution of data around DT(Average) for the low power rods in comparison with those of the high power rod data. All the low power rod data were included within a range between - 126 and + 90 K around DT(Average) which reached a maximum value of 311 K and showed similar but slightly lower values as that of high power rod data.

(c) The non-heated rod temperature responses differed slightly from the above two data. Namely, heatup responses of the non-heated rods were not so widely distributed in the heatup initiation period, but showed similar responses in a later period as those of of low power rods. The non-heated rod temperature data distributed within a range between - 68 and + 107 K around DT(Average). These heatups of non-heated rods are due to

radiation and convection flow effects from adjacent heater rods. The higher value of non-heated rod data than those of the low power rods is ascribed to data of a rod in the high power bundle.

(d) Figure 4.2.12 includes all these core heatup responses at the core top (Pos.9). All these data were included within - 131 and + 125 K around DT(Average) for the boil-off heatup period.

(3) Correspondence of Temperature rises between CETs and Heated Core

Then, the DT(Average) of all rods at the core top is compared with that of CETs during a time period from 5500 to 7500 s in Fig.4.2.13. The core top temperature increases are given by horizontal scales, DTAVE(P9T), and the CET temperature increases are given by vertical scales, DTAVE(UCP Outlet). This comparison is valuable to visualize an overall correspondence between them during the boil-off core heatup process.

It is shown that the CET average temperature increases were almost proportional to the average rod temperature increases at the core top except for the initial detection delay time (before 6280 s) and the temporary cooling period (between 7000 and 7100 s). Namely, most of the average core top temperature increases were represented by the average CET temperature increases as,

$$DTAVE(P9T) = 1.88 \times DTAVE(UCP\ Outlet) + 40\ K$$

within a discrepancy of ± 21 K except for the temporary cooling in the CET data. This discrepancy is very small compared with the maximum distribution around the average CET data (± 125 K) or that around the average core heatup data (- 131 and + 125 K).

It is concluded that the average CET temperature increase data corresponded well to the average temperature increase data at the core top region (Pos.9) during the boil-off process in which the local cooling by fall-back water significantly affected both CETs and core top temperatures to cause a wide temperature distribution of less than ± 131 K around their average temperature data. The limited CET responses during the LSC process and valuable CET responses for core heatup detection during the boil-off process are both clarified in this report. In general, a small number of temperature measurements by CETs is not preferable to accurately detect the core heatup behaviors including the local fall-back cooling effect under a secondary depressurization action.

4.2.4 Detection of Core Heatup by Upper Plenum and Hot Legs Temperatures in Boil-off Process

An alternative measurement to detect the core heatup behaviors can be conducted by the

fluid temperature measurements in the upper plenum or in the hot legs. On this view point, the measured fluid temperatures in these primary regions are comapred here with the core heatup temperature responses.

Figure 4.2.14 shows measured fluid temperatures at the bottom (EL 4.850m), middle (EL 5.503m) and top (EL 6.038 m) in the upper plenum (each T/C was overhanged from surfaces of the control rod guide tubes located far from the hot leg sides) in addition to the reference saturation temperature.

It is shown that all the upper plenum temperatures showed uniform increases after 6125 s, non-uniform increases after the PORV open, decreases after the core power decrease (from 7109 s), and a temporary increase in the core reflooding process (after the LPI actuation at 7371 s). The temperature decreases after 7109 s are ascribed to a decrease of uprising steam flow from the heated core (after the core power decrease) under the decreasing saturated temperature. Consequently, these upper plenum temperatures showed increases in a shorter time after the boil-off core heatup started, rather higher values and uniform data compared with the CET responses (refer Figs. 4.2.4 and 4.2.5). These indicate less influences of the fall-back water on the upper plenum temperature measurements in comparison with the CET measurements.

Figure 4.2.15 compares an average increase of the upper plenum middle temperatures above the saturation condition, DTAVE(UP Middle), with the average increase of core top rod temperatures, DTAVE(P9T), between 5500 and 7500 s. The upper plenum middle temperatures started to increase at the average core top temperature of 28 K and well corresponded to the increasing speed of the average core top temperature until the PORV opened. After the PORV opened, the upper plenum temperature increasing rate slightly decreased. Thus, the average core top temperature increase was represented in two straight lines given by the following equations,

$$DTAVE(P9T) = 1.20 \times DTAVE(UP\ Middle) + 19\ K$$
$$(6200\ s \leqq t \leqq 6568\ s,\quad 0\ K \leqq DTAVE(UP\ Middle) \leqq 87\ K),$$
$$DTAVE(P9T) = 2.42 \times DTAVE(UP\ Middle) - 89\ K$$
$$(6568\ s \leqq t \leqq 7100\ s,\quad 87\ K \leqq DTAVE(UP\ Middle) \leqq 170\ K),$$

within an discrepancy of $\pm$ 13 K. These relations are not held after the core power was degraded at 7109 s.

It is concluded that the upper plenum temperature measurements can be used as an alternative core heatup detection method to the CET measurements during the boil-off heatup process.

The hot leg fluid temperatures during the boil-off process were measured as shown in Fig. 4.2.16 at the A-Loop and in Fig. 4.2.17 at the B-Loop, respectively. The HL-A fluid temperatures were almost in a saturation condition during the primary pressurization process and did not steadily detect an arrival of superheated steam from the core for more than 600 s from the core heatup initiation. The PORV and SV opening actions caused a steam flow from the core to pressurizer and resulted in abrupt increases of the HL-A temperatures.

On the other hand, some of the HL-B fluid temperatures started to slightly increase at approximately 6125 s and showed an increase of 18 K above the saturation temperature at 6500 s indicating an arrival of the upper plenum steam at the HL-B despite the condensed water flow at the bottom of HL-B line. The HL-B temperature increases, however, diminished after the PORV opening and thereafter all the HL-B temperatures showed decreases along the saturation temperature for more than 180 s, slightly higher values above the saturation temperature after 6940 s and a temporary increase in the later core reflooding process. Thus, the HL-B temperature measurements detected an arrival of the upper plenum steam flow for a short time period before the PORV but the increased temperatures were not so high as the upper plenum temperatures. The later temperature increases in the HL-B temperature measurements did not well correspond to the upper plenum temperature responses except for the temporary increase in the core reflooding process.

It is clear that both the secondary and primary depressurization actions significantly affected the hot leg fluid temperatures to result in unstable heatup detection and less corresponding temperature increases to the upper plenum temperatures. Concludingly, the hot leg fluid temperature measurements are less effective than the CETs or the upper plenum temperatures with respect to the core heatup detection during the boil-off process with the secondary depressurization action.

4.3 Primary Mass Distribution Related to Repeated Core Heatups

It is valuable to understand the core heatup behaviors in relation to the primary water level responses or a decreased total primary mass inventory in order to prognosticate an inadequate core cooling condition. In this section, a total primary mass inventory is estimated at first, secondly ineffective AIS contribution to the primary mass recovery is shown, thirdly major events including the core heatups are related to the primary inventory and at last the repeated LSC and reformation processes are precisely described.

4.3.1 Estimated Primary Mass Inventory

An initial primary mass (M_0) was determined by cumulating initial regional fluid masses (M_i in i-th region) which were calculated by using a revised volume (V_i) distribution data base for the primary system (all the active dead volumes such as the connected pipe volumes are included) and fluid density (ρ_i) in each primary region as,

$$M_0 = \Sigma_i M_i \ (t \leqq 0 \text{ s}) = \Sigma_i (\rho_i V_i) = 5401 \text{ kg}. \quad (4.3.1)$$

Therefore, this mass value is sufficiently correct and is consistent to the other LSTF experiments with the same primary system using the second simulated fuel assembly.

In general, a transient mass in the LSTF primary system can be estimated in two ways, i.e., one is a cumulated value (M_C) of the transient regional masses which are accounted by the measured regional fluid density or the collapsed water level reduced from DP data (or gamma-densitometer data) in addition to the revised configurational data base as,

$$M_C = \Sigma M_i \ (t > 0 \text{ s}). \quad (4.3.2)$$

The DP data, however, generally include a frictional pressure loss in the forced circulation flow and an acceleration pressure loss in the rapid pressure transient. These result in increase of mass uncertainty which is not easy to estimate at each time. Therefore, the primary mass M_C reduced from the DP data should be carefully treated in order to lower these mass uncertainties.

The other one is a calculated value by using the following mass balance equation between a total discharged primary mass (M_D), a total injected ECC water mass (M_I), an initial primary mass (M_0) and a total remained mass (M_R) as,

$$M_R = M_0 - M_D + M_I. \quad (4.3.3)$$

The M_D is a sum of masses discharged from the break unit (M_{D1}; $t \geqq 0$s) and from the pressurizer valves of PORV and SV (M_{D2}; $t \geqq 6568$s), while the M_I is a sum of injected masses from the AIS (M_{I1}; $t \geqq 2110$s) and from the LPI system (M_{I2}; $t \geqq 7371$s) as,

$$M_D = M_{D1} + M_{D2}, \quad (4.3.4)$$

$$M_I = M_{I1} + M_{I2}. \quad (4.3.5)$$

The discharged mass of M_{D2} was not measured in this experiment but was calculated from the equation (3) by using a cumulated primary mass of M_C in equation (2) instead of the remained primary mass of M_R. In this calculation, it is necessary that the cumulated primary mass of M_C should be cosistent to the M_R estimated by the mass balance equation at a time before 6568 s. Actually, there was a slight discrepancy of 70 kg (1.3% of M_0) between M_R and M_C at 6504 s,

$M_R = M_C + 70$ (kg) (at t=6504s). (4.3.6)

This discrepancy was the least value during the experiment time, since there was no void in the pressurizing primary water except for the core, there was no forced circulation flow in the primary loops and the remained mass significantly decreased. Concludingly, a corrected primary mass of (M_C + 70 kg) was used to determine the discharged mass of M_{D2} after the time of PORV open (t≧6568s).

Table 4.3-1 shows estimated results of the transient primary mass (M_R; 8016s≧t≧-48s) in this experiment in addition to the total discharged mass, the total injected mass and a ratio of the transient primary mass to the initial mass ($M^* = M_R/M_0$). An uncertainty of the transient primary mass before the PORV actuation was represented by the most influential term of discharged mass through the break ($\Delta M_{D1} = \pm 324$ kg[14]). It should be noted that fluctuations in the discharged masses (M_D) reflected to the transient primary masses (M_R).

4.3.2 Less Mass Accumulation during Accumulator Injection Periods

Figure 4.3.1 shows the primary mass inventory ratio (M^*) in this experiment, SB-CL-24, related to times of the three LSCs, the repeated core heatups, the ECCS injection and other events. The least primary mass ($M^* = 0.168$) was observed when the LPI started.

It is shown in the figure that the primary mass discharge rate slightly increased after the secondary depressurization action started at 600 s and, on the other hand, it gradually decreased after the two-phase flow discharged through the break (at approximately 750 s). Thereafter, the mass discharge rate repeated an apparent decrease and a recovery in the repeated LSC processes. Namely, the mass discharge rate before the AIS actuation (from 1548 to 2052 s) was 0.46 kg/s while that after 2110 s (from 2136 to 2808 s) apparently increased to 1.65 kg/s (more than 3 times as large as the former period). Thus, the primary mass decrease was promoted after the AIS actuation and the mass recovered after the first LSC because of the steam discharge through the break and the increased AIS injection flow rates. This mass change was repeated at the second LSC process.

The increased break flow rates prior to the first and second LSCs are also shown in Fig. 4.1.2. Namely, the CL-B fluid density before 2110 s detected a steam phase at the top (Beam A) and a two-phase fluid at Beams B and C (refer Fig. 4.1.10), respectively. These densities rapidly increased after 2110 s indicating steam condensation and full of water in the CL-B pipe. The subcooled water temperatures were detected in the CL-B after the AIS actuation. These steam condensation and full-of-water condition in the CL-B were al-

so observed during the second AIS injection period (3026 to 4086 s).

At 2110 s, the primary mass remained approximately 41% of M_0. A total amount of injected water from the ACC and ACH was 2229 kg (from 2110 to 4086 s) which was also 41% of M_0. The AIS injection, however, did not increase the primary mass inventory ratio (M^*) over the 41% level during all the experiment. On the other hand, the discharged primary mass during the AIS injection period was M_{D1} = 2478 kg (approximately 46% of M_0) which was larger than the total amount of AIS injected water mass. Therefore, the AIS did not contribute to increase the primary mass inventory above the previous mass level (before the AIS actuation time) but slightly recovered the primary mass by 8 to 4% of M_0 after the first and second LSCs.

In the third LSC process (after termination of the AIS injection), the break mass flow rate slightly increased between 4868 and 5138 s as shown in Fig. 4.1.2. In this period, the CL-B top region was filled with steam (see Beam A in Fig. 4.1.32) and middle to bottom region was filled with almost saturated water when the water level was at approximately 0.12 m. Thus, the break flow increase in the third LSC process was ascribed to the increased fluid density at the break unit which was 0.1 m above the cold leg bottom. The CL-B fluid density increase in the third LSC process was caused by water mass transport from the downcomer region due to a manometric pressure balance during the second loopseal reformation process described in Section 4.3.4.

4.3.3 Repeated Core Heatups Related to Water Level Measurements

The major events including the repeated core heatups during the LSCs and the boil-off processes, and the water levels in the primary system are related to the primary mass inventory as shown in Fig. 4.3.1.

The following are found during this experiment.

(a) The pressurizer water level indication showed zero level at 216 s when the primary mass decreased to M^*= 0.86. Thereafter, no pressurizer level was indicated during the experiment.

(b) The primary mass decreased to M^*= 0.67 when the secondary depressurization started at 600 s. This mass ratio corresponded to water level formation in the primary regions including upper half of the SG U-tubes in both loops and upper parts of the upper head, the upper plenum, the hot and cold legs, and the downcomer, respectively. When the upper plenum collapsed level started to decrease again at 2440 s, the primary mass was

approximately M^* = 0.37. Thus, the upper plenum collapsed water level (see Fig. 4.1.3) remained at a constant value of approximately 1.0 m above EL 4.044 m when the primary mass decreased from 67 to 37% of M_0. This constant collapsed level of 1.0 m in the upper plenum corresponds to the hot leg level at 0.12 m by estimating an average upper plenum void fraction as 0.32.

(c) The three LSCs occurred at similar primary mass conditions (M^*= 0.33 to 0.30), and these mass ratios corresponded to the water mass distribution in the primary regions as typically shown in Figs. 4.3.2 (t=2831.6s) and 4.3.3 (t=5119.4s). Major difference between these figures is due to the different collapsed water levels in the cold legs. At the first LSC time, the collapsed water levels in cold legs were approximately at 0.17 m in CL-A and 0.18 m in CL-B, while those at the third LSC time were approximately at 0.10 m in CL-A and 0.11 m in CL-B, respectively. The total water masses at the times of LSCs corresponded to from 25 to 23% of the total primary volume of 8.03 m^3.

(d) In the boil-off core heatup process, the upper plenum water level began to decrease at approximately M^*= 0.30 and it reached the core top region at M^*= 0.27. Thus, the upper plenum level decrease in the boil-off process corresponded to the primary mass decrease from 30 to 27% of M_0.

(e) Both DP and CP data for the water level measurement between the SG outlet plenum and the loopseal bottom in each loop were also related to the primary mass decrease prior to the core heatup initiation. Namely, the water level in SG-A outlet region started to decrease at approximately 900 s (which was 350 s earlier than the SG-A inlet plenum level decrease) and it corresponded to the primary mass ratio of M^* = 0.56. On the other hand, the water level decrease in SG-B outlet region started at M^* = 0.49. These level decreases continued until the first LSC occurred at M^* = 0.32.

(f) The temporary core heatups during three LSC processes started at M^* = 0.33 to 0.32 and the boil-off core heatup started at M^* = 0.27. When the middle core (EL 1.830 m) was heated up, the primary mass was approximately M^* = 0.24.

(g) The primary mass further decreased by the opening actions of the PORV and SV, and started to recover after the LPI actuation. The core quench caused by the LPI injection occurred at M^* = 0.25.

4.3.4 Investigation on Loopseal Clearing and Reformation Processes

In this section, the loopseal clearing and reformation processes are separately shown. Experiment data of the collapsed water levels in both upflow-side and downflow-side of the loopseal-B region and the calculated primary mass distribution were investigated to clarify mechanisms of the loopseal reformation, i.e., water fall-back from the CL-B region and condensed water fall-back from the SG-B U-tubes.

(1) Time Ranges of Loopseal Clearing and Reformation Processes

The LSC is defined as a phenomenon of water mass sweepout from the cross-over leg (loop-seal region), which enabels to discharge steam cumulated in the primary system out of the break location at CL-B. In this report, a LSC process is defined as a time period of water level decrease at the loopseal downflow region, which terminated by a loopseal occurrence, and a loopseal reformation process is defined as that of the water level increase in the same region. Prior to the end of each LSC process, a rapid water mass loss occurres in the upflow region indicating violent steam passage from the downflow-side to upflow-side of the loopseal region and therefore, this time is defined as an initiation of a LSC, i.e., 2831 s for the first LSC, 4009 s for the second LSC, and 5122 s for the third LSC, respectively.

Figure 4.3.4 shows DP data between the upper plenum and the downcomer during the repeated LSC processes. The first to third LSC processes are noted by C1 to C3 in the figure and the first and second loopseal reformation processes are noted by R1 and R2, respectively. After the C3 process, the third loopseal reformation process (R3) started like as the R2 process. Figure 4.3.5 shows two DP data both in upflow and downflow sides of the loopseal-B region during the same time period. Each loopseal reformation process was divided into several steps, i.e., an early stage of each reformation process with gradual water level increases in the horizontal leg (R1-1, R2-1), and a later stage of each reformation process with rapid level increases both in upflow and downflow sides (R1-2, R2-2 and R2-3). The middle stage of R2-2 in the second reformation process can be distinguished by (a) a contant water level in the downflow-side and (b) a gradual level increase in the upflow side, from the R2-3 stage with their rapid increases.

The numbers ① through ⑤ in these figures denote selected phases for the primary mass distribution shown later. Figures 4.3.6 and 4.3.7 show DP data across the primary coolant pump B and SG-B plena, respectively. Figures 4.3.8 and 4.3.9 show DP data in the loopseal A region and those across the SG-A plena, respectively. It is apparent in Fig. 4.3.8 that the LSC did not take place in the loopseal A region except for a manometric water level depression in the downflow-side. Figures 4.3.10 through 4.3.13 show the mass distribution maps at four selected phases (phases ① through ⑤ except ④ at which the mass distribution map is already shown in Fig. 4.1.33). The loopseal-B water levels at selected phases are presented later (see Fig. 4.3.14).

(2) The First LSC Process (C1)

The first LSC process in loopseal-B region started at approximately 2270 s and ended at

approximately 2855 s when the water level in the loopseal-B downflow-side diminished (see Fig. 4. 3. 5). During this process, the collapsed water level in the core reached a minimum level at EL 2. 0 m (see Fig. 4. 1. 34) and a pressure difference between the upper plenum and the downcomer at EL 5. 503m decreased to a minimum value of -28 kPa.

A rapid mass transport from the loopseal-B to the CL-B at the first LSC was detected by an increased DP data across the primary coolant pump B as shown in Fig. 4. 3. 6. A similar increase was observed in the DP data across the inlet and outlet plena of SG-B as shown in Fig. 4. 3. 7. Although there was no water level in both SG-B plena, some amount of condensed water could be existed in the lower part of U-tubes through which the primary-to-secondary heat transfer continued. In fact, subcooled water temperatures were detected a t the exit of instrumented U-tubes (No. 2 through No. 5 tubes, see Section 4. 4) during the first LSC process. Therefore the increased DP across the SG-B plena can be ascribed to a temporary increase of flow resistance through these U-tubes when the cumulated steam violently passed the SG-B U-tubes in which some amount of condensed water existed.

In the loopseal-A region, water was not completely swept out during the first LSC process. Moreover, there was no DP increase across the SG-A plena during this process as shown in Fig. 4. 3. 9. Therefore, the cumulated steam in the primary system mainly passed the SG-B U-tubes and flowed out of the break. It should be noted that significant pressure oscillations were observed in the DP data between the upper plenum and downcomer, and in both loopseal regions (see Figs. 4. 3. 4 and 4. 3. 5). These oscillations are due to the cyclic SG-RV opening actions and the accompanied AIS injection flow oscillations.

(3) The First Loopseal Reformation Process (R1-1 and R1-2)

The first loopseal reformation process (R1) started at 2855 s and completed by the rapid water refilling in the loopseal-B region at 3352 s (see Fig. 4. 3. 5). After the first LSC, water mass gradually accumulated in the loopseal-B region (stage R1-1) from two ways, i. e., one from the CL-B in which the ACH water was injected and other one from the SG-B U-tube outlets from which some amount of condensed water flowed down. At approximately 3240 s, the collapsed water level in the loopseal-B upflow-side was 0. 08 m above the bottom (EL 1. 701m) and that in the loopseal-B downflow-side was 0. 06 m, respectively. After 3240 s (stage R1-2), the upflow-side DP started to increase faster than the previous period indicating rapid water accumulation in the upflow-side, and the downflow-side DP increased rapidly from 3341 s.

An average water volume increasing rate in the loopseal-B region was calculated during the R1-1 stage (from 2892 to 3228s) as 3.8×10^{-5} m^3/s, and that in R1-2 stage (from 3240

to 3341s when the collapsed water level in the loopseal-B downflow-side was 0.12 m and that in the upflow-side was 0.97 m) was 3.9×10^{-4} m^3/s. Thus, the latter was more than 10 times as large as the former. This rapid loopseal reformation in RI-2 stage is a result of immediate mass transport from the CL-B to loopseal-B region, which can be enabled by a counter current flow limination (CCFL) break at the loopseal-B upflow-side to the primary pump B region.

Figure 4.3.10 shows a mass distribution map at 3247 s (Phase ①, start of RI-2 stage) when the loopseal-A region was filled with water, water accumulation in the loopseal-B region started prominently, the CL-A and CL-B were not completely filled with AIS water, and water remained in the HL-A, HL-B and SG-B inlet plenum. Figure 4.3.11 shows a mass distribution map at 3398 s (Phase ②, after RI-2 stage) when the loopseal reformation was completed in the loopseal-B region, and the CL-A and CL-B were almost filled with water. It is shown that total primary masses in these two maps were almost the same as shown in Fig. 4.3.1 and that the water mass in the SG-B inlet plenum (Phase ①) was consequently redistributed both to the cold legs and the loopseal-B region through this RI process.

The DP across the primary pump B gradually decreased in the first reformation process with intermittent increases after the AIS injection restarted at 3026 s, and finally became negative value in the RI-2 stage indicating water fall-back from the CL-B to the loopseal-B region (see Fig. 4.3.6). During the RI-1 stage, the DP across the SG-B plena showed similar intermittent increases which are a result of intermittent flow resistance increases in the U-tubes when the SG-B secondary system was periodicly depressurized and steam flow through the SG-B was promoted by steam condensation in the CL-B during the intermittent AIS injection periods. There was no prominent DP increase across the SG-B plena during the RI-2 stage indicating steam flow stagnation through the SG-B U-tubes and the loopseal-B region.

(4) The Second LSC Process (C2)

After a short time from the first loopseal reformation completed, steam generated in the core gradually accumulated in the primary hot regions and caused both a loopseal-B water level decrease at 3372 s and an increase of the pressure difference between the upper plenum and the downcomer. Due to this manometric pressure balance in the primary system, the core water level decreased to result in the temporary core heatup. The AIS injection in the CL-B terminated at 3537 s and that in the CL-A intermittently continued until 4086 s. In the second LSC process (C2) until 4042 s, the hydraulic behaviors observed during the first LSC process were similarly repeated in the primary system.

(5) The Second Loopseal Reformation Process (R2-1 to R2-3)

The 2nd loopseal reformation process (R2) started at 4042 s and passed three stages of water accumulation (from R2-1 to R2-3) until 4890 s as shown in Figs. 4.3.4 and 4.3.5. The mass distribution maps at the middle stage (Phase ③ at 4160 s) and the end stage (Phase ④ at 4377 s) of this R2-1 stage are shown in Figs. 4.1.33 and 4.3.12, respectively.

In the first stage of loopseal reformation process (R2-1), water mass gradually accumulated in the loopseal-B horizontal leg similarly as in the R1-1 process, and steamflow from the SG-B passed an upper region above the water level. The collapsed water level reached approximately 0.10 m above the leg bottom at the end of R2-1 stage (at 4377 s). On the other hand, there was less mass in both cold legs during R2-1 process compared to the R1-1 stage since the AIS injection already stopped in this early stage. Thus, the water mass accumulated in the loopseal-B was mainly supplied by the SG-B condensed waterduring the R2-1 stage. The loopseal-A was continuously filled with water during the R2 process.

The downcomer collapsed water level started to increase at the same time of R2-2 stage initiation (4377 s) and the water accumulation in the loopseal-B upflow-side was apparently promoted from this time. The collapsed water level in the downflow-side was kept constant at approximately 0.1 m while the upflow-side collapsed water level increased to 1.54 m at the end of R2-2 stage (4820 s). This water distribution in the loopseal-B is possible only by a significant steam flow passing through the upper region of horizontal leg, which limited water fall-back from the loopseal-B upflow-side (a CCFL at the bend of upflow-side). The R2-3 is a rapid refilling stage until 4890 s in the loopseal-B region caused by a CCFL break at the upflow-side bend and water fell back from the CL-B.

An average water volume accumulation rate in the loopseal-B region for R2-1 stage (from 4068 to 4377 s) was calculated as 6.3×10^{-5} m^3/s and that for R2-2 stage (from 4377 to 4718 s) as 9.7×10^{-5} m^3/s, respectively. The water accumulation rate in R2-2 stage was approximately 50% higher than that in R2-1 stage. An average water volume accumulation rate in R2-3 process was calculated as 1.9×10^{-3} m^3/s (from 4824 to 4890 s) which was more than 10 times as large as those in the R2-1 and R2-2 stages.

The mass distribution map at the begining of R2-3 stage (Phase ⑤ at 4828 s) is shown in Fig. 4.3.13. As a result, water mass remained in the SG-B inlet plenum and a part of mass in hot legs (see Fig. 4.3.12) were transported to the cold legs and the loopseal-B region

during the R2-2 stage. At the end of R2-3 stage, the collapsed water level in the loop-seal-B upflow-side was 3.48 m and that in downflow-side was 1.59 m which is fairly lower than the downflow-side level at the R1-2 end time. Moreover, the CL-B water level height at the end of R2-3 stage was almost half of that at the end of R1-2 stage. Thus, there was not sufficient water mass in the primary system at the R2-3 stage to fully refill the loopseal-B region.

(6) The Third LSC Process (C3) and Aftermath

The third LSC process (C3) started at 4890 s and ended at 5130 s. During the C3 process, the pressure difference between the upper plenum and the downcomer increased faster than that in C2 process as shown in Fig. 4.3.4, and reached a minimum value of approximately -30 kPa which is nearly the same as that in C2 process. The DP data in the loopseal-B downflow-side in C3 process also changed faster than those in C2 process as shown in Fig. 4.3.5. These indicate that steam accumulated in the primary system with a higher accumulation rate in C3 process than in C2 process despite the slightly lower core power in the former. A reason of this higher steam accumulation rate in C3 process is ascribed to less steam condensation at the SG U-tubes, which resulted in the primary pressurization, in comparison with C2 process, in which the primary system was still depressurized by the SG-RV cyclic opening actions.

The core water level decreased in the C3 process and temporarily caused the third core heatup as shown in Section 4.1.3. After the C3 process, water accumulated again in the loopseal-B region (in R3 process started at 5130 s). A water volume accumulation rate in the upflow-side during R3 process was fairly lower than that during R2-2 stage, and the downflow-side collapsed water level was kept constant at the same level at R2-2 stage initiation (Phase ④). The primary mass inventory gradually decreased through the C3 and R3 processes due to steam discharge through the break unit, and the boil-off process started by the upper plenum mixture level decrease (in a short time after the third LSC).

An erroneous measurement is commonly shown after 5100 s in the following DP data. Namely, DP measurements with impulse lines at SG inlet plenum such as DP 118 and DP 119 (see Fig. 4.3.7) and DP 116 and DP 117 (Fig. 4.3.9) showed an abrupt decrease at 5100 s and a recovery to the previous conditions. The DP 120 in Fig. 4.1.28 and DP 122 in Fig. 4.1.30 also showed an abrupt increase and a recovery. All these behaviors have no meaning but a measurement failure.

(7) Collapsed Water Levels in Loopseal Reformation Processes

Figures 4.3.14 (a) and (b) illustrate collapsed water levels (CLs) in the loopseal-B re-

gion at three typical times during the R1 and R2 processes, respectively. In these figures, the loopseal configuration (pipe diameter, pipe length and bend parts) is accurately scaled to the design data so that transient water levels and steam flow paths can be correctly refered. The collapsed levels were calculated from the measured DP data, i.e., DP 41 between the SG-B outlet plenum and the loopseal-B bottom, and DP 42 between the loopseal-B bottom and the primary pump B (PC-B) suction.

At the begining of R1-2 stage (3240s), collapsed levels in loopseal-B were lower than the middle height of horizontal leg, and steam flowed from the SG-B side (left side top) to the CL-B (right side top) passing through the upper half of horizontal leg. The collapsed level in upflow-side started to rise at 3240 s and finally reached the top part (3.46 m above the horizontal leg bottom) at 3352 s. Those in the downflow-side also increased to 2.27 m during this period. It is easy to understand that water fall-back from the CL-B was restricted at the pump-B before 3240 s and that water flow from the upflow-side to the horizontal leg was restricted at the lower bend (radius/pipe diameter= 2.98) of the upflow-side region after 3240 s. The collapsed levels at 3341s shows an instantaneous stage of the water refilling process of R1, and a rapid water fall-back from the CL-B occurred after 3341 s due to a CCFL break at the pump-B. This CCFL break was a result of decreased uprising steam flow which was mainly restricted at the lower part of loopseal-B upflow-side covered with two-phase mixture.

Similar but slightly different conditions were observed during the R2 process as shown in Fig. 4.3.14 (b) comparing with the R1 process. At the begining of R2-2 process (4377s), collapsed levels in the horizontal leg were slightly higher than the middle height and steam passed the upper region above the water level. An intermediate stage at 4820 s, when rapid water fall-back from the CL-B started, was observed with similar water levels as the instantaneous stage of R1-2 process (3341s). A time period between 4377 and 4820s is, however, more than four times as long as the time period in R1-2 process (between 3240 and 3341 s), and the upflow-side collapsed level at 4820 s was approximately 50% higher than that at 3341 s. Reasons of this slower level increase and higher level in the upflow-side in R2-2 stage compared to the early R1-2 stage can be ascribed to (a) less water mass in the CL-B, (b) less condensed water at SG-B U-tube outlets and (c) a higher steam flow rate at the loopseal-B region due to the degraded steam condensation effect at both SGs in the second loopseal reformation process.

4.4 Mass and Energy Balance at Steam Generators

The secondary depressurization action largely contributed to lower the primary pressure by increasing primary-to-secondary temperature differences, but the primary pressure finally turned to increase at 4163 s when the secondary water level almost reached bottom. On the other hand, the loopseal reformation was twice repeated at the loopseal-B region by accumulating condensed water from the SG-B U-tubes in addition to the fall-back water from the CL-B region. In this section, the primary-to-secondary heat transfer and fluid conditions in the secondary systems are investigated for the repeated LSC processes.

4.4.1 Secondary Mass Balance during Repeated LSC Processes

Figure 4.4.1 shows the primary and secondary pressures between 2400 and 5400 s in which the LSC process was repeated. The secondary pressures continuously decreased by cyclic opening of the RVs at both SGs and promoted the primary depressurization until 4163 s. In this figure, six time periods are shown for the following estimation of the secondary mass balance (i.e., before and after each time of three LSCs). In the core, approximately 1.0 MW power was supplied to generate steam during the repeated LSC processes.

Figures 4.4.2 and 4.4.3 show a steam discharge flow rate and fluid temperatures in both the steam RV line and bottom of the boiling section in the SG-A and those in the SG-B, respectively. It is shown in these figures that (a) the steam discharge flow rate gradually decreased as the secondary pressure decreased, (b) the discharged steam temperature was significantly higher than the bottom fluid temperature which was nealy in saturated conditions in each SG and (c) the flow rate included zero-shift. A total discharged steam mass was obtained by correcting the zero-shift which was rather higher than an uncertainty of steam discharge flow rates (FE 19 and FE 27) of approximately ± 0.09 kg/s. Figure 4.4.4 shows the collapsed water levels in both SGs. These level data also included zero-shifts which were higher than a nominal uncertainty of the water level measurement (LE 3 and LE 6) of ± 0.05 m.

Mass balance in the secondary system was estimated in six time periods, i.e., before and after three LSC times. Each time period included some RV cyclic open actions except for the last period (after the 3rd LSC) in which only one RV open action was included. These time periods are shown in Figs. 4.4.1 and 4.4.4. A total discharged steam mass (ΔM_D in kg) in each time period was accounted by cumulating an average steam flow rate (W_{ave} in kg/s) in each RV open cycle (j) multiplied by each time length (Δt in s) as,

$$\Delta M_D = \Sigma_j \{W_{ave,j} \times \Delta t_j\}. \quad (4.4.1)$$

On the other hand, a fluid mass loss was also calculated by estimating both mass changes in water and steam phases for each time period. The water volume (V_L in m^3) was obtained from the collapsed water level data with zero-shift correction by using the revised correlation (Appendix A in Reference 13) for elevation and fluid volume in both SGs. Thus, a water mass loss in the secondary side (ΔM_L in kg) is obtained as a difference of water masses at initial time (i) and final time (f) by using a saturated water density of (ρ_L in kg/m^3) as,

$$\Delta M_L = \{V_L \times \rho_L\}_i - \{V_L \times \rho_L\}_f. \quad (4.4.2)$$

In order to minimize effects of void distribution in the water phase, the initial and final times were chosen in a secondary pressurization period when the RV was closed.

The steam phase in the secondary system was divided into three subnodes to take account of the significant temperature distribution in the steam dome (see next section), i.e., two subnodes between EL 7.96 and 13.74 m and between EL 13.74 and 18.58 m (approximately 20% of total secondary volume (V_0) for each one) and one subnode in the upper SG region (above EL 18.58 m, approximately 60% of V_0). For the lower steam subnode, a steam volume (V_{G1}) at each time is given by ($0.2V_0 - V_L$) and the other two steam volumes are given as $V_{G2} = 0.2V_0$ and $V_{G3} = 0.6V_0$.

Thus, a total steam mass change (ΔM_G) in the secondary system during a time period was obtained by using the local steam densities ρ_{Gk} (k=1, 2 and 3) as,

$$\Delta M_G = \Sigma_k \{V_{Gk} \times \rho_{Gk}\}_i - \Sigma_k \{V_{Gk} \times \rho_{Gk}\}_f. \quad (4.4.3)$$

Therefore, a total mass loss in the SG secondary system is given as ($\Delta M_L + \Delta M_G$) and is compared with the total steam discharged mass of ΔM_D to check the secondary mass balance. The measurement list for this mass balance check is shown in Table 4.4-1. Tables 4.4-2 and 4.4-3 show the estimated mass balance at the SG-A and SG-B, respectively. The following are derived.

(a) Similar results of mass balance were obtained for both SG-A and SG-B.

(b) The total discharged steam mass agreed well with the total fluid mass loss in six time periods within a discrepancy of ±26 kg. A nominal uncertainty of the discharged steam mass can be estimated as $\pm 0.09(kg/s) \times \Delta t_{ave} = \pm 35$ kg while a nominal uncertainty of the collapsed water level (±0.05 m) is equivallent to a water mass uncertainty of ±12 kg in the lower boiler region. Thus, a difference of these two masses has an uncertainty of ±37 kg. It is clear that the mass discrepancy of ±26 kg was relatively lower than the uncertainty of ± 37kg.

(c) The steam mass discharged through the RV is used to calculate steam enthalpy discharged through the RV during each time period (see Section 4.4.3).

4.4.2 Vertical Temperature Distribution in Secondary Fluid and U-tubes

The RV cyclic open actions caused not only the fluid mass loss but also a significant temperature distribution both in the secondary fluid and the U-tubes as shown below.

(1) Temperature Distribution in Secondary System

Figure 4.4.5 shows fluid temperatures measured at eight vertical locations in the SG-A secondary-side between 2400 and 5400 s. TE 429 was measured at Pos.1 (0.65 m above the secondary bottom of EL 7.964 m), and TE 442 was measured at 16.546 m above the bottom (the highest region in SG-A). The fluid temperature at Pos.1 was almost in a saturated condition. The temperatures at Pos.5 and Pos.3 showed departures from the Pos.1 fluid temperature after the water level passed each T/C location. The fluid temperatures in the steam dome were kept nearly constant during all the time period. Thus, the temperature differences between top and bottom of the SG secondary system increased as the water level decreased. After the primary system pressure started to increase at 4163 s, some of the secondary fluid temperatures (in the lower boiler region) also started to increase. Thus, a significant thermal stratification was observed in the secondary fluid. Similar thermal stratification was observed in the SG-B secondary fluid.

(2) SG Vessel Wall Temperatures

Figure 4.4.6 shows metal temperatures measured at four locations of the vessel wall inner surface. These showed similar trends but slightly different behaviors compared with the fluid temperatures (Fig.4.4.5). TW 466 at the steam dome and TW 465 at Pos.10 were higher than the corresponding fluid temperatures (TE 442 and TE 436) indicating that these vessel walls were heat sources to the secondary fluid. On the other hand, TW 464 at Pos.7 showed lower values than the corresponding fluid temperature (TE 433) until approximately 3100 s and thereafter it turned to increase. This temperature increase at Pos.7 is not a result of the water level passage through the T/C location but probably due to a result of some local cooling effect which was not determined. The bottom part of secondary wall (TW 463) showed slightly lower value than the corresponding fluid temperature (TE 429) when the metal wall measuring location was covered by the water level.

(3) U-tube Wall Temperatures

Figure 4.4.7 shows metal temperatures measured at six different elevations of the outer surfaces of SG-B No.2 U-tube. The U-tube T/Cs were installed at the same elevation of

inlet-side (IN) and outlet-side (EX) except for the top bend (Pos. 10). These temperature data were bounded by three typical temperatures, i.e., One is the highest temperature at the outlet-side of Pos. 9 (TW 533), next one is the lowest temperature at Pos. 1 (TW 510 and TW 511) and the last one is the increasing primary saturation temperature. Some interesting temperature behaviors were observed as shown below.

(a) The highest U-tube wall temperature was detected at the outlet-side of Pos. 9. The U-tube wall temperature at Pos. 10 was rather lower than those of lower parts. On of possible reasons is a disconnection of welding at the T/C sensing part.
(b) The U-tube wall temperatures at both sides of Pos. 5 showed simultaneous increases after the water level passed the T/C location, while they showed different behaviors after the first and second LSCs. Namely, the inlet-side temperature slightly decreased after the LSCs while the outlet-side temperature slightly increased after the LSCs. These behaviors were similarly observed in the U-tube temperatures at Pos. 7 and Pos. 3 suggesting an increased primary flow after each LSC time.
(c) These temperature behaviors were similarly observed in the shortest U-tubes (No. 1) and the longest U-tubes (No. 3) with instrumentations among the 141 U-tubes. Therefore, these temperature behaviors support an increased steam flow in every SG-B U-tube after each LSC occurrence.

(4) Saturated temperatures in Both SG Plena

Figure 4.4.8 show the fluid temperatures both in the inlet and outlet plena of SG-B. It is clear that these SG plena was maintained in the same saturated condition during the repeated LSC processes, and no super-heated steam temperature was detected even in the SG-B outlet plenum. By considering the super-heated temperatures at the U-tube walls (see Fig. 4.4.7) and an increased U-tube steam flow toward the CL-B break location after each LSC, sufficient steam condensation should be necessary at the U-tube outlets to maintain the SG-B outlet plenum temperature in saturated conditions. The same saturated condition was observed in the inlet and outlet plena of SG-A suggesting similar steam condensation at the SG-A U-tube outlets as in the SG-B U-tubes.

4.4.3 Primary-to-secondary Temperature Distribution across U-tubes

In order to clarify the primary-to-secondary energy flow direction across the U-tubes in the repeated LSC processes, horizontal temperature distribution at four vertical elevations and spatial temperature distribution along the SG-B No. 2 U-tube at six typical times are shown below.

(1) Horizontal Temperature Distribution at Four Elevations around No. 2 U-tube

Figures 4.4.9, 4.4.10, 4.4.11 and 4.4.12 show primary-to-secondary temperature distribution around the No. 2 U-tube at Pos. 1, Pos. 3, Pos. 5 and Pos. 9, respectively. Namely, the fluid temperatures both in inlet and outlet sides of the U-tube are compared with the U-tube wall temperatures in addition to the secondary fluid temperature at the same elevation.

It is shown in Fig. 4.4.9 that the U-tube wall temperatures at both sides of Pos. 1 agreed well with the secondary fluid temperature until approximately 4050 s (until the water level uncovered the Pos. 1 T/Cs). As shown in Fig. 4.4.1, the SG-B secondary pressure was kept lower than the primary pressure in the period (2400 to 5400 s) except for a short time after the first LSC. Therefore, the U-tube wall temperatures at Pos. 1 were almost kept in subcooled conditions until 4050 s for the primary fluid in the U-tube. On the other hand, the primary fluid temperature at the inlet-side of Pos. 1 was maintained at saturated conditions like as the SG-B inlet plenum temperature.

The primary fluid temperature at the outlet-side of Pos. 1, however, showed slightly different behaviors from the inlet-side temperatures, i.e., the outlet-side temperature stably showed a subcooled condition until the first LSC indicating existence of subcooled water flowing down to the SG-B outlet plenum. After the first LSC, it showed superheated temperature until approximately 3330 s and thereafter it agreed with the inlet-side fluid temperature until the second LSC. After the second LSC occurred, the outlet-side temperature turned to increase indicating a super-heated steam flow in the U-tube. And both side temperatures finally agreed with the saturation temperature after approximately 4860 s.

Similar temperature distributions were observed around the No. 1 and No. 3 U-tubes (Pos. 1). It is concluded that a primary-to-secondary energy flow direction was confirmed across the lowest part of SG-B U-tubes (Pos. 1) during the repeated LSC processes.

At Pos. 3 elevation, similar but slightly different temperature behaviors were observed as shown in Fig. 4.4.10. Namely, the secondary fluid temperature showed saturated conditions until approximately 3900 s and thereafter it turned to increase as the U-tube wall temperatures increased. The U-tube wall temperatures at both sides were almost equal to the secondary fluid temperature until 3300 s, and thereafter only the inlet-side wall temperature showed the primary saturation condition. After 3300 s, the outlet-side wall temperature gradually increased from the inlet-side wall temperature and showed an apparent increase after the second LSC. Thus, the Pos. 3 U-tube walls were limited to the

secondary fluid temperature as long as the T/Cs were covered by the secondary water level, while they were affected by the primary fluid temperature when the T/Cs were uncovered by the secondary water level.

The primary fluid temperatures at the outlet-side of U-tube showed the highest value after the first LSC among the temperature data at Pos. 3, and it showed another increase after the second LSC indicating arrival of hotter steam from the higher region after each LSC. On the other hand, the primary fluid temperature at the inlet-side showed almost saturated condition as in the SG-B inlet plenum, and it was rather higher than the U-tube wall inlet-side temperature. All the fluid and wall temperatures at Pos. 3 finally agreed with the primary saturation temperature after approximately 4950 s.

Figure 4.4.11 shows the fluid and U-tube wall temperatures at Pos. 5. These showed superheated steam conditions except for short time periods before the first LSC and after 4700 s. Both of fluid and wall temperatures at the outlet-side were maintained higher than those at the inlet-side. At the outlet-side, the primary fluid temperature was higher than the wall temperature, while at the inlet-side, the primary fluid temperature was rather lower than the wall temperature after the first LSC. The secondary fluid temperature at Pos. 5 became rather higher than the U-tube inlet-side wall temperature after 2850 s. Thus, a transverse energy flow direction was observed at Pos. 5, i.e., from the U-tube outlet-side fluid to the secondary fluid and then to the inlet-side primary fluid.

All these primary fluid and U-tube wall temperatures at Pos. 5 became the primary saturated condition in the later pressurization process. The secondary fluid temperature data (TE 550) showed an abrupt decrease after 5300 s (probably due to a local cooling effect caused by water fall-back).

Figure 4.4.12 shows that fluid temperatures and U-tube wall temperatures at Pos. 9 (near the top part of No. 2 U-tube) showed almost the same values within 10 K and they were always higher than 500 K between 2400 and 5400 s. It is clear that Pos. 9 temperatures are the highest among the experiment data shown in Figs. 4.4.9 through 4.4.12. It is also shown that the inlet-side fluid temperature was lower than the others, and the highest temperature was detected at outlet-side temperatures (both fluid and U-tube wall) among these temperature data.

(2) Spatial Temperature Distribution around No. 2 U-tube at Six Time Phases

More precise temperature distribution along the steam flow path in SG-B No. 2 U-tube was

investigated below in addition to the U-tube wall temperatures and secondary fluid temperatures at six selected times during the repeated LSC processes.

Figures 4.4.13 (a) and (b) show these spatial temperature distributions and the collapsed water level at times before and after the first LSC. The SG wall surface temperatures at three elevations are also included. The U-tube wall temperature at Pos.10 (TW 537 in Fig.4.4.7) is not indicated in Fig.4.4.13 since it showed questionable behaviors. Figures 4.4.14 (a) and (b) show similar spatial temperature distribution before and after the second LSC, and Figs.4.4.15 (a) and (b) show that before and after the third LSC. Notations of symbols in these figures are presented in right side of Fig.4.4.13 (b). The following are derived from these figures.

(a) During the repeated LSC processes (except for a time after the third LSC), the primary fluid passed the SG-B U-tubes from the inlet-side to outlet-side showing a vertical temperature increase in the inlet-side and a recovery to saturation conditions in the outlet-side. These temperature changes were caused by heat transfer between the flowing primary steam and the surrounding U-tube wall, i.e., the primary fluid was heated by the hotter U-tube walls in the inlet-side (above the secondary water level), reached a maximum temperature at the U-tube outlet-side location with the highest wall temperature, and cooled by the colder tube walls in the lower outlet region (including the subcooled wall temperatures below the secondary water level). Thus, a horizontal temperature gradient was detected between the inlet-side and outlet-side tube walls above the secondary water level.

(b) The secondary depressurization action contributed to maintain the U-tube wall temperatures in subcooled conditions below or close to the secondary water level, and the primary-to-secondary energy transfer was mainly conducted at this lower boiler region by steam condensation in the U-tube inner surfaces. A subcooled primary temperature at the U-tube outlet (see Fig.4.4.13 (a)) and a larger magnitude of fluid temperature decrease in the U-tube outlet than a temperature increase in the U-tube inlet-side mean a smaller amount of steam flow rate in outlet-side than that in inlet-side. Namely, a part of the primary steam flow which was condensed in the U-tube inlet-side flowed down to the SG-B inlet plenum, and a decreased steam flow arrived at the outlet-side with a larger temperature decrease including the subcooled temperature shown above.

(c) The maximum primary fluid temperature was detected at a location between Pos.7 and Pos.9 in the outlet-side in every case (except for a time after the third LSC). In each case after the first or second LSC, the maximum temperature location shifted to a lower region (downflow-side) compared to a case before each LSC indicating an increased steam flow rate after these LSCs. On the other hand, a maximum tube wall tem-

perature which was detected mainly at outlet-side Pos. 9, was lower than the maximum primary fluid temperature in some cases (see times after the first and second LSCs). A tube wall temperature at Pos. 8 (no T/C had been installed at Pos. 8 nor Pos. 6) was estimated for these cases by extraporating the wall temperatures at Pos. 5 and Pos. 7 to Pos. 8 location, and concludingly the extraporated wall temperature at the outlet-side of Pos. 8 agreed well with the maximum fluid temperature in these cases.

(d) In a case after the third LSC (Fig. 4. 4. 15 (b)), all the primary fluid temperatures in No. 2 U-tube showed the same value which agreed well with the primary saturation temperature within an uncertainty range of ± 6. 3 K suggesting steam condensation in every part of the tube wall innner surfaces. The tube wall temperatures also showed an uniform temperature distribution which was mainly controlled by the primary fluid temperature. In this case, there was no water in the boiler region and the primary system was pressurized to 3. 1 MPa (the secondary pressure was 0. 90 MPa).

(e) The SG vessel wall temperature in the upper region (EL 17. 844 m) was significantly higher than the temperatures of the secondary fluid and U-tube wall in the same horizontal domain and was kept at nearly constant value indicating a large amount of metal stored heat which was a heat source to the secondary fluid and the U-tubes. On the other hand, the SG vessel wall temperature at the secondary bottom (EL 8. 614) was equal to or slightly lower than the secondary fluid temperature at the same elevation indicating that the SG wall was a heat sink to the secondary fluid. The SG vessel wall at the middle boiler region (EL13. 744m) which was above the water level, was kept almost constant temperature and became a heat source or a heat sink to the secondary fluid accoding to the varied secondary fluid temperature.

4. 4. 4 Secondary Energy Balance during Repeated LSC Processes

In order to estimate an overall primary-to-secondary heat transfer rate, an energy balance was investigated for both SGs. Namely, energy balance equations were derived for the secondary metal structures, the U-tube walls and the secondary fluid system during each one of the six time periods (refer Section 4. 4. 1), and finally a total heat transfer rate across the SG U-tubes was derived. The experiment data for this estimation and the regional configuration data are shown in Table 4. 4-1.

(1) Energy Balance in SG Vessel Wall and Other Structures

A total energy transfered to the secondary fluid from the SG vessel wall and other metal structures (Q_w in unit kJ) in a time period of Δt (in unit s) is given from a stored energy loss in the SG wall and other structures (ΔQ_w in kJ), and an environmental heat loss (Q_{HL} in kJ) by using a following equation.

$$Q_W = \Delta Q_W - Q_{HL}, \quad (4.4.4)$$

$$\Delta Q_W = \Sigma_k \{M_{Wk} \times C_{Pk} \times \Delta TW_k\}, \quad (4.4.5)$$

where M_{Wk} (in kg) is a metal mass at k-th component, C_P (in kJ/kg/K) is an average specific heat of the metal during a time period, and ΔTW (in K) is a difference of wall temperature between the initial and final times during a time period. The SG vessel wall and structures were divided into eight components (k=1 to 8), i.e., a tube-sheet, four vessel wall components, a steam line, downcomer pipes and some internal structures as shown in Table 4.4-1. The same components and metal weights were assumed to both SGs.

An average metal temperature of (TW - DT/2) was defined for a thick SG wall instead of the measured wall temperature, where DT (in K) is the measured temperature difference between the inner and outer surface temperatures. On the other hand, an average metal temperature in the tube-sheet was assumed to be given by a mean value between the vessel wall temperature at Pos.1 and the SG plenum fluid temperature. An uniform temperature distribution was assumed to thin metal walls such as the steam line pipe walls and the internal structures. A mean value of four downcomer wall temperatures ($TW = \Sigma_k TW_k/4$) was defined for the downcomer region average temperature.

The environmental heat loss from the SG vessel at an average wall temperature was estimated from the previously determined results[14].

(2) Energy balance in U-tube Wall

A total energy transfered from the primary fluid to the SG U-tubes (Q_S in kJ) was given from a stored energy loss in the U-tube walls (ΔQ_U in kJ) during a time period of Δt (in s) and a transfered energy from the U-tube outer surfaces to the secondary fluid (Q_U in kJ) as,

$$Q_S = Q_U - \Delta Q_U, \quad (4.4.6)$$

$$\Delta Q_U = \Sigma_k \{M_{Uk} \times C_{Pk} \times \Delta TW_k\}, \quad (4.4.7)$$

where M_{Uk} (in kg) is a U-tube metal mass at k-th component, C_P (in kJ/kg/K) is an average specific heat of the metal during a time period, and ΔTW (in K) is a wall temperature difference between the initial and final times of each time period. The U-tubes were divided into five components (k=1 to 5) and an average metal temperature at each component was given by a mean value of U-tube wall temperatures measured at the inlet and outlet sides (refer Table 4.4-1). The primary-to-secondary transfered energy (Q_S) was determined by solving simultaneous equations as shown later.

(3) Energy balance in Secondary Fluid and Steam Discharge Flow

An energy balance in the secondary fluid during a time period was roughly given as,

$$Q_U + Q_W - Q_D + \Delta Q_F = 0, \quad (4.4.8)$$

where Q_D (in kJ) is a total enthalpy of dischrged steam during a time period and ΔQ_F (in kJ) is an enthalpy decrease in the secondary fluid. Q_D is given as,

$$Q_D = \Sigma_j \{W_{ave.,j} \times h_{ave.,j} \times \Delta t_j\}, \quad (4.4.9)$$

where $h_{ave.,j}$ (in kJ/kg) is an average value of specific enthalpy at j-th RV open cycle. ΔQ_F is given by a difference of total fluid enthalpies between the initial and final times of a time period as,

$$\Delta Q_F = \Sigma_k \{V_k \times \rho_k \times h_k\}_i - \Sigma_k \{V_k \times \rho_k \times h_k\}_f. \quad (4.4.10)$$

By introducing equations (4.4.4) and (4.4.6) into (4.4.8), a primary-to-secondary transfered energy of Q_S can be derived for each time period as,

$$Q_S = -\Delta Q_W + Q_{HL} - \Delta Q_U - \Delta Q_F + Q_D. \quad (4.4.11)$$

(4) Results of Secondary Energy Balance during Repeated LSC Periods

Tables 4.4-4 and 4.4-5 show results of the estimated values of each energy term during the time periods from (1) through (6) at the SG-A and SG-B, respectively. In these tables a time average value of $Q_S/\Delta t$ (in kJ/s) during each time period is added. The following are derived from these results.

(a) The steam outflow had a maximum contribution to the secondary energy balance shown in Tables 4.4-4 and 4.4-5. Namely, the secondary depressurization actions significantly controlled the secondary fluid conditions at two SGs.

(b) The primary-to-secondary transfered energy (Q_S) was approximately 37% to 56% of the discharged steam energy (Q_D) as long as the secondary water level existed in both SGs (time periods (1) through (4)). After the secondary water level became almost zero, the primary-to-secondary transfered energy became low values. It is also shown that the energy of Q_S at SG-B was rather higher than that at SG-A indicating an improved heat transfer due to a larger steam flow in the SG-B U-tubes than in the SG-A U-tubes.

(c) The energy of Q_S before the first LSC was fairly larger than that after this LSC. This was also found for the second LSC time. Therefore, steam condensation at two SGs more strongly occurred before these LSC times than that after the LSC times.

(d) In the primary depressurization phase (time periods of (1) through (3)), a sum of the time average rates ($Q_S/\Delta t$) at two SGs was more than or equal to 70% of the core power while it was less than 50% of the core power in the primary re-pressurization.

(e) The environmental heat loss from the SG walls had minor contribution to the secondary energy balance as shown in above tables. A total energy stored in the U-tubes had less contribution to the secondary enegy balance as well as the stored energy in SG vessel walls.

Table 4.1-1 Sequence of events in experiment SB-CL-24

Event	Time (s)
·Break initiation	**0.0**
Primary pump speed started to increase	0.0
·Trace heater powers tripped off	2 - 4
·PZR heaters were terminated on low PZR level	70 - 77
·PZR pressure reached Scram setpoint (12.97 MPa)	**75**
·SG-A/B steam and feedwater lines were closed	78 - 81
·Primary coolant pumps started to coast down	**80**
·Boiling started in the upper core region	91
PZR pressure started to temporarily recover	91
·Water level formed in upper plenum	95
·Core power decay from 10 MW started	**110**
·Boiling started in HL-A and HL-B	111 - 116
·SG-A relief valve cyclicly opened	116
·PZR pressure started to decrease again	125
·Water level formed in upper head	180
·PZR level decreased to zero level	216
·Primary coolant pump-A stopped	332
·Primary coolant pump-B stopped	513
·Both SGs depressurization started	**600**
·Level formed in CL-A	635
·Level formed in SG-A outlet plenum	840
·Level formed in SG-B outlet plenum	1200
·ACC and ACH injection to CLs started	**2110**
·The 1st loopseal clearing occurred	**2831**
·ACH and ACC injection temporarily terminated	2886 - 3026
·ACH injection was terminated	3537
·The 2nd loopseal clearing occurred	**4009**
·ACC injection was terminated	4086
·Primary pressure started to increase	4163
·The 3rd loopseal clearing occurred	**5122**
·Core water level began to decrease	5810
·Core heatup started at the top (Pos.9)	**5929**
·PORV was opened by detecting core heatup	**6568**
·PZR safety valve was manually opened	**6610**
·Core decay power was limited to 75%	7109
·Core decay power was limited to 50%	7156
·Core decay power was limited to 25%	7161
·Core decay power was limited to 10%	7166
·LPI injection to CLs started	**7371**
·Heated core was completely quenched	7675
·Core power supply was terminated	7822
·Break valve was closed at the test end	**7844**
·LPI injection to CLs was terminated	7860
·PORV and PZR-SV were closed	7862 - 7865
·Data recording was terminated	8300

Table 4.3-1 Primary mass inventory in experiment SB-CL-24

Time (s)	M_D (kg)	M_I (kg)	M_R (kg)	M*= M_R/M_o
- 48	0	0	5401	1.000
36	158	0	5243	0.971
120	469	0	4932	0.913
204	713	0	4689	0.868
288	951	0	4450	0.824
372	1189	0	4213	0.780
456	1426	0	3975	0.736
540	1585	0	3816	0.707
624	1823	0	3578	0.662
708	2061	0	3340	0.618
792	2220	0	3181	0.589
876	2333	0	3068	0.568
960	2458	0	2943	0.545
1044	2538	0	2863	0.530
1128	2617	0	2784	0.515
1212	2697	0	2704	0.501
1296	2776	0	2625	0.486
1380	2783	0	2619	0.485
1464	2856	0	2545	0.471
1548	2935	0	2466	0.457
1632	3015	0	2386	0.442
1716	3015	0	2386	0.442
1800	3085	0	2316	0.429
1884	3095	0	2307	0.427
1968	3095	0	2306	0.427
2052	3168	0	2233	0.413
2136	3174	27	2253	0.417
2220	3254	82	2229	0.413
2304	3412	127	2116	0.392
2388	3571	210	2040	0.378
2472	3730	273	1944	0.360
2556	3888	357	1869	0.346
2640	4020	449	1830	0.339
2724	4130	519	1791	0.332
2808	4285	635	1751	0.324
2892	4380	919	1940	0.359
2976	4399	925	1928	0.357
3060	4438	1069	2032	0.376
3144	4445	1161	2118	0.392
3228	4524	1228	2105	0.390
3312	4603	1299	2097	0.388
3396	4695	1379	2086	0.386
3480	4841	1471	2031	0.376
3564	4921	1557	2037	0.377
3648	5079	1614	1936	0.358
3732	5204	1685	1882	0.348
3816	5317	1761	1845	0.342
3900	5430	1853	1824	0.338
3984	5555	1930	1776	0.329
4068	5635	2158	1925	0.356
4152	5635	2220	1986	0.368
4236	5635	2219	1986	0.368
4320	5635	2220	1986	0.368
4404	5656	2219	1964	0.364
4488	5690	2220	1931	0.357
4572	5681	2220	1941	0.359
4656	5693	2221	1929	0.357
4740	5715	2221	1907	0.353
4824	5715	2221	1908	0.353
4908	5794	2222	1829	0.339
4992	5870	2222	1753	0.324
5076	5953	2222	1670	0.309
5160	6032	2222	1591	0.295
5244	6032	2222	1591	0.295
5328	6044	2223	1580	0.292
5412	6063	2223	1562	0.289
5496	6100	2324	1526	0.282
5580	6100	2224	1526	0.282
5664	6130	2223	1494	0.277
5748	6142	2224	1482	0.274
5832	6161	2224	1464	0.271
5916	6176	2224	1449	0.268
6000	6183	2224	1443	0.267
6084	6219	2224	1406	0.260
6168	6225	2224	1400	0.259
6252	6235	2224	1390	0.257
6336	6256	2225	1370	0.254
6420	6284	2225	1342	0.248
6504	6299	2224	1326	0.246
6588	6312	2224	1313	0.243
6672	6362	2226	1265	0.234
6756	6433	2226	1194	0.221
6840	6478	2224	1147	0.212
6924	6527	2225	1099	0.203
7008	6569	2225	1057	0.196
7092	6607	2225	1019	0.189
7176	6641	2225	985	0.182
7260	6674	2225	953	0.176
7344	6707	2225	920	0.170
7428	6734	2240	907	0.168
7512	6792	2360	969	0.179
7596	6801	2566	1166	0.216
7680	6835	2797	1364	0.252
7764	6834	3080	1647	0.305
7848	6812	3363	1952	0.361
7932	6843	3378	1937	0.359
8016	6841	3379	1939	0.359

$M_R = M_o - M_D + M_I$, M_D includes break and PORV flows. M_I includes ACC and LPI flows.

Table 4.4-1 Measurement list for mass and energy estimation

Item / Region (Elevation / Material, Weight)	Pressure	Flow Rate	Water Level	Fluid Temp.	Metal Wall Temperature
SG-A Steam Flow at RV Line		FE 19			
SG-A Steam Enthalpy at RV Line	PE 19	FE 19		TE 57	
SG-B Steam Flow at RV Line		FE 27			
SG-B Steam Enthalpy at RV Line	PE 21	FE 27		TE 61	
SG-A Fluid Mass & Enthalpy (*)					
· Lower Part (EL 7.96-13.74 m)	PE 19		LE 3	TE429	
· Middle Part (13.74-18.58 m)	PE 19			TE435	
· Steam Dome (18.58-25.69 m)	PE 19			TE442	
SG-B Fluid Mass & Enthalpy					
· Lower Part (EL 7.96-13.74 m)	PE 21		LE 6	TE548	
· Middle Part (13.74-18.58 m)	PE 21			TE554	
· Steam Dome (18.58-25.69 m)	PE 21			TE561	
Stored Heat in SG-A Wall & Structures					
· Tube Sheet (EL 7.63- 7.96 m) (Carbon Steel, 1118 kg)				TE324	TW463
· Lower Vessel (7.96-10.54 m) (Carbon Steel, 1823 kg)					TW463, DT139
· Middle Vessel (10.54-15.02 m) (Carbon Steel, 2644 kg)					TW464, DT140
· Middle Vessel (15.02-18.58 m) (Carbon Steel, 2430 kg)					TW465, DT141
· Upper Vessel (18.58-25.66 m) (Carbon Steel, 6356 kg)					TW466, DT142
· Steam Line Pipes (Stainless Steel, 901 kg)				TE442	
· Downcomer Pipes (Stainless Steel, 787 kg)					TW14, 15, 16, 17
· Other Internals (Stainless Steel, 729 kg)				TE442	
Stored Heat in SG-B Wall & Structures					
· Tube Sheet (EL 7.63- 7.96 m) (Carbon Steel, 1118 kg)				TE443	TW504
· Lower Vessel (7.96-10.54 m) (Carbon Steel, 1823 kg)					TW504, DT174
· Middle Vessel (10.54-15.02 m) (Carbon Steel, 2644 kg)					TW505, DT175
· Middle Vessel (15.02-18.58 m) (Carbon Steel, 2430 kg)					TW506, DT176
· Upper Vessel (18.58-25.66 m) (Carbon Steel, 6356 kg)					TW507, DT177
· Steam Line Pipes (Stainless Steel, 901 kg)				TE561	
· Downcomer Pipes (Stainless Steel, 787 kg)					TW18, 19, 20, 21
· Other Internals (Stainless Steel, 729 kg)				TE561	
Stored Heat in SG-A U-tubes Wall					
· Region 1 (EL 7.96- 9.26 m) (Stainless Steel, 598 kg)					TW469, 470
· Region 2 (9.26-10.54 m) (Stainless Steel, 589 kg)					TW475, 476
· Region 3 (10.54-12.46 m) (Stainless Steel, 883 kg)					TW481, 482
· Region 4 (12.46-15.02 m) (Stainless Steel, 1178 kg)					TW487, 488
· Region 5 (15.02-18.58 m) (Stainless Steel, 1284 kg)					TW491, 492
Stored Heat in SG-B U-tubes Wall					
· Region 1 (EL 7.96- 9.26 m) (Stainless Steel, 598 kg)					TW510, 511
· Region 2 (9.26-10.54 m) (Stainless Steel, 589 kg)					TW516, 517
· Region 3 (10.54-12.46 m) (Stainless Steel, 883 kg)					TW522, 523
· Region 4 (12.46-15.02 m) (Stainless Steel, 1178 kg)					TW528, 529
· Region 5 (15.02-18.58 m) (Stainless Steel, 1284 kg)					TW532, 533

* SG fluid volumes in lower, middle and steam dome regions are roughly 20%, 20% and 60% of total volume (V_0), respectively (V_0 = 6.996 m^3 in SG-A and 7.023 m^3 in SG-B).

Table 4.4-2 Mass balance in SG-A secondary system

Time Period (s)		No. of RV Open Cycles	Steam Mass Loss in SG ΔM_G (kg)	Water Mass Loss in SG ΔM_L (kg)	Discharged Steam Mass ΔM_D (kg)	Difference $\Delta M_G+\Delta M_L-\Delta M_D$ (kg)
(1)	2438.2 - 2817.2	7	19.6	154.5	153.5	20.6
(2)	3067.3 - 3416.4	5	12.8	82.8	86.7	8.9
(3)	3553.9 - 3989.6	6	13.4	113.7	114.5	12.6
(4)	4071.7 - 4468.2	5	10.1	74.5	73.7	10.9
(5)	4636.4 - 5109.7	4	8.1	53.4	36.0	25.5
(6)	5165.8 - 5452.2	1	5.2	5.2	6.9	- 1.7

Table 4.4-3 Mass balance in SG-B secondary system

Time Period (s)		No. of RV Open Cycles	Steam Mass Loss in SG ΔM_G (kg)	Water Mass Loss in SG ΔM_L (kg)	Discharged Steam Mass ΔM_D (kg)	Difference $\Delta M_G+\Delta M_L-\Delta M_D$ (kg)
(1)	2438.2 - 2817.2	7	16.3	163.0	174.5	4.8
(2)	3067.3 - 3416.4	5	9.4	88.5	104.1	- 6.2
(3)	3553.9 - 3989.6	6	12.9	125.2	147.8	- 9.7
(4)	4071.7 - 4468.2	5	9.1	74.6	71.9	11.8
(5)	4636.4 - 5109.7	4	9.8	48.8	35.0	23.6
(6)	5165.8 - 5452.2	1	5.1	0.0	5.0	0.1

Table 4.4-4 Energy balance in SG-A secondary system

Time Length Δt (s)	Thermal Energy in Each Term ($\times 10^5$ kJ) Loss in SG Wall ΔQ_W	Heat Loss from SG Q_{HL}	Loss in U-tubes ΔQ_U	Loss in Fluid ΔQ_F	Steam Outflow Q_D	Transfered to U-tubes Q_S (*)	Time Average $Q_S/\Delta t$ (kJ/s)
(1) 379.0	0.33	0.09	0.15	2.38	4.42	1.65	440
(2) 349.1	0.19	0.07	0.11	1.33	2.52	0.96	270
(3) 435.7	0.26	0.09	0.12	1.53	3.36	1.54	350
(4) 396.5	0.33	0.08	0.03	0.98	2.17	0.91	230
(5) 473.3	0.48	0.09	- 0.14	0.67	1.06	0.14	30
(6) 286.4	- 0.01	0.05	- 0.07	0.15	0.20	0.18	63

Table 4.4-5 Energy balance in SG-B secondary system

Time Length Δt (s)	Thermal Energy in Each Term ($\times 10^5$ kJ) Loss in SG Wall ΔQ_W	Heat Loss from SG Q_{HL}	Loss in U-tubes ΔQ_U	Loss in Fluid ΔQ_F	Steam Outflow Q_D	Transfered to U-tubes Q_S (*)	Time Average $Q_S/\Delta t$ (kJ/s)
(1) 379.0	0.37	0.10	0.16	2.45	5.03	2.15	570
(2) 349.1	0.25	0.09	0.12	1.26	3.03	1.49	430
(3) 435.7	0.23	0.10	0.12	1.64	4.33	2.44	560
(4) 396.5	0.26	0.09	0.03	0.95	2.11	0.96	240
(5) 473.3	- 0.04	0.10	- 0.14	0.69	1.03	0.62	130
(6) 286.4	0.0	0.06	- 0.07	0.15	0.15	0.13	45

* $Q_S = -\Delta Q_W + Q_{HL} - \Delta Q_U - \Delta Q_F + Q_D$.

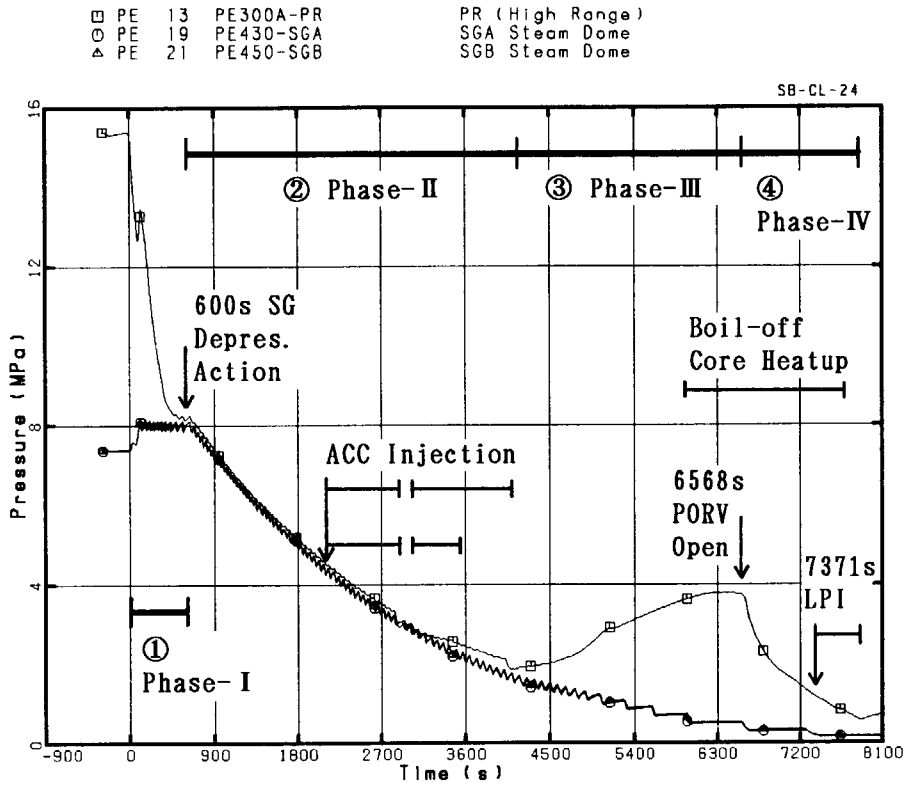

Fig. 4.1.1 Transient system pressures and major events in four phases

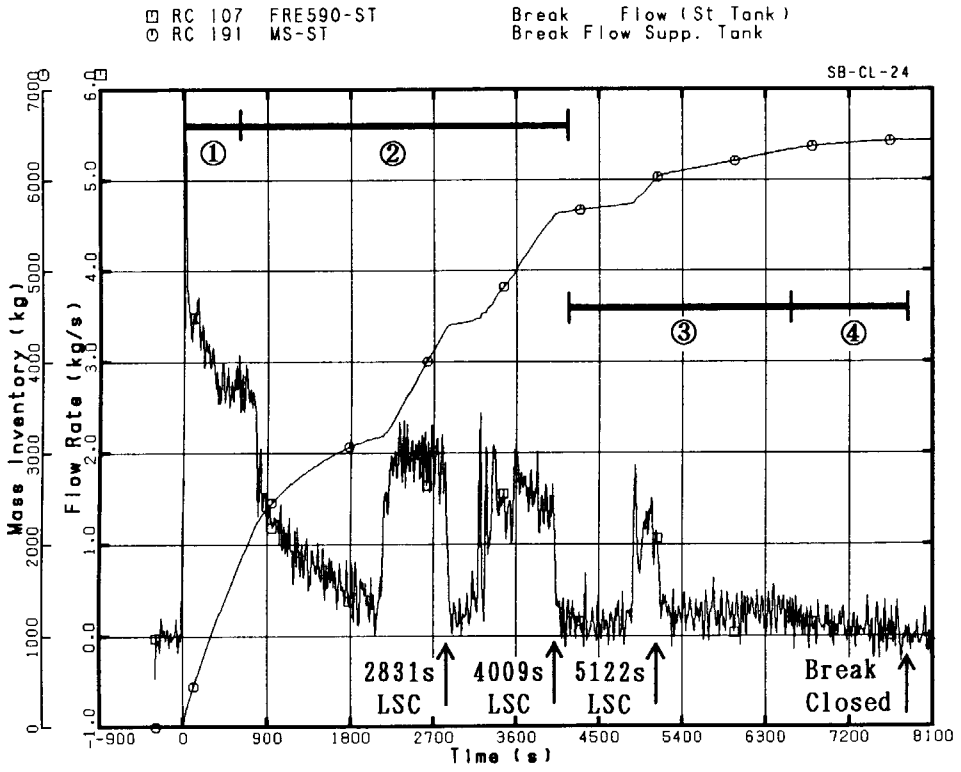

Fig. 4.1.2 Discharged mass and break flow rate in four phases

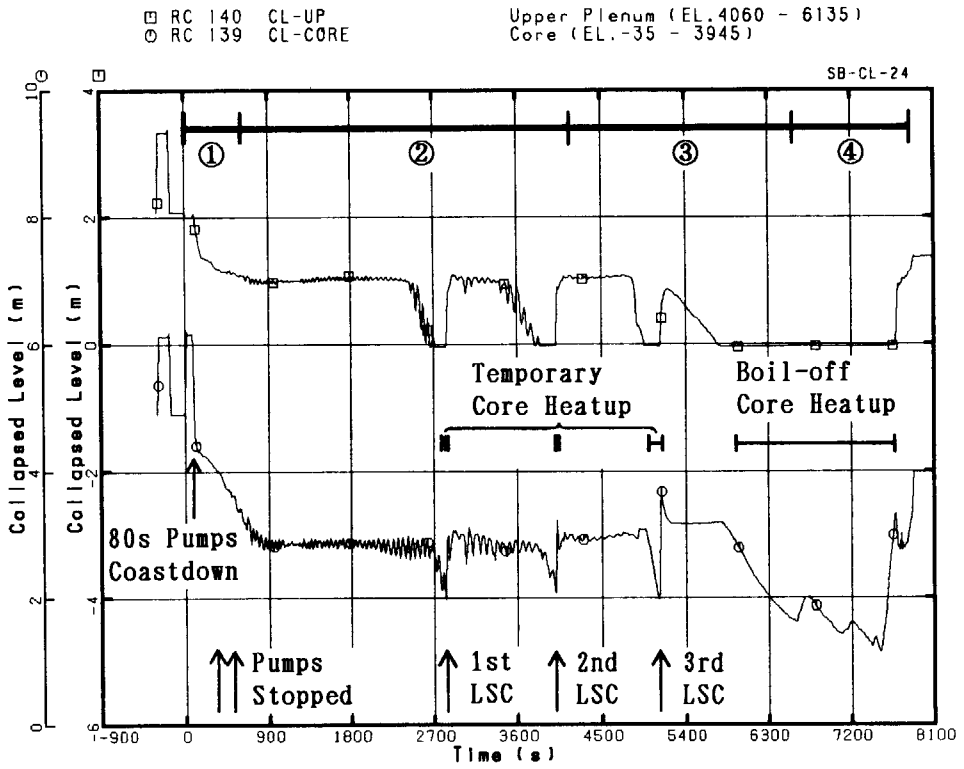

Fig. 4.1.3 Collapsed liquid levels in upper plenum and core in four phases

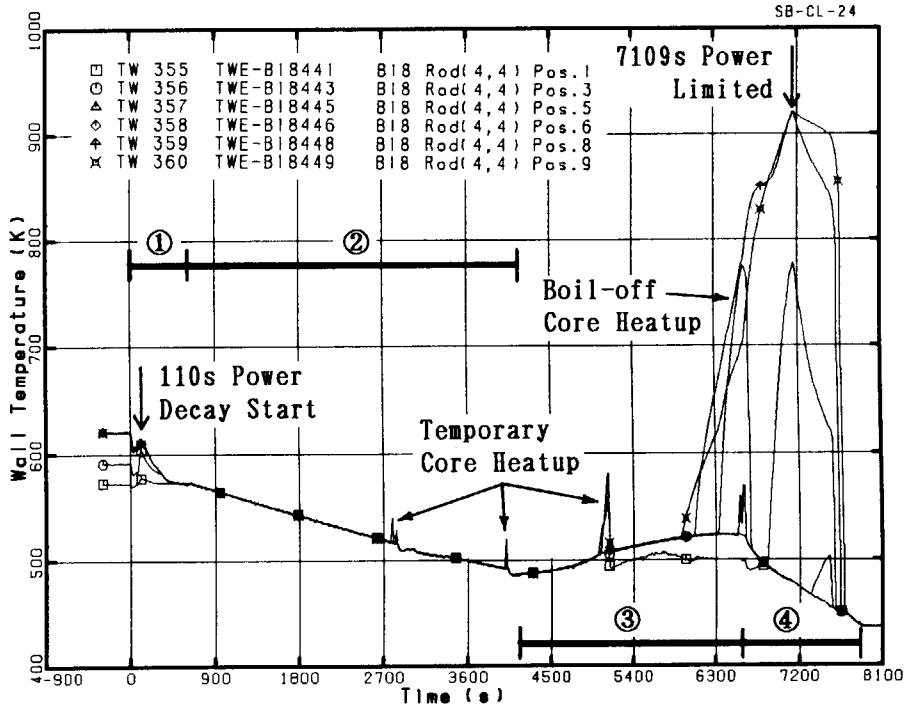

Fig. 4.1.4 Representative heater rod temperatures in four phases

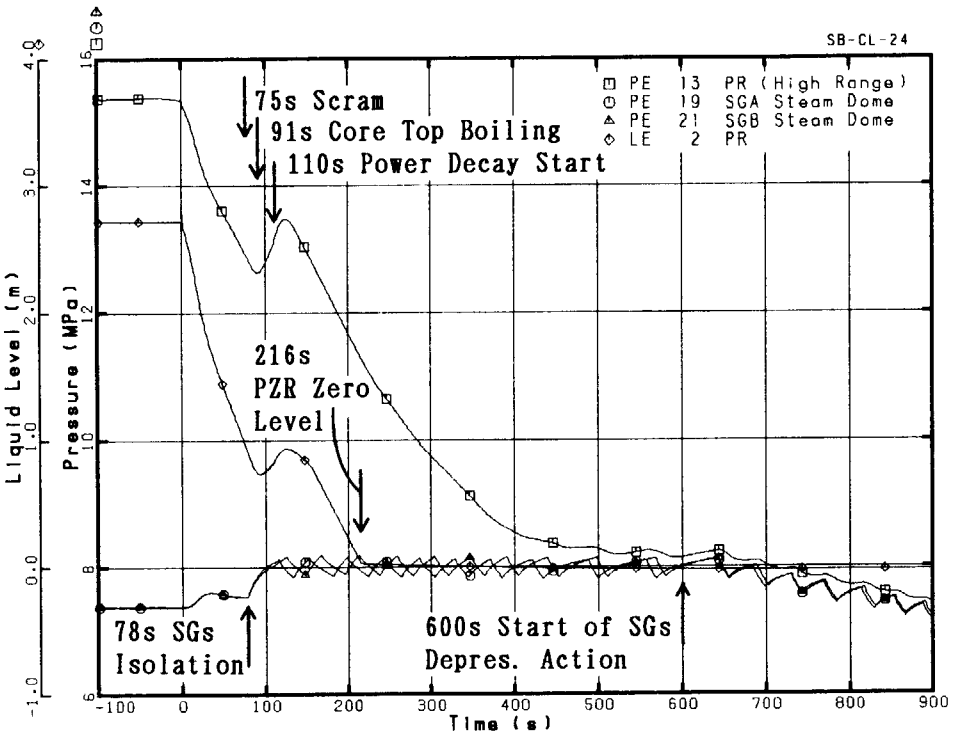

Fig. 4.1.5 Initial responses in pressurizer and SGs

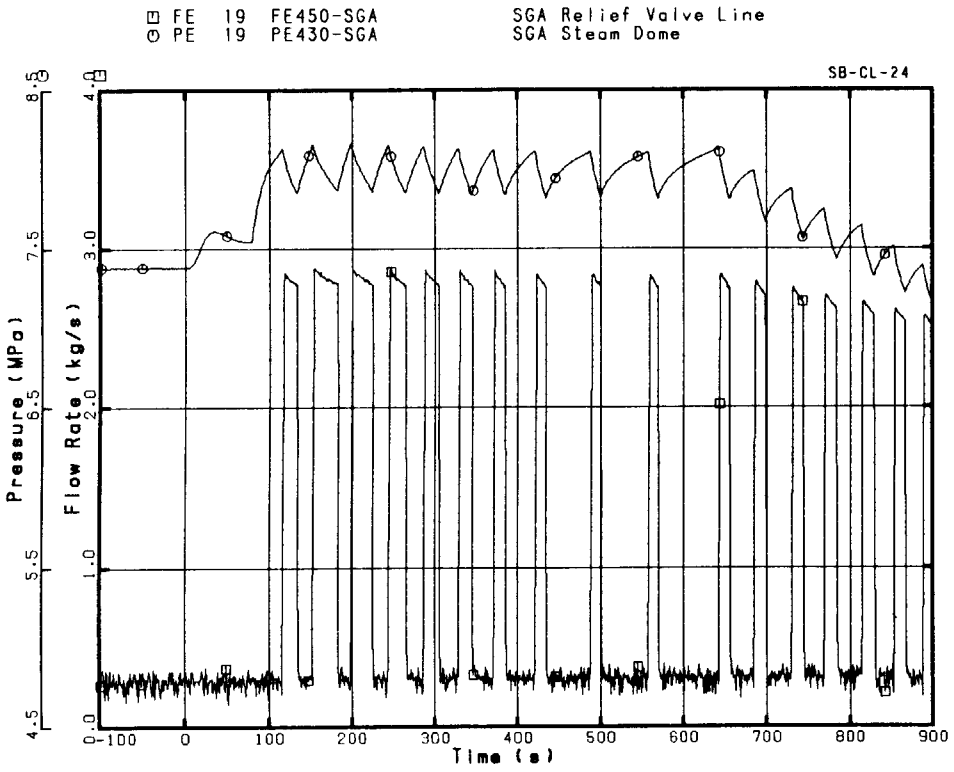

Fig. 4.1.6 Steam flow and pressure during SG-A relief valve cyclic operation

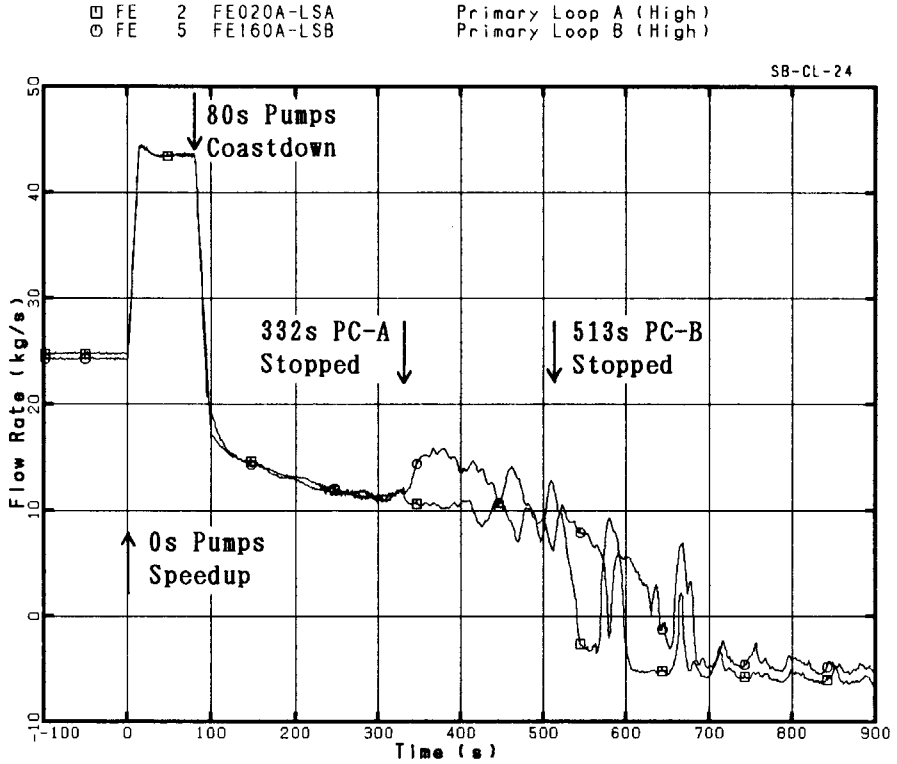

Fig. 4. 1. 7 Primary loop flow rates in initial transient

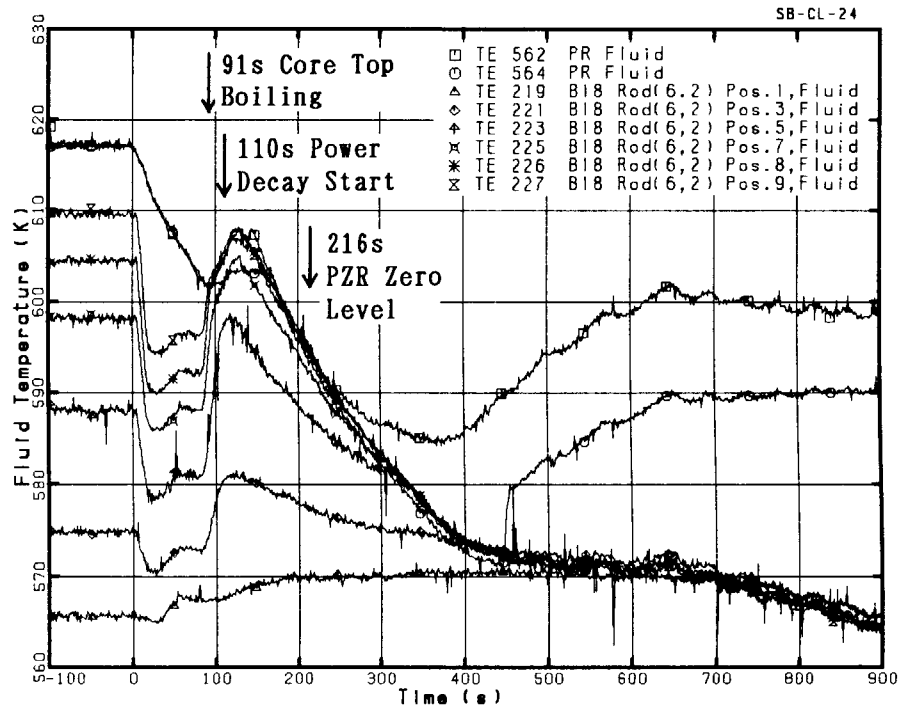

Fig. 4. 1. 8 Fluid temperatures in pressurizer and core in initial transient

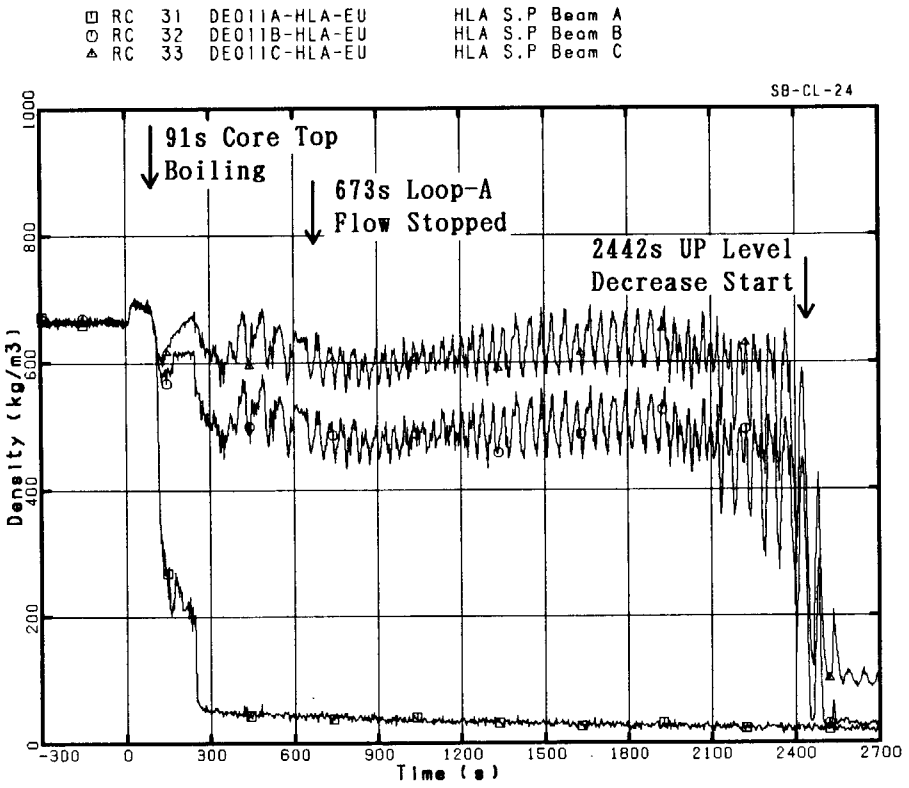

Fig. 4.1.9 Three-beam density data at hot leg A

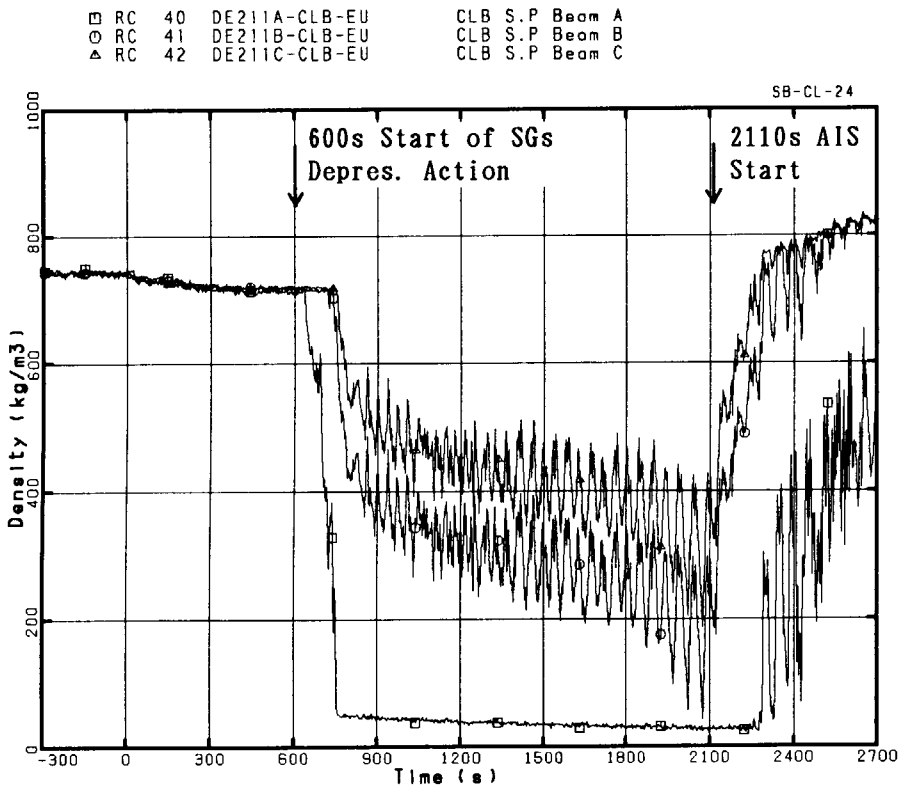

Fig. 4.1.10 Three-beam density data at cold leg B

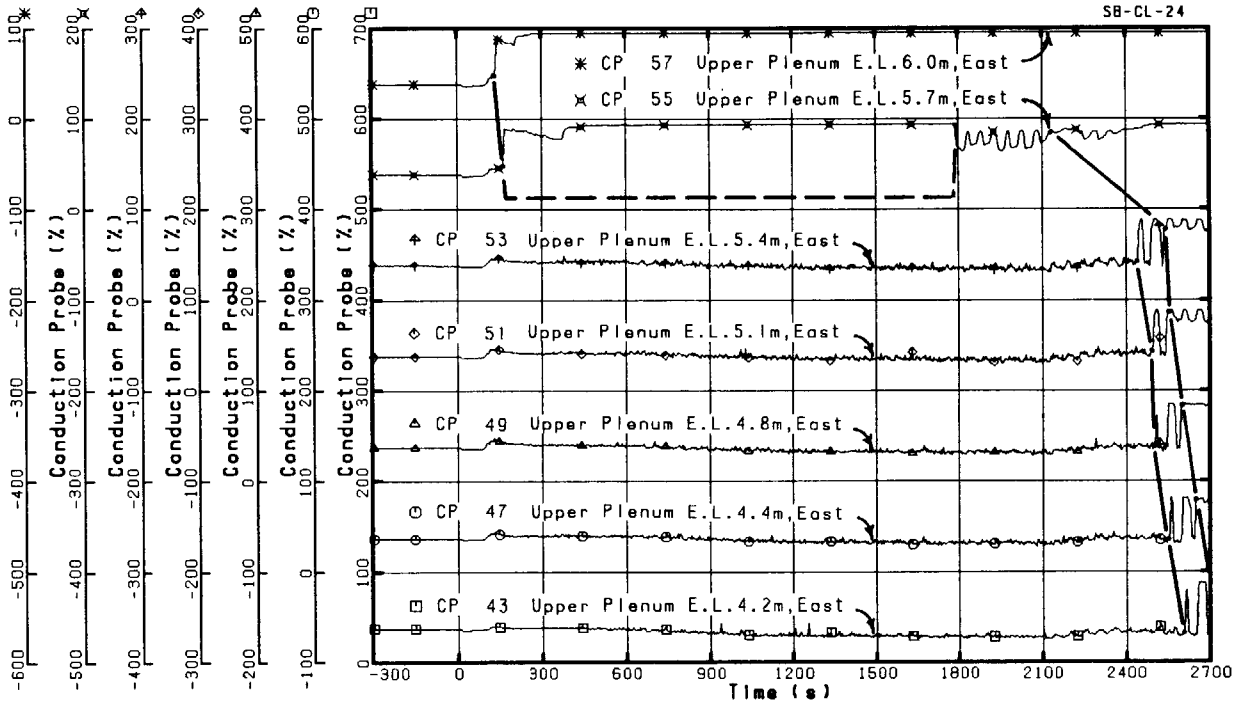

Fig. 4.1.11 CP data for mixture level detection in upper plenum

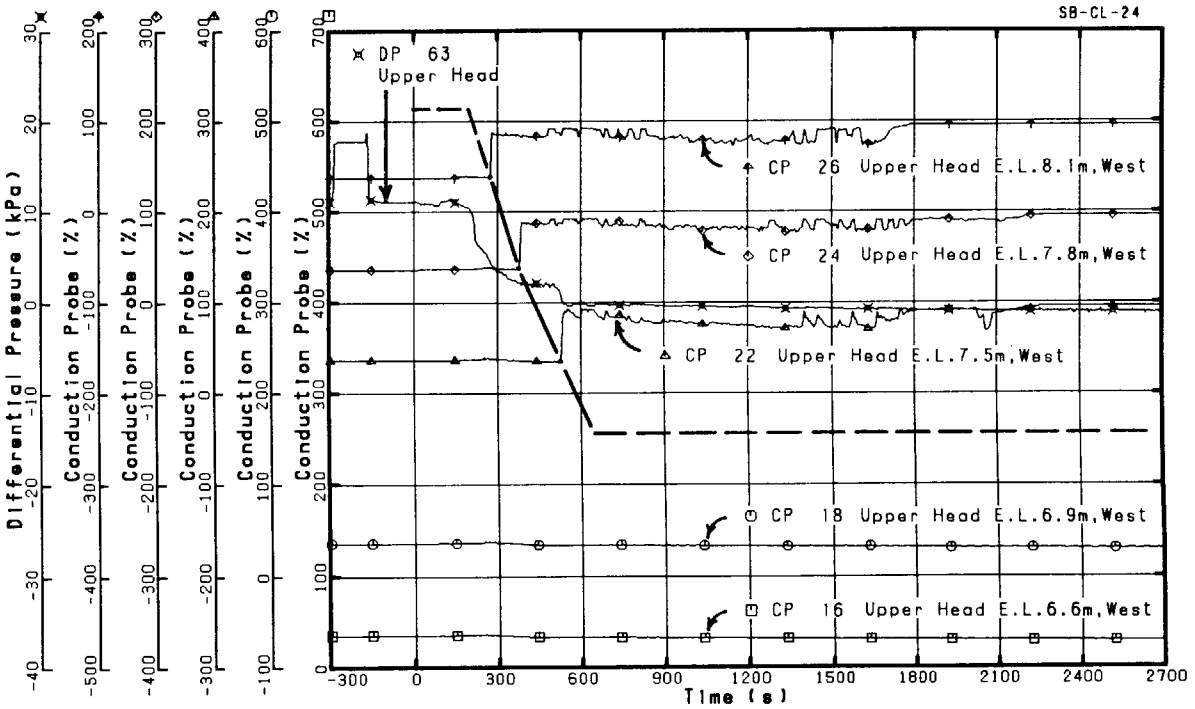

Fig. 4.1.12 CP data for mixture level detection in upper head

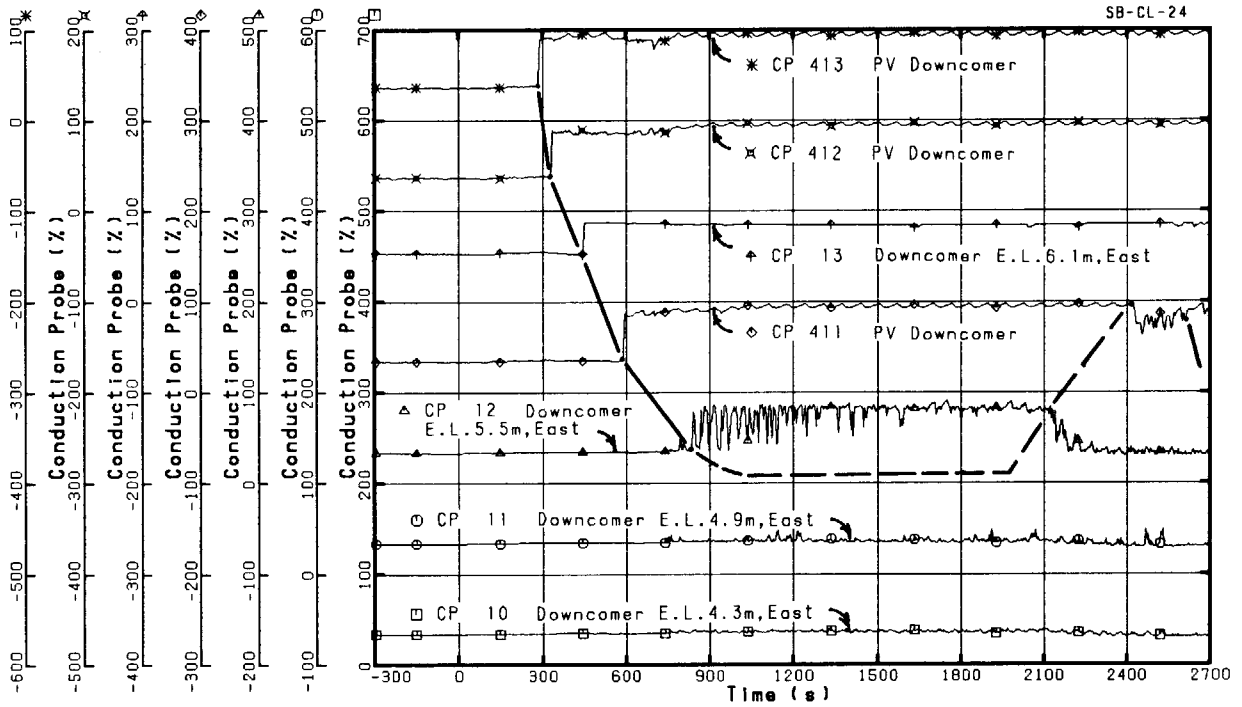

Fig. 4. 1. 13 CP data for mixture level detection in upper downcomer

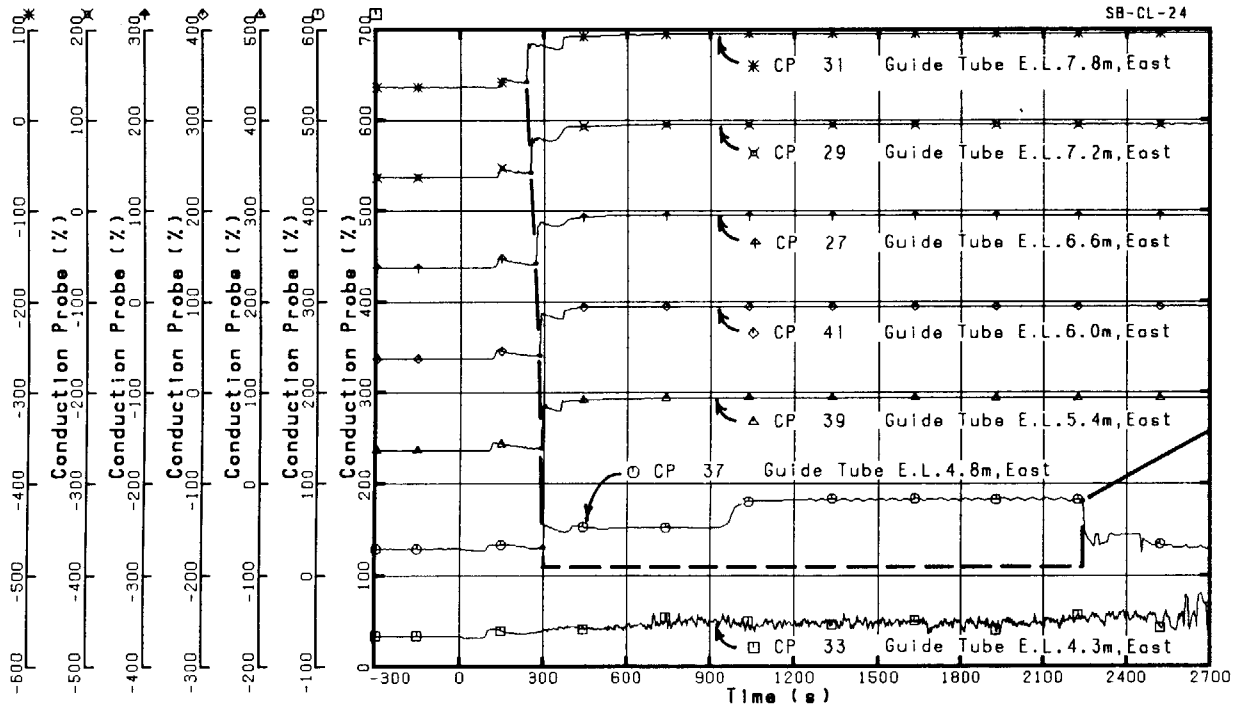

Fig. 4. 1. 14 CP data for mixture level detection in control rod guide tube

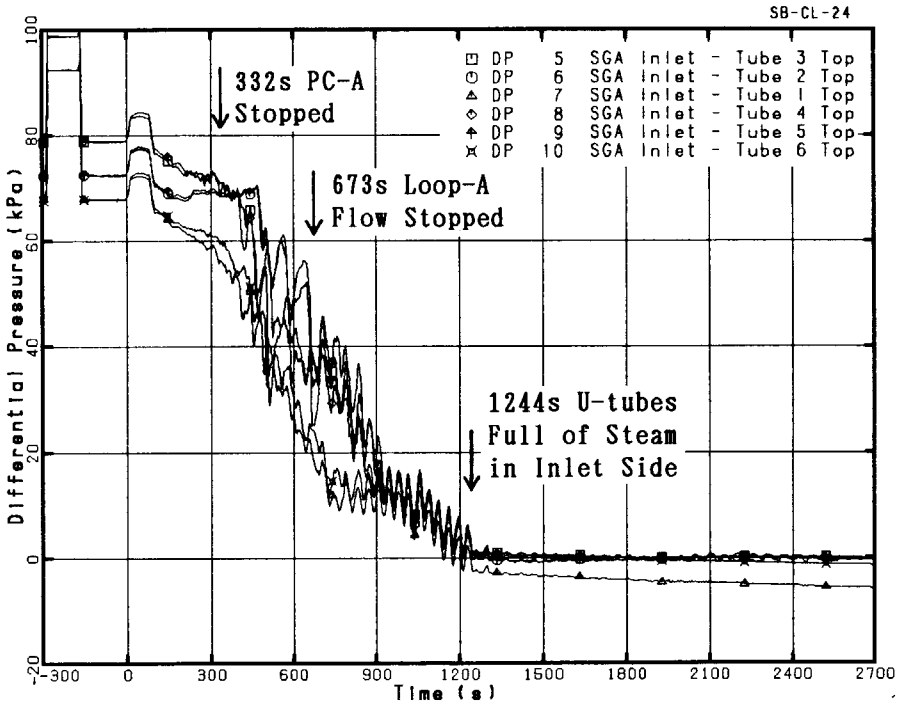

Fig. 4. 1. 15 DP data in U-tube inlet sides at SG-A

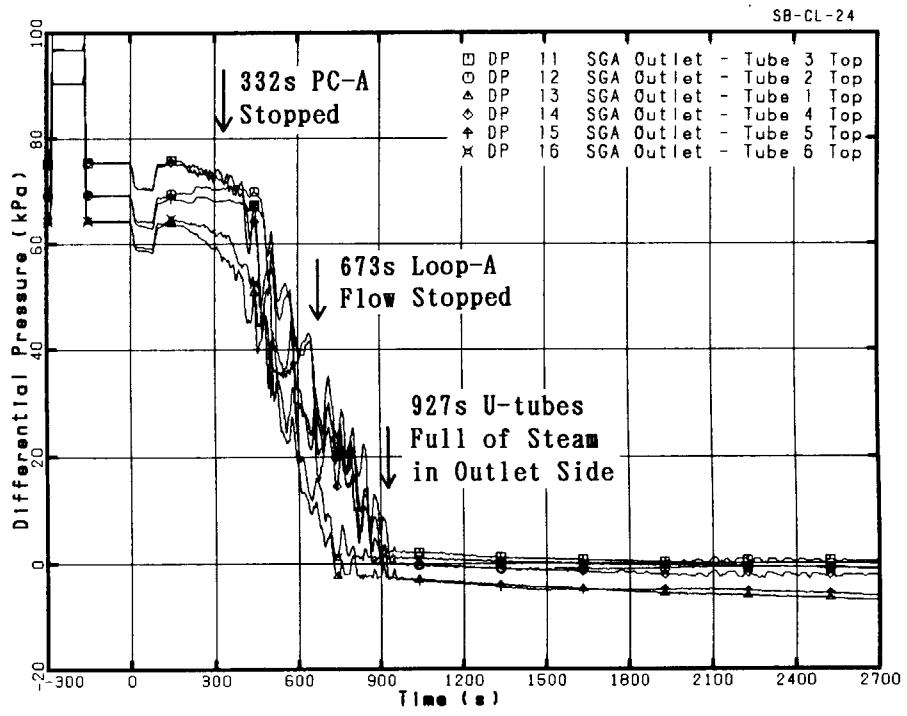

Fig. 4. 1. 16 DP data in U-tube outlet sides at SG-A

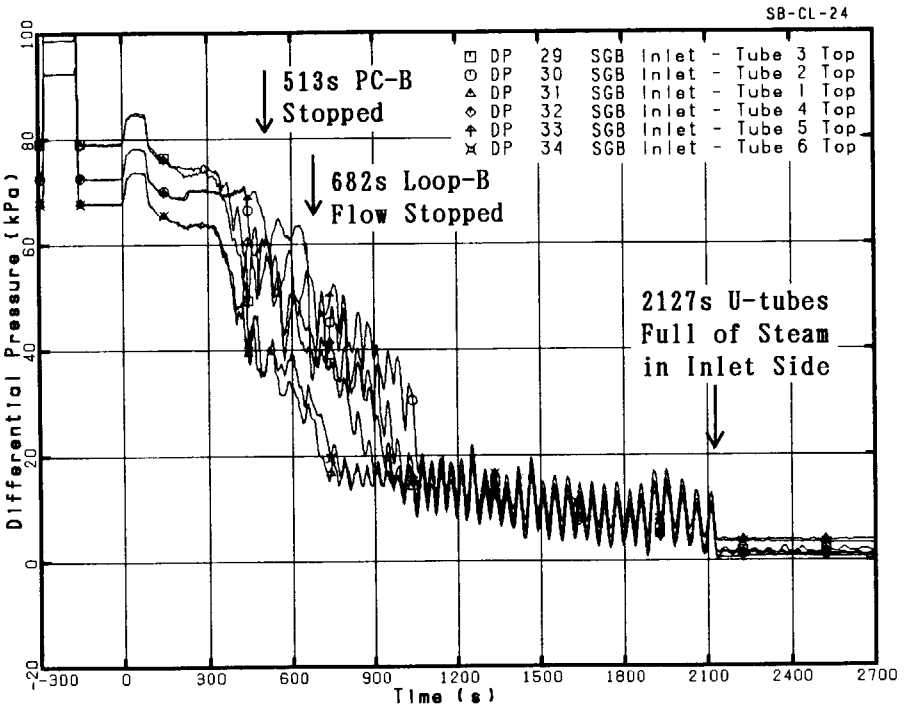

Fig. 4.1.17 DP data in U-tube inlet sides at SG-B

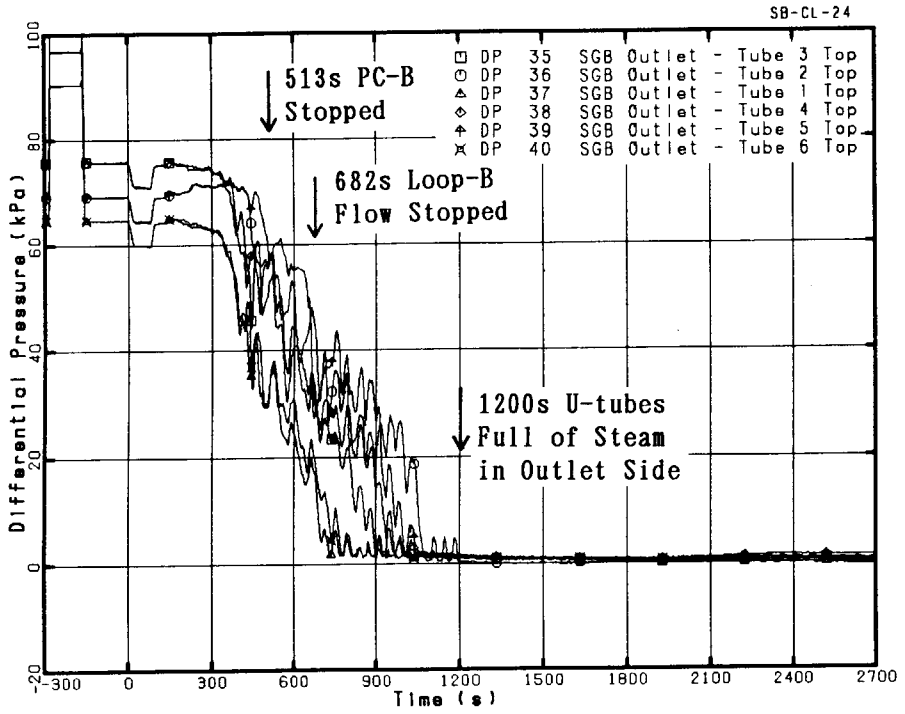

Fig. 4.1.18 DP data in U-tube outlet sides at SG-B

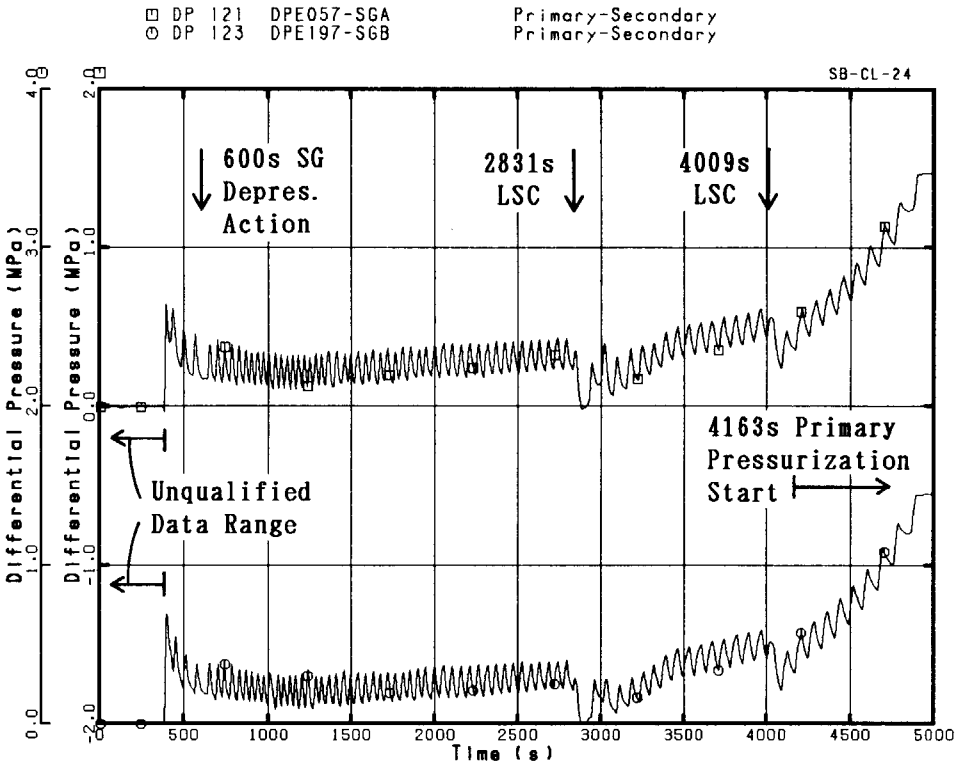

Fig. 4.1.19 Pressure differences between primary and secondary sides

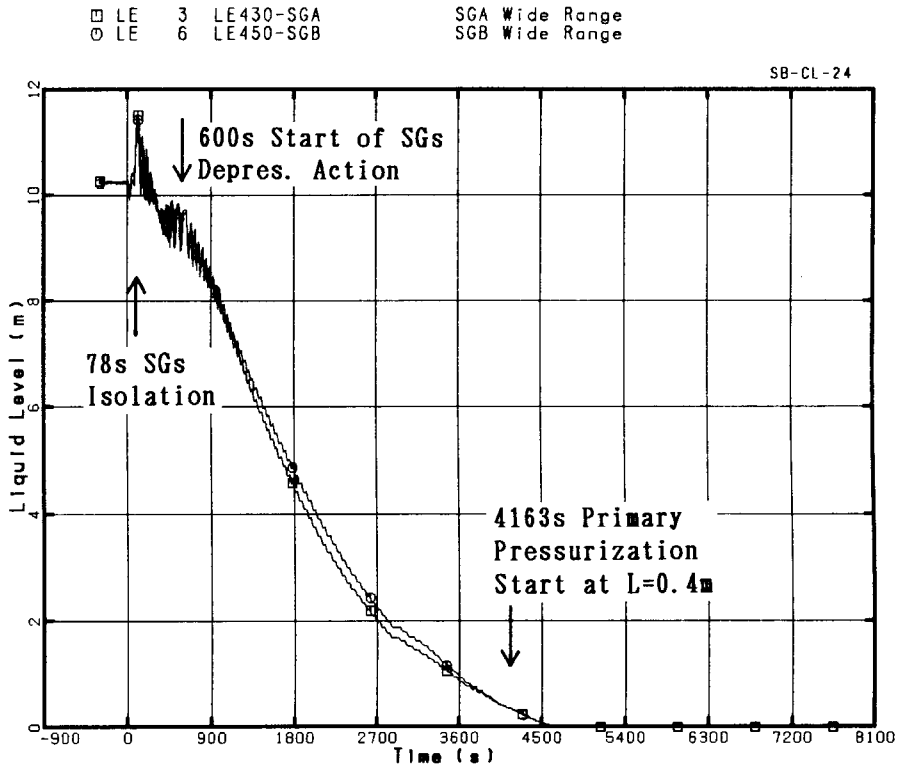

Fig. 4.1.20 Wide-range collapsed water levels in SG secondary sides

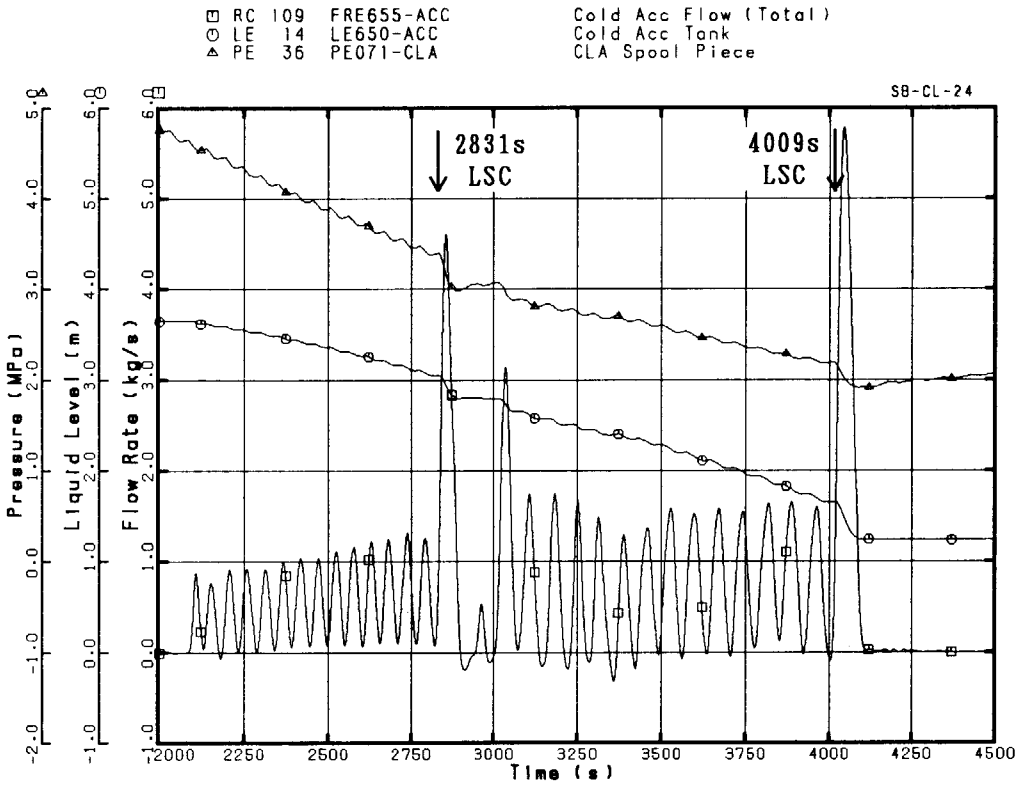

Fig. 4. 1. 21 Accumulator injection to cold leg A (ACC)

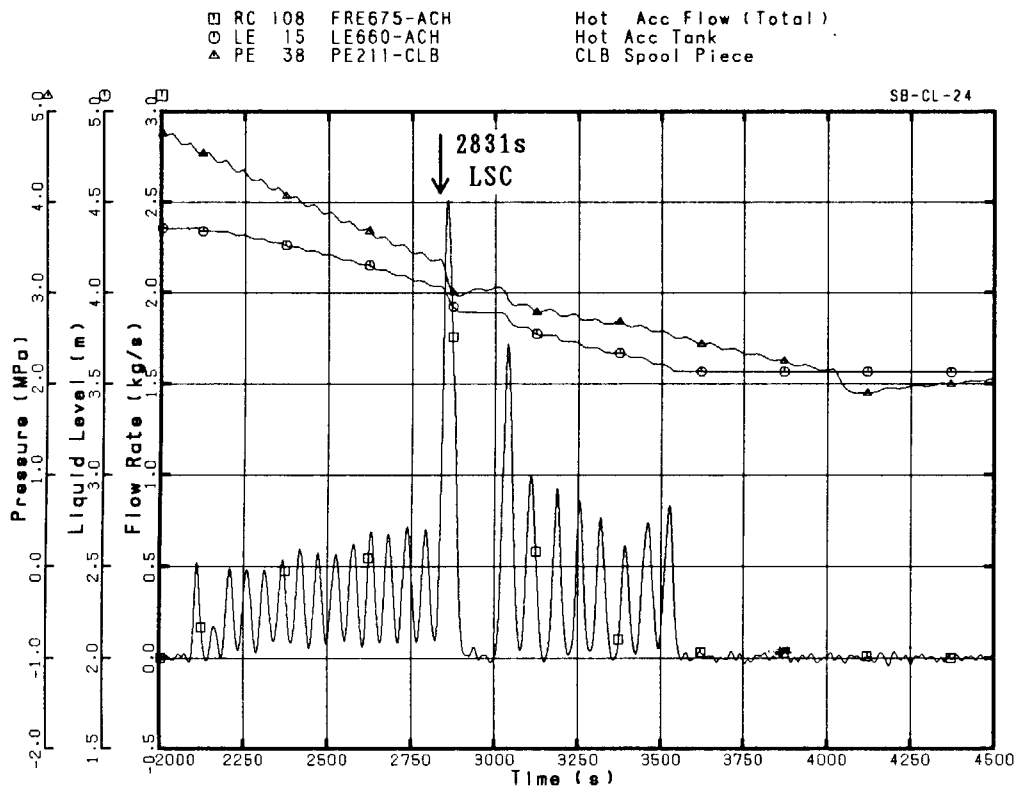

Fig. 4. 1. 22 Accumulator injection to cold leg B (ACH)

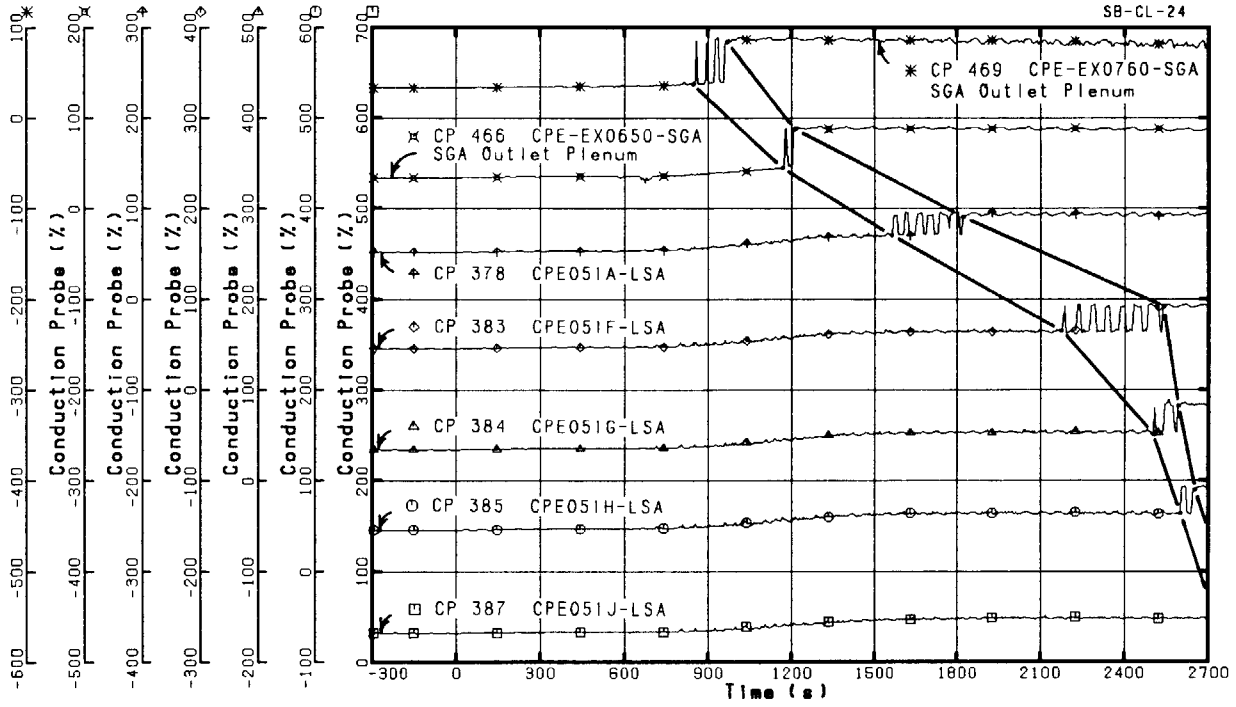

Fig. 4. 1. 23 CP mixture level data in SG-A outlet plenum and loopseal A (0 - 2700 s)

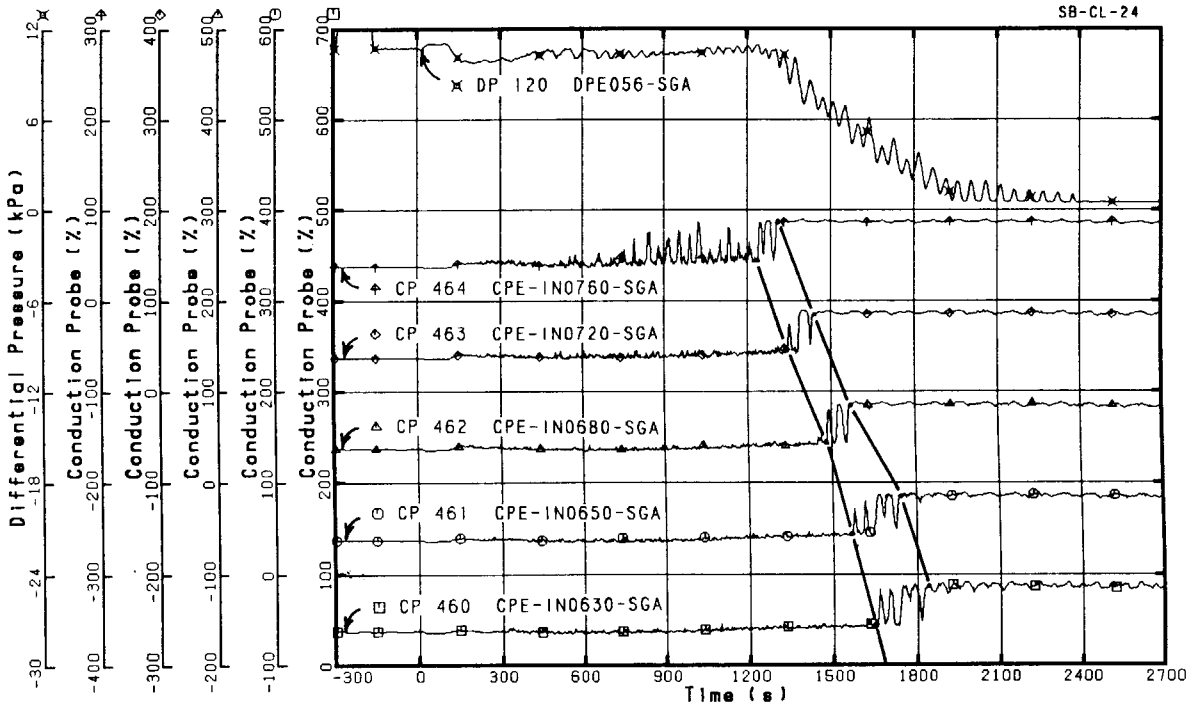

Fig. 4. 1. 24 CP mixture level and DP data in SG-A inlet plenum (0 - 2700 s)

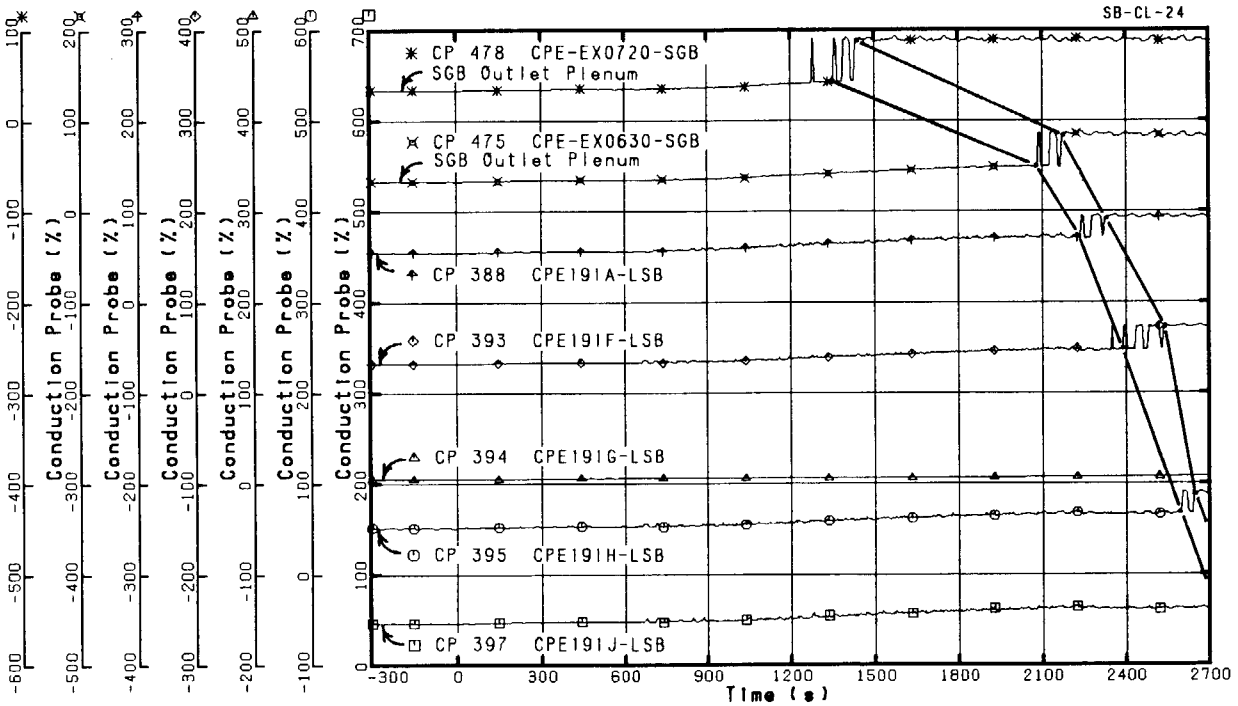

Fig. 4. 1. 25 CP mixture level data in SG-B outlet plenum and loopseal B (0 - 2700 s)

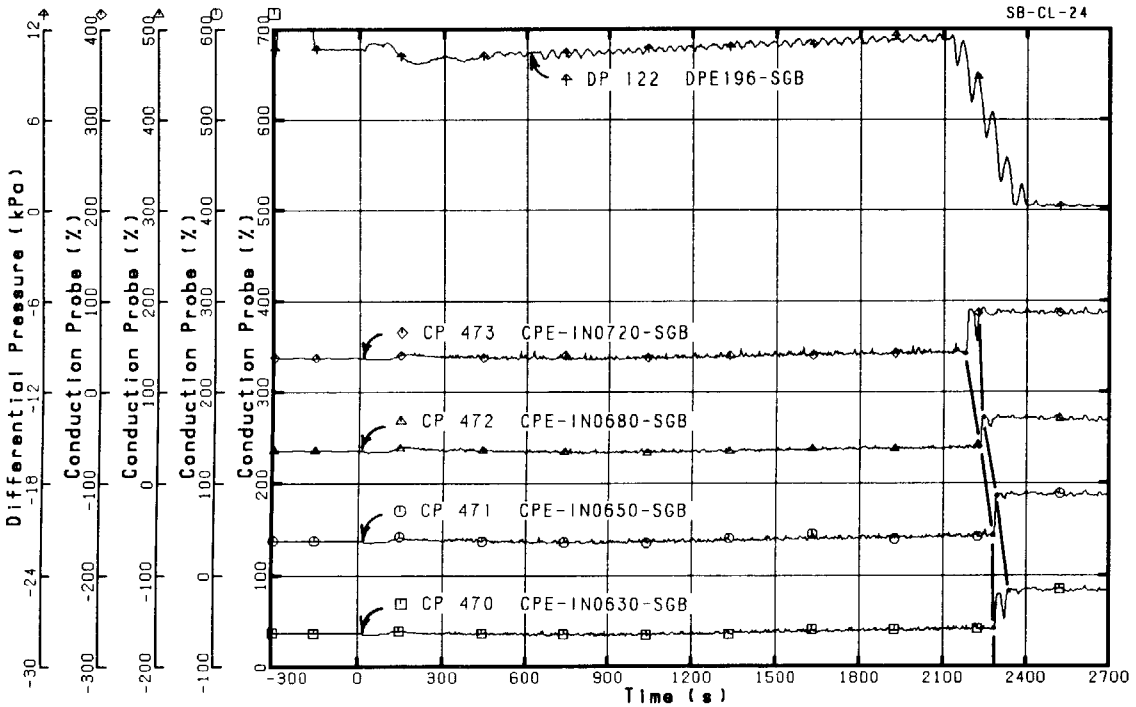

Fig. 4. 1. 26 CP mixture level and DP data in SG-B inlet plenum (0 - 2700 s)

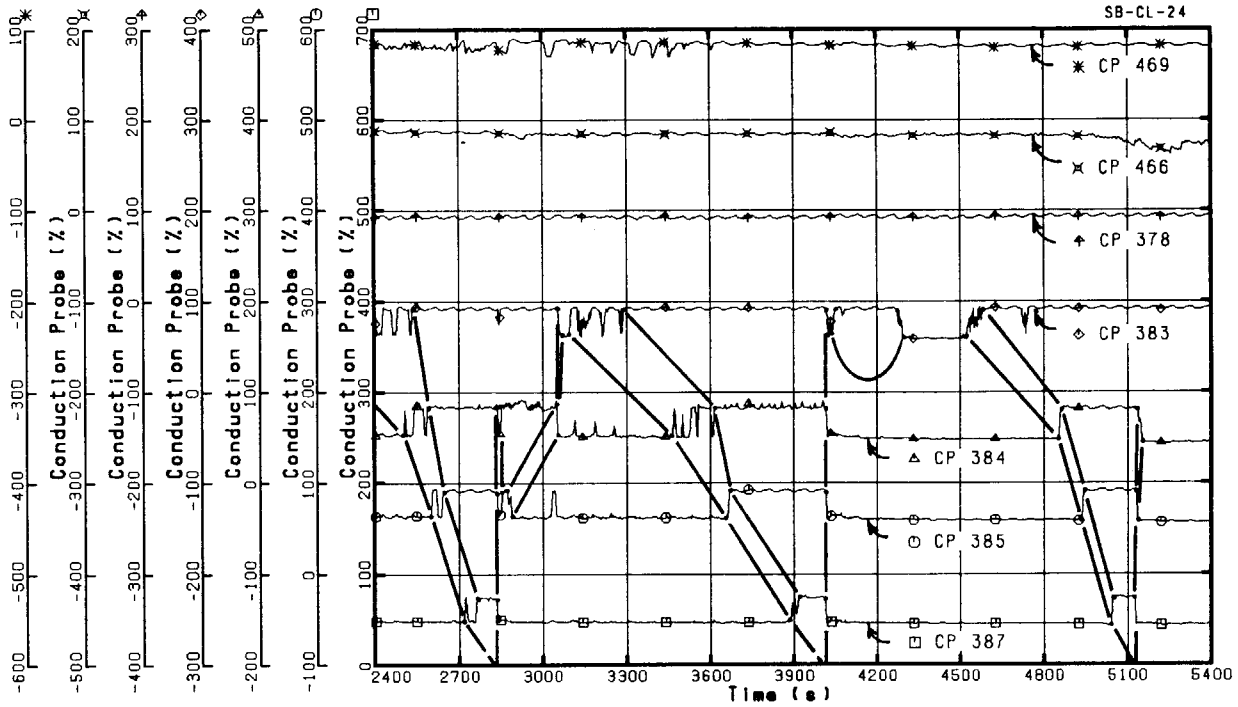

Fig. 4.1.27 CP mixture level data in SG-A outlet plenum and loopseal A (2400 - 5400 s)

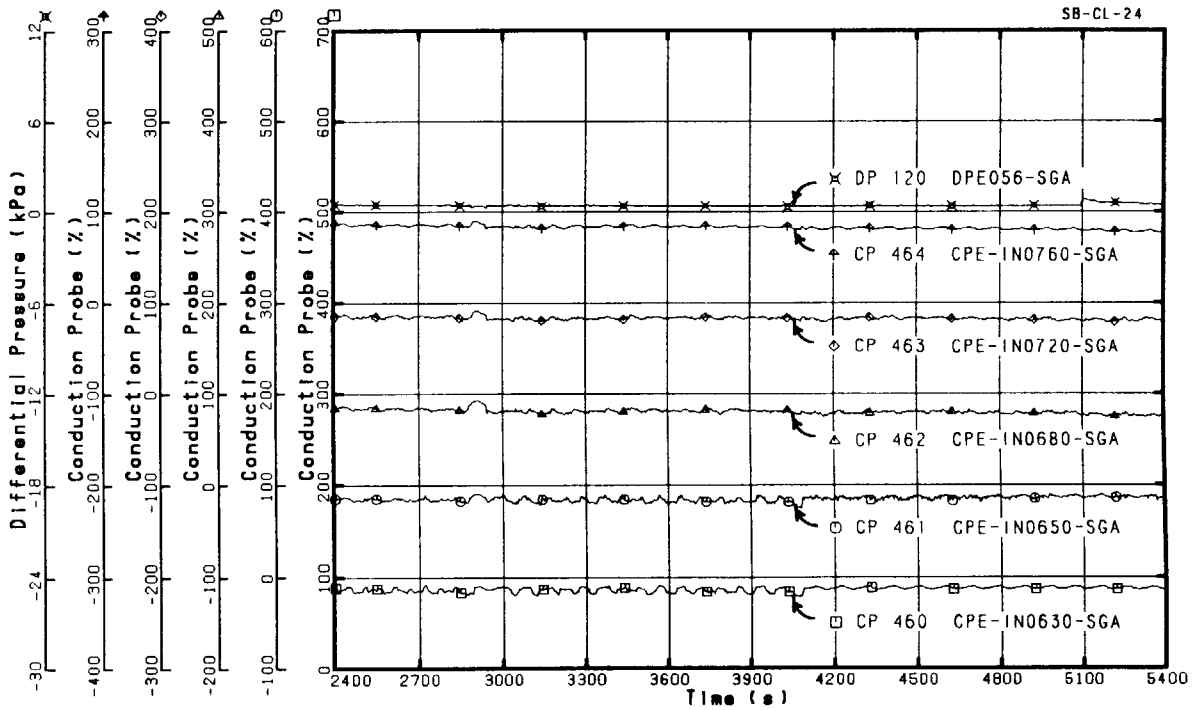

Fig. 4.1.28 CP mixture level and DP data in SG-A inlet plenum (2400 - 5400 s)

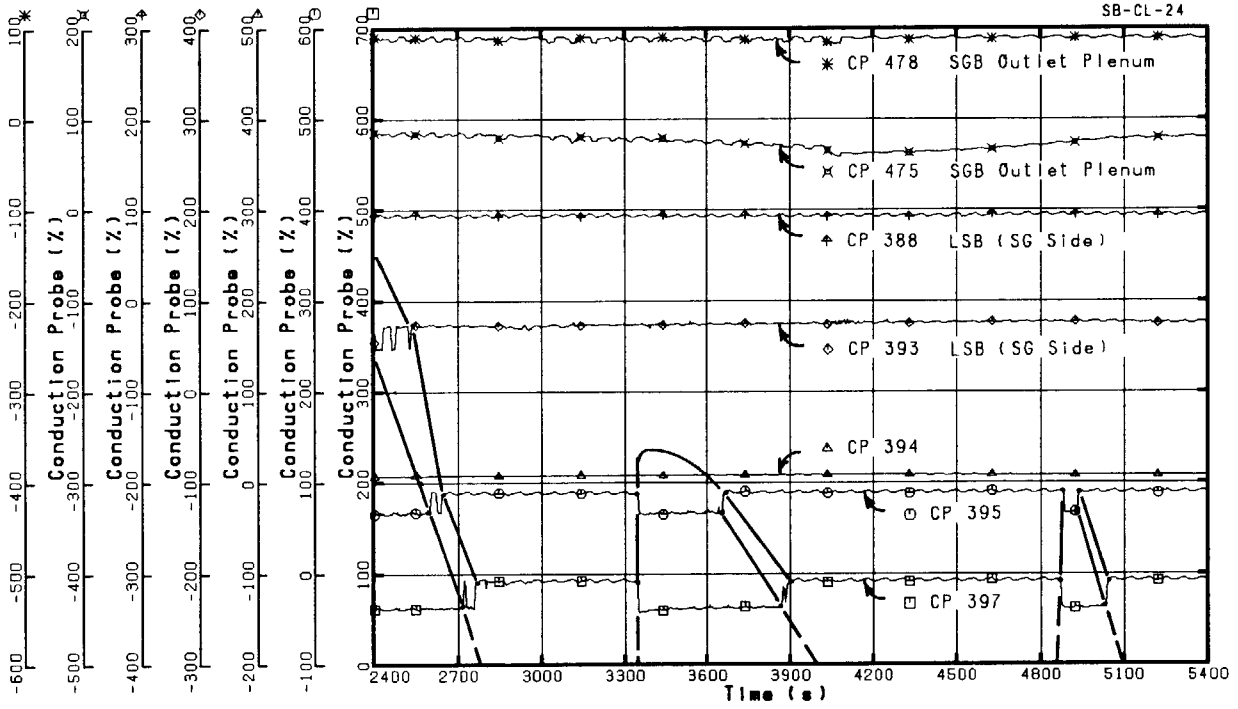

Fig. 4. 1. 29 CP mixture level data in SG-B outlet plenum and loopseal B (2400 - 5400 s)

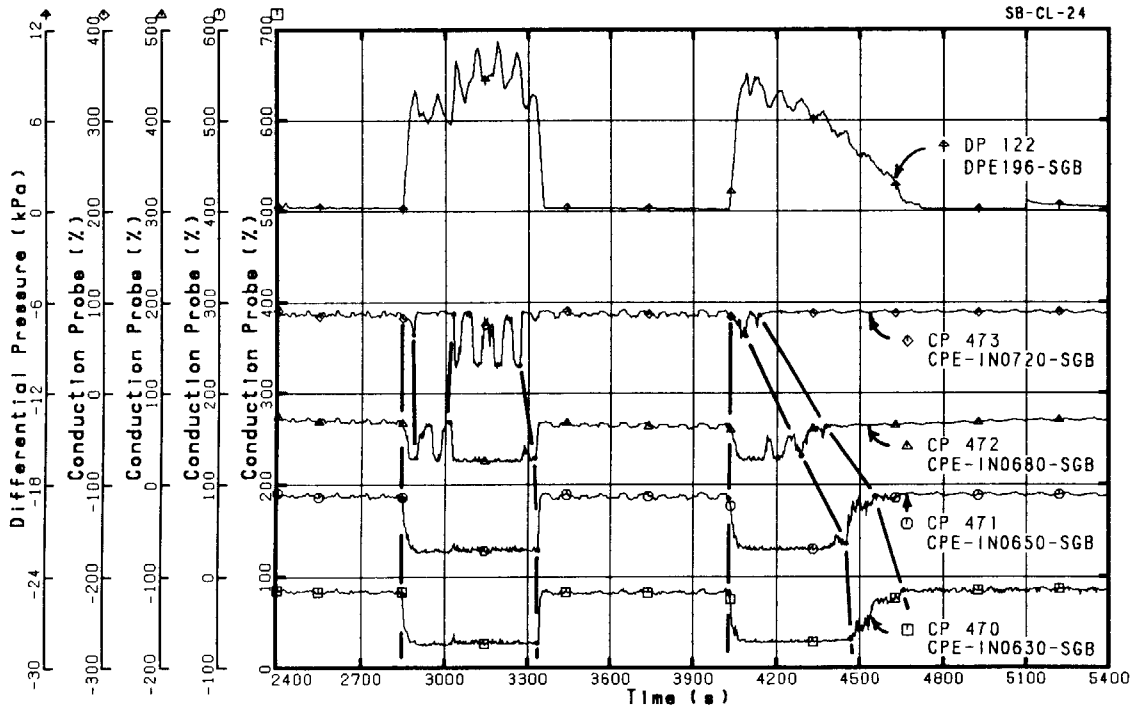

Fig. 4. 1. 30 CP mixture level and DP data in SG-B inlet plenum (2400 - 5400 s)

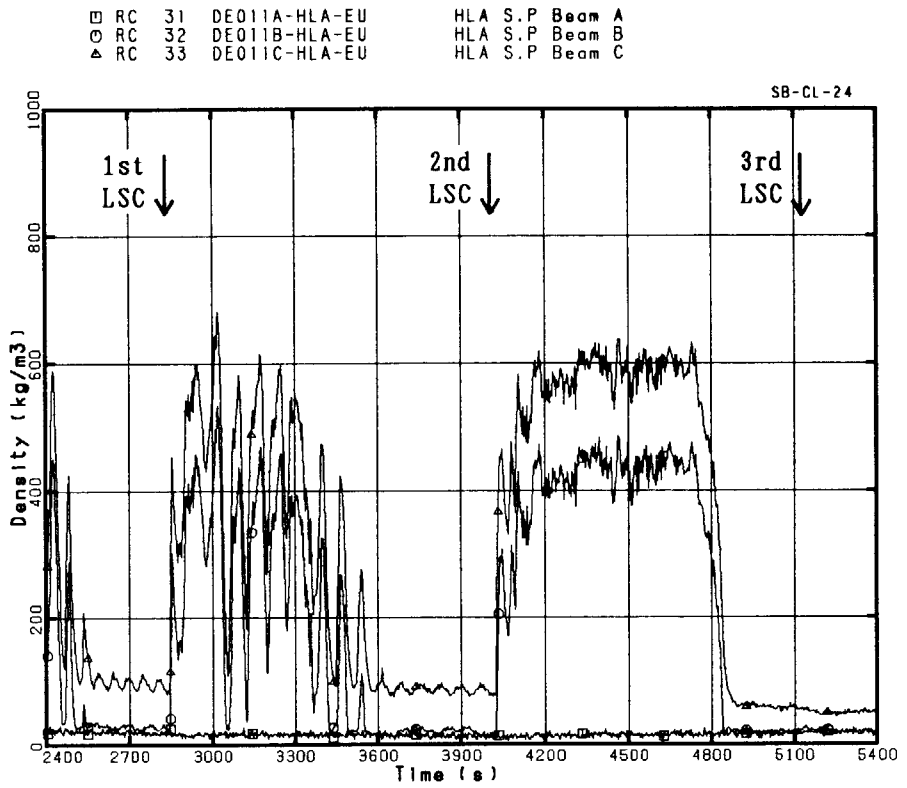

Fig. 4. 1. 31 Three-beam density data at hot leg A (2400 - 5400 s)

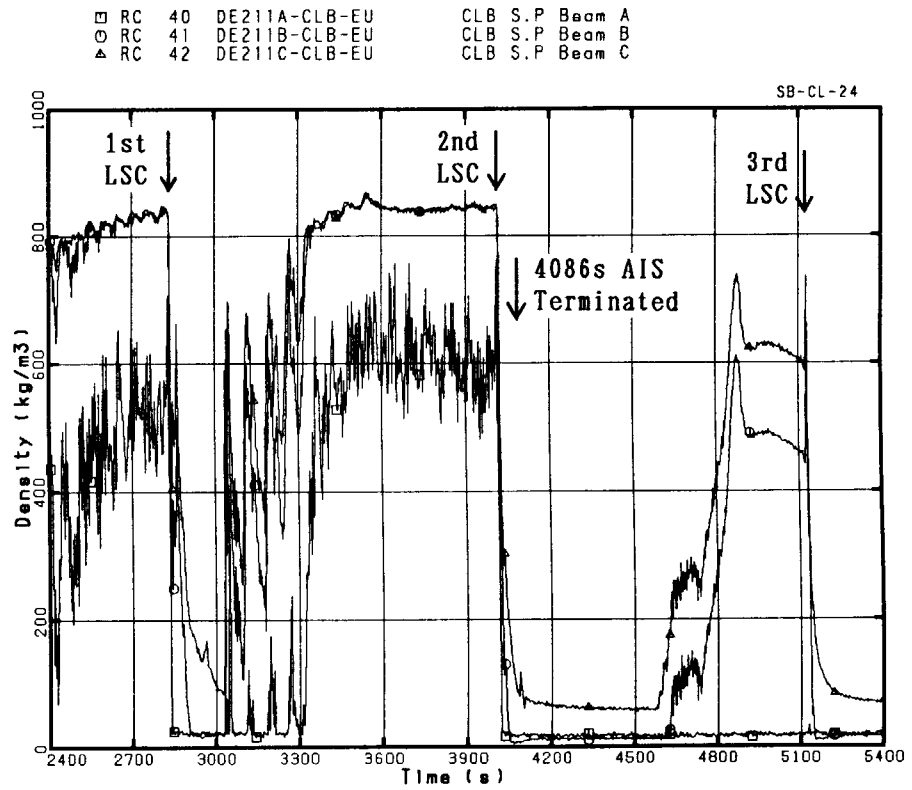

Fig. 4. 1. 32 Three-beam density data at cold leg B (2400 - 5400 s)

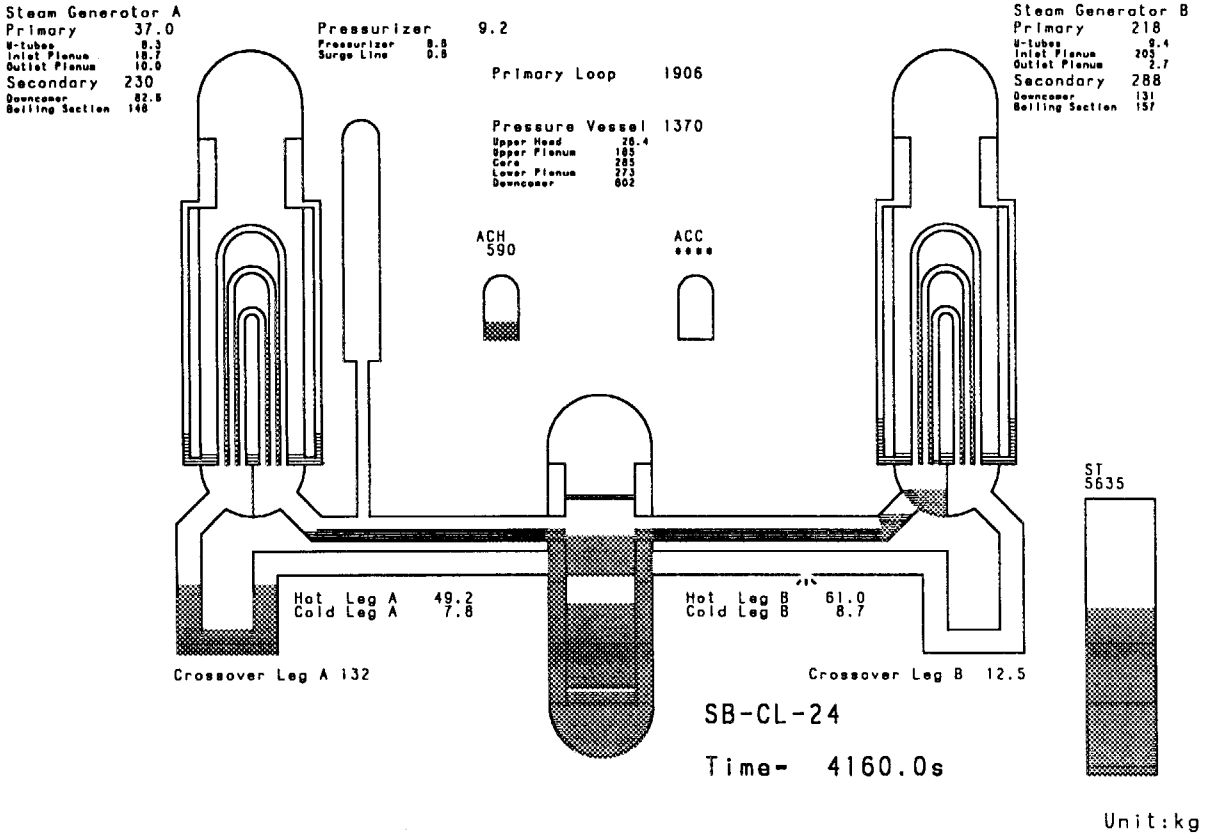

Fig. 4.1.33 Fluid mass distribution at primary pressurization start (4160 s)

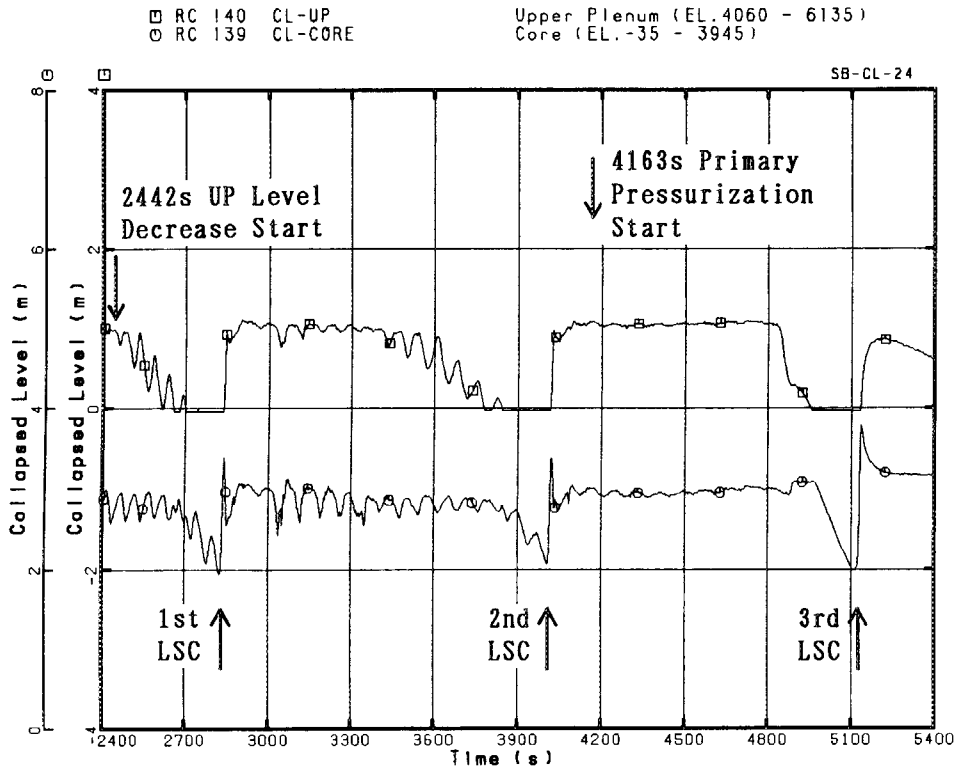

Fig. 4.1.34 Collapsed levels in upper plenum and core (2400 - 5400 s)

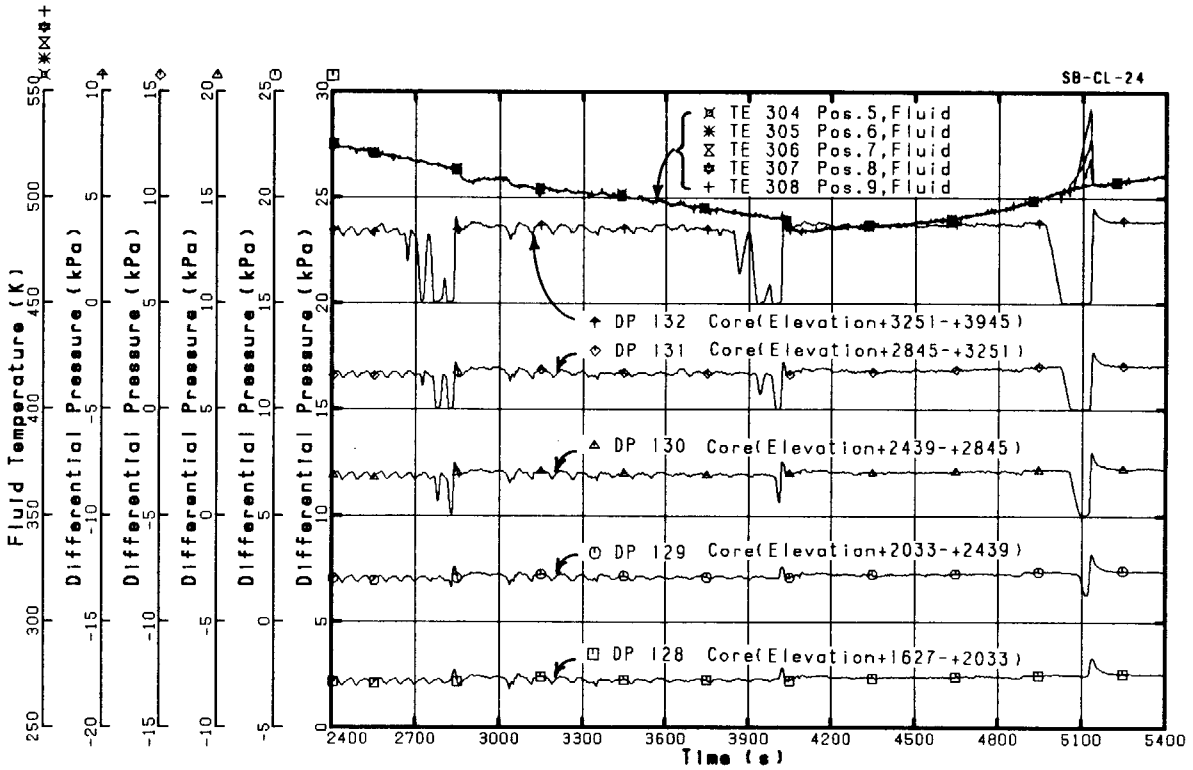

Fig. 4.1.35 Regional DP data and fluid temperatures in upper half core (2400 - 5400 s)

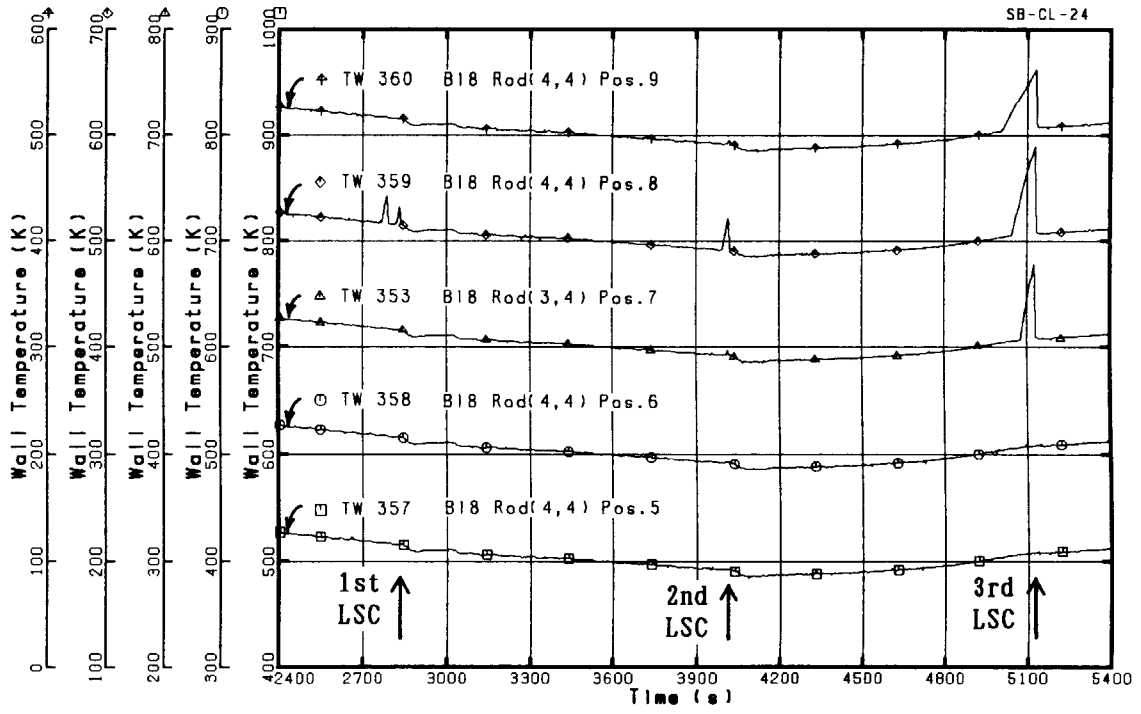

Fig. 4.1.36 Representative heater rod temperatures in upper half core (2400 - 5400 s)

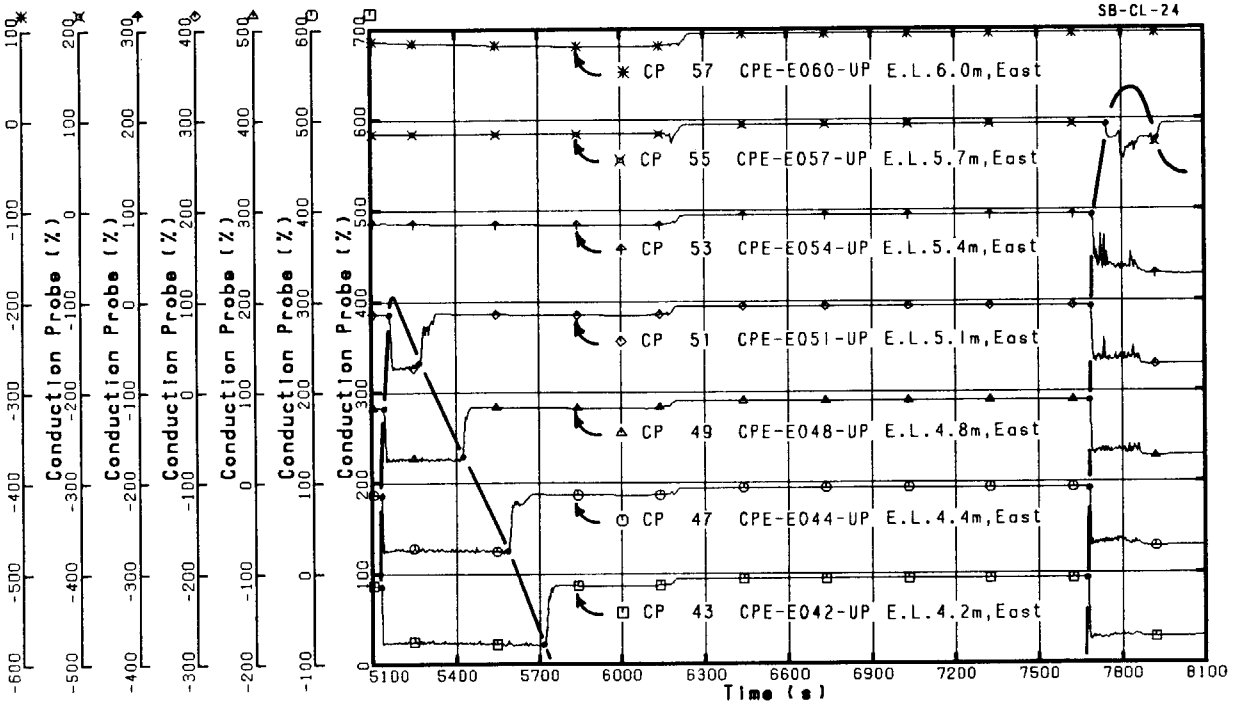

Fig. 4. 1. 37 CP data mixture level in upper plenum during boil-off process

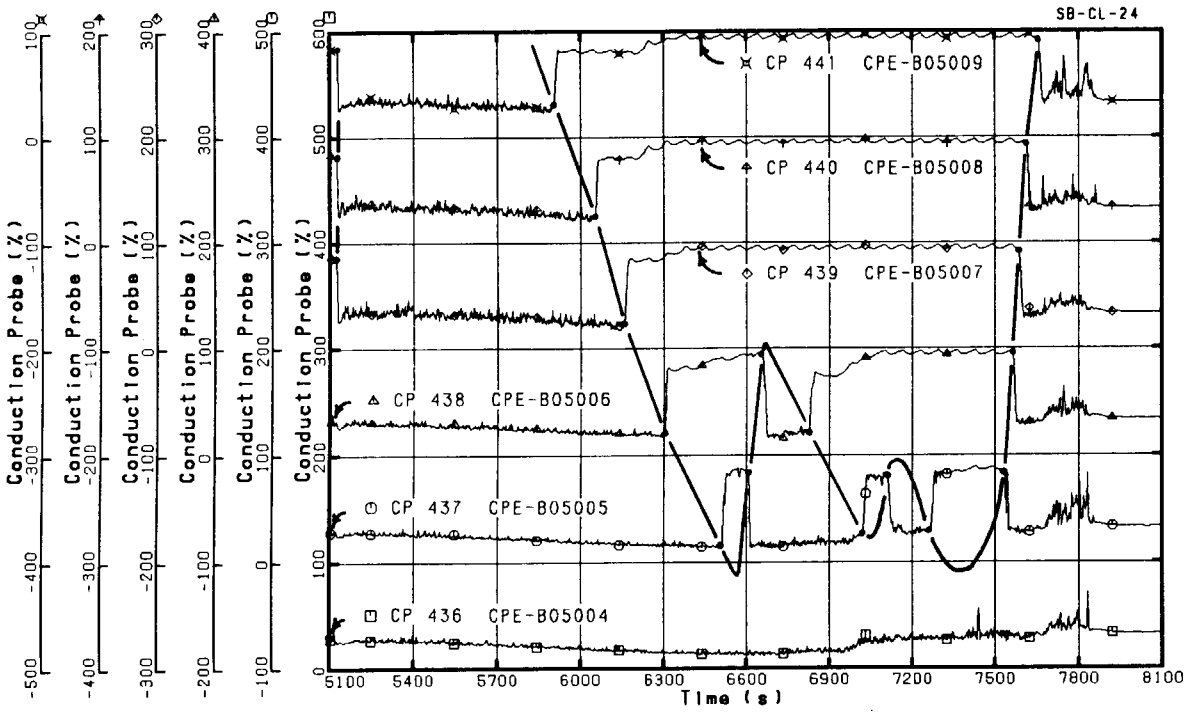

Fig. 4. 1. 38 CP data mixture level in core during boil-off process

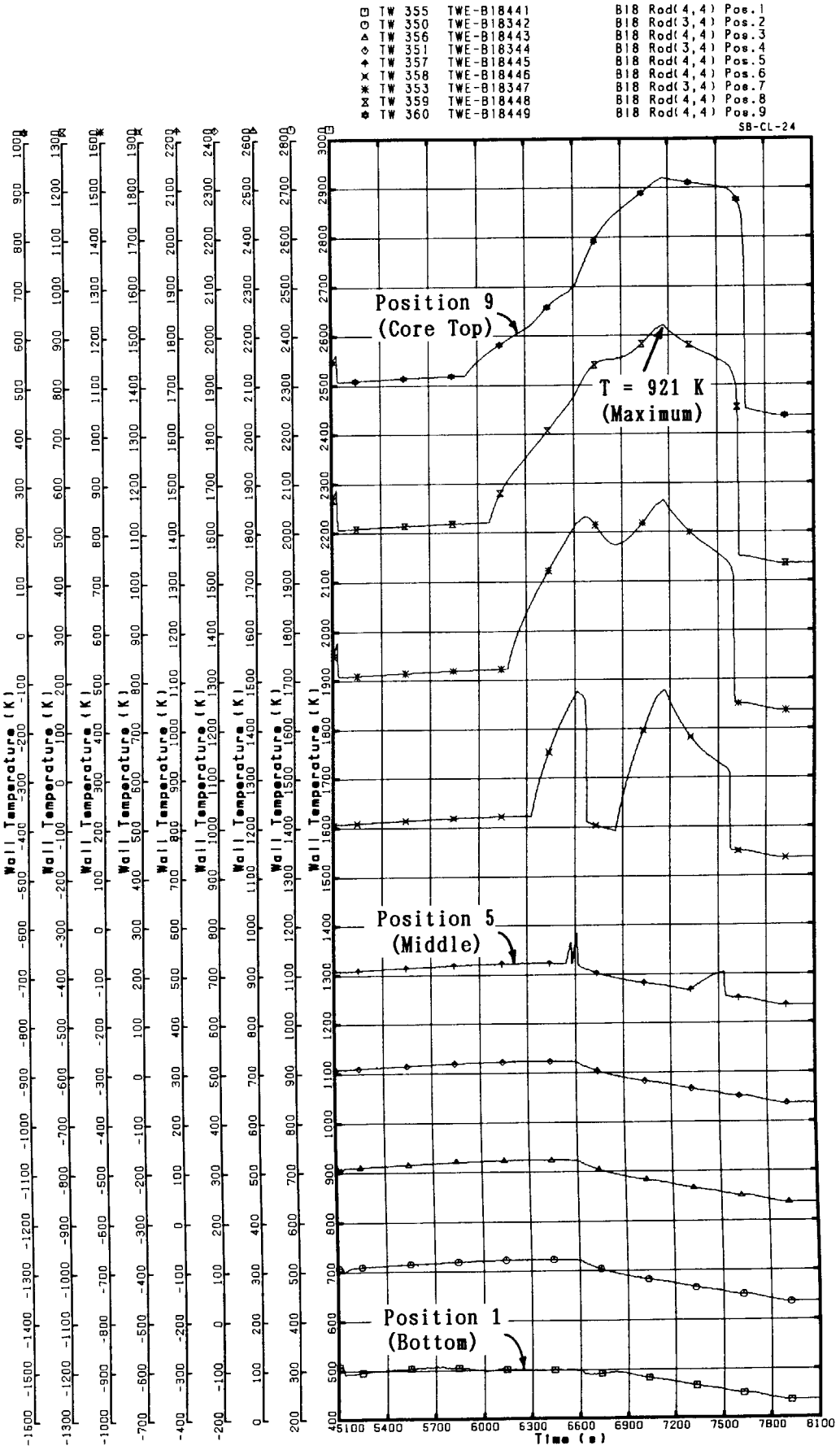

Fig. 4. 1. 39 Representative heater rod temperatures during boil-off process

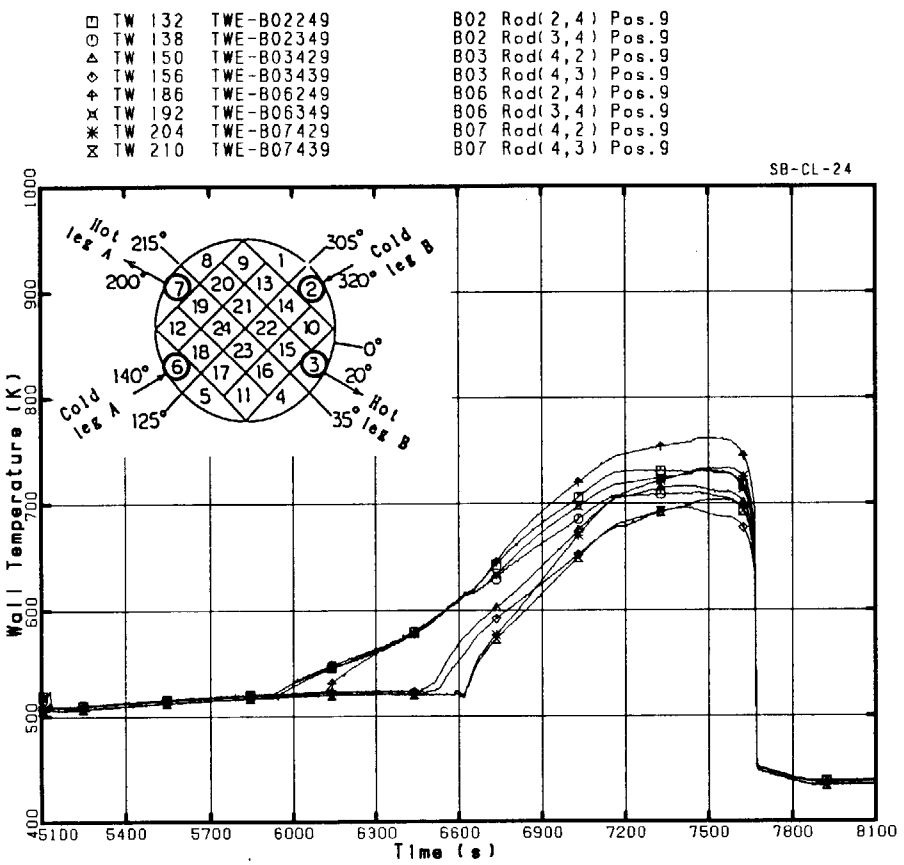

Fig. 4. 1. 40 Heater rod temperatures in peripheral bundles at Position 9

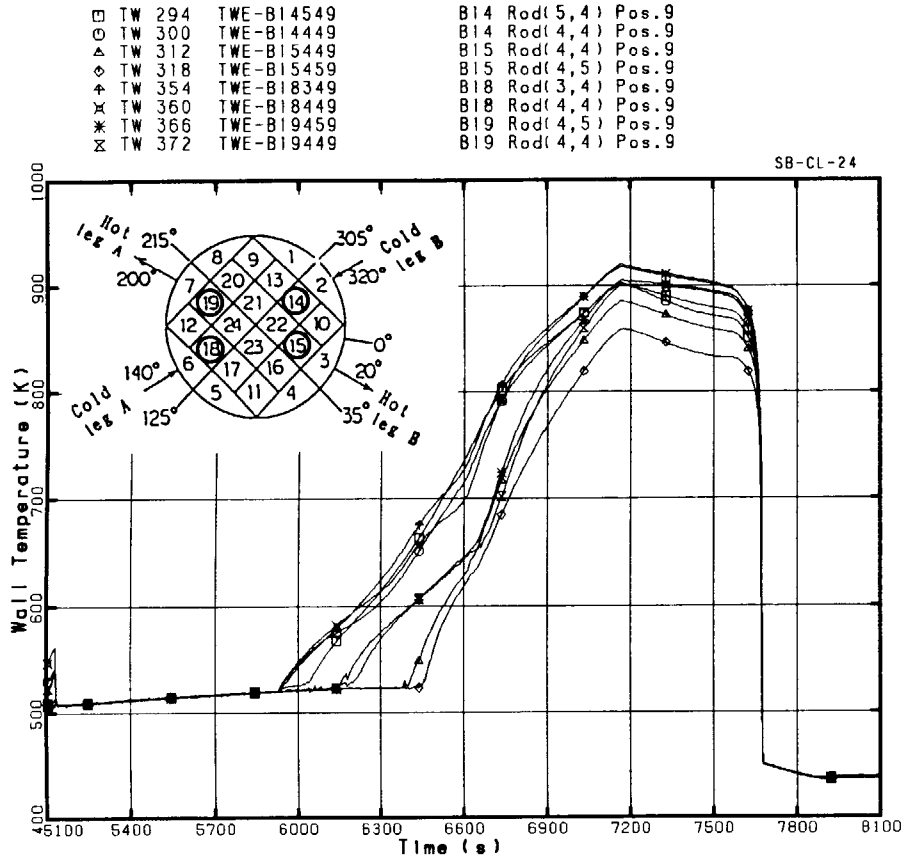

Fig. 4. 1. 41 Heater rod temperatures in high power bundles at Position 9

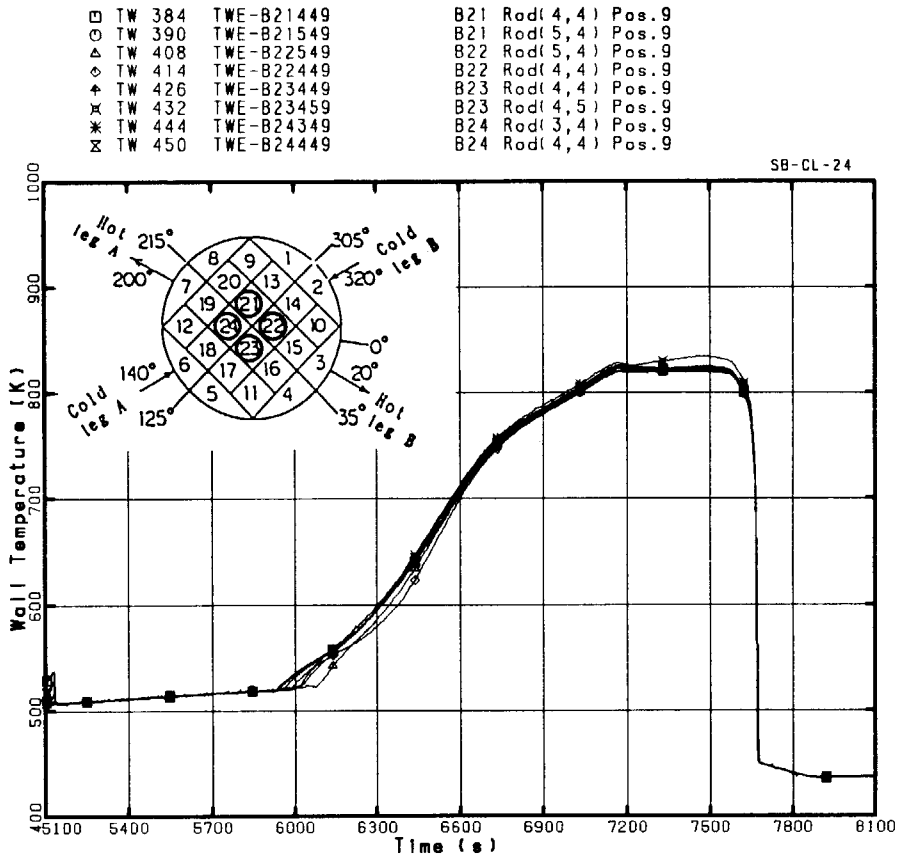

Fig. 4.1.42 Heater rod temperatures in central bundles at Position 9

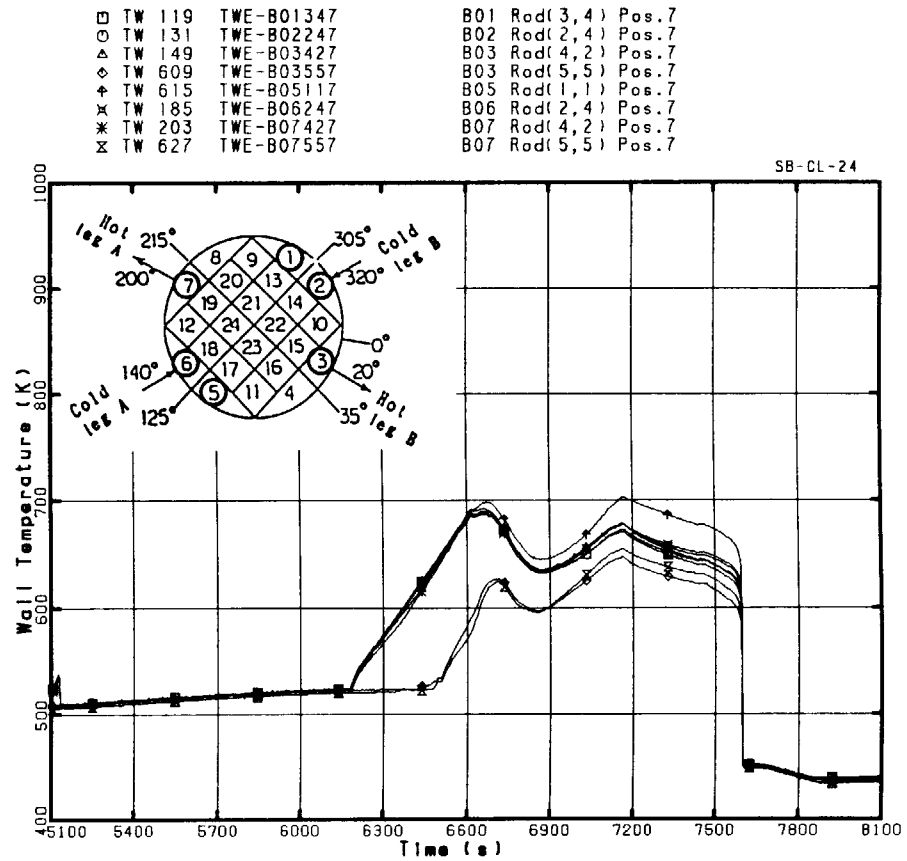

Fig. 4.1.43 Heater rod temperatures in peripheral bundles at Position 7

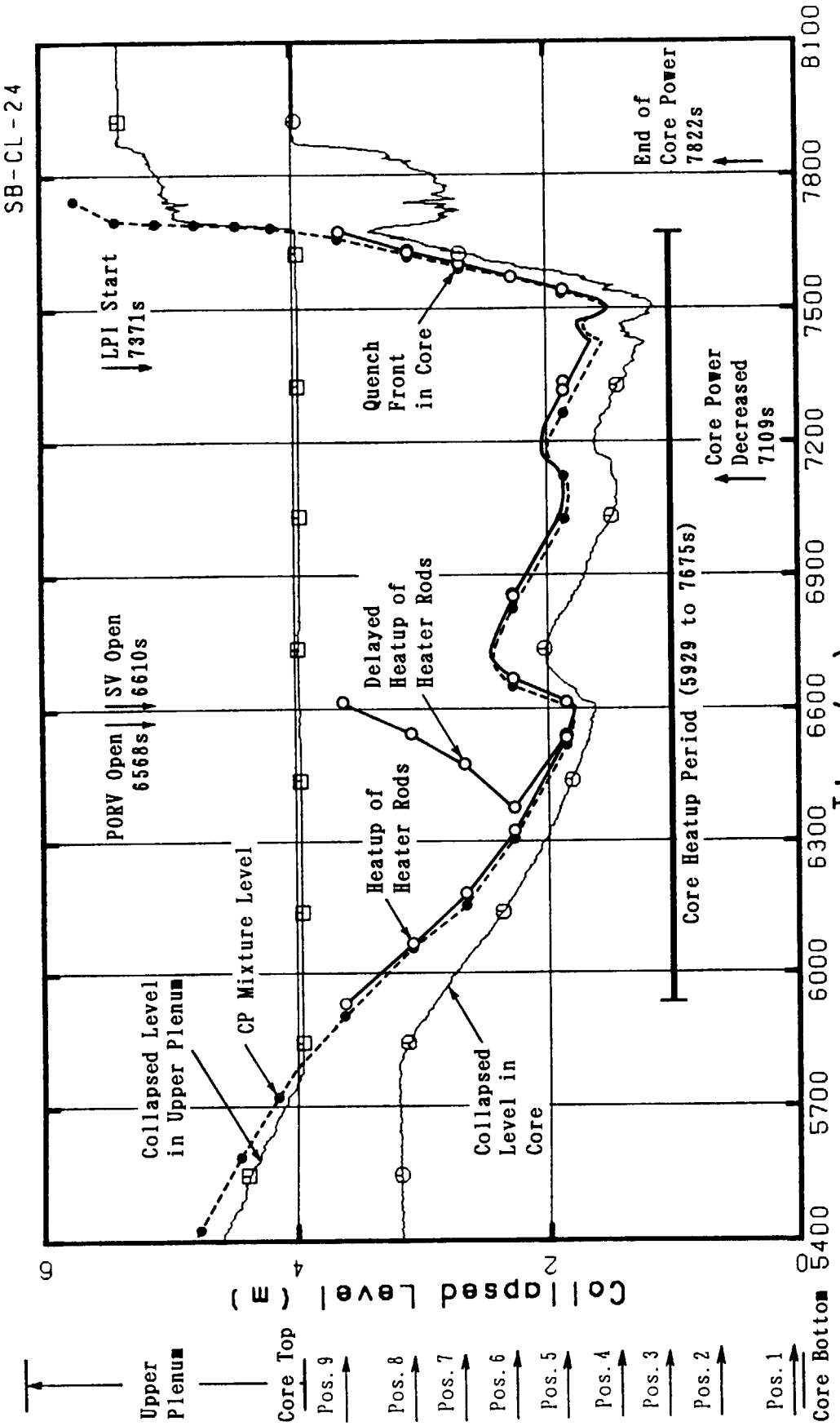

Fig. 4.1.44 Water levels and core heatup behaviors during boil-off process

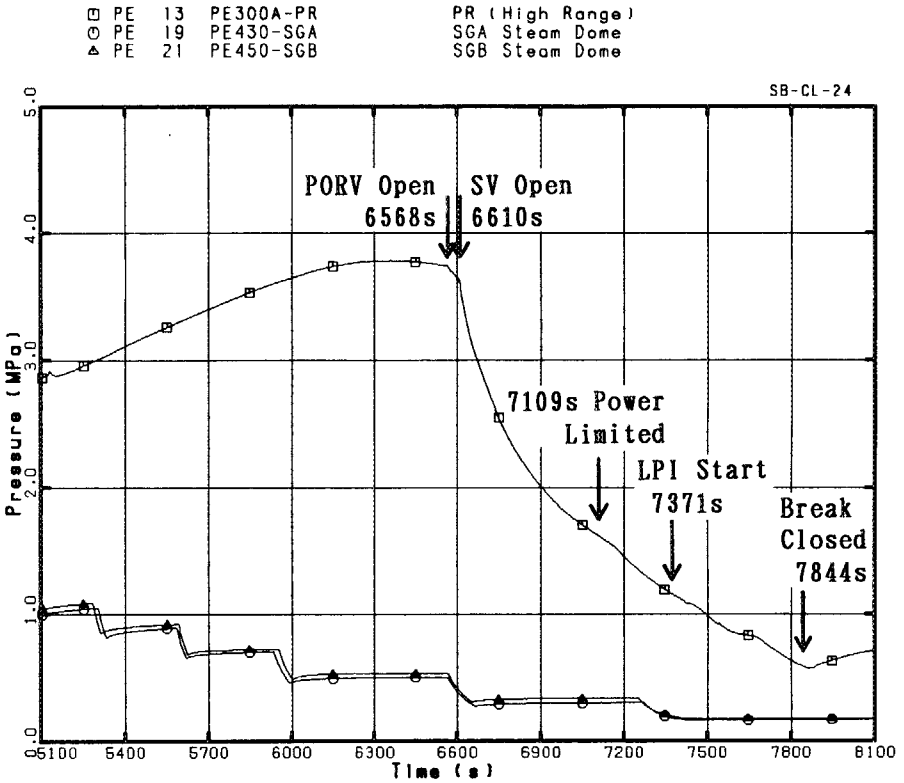

Fig. 4.1.45 Primary and secondary pressures in later phase

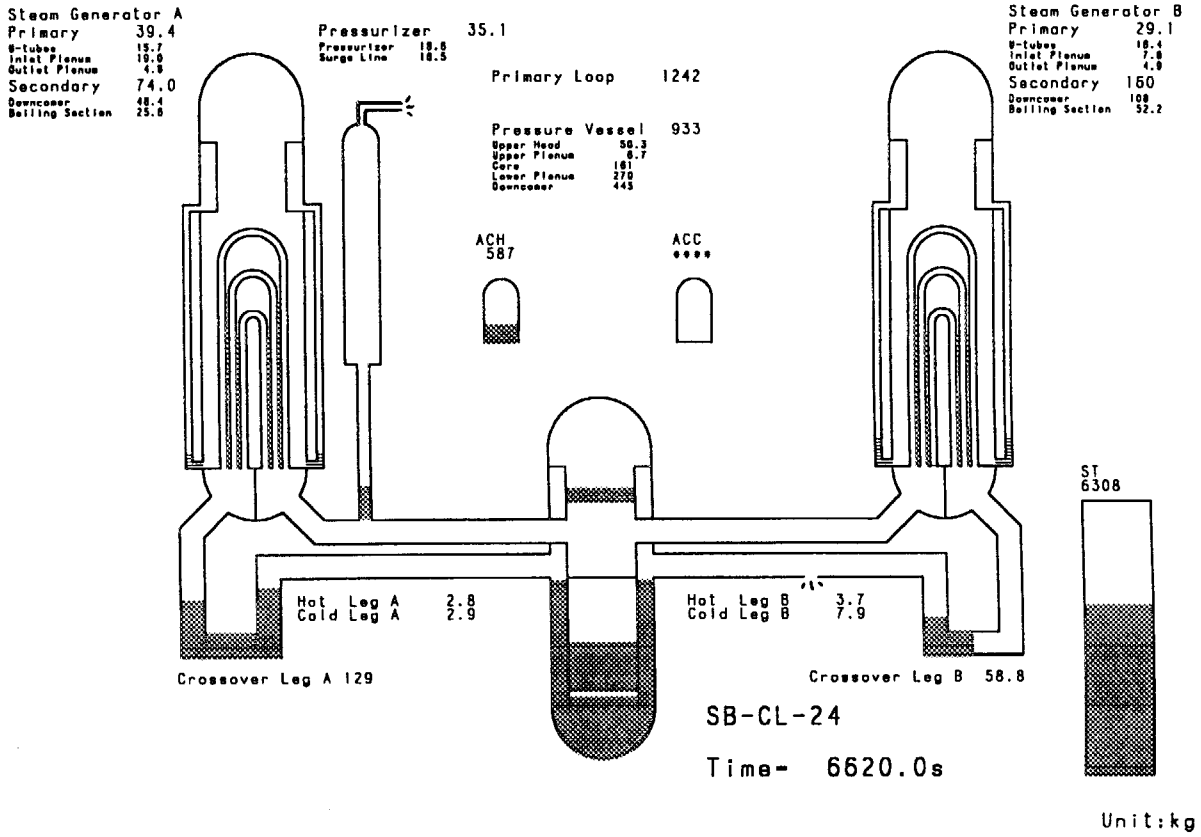

Fig. 4.1.46 Fluid mass distribution just after the pressurizer SV opened (6620 s)

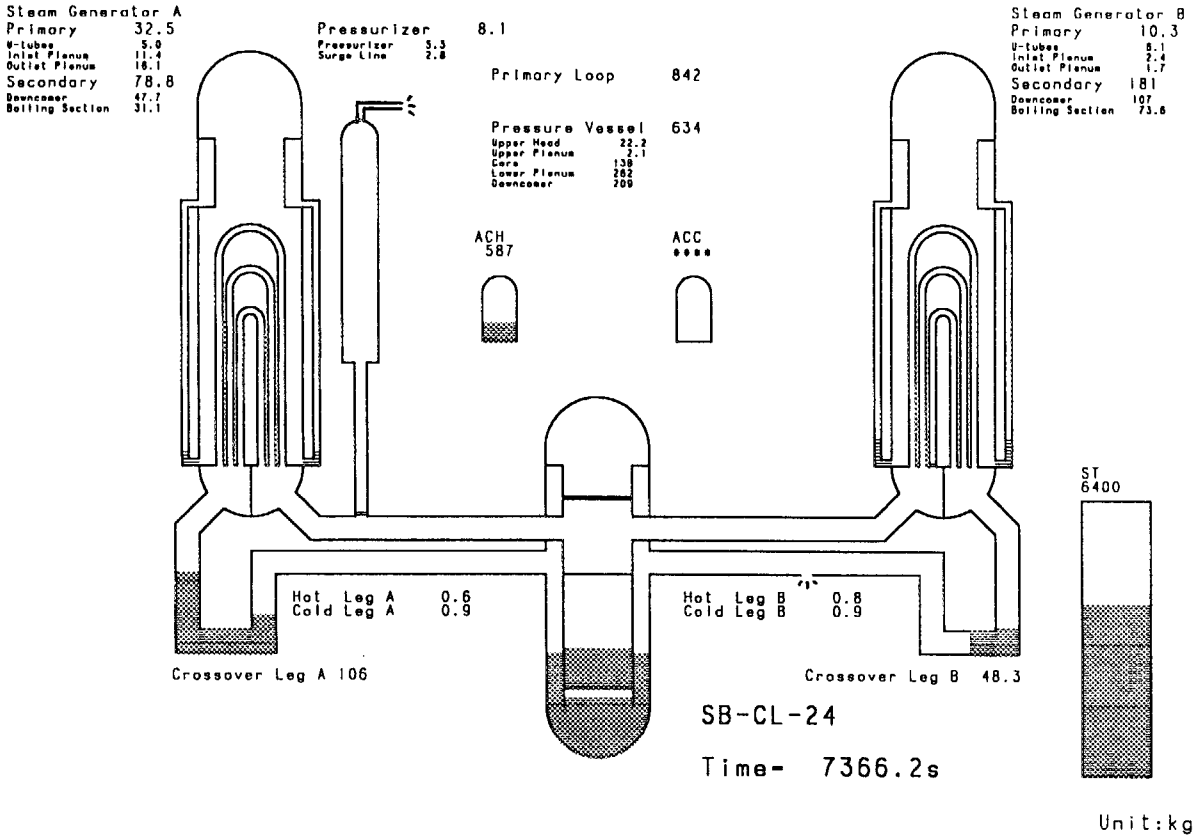

Fig. 4. 1. 47 Fluid mass distribution just before the LPI initiation (7366. 2 s)

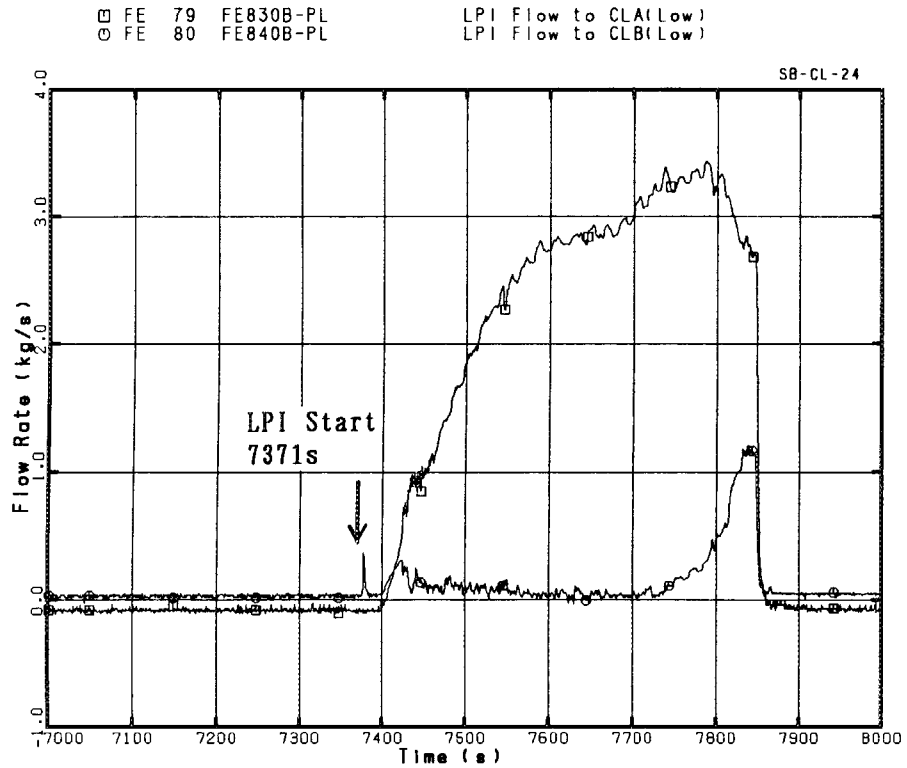

Fig. 4. 1. 48 LPI injection flow rates to cold legs

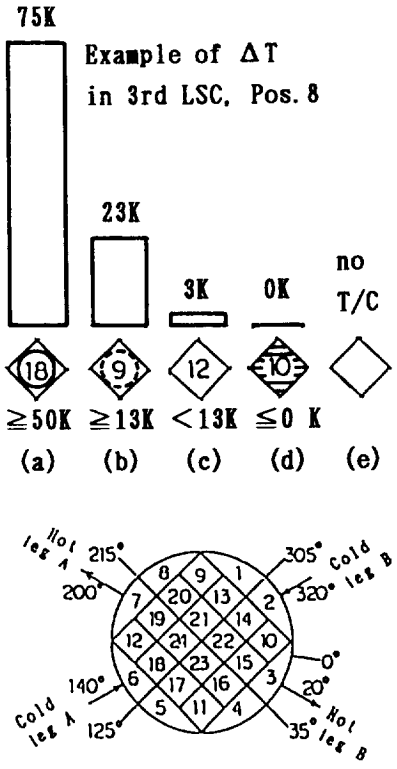

Heatup Distribution
and Bundle Arrangement

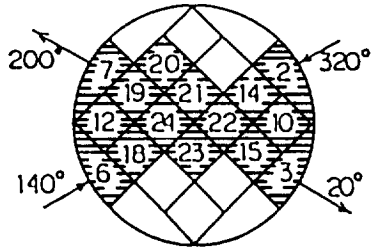

(1st LSC, Pos. 9)
No Heatup

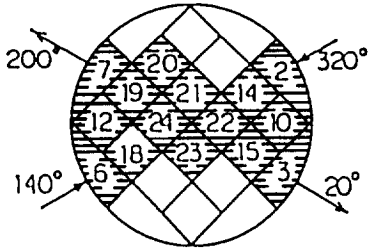

(2nd LSC, Pos. 9)

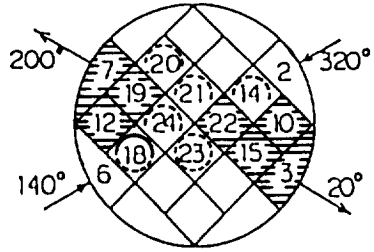

(3rd LSC, Pos. 9)

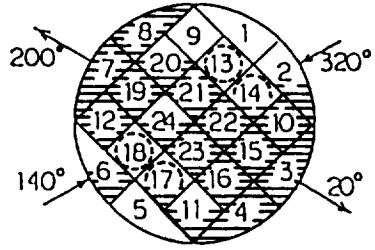

(1st LSC, Pos. 8)

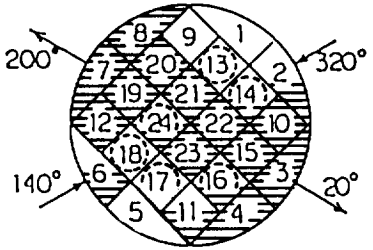

(2nd LSC, Pos. 8)

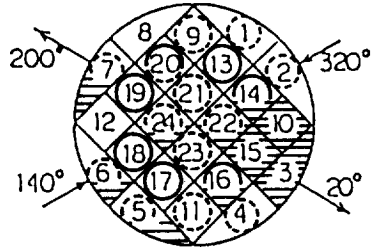

(3rd LSC, Pos. 8)

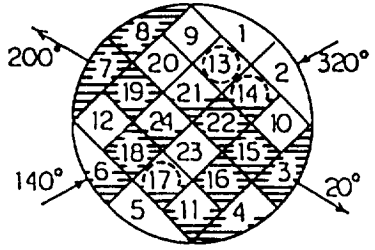

(1st LSC, Pos. 7)

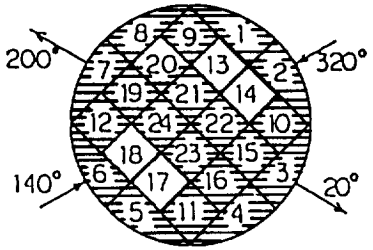

(2nd LSC, Pos. 7)

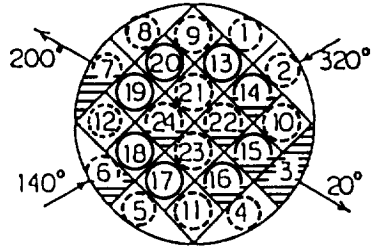

(3rd LSC, Pos. 7)

Fig. 4. 2. 1 Heatup distribution in upper core region during three LSC processes

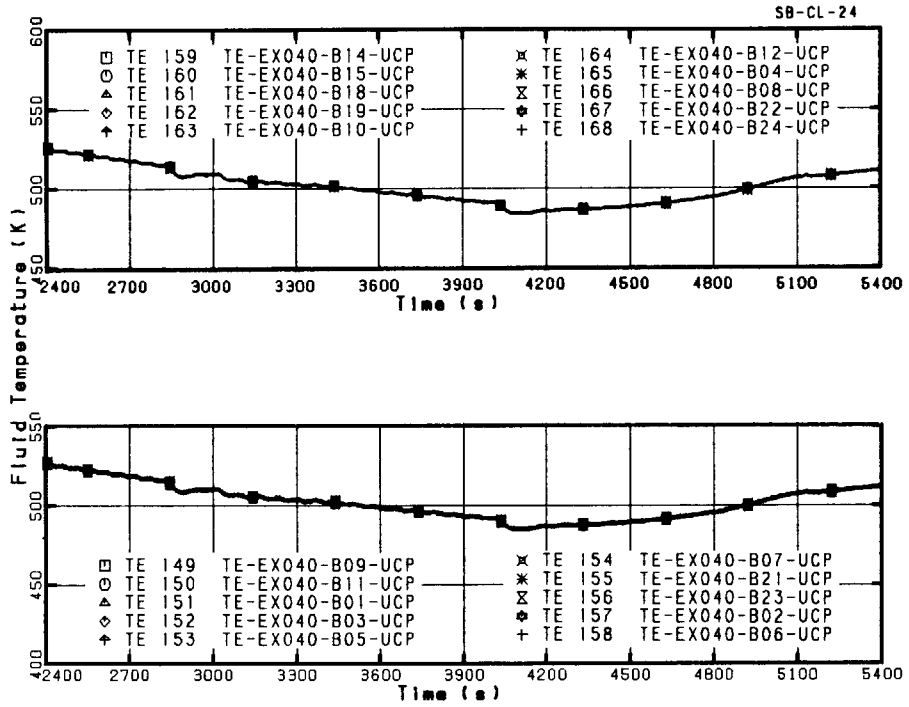

Fig. 4. 2. 2 Core exit fluid temperatures during LSC processes

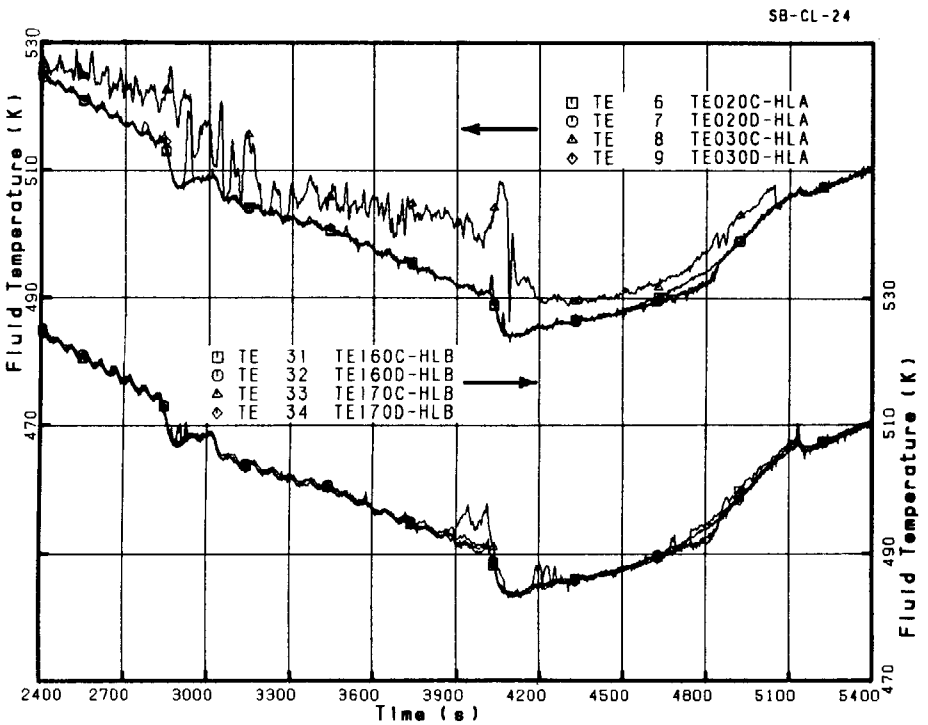

Fig. 4. 2. 3 Fluid temperatures in both hot legs during LSC processes

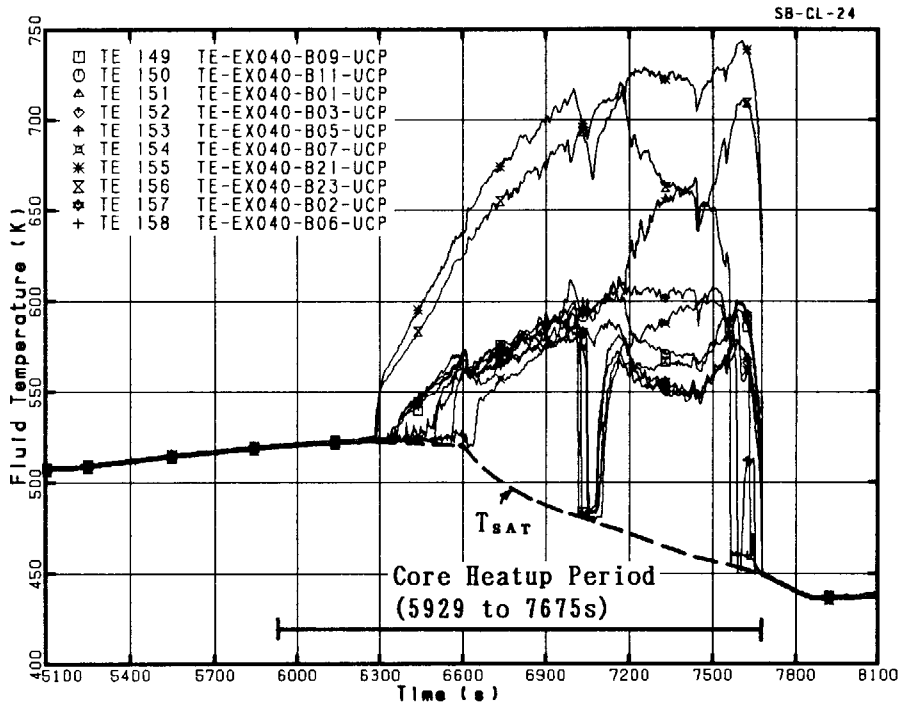

Fig. 4. 2. 4 Core exit temperaures in boil-off process (A)

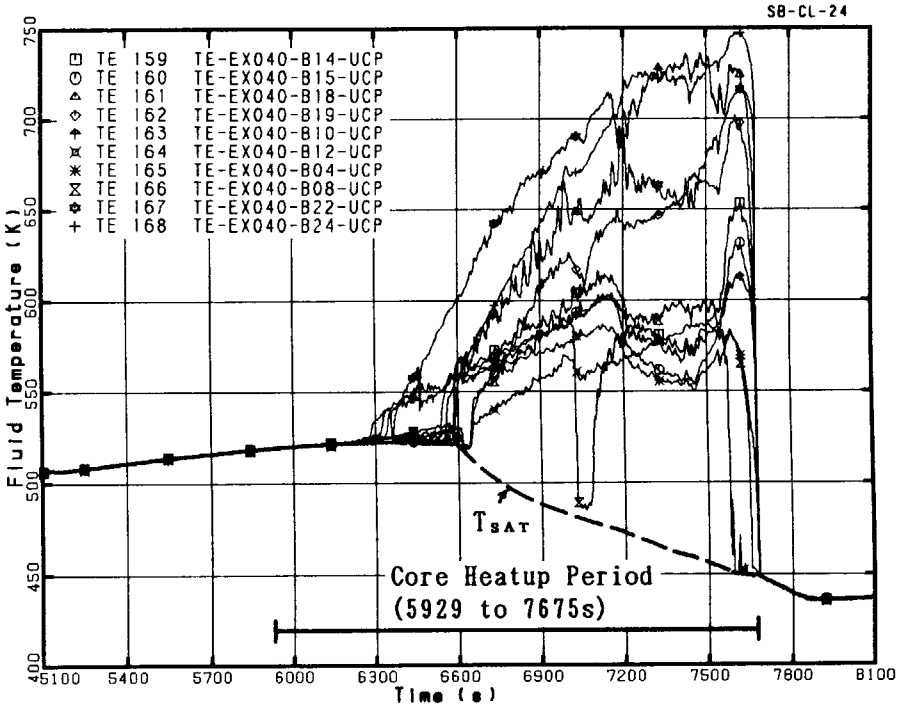

Fig. 4. 2. 5 Core exit temperaures in boil-off process (B)

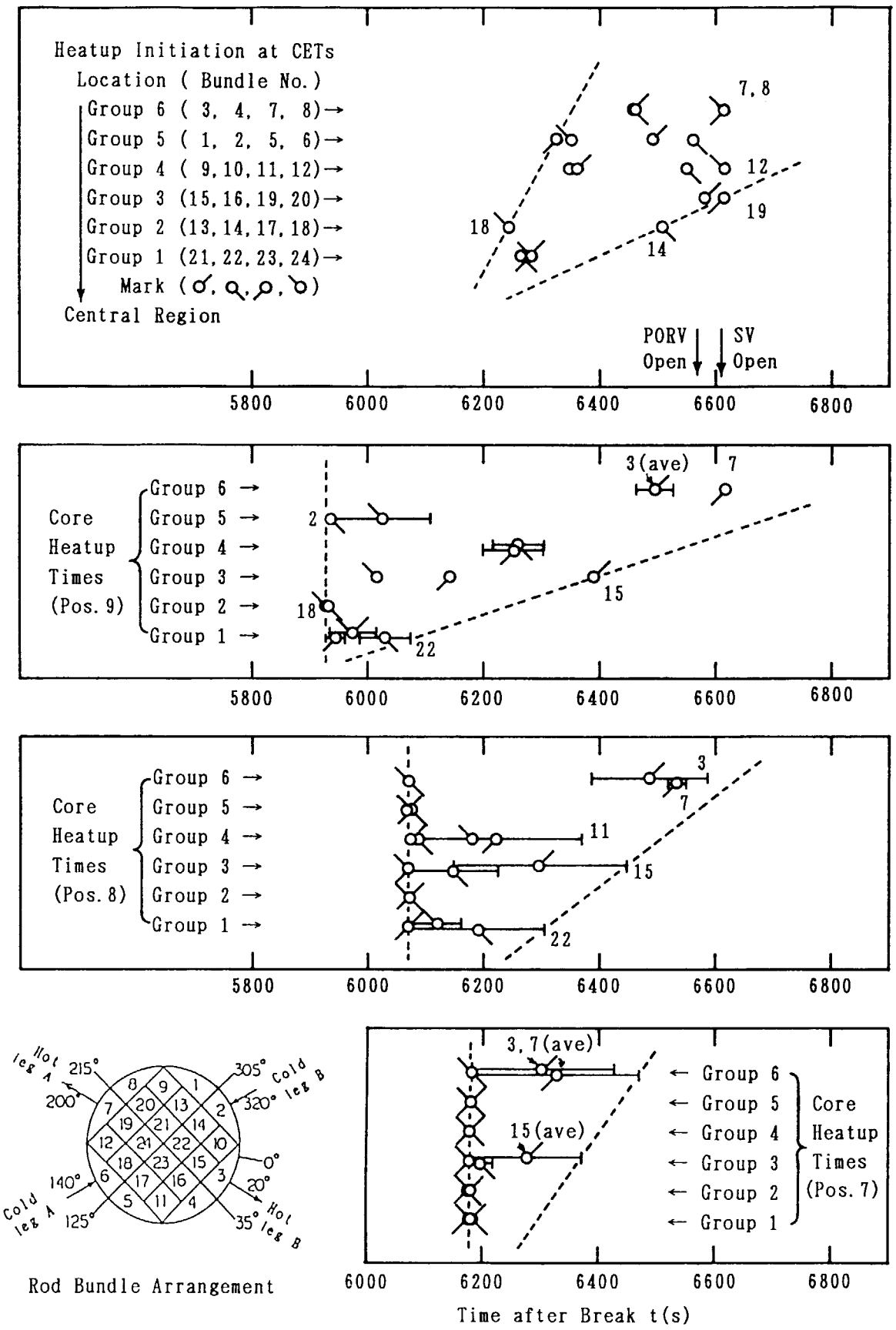

Fig. 4. 2. 6 Heatup distribution at CETs and upper core during boil-off process

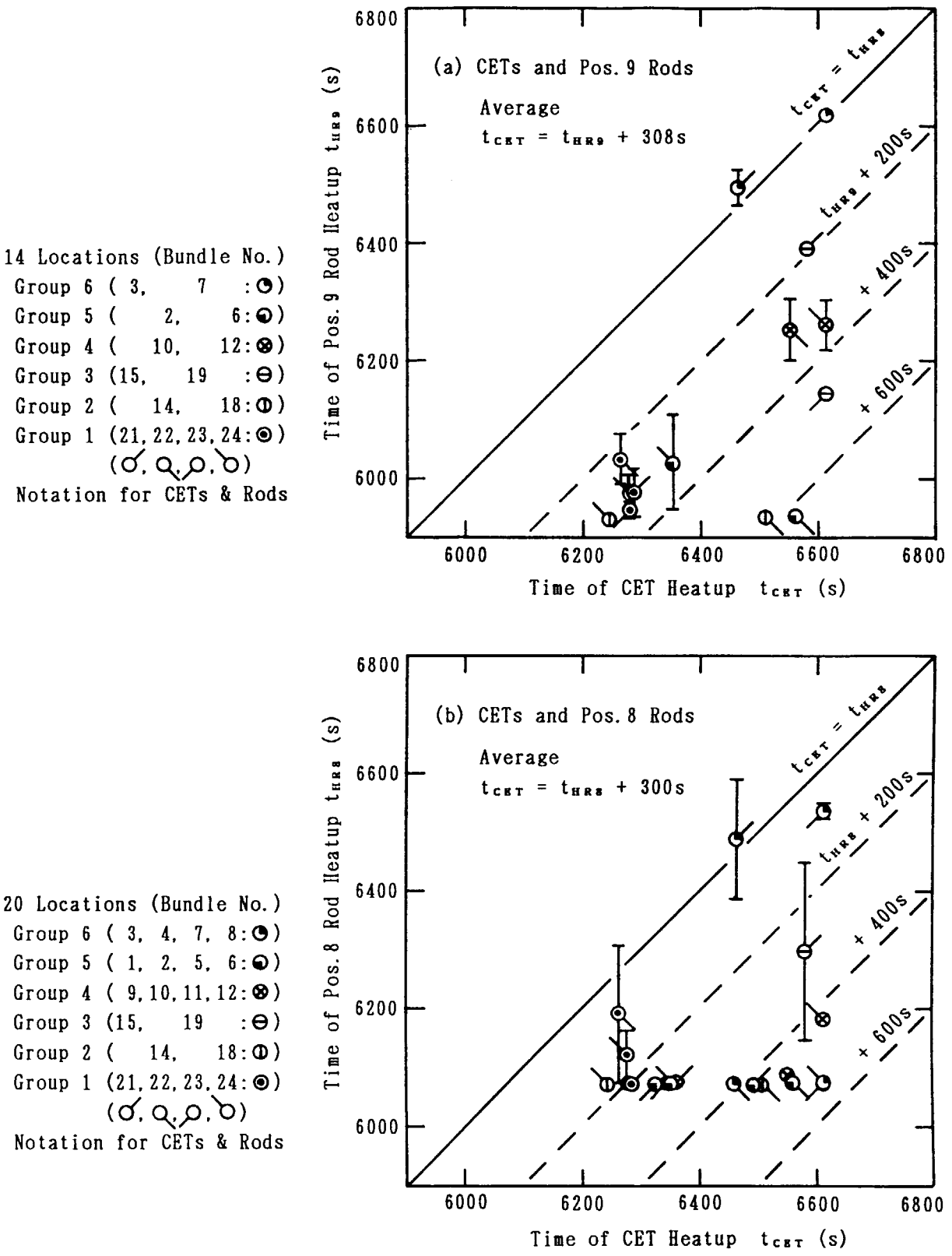

Fig. 4. 2. 7 Delayed CET heatup from corresponding rod bundle heatup initiation

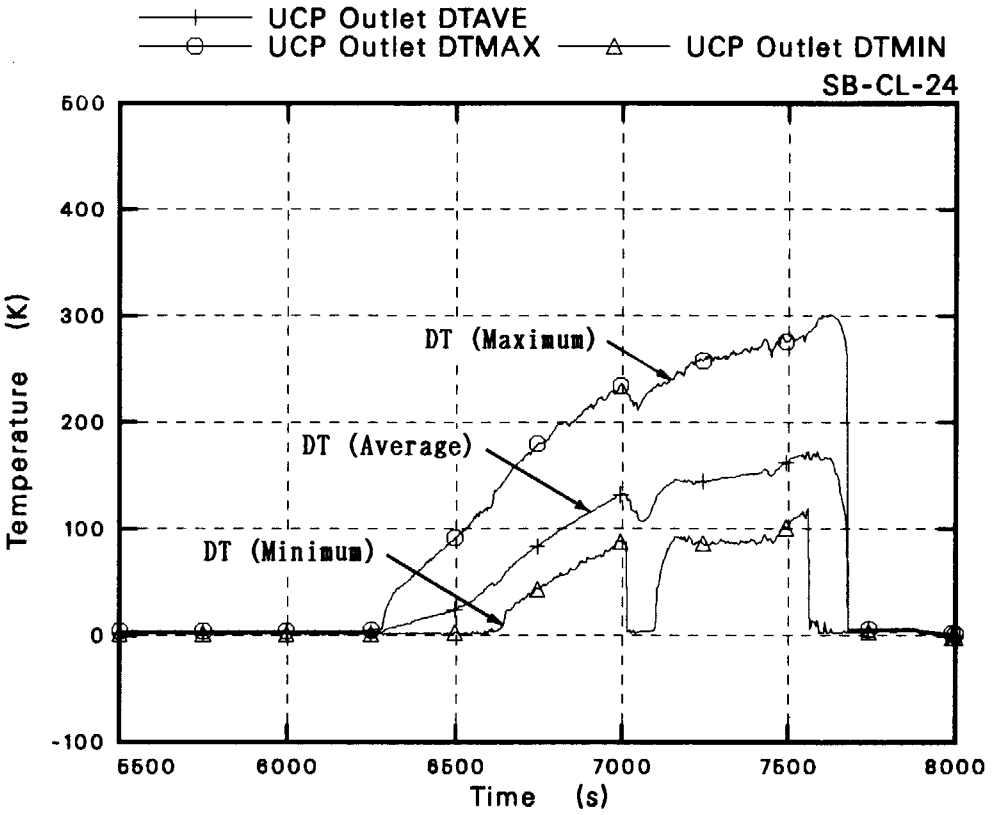

Fig. 4. 2. 8 Data analysis on CET temperature increases above saturation

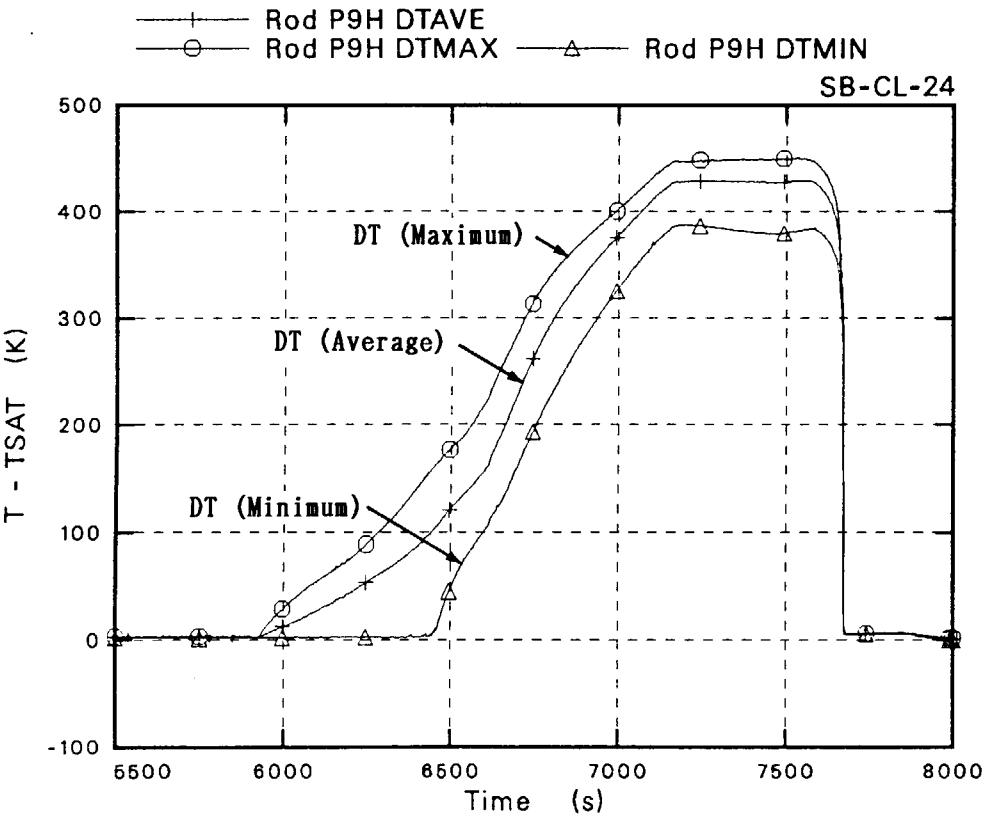

Fig. 4. 2. 9 Data analysis on high power rod temperature increases at core top

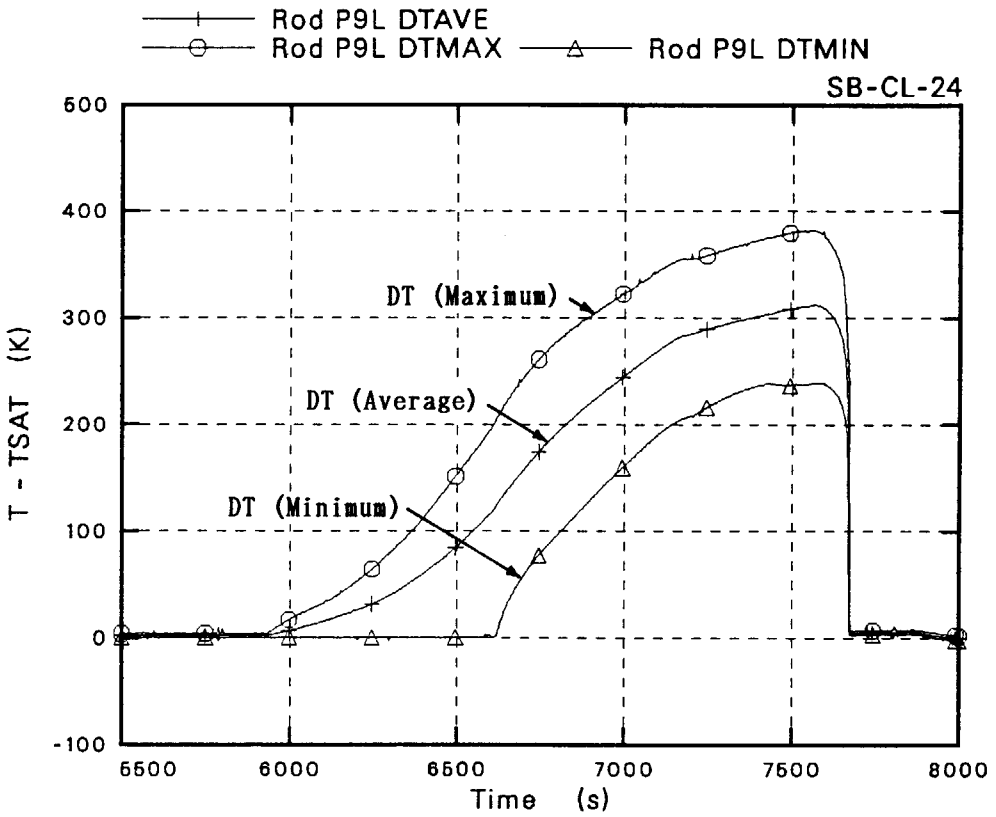

Fig. 4. 2. 10 Data analysis on low power rod temperature increases at core top

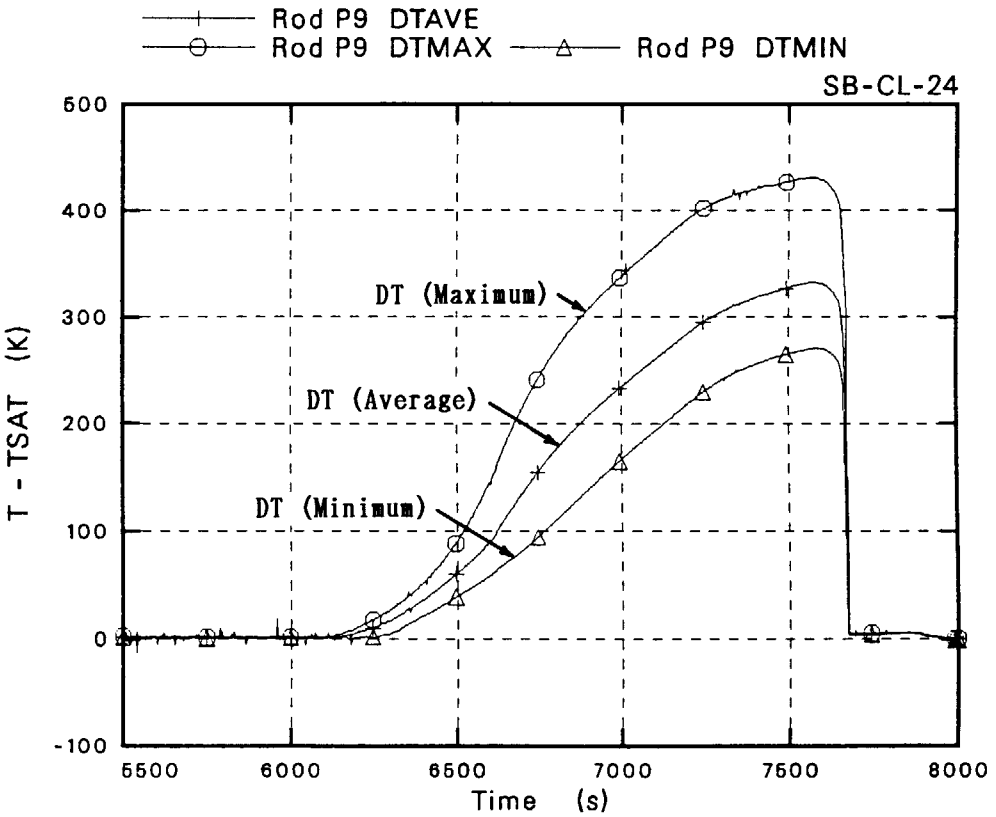

Fig. 4. 2. 11 Data analysis on nonheated rod temperature increases at core top

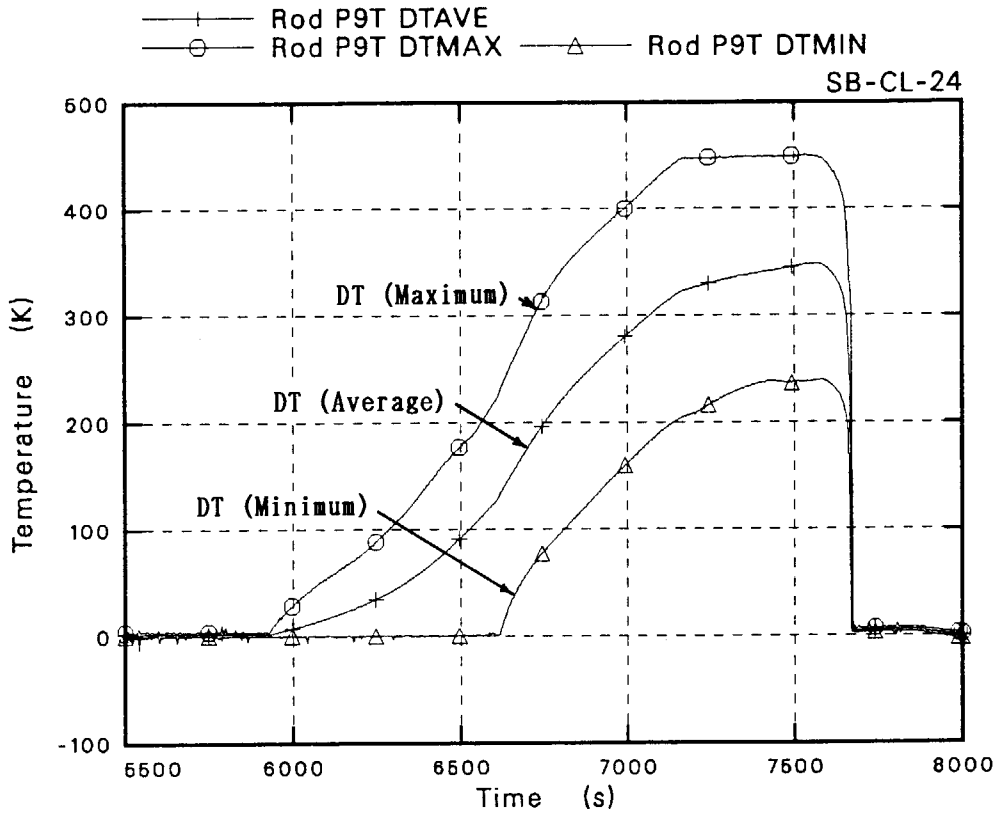

Fig. 4. 2. 12 Data analysis on total rod temperature increases at core top

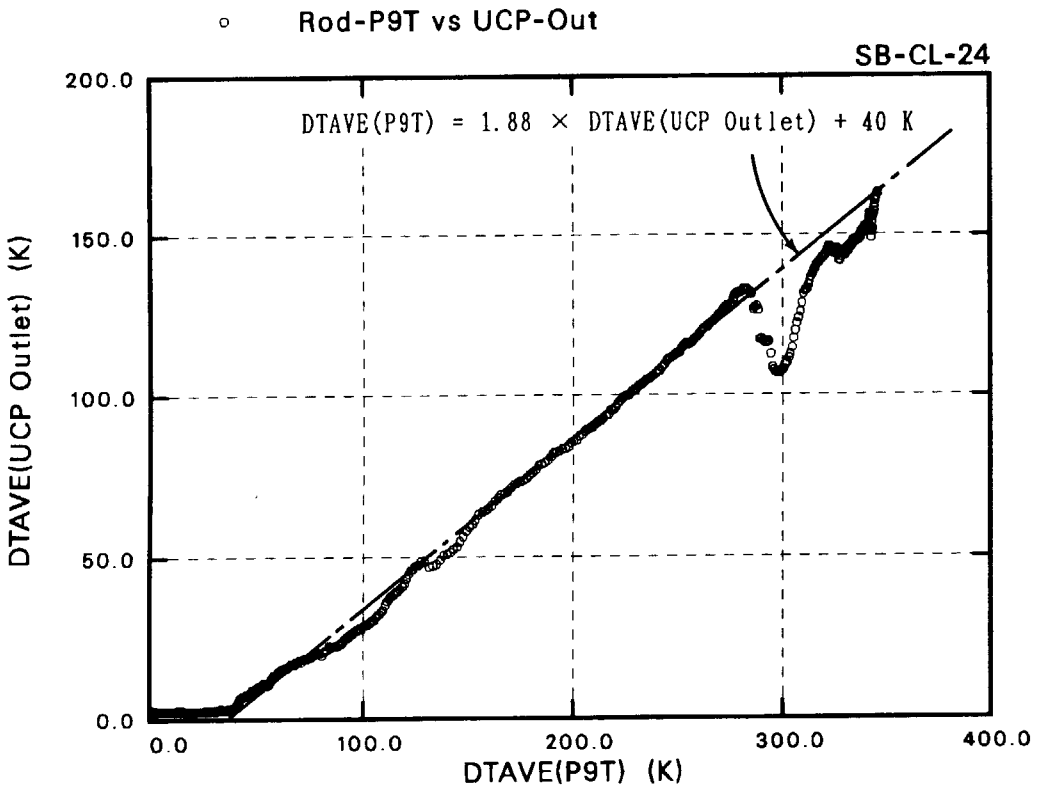

Fig. 4. 2. 13 Correspondence of average temperature increases between CETs and rod temperatures at core top

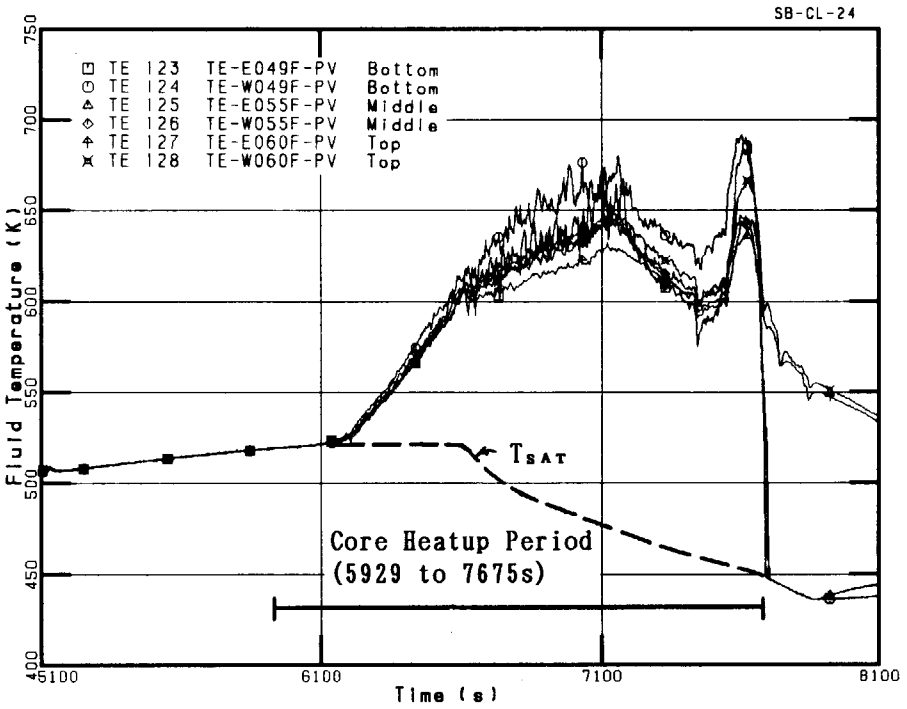

Fig. 4. 2. 14 Fluid temperatures in upper plenum during boil-off process

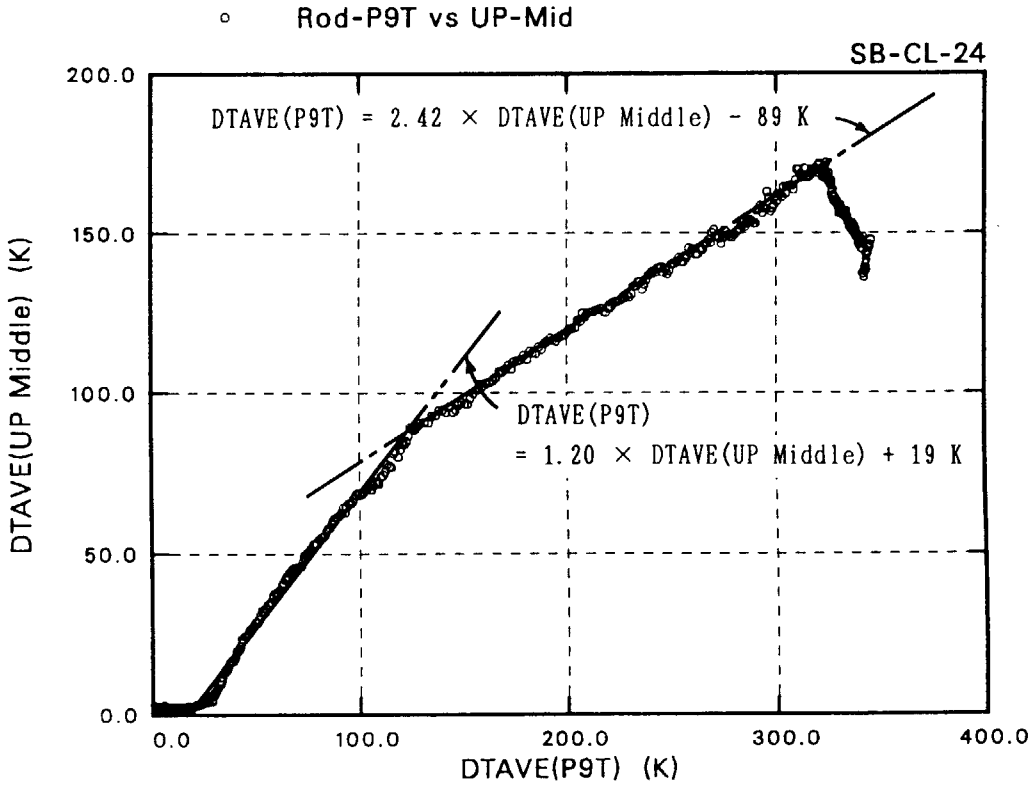

Fig. 4. 2. 15 Correspondence of average temperature increases between upper plenum fluid temperatures and rod temperatures at core top

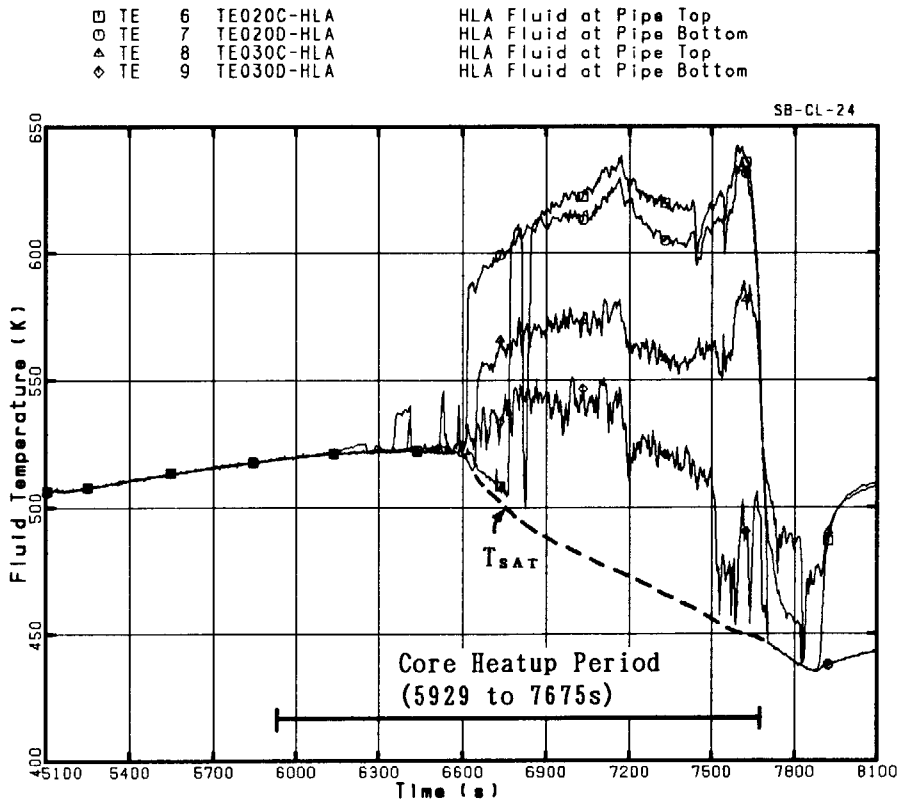

Fig. 4. 2. 16 Fluid temperatures in hot leg A during boil-off process

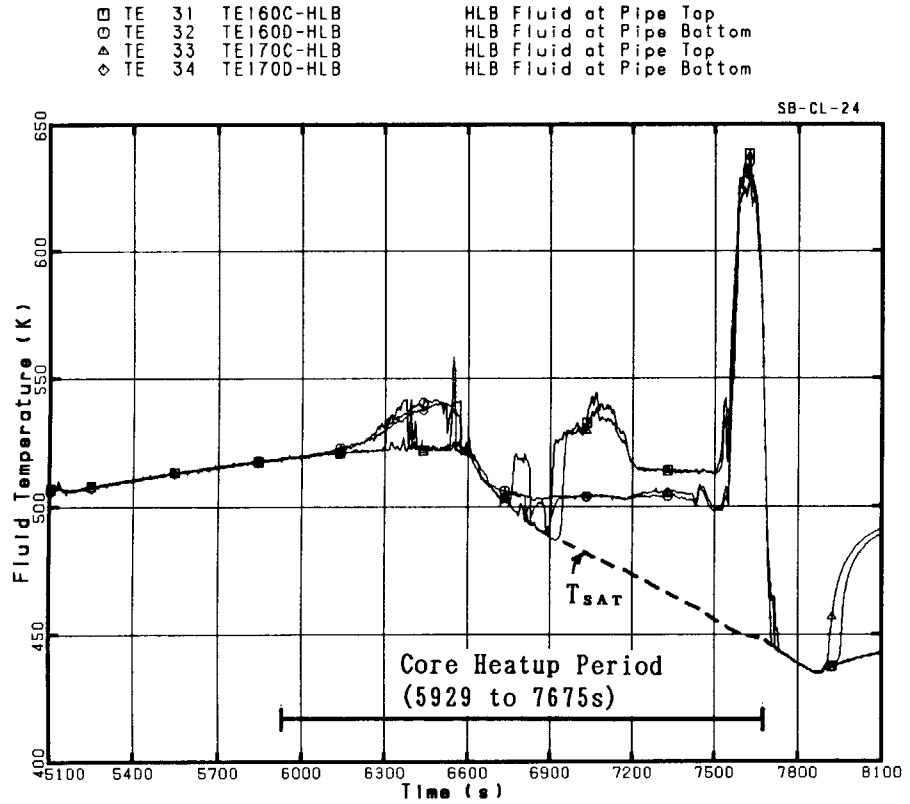

Fig. 4. 2. 17 Fluid temperatures in hot leg B during boil-off process

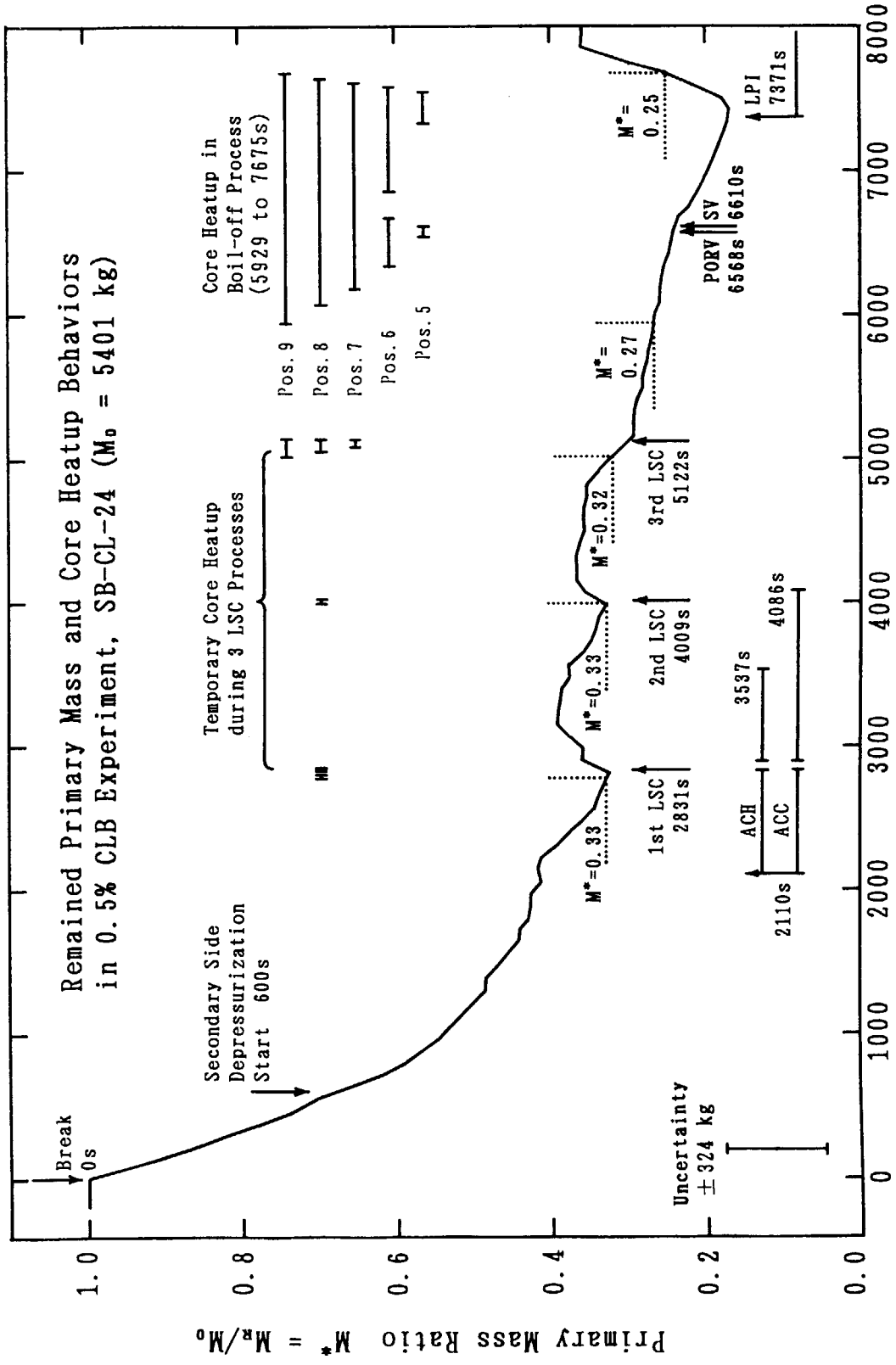

Fig. 4.3.1 Primary mass inventory related with core heatups in Experiment SB-CL-24

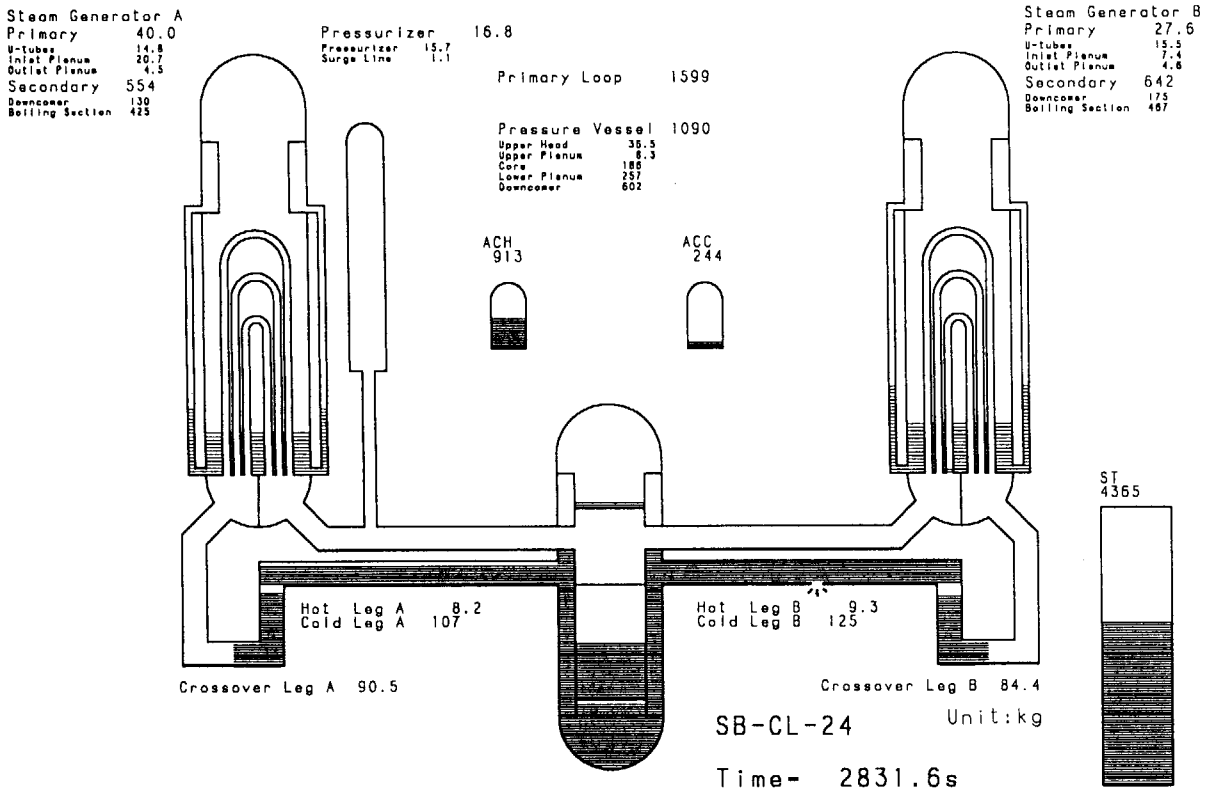

Fig. 4.3.2 Fluid mass distribution at the first LSC (2831.6 s)

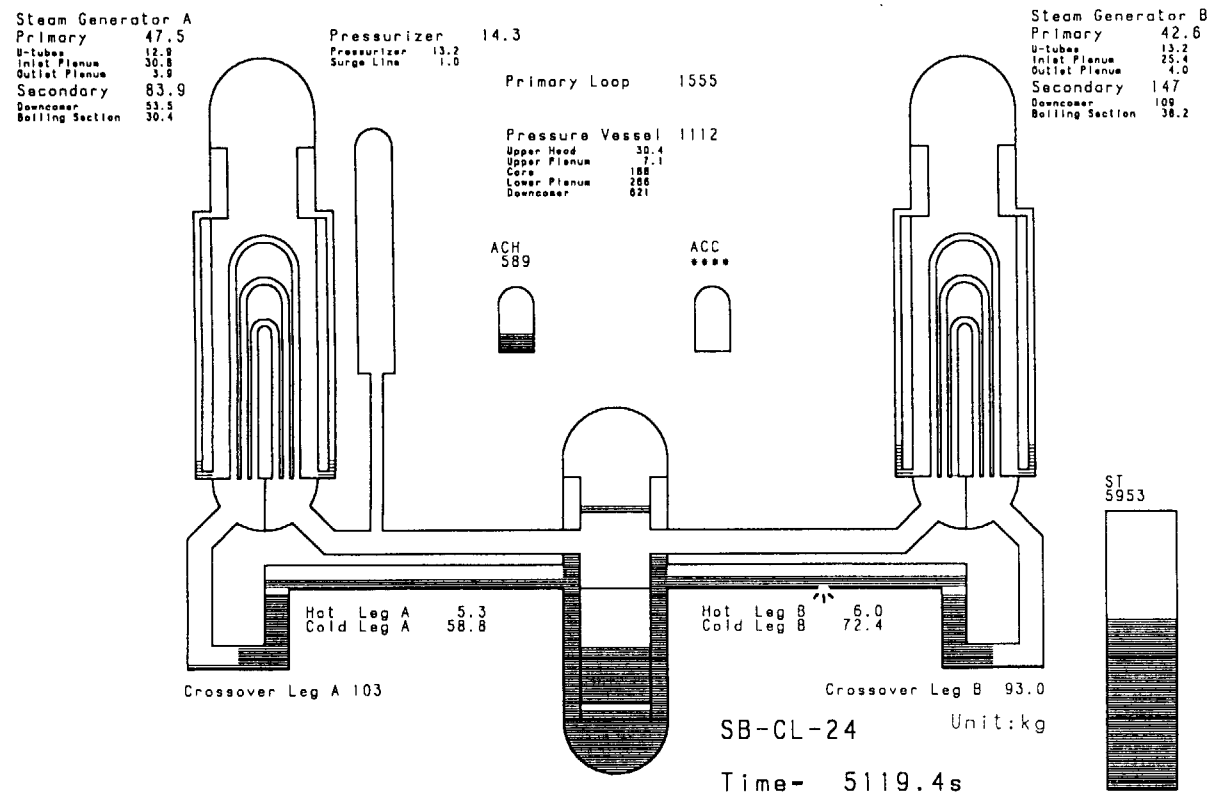

Fig. 4.3.3 Fluid mass distribution at the third LSC (5119.4 s)

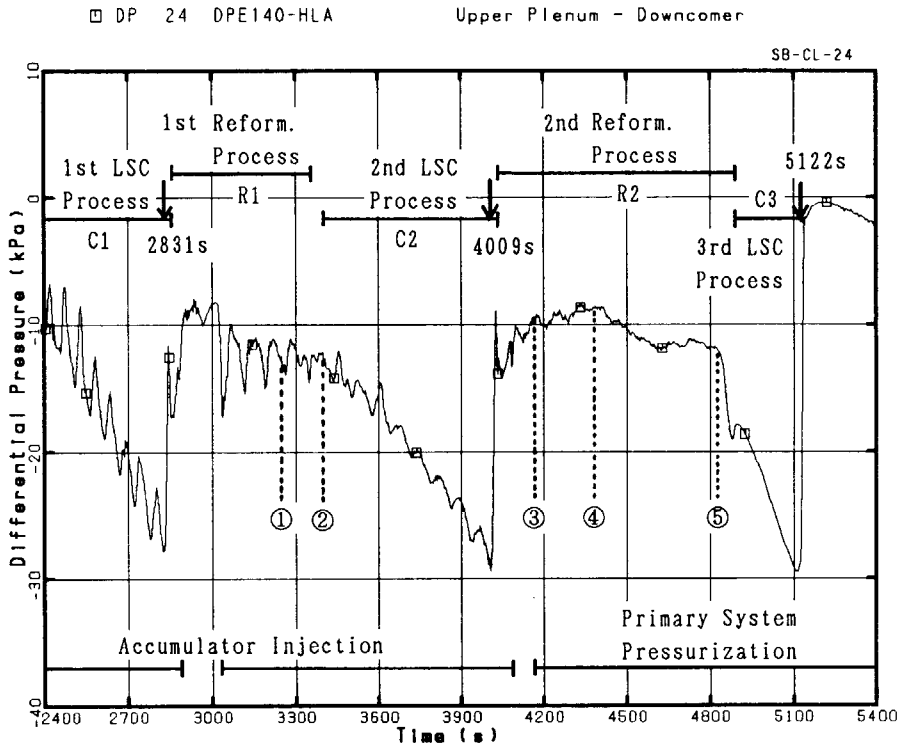

Fig. 4. 3. 4 DP data between upper plenum and downcomer during LSC and reformation processes

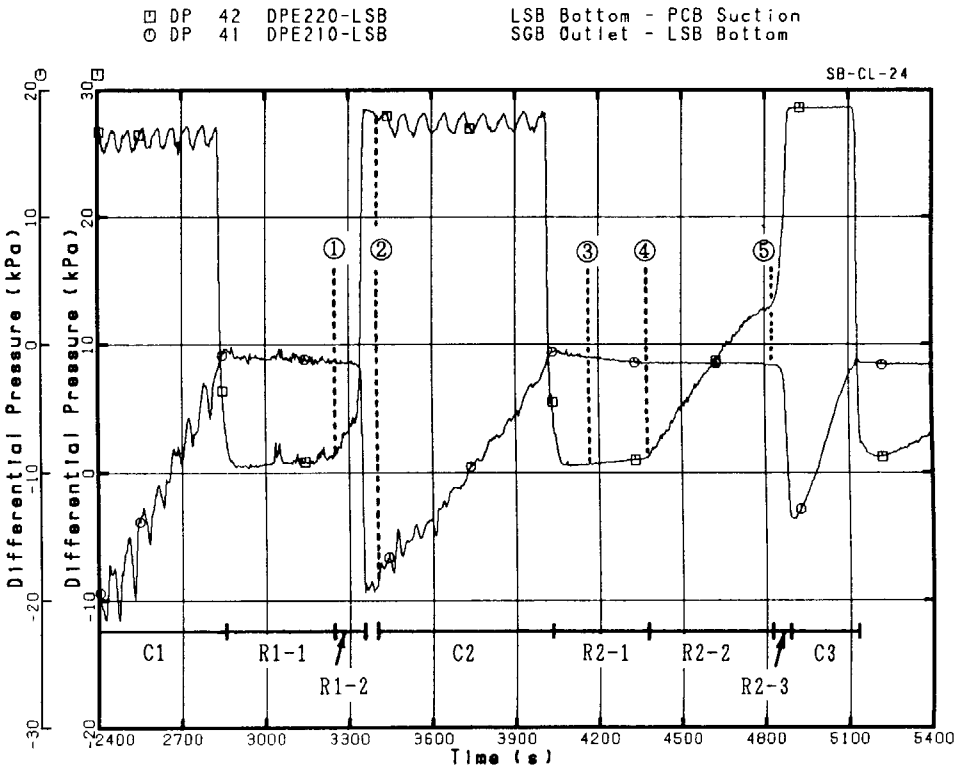

Fig. 4. 3. 5 DP data in loopseal B region during LSC and reformation processes

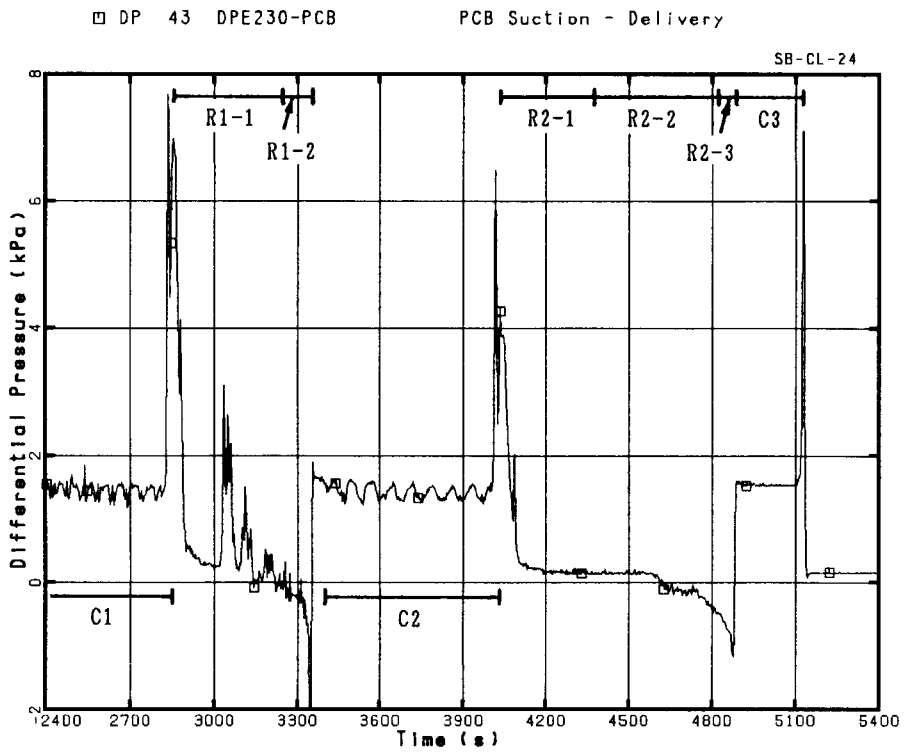

Fig. 4. 3. 6 DP data across primary coolant pump B during repeated LSC processes

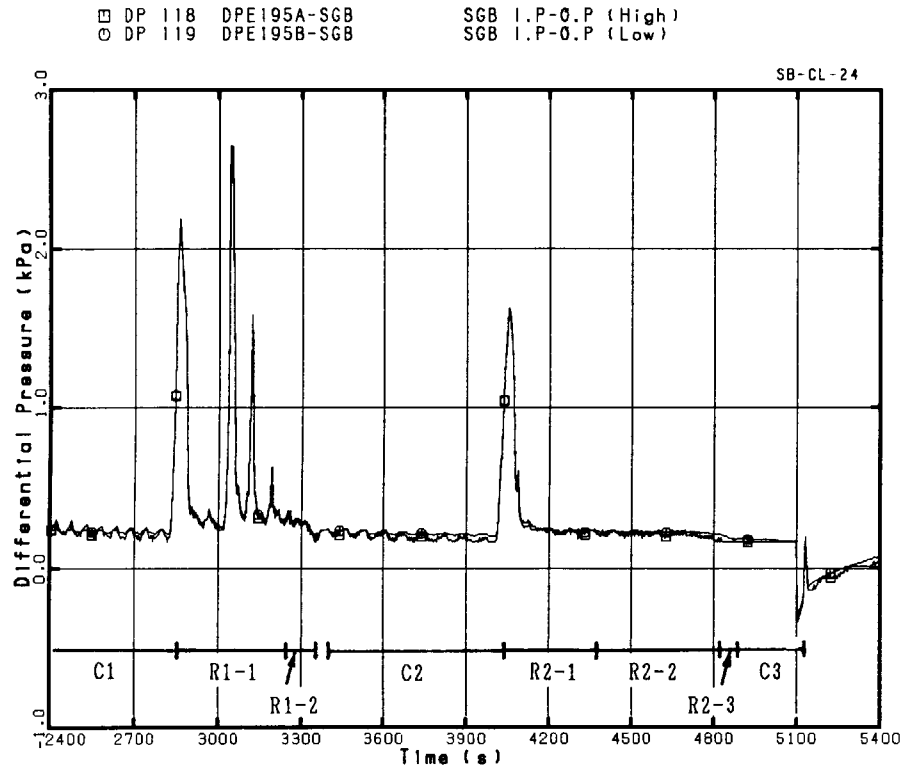

Fig. 4. 3. 7 DP data across inlet and outlet plena of SG-B during repeated LSC processes

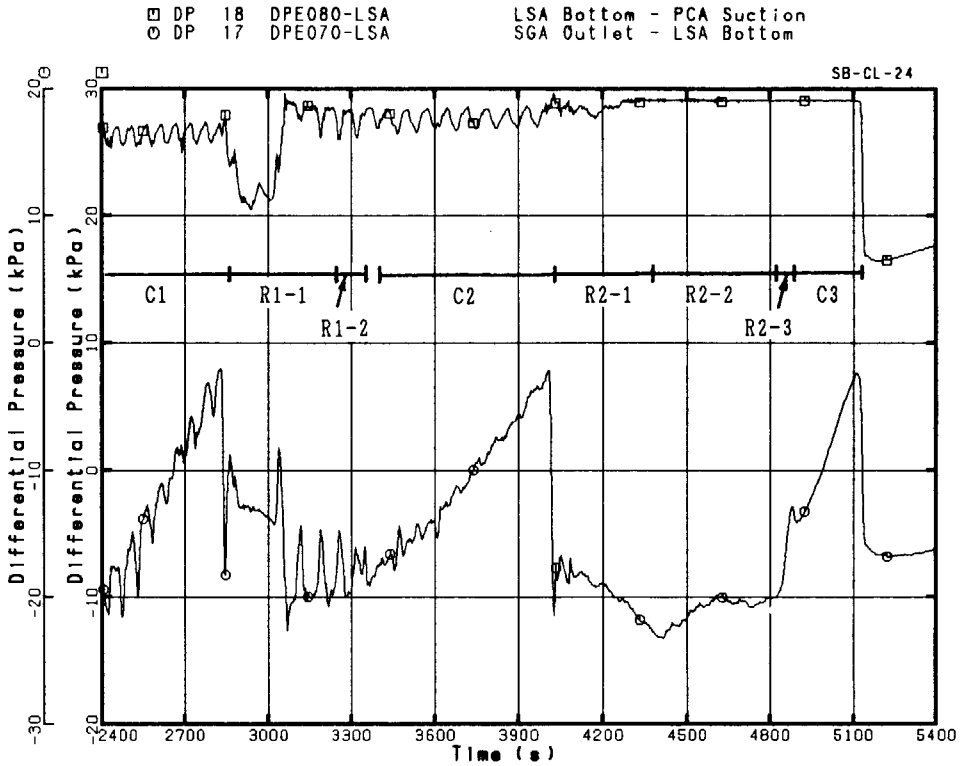

Fig. 4. 3. 8 DP data in loopseal A region during repeated LSC processes

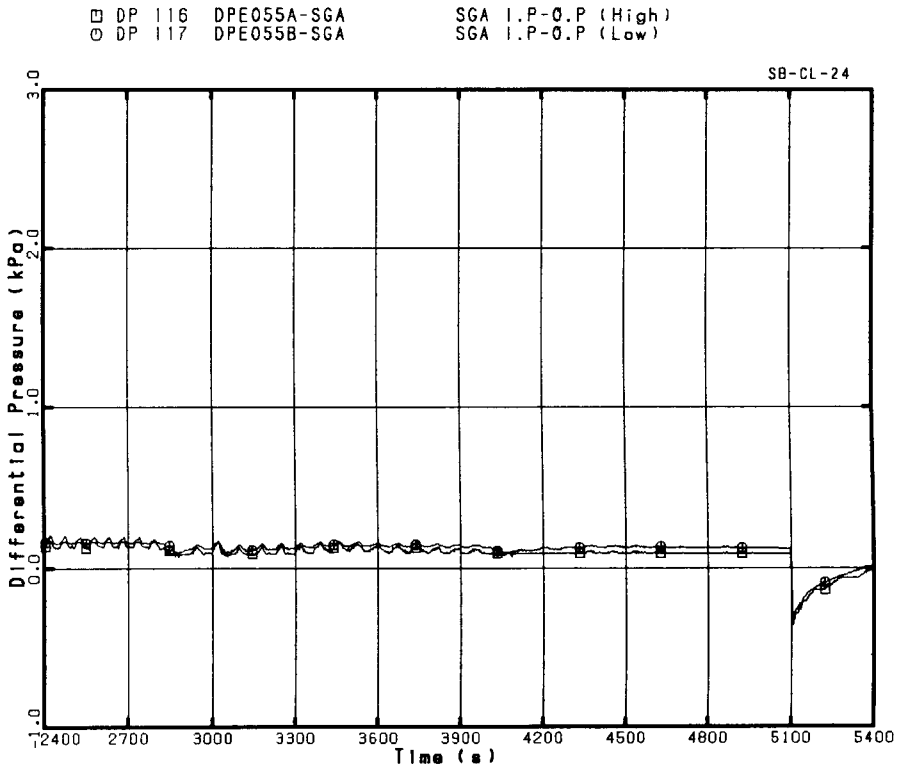

Fig. 4. 3. 9 DP data across SG-A plena during repeated LSC processes

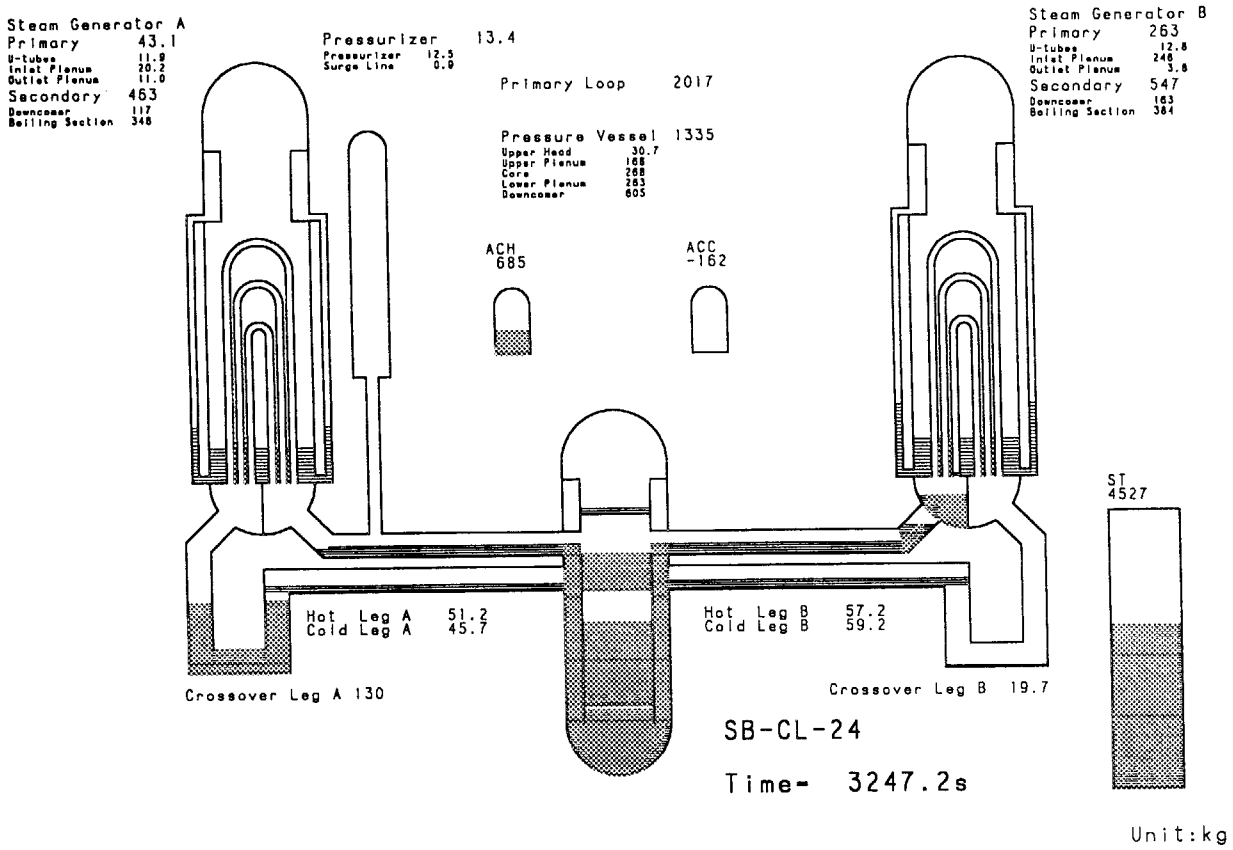

Fig. 4.3.10 Fluid mass distribution in early stage of the first loopseal reformation process (①; 3247.2 s)

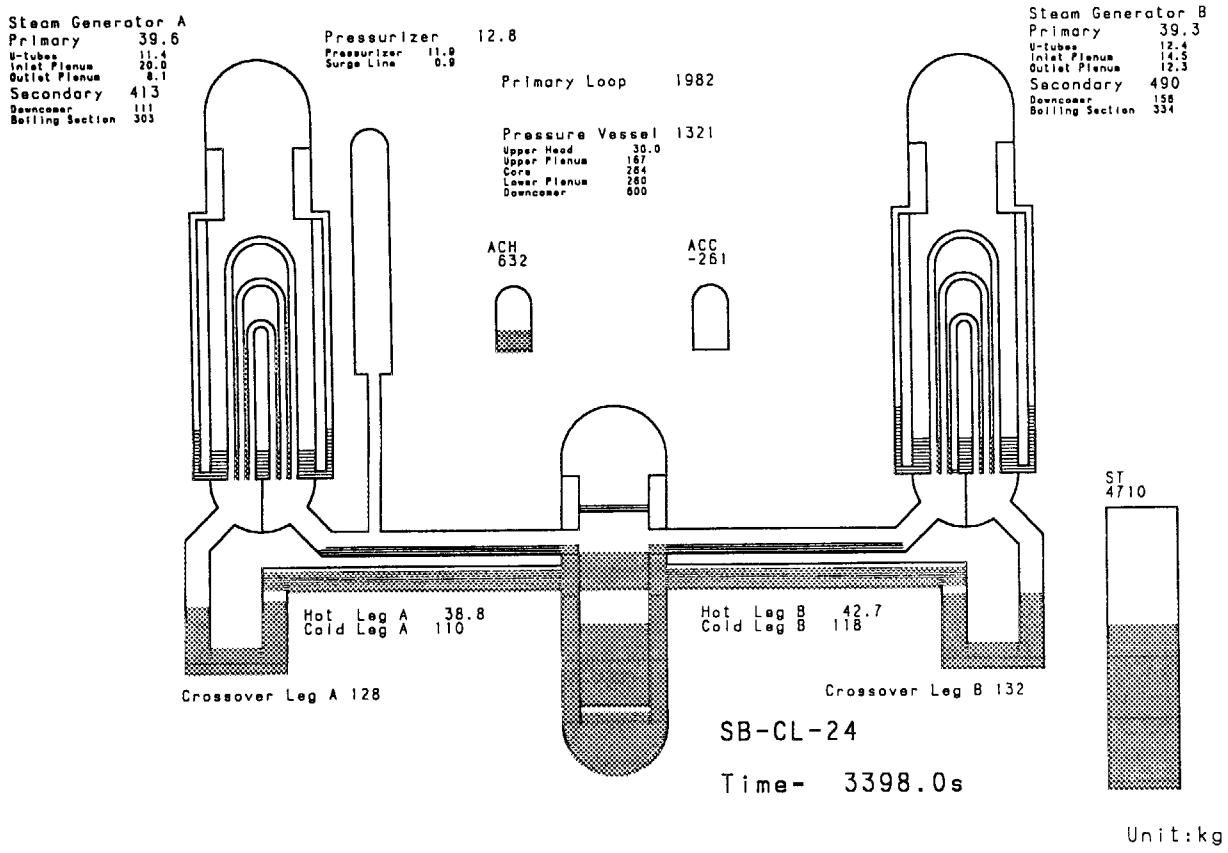

Fig. 4.3.11 Fluid mass distribution at the first loopseal reformation process (②; 3398 s)

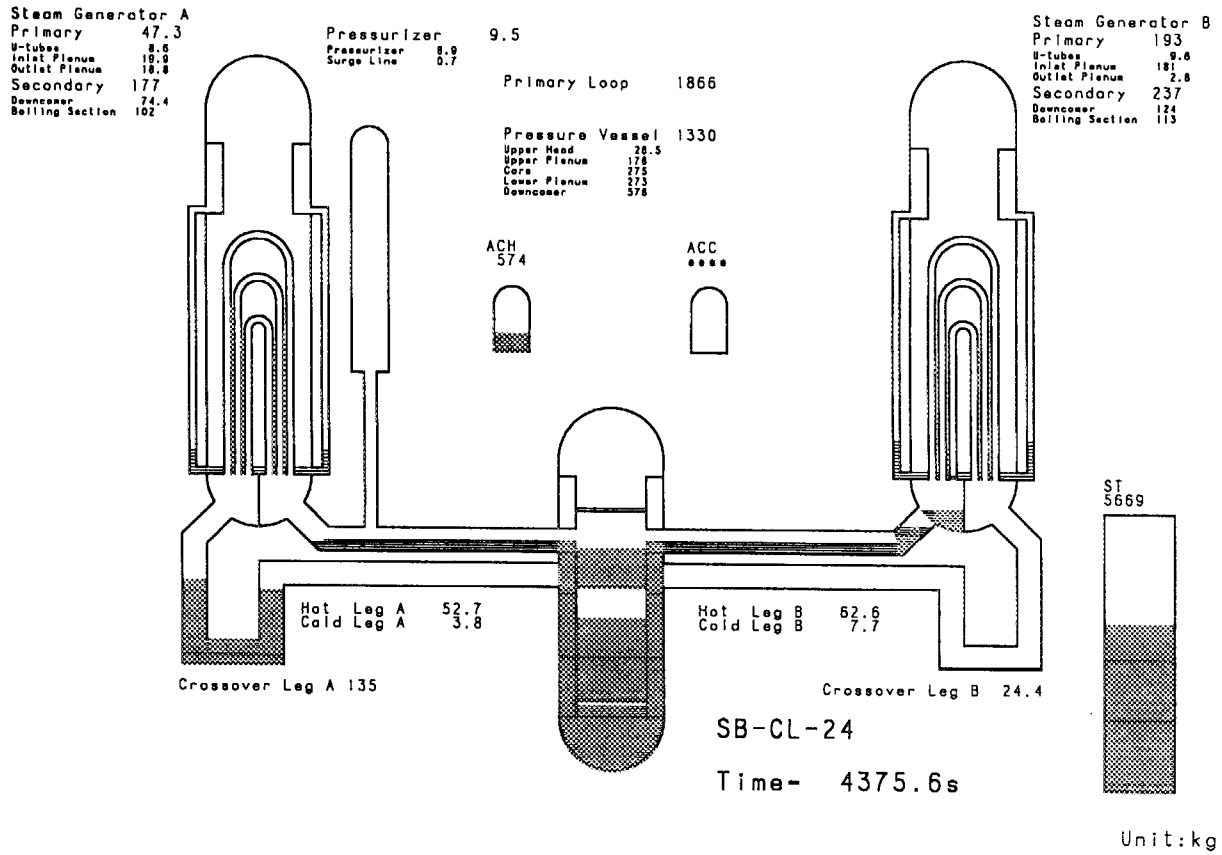

Fig. 4. 3. 12 Fluid mass distribution in early stage of the second loopseal reformation process (④; 4375.6s)

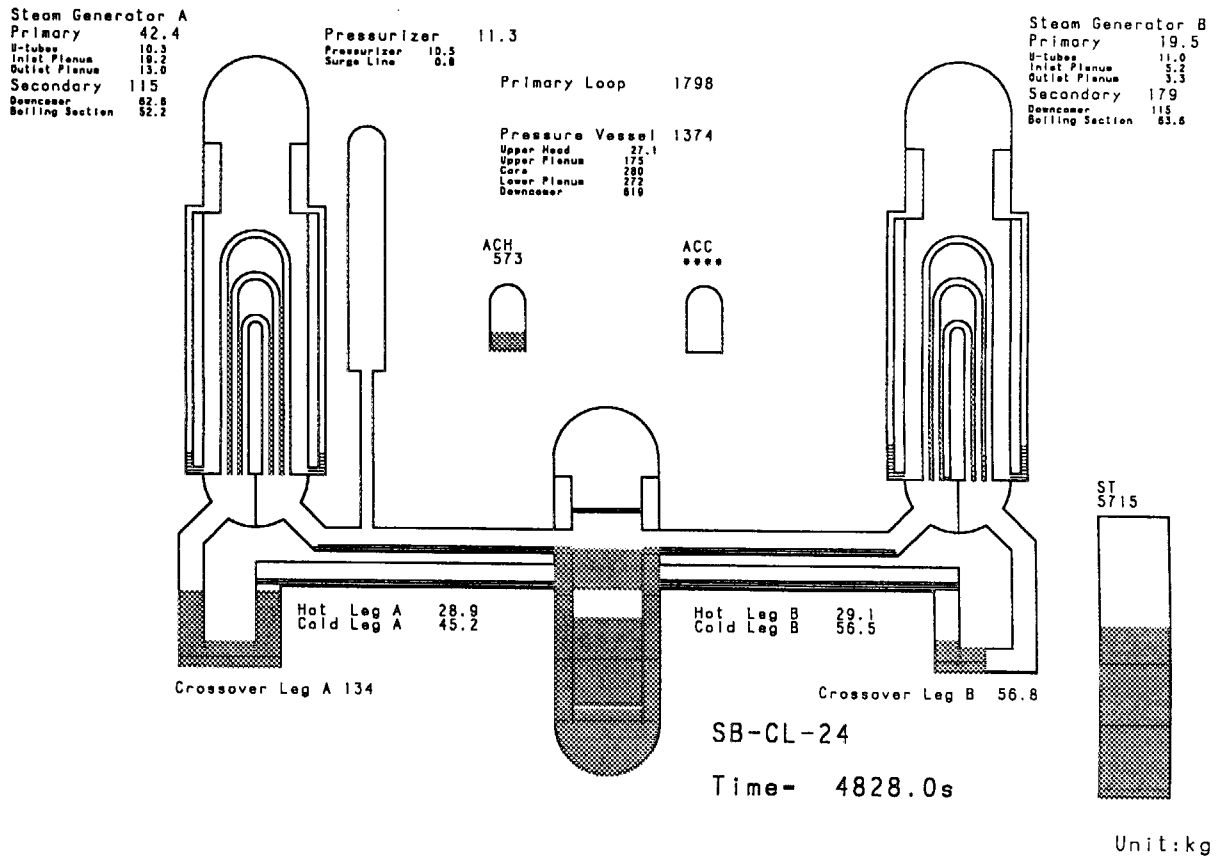

Fig. 4. 3. 13 Fluid mass distribution in middle stage of the second loopseal reformation process (⑤; 4828s)

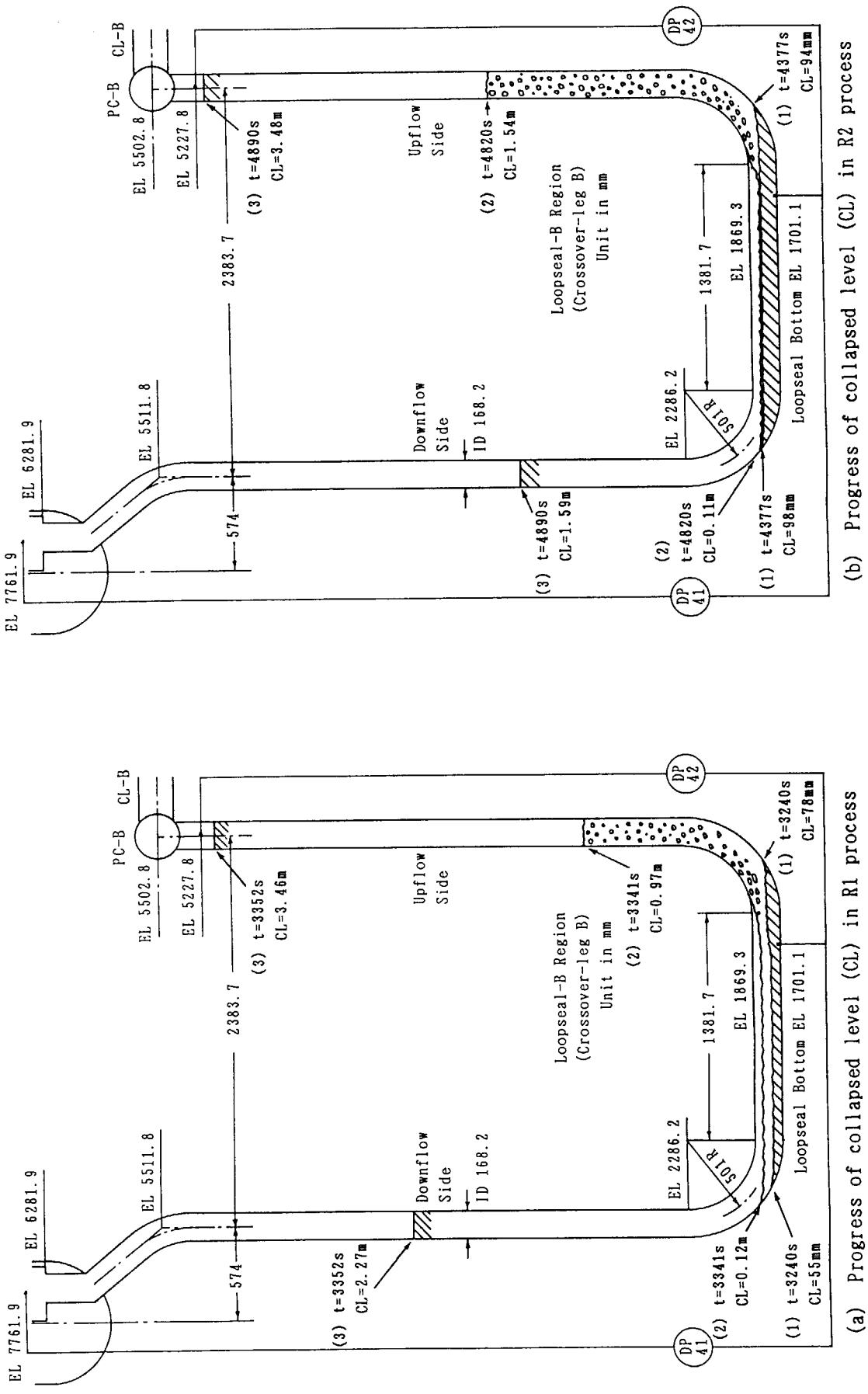

(a) Progress of collapsed level (CL) in R1 process

(b) Progress of collapsed level (CL) in R2 process

Fig. 4.3.14 Loopseal reformation process in loopseal-B region (Experiment SB-CL-24)

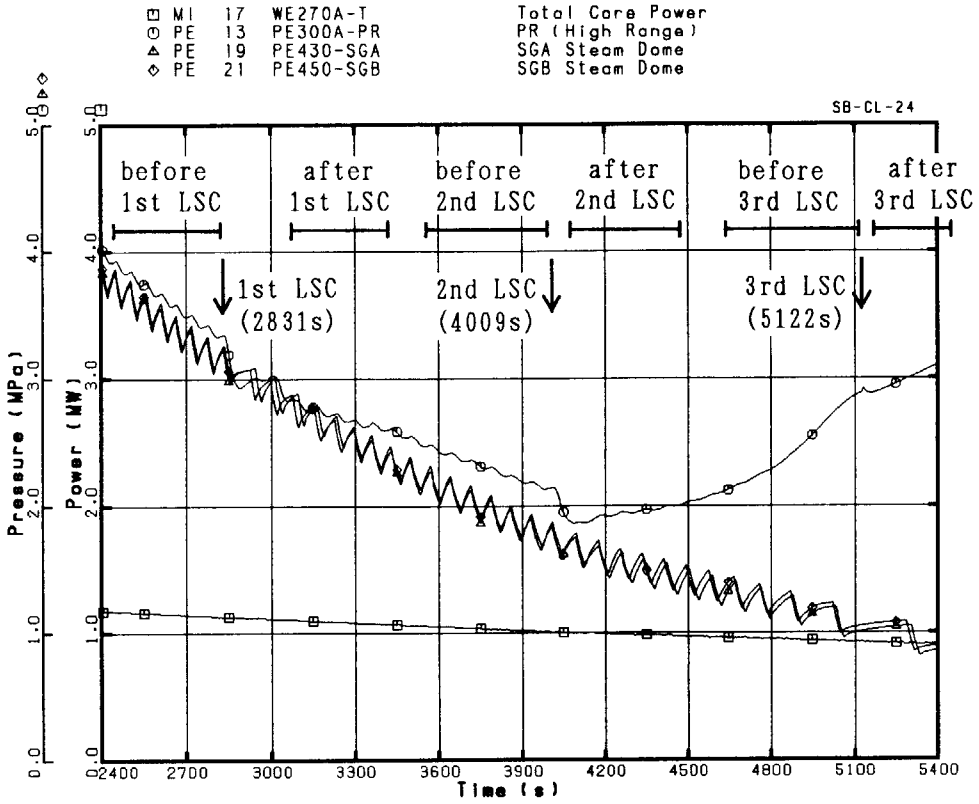

Fig. 4. 4. 1 Transient pressures and core power (2400 to 5400 s)

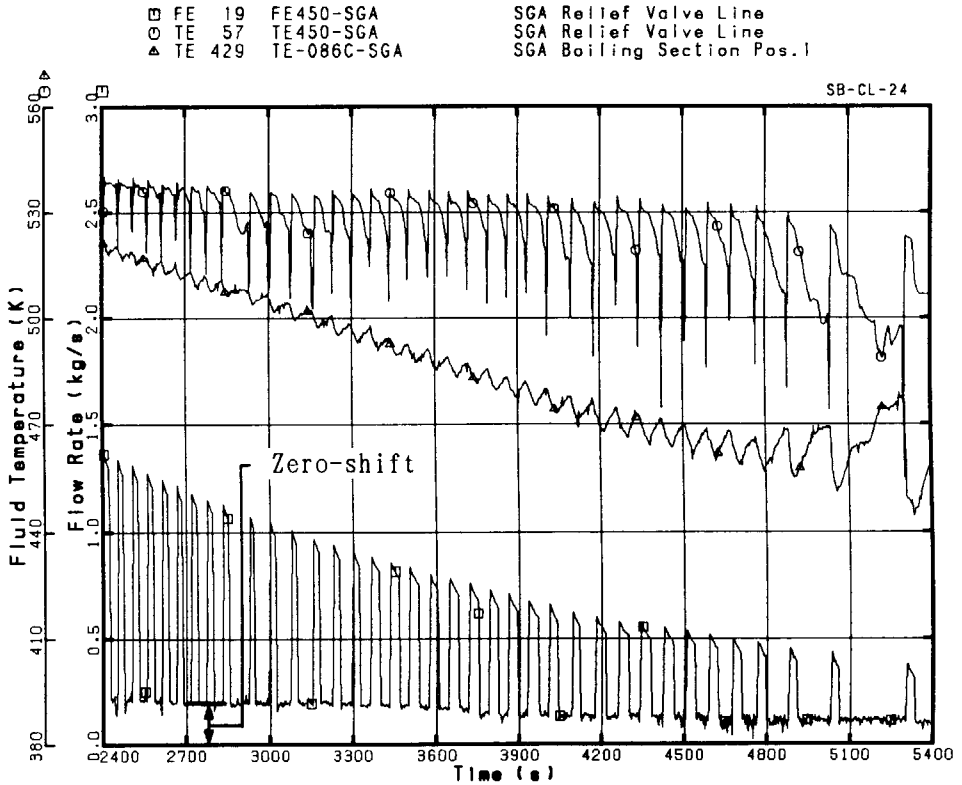

Fig. 4. 4. 2 Steam discharge flow rate and secondary fluid temperatures in SG-A

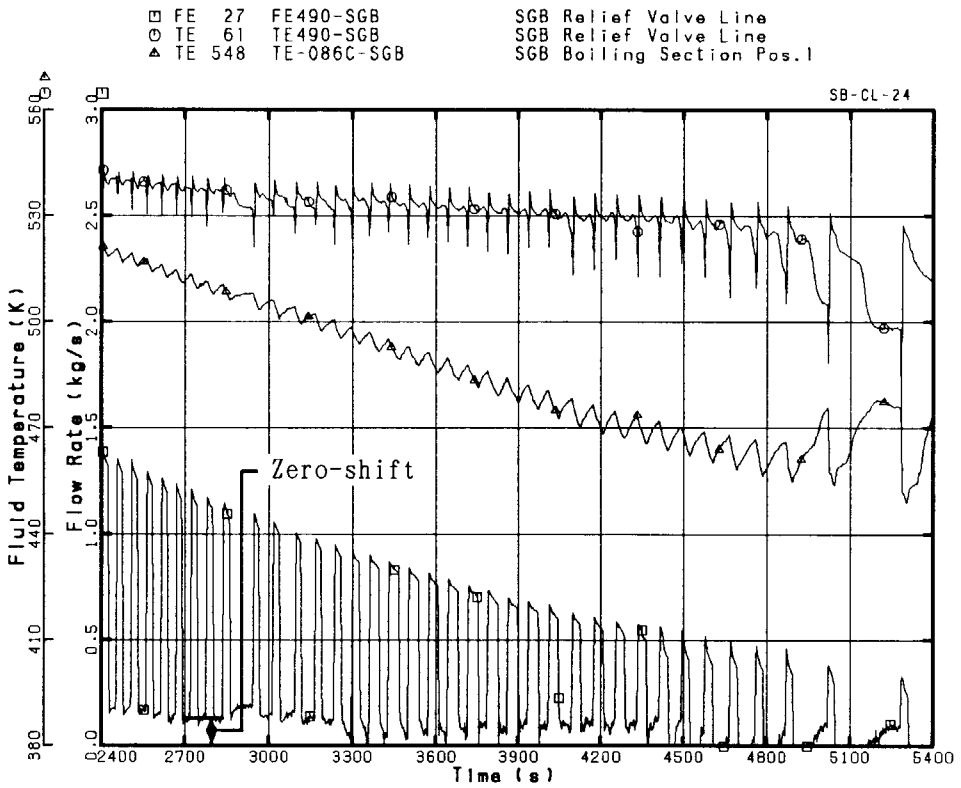

Fig. 4. 4. 3 Steam discharge flow rate and secondary fluid temperatures in SG-B

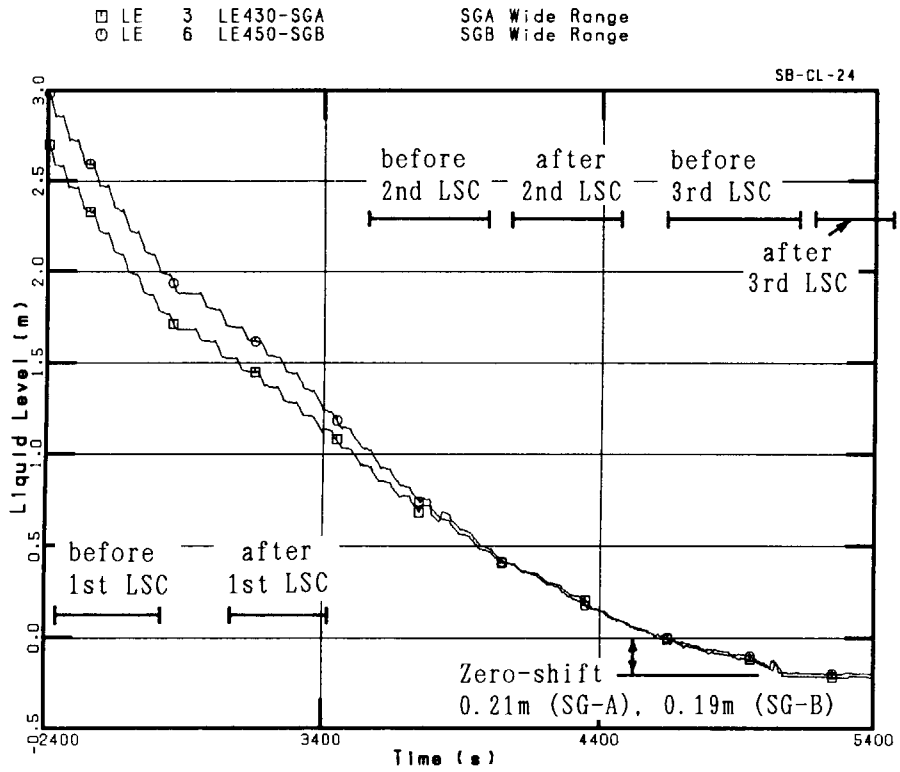

Fig. 4. 4. 4 Collapsed water levels in SG secondary systems

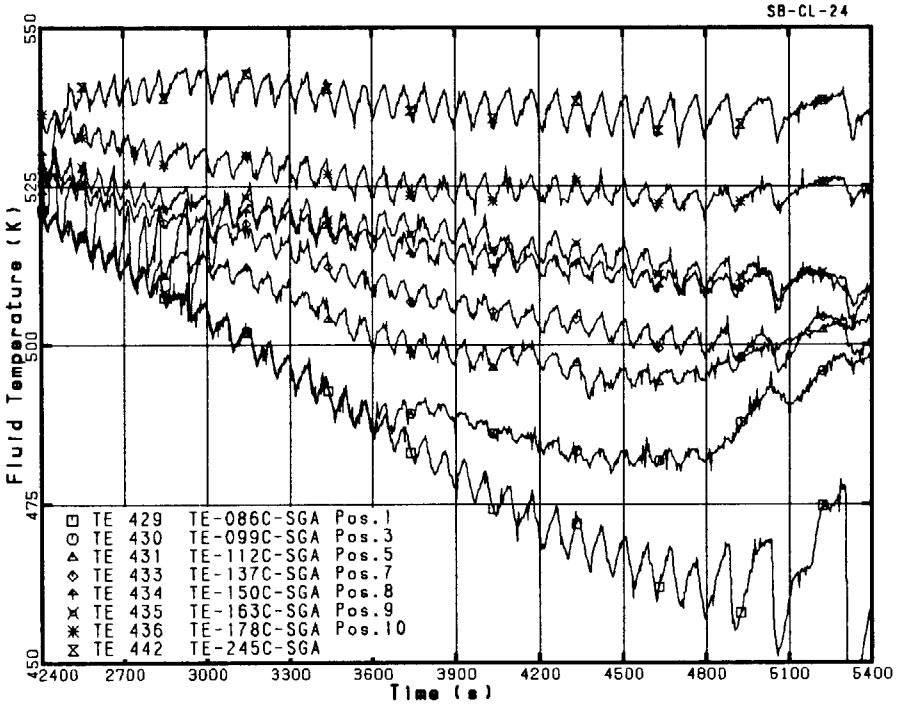

Fig. 4. 4. 5 Thermal stratification in secondary side fluid (SG-A)

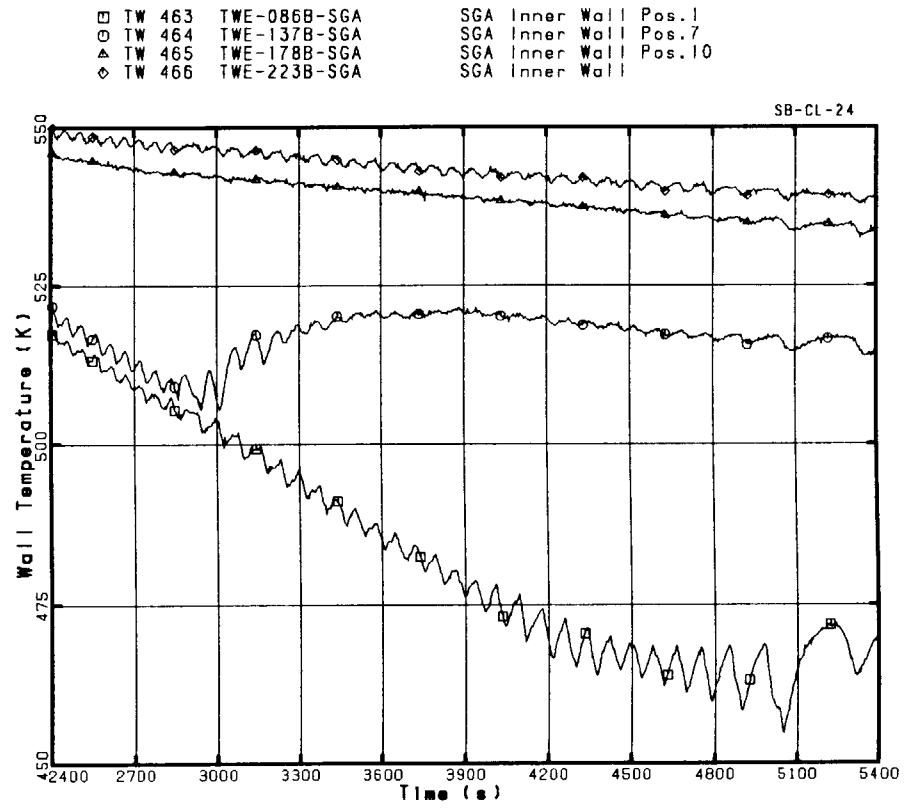

Fig. 4. 4. 6 Temperature distribution at SG-A vessel wall

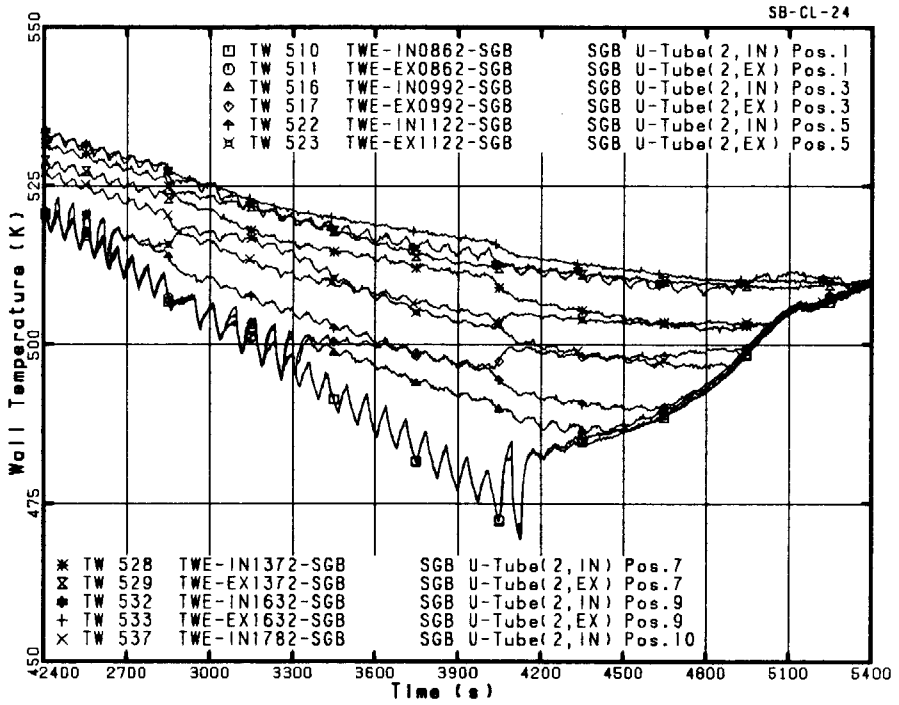

Fig. 4. 4. 7 Temperature distribution at U-tube walls (SG-B, tube No. 2)

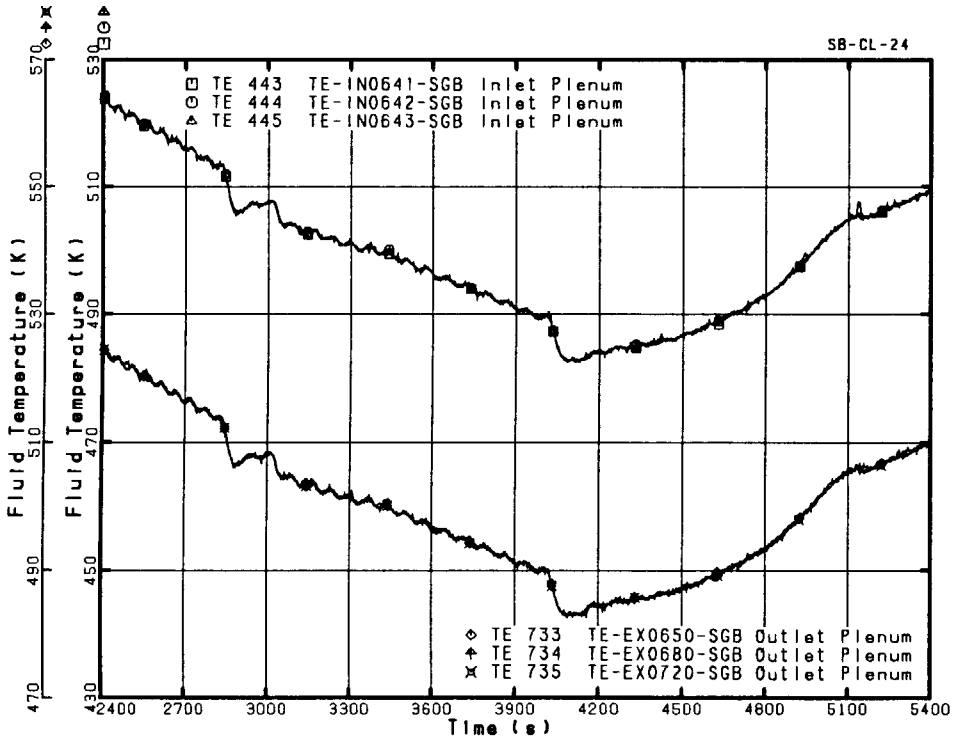

Fig. 4. 4. 8 Saturated fluid temperatures in inlet and outlet plena (SG-B)

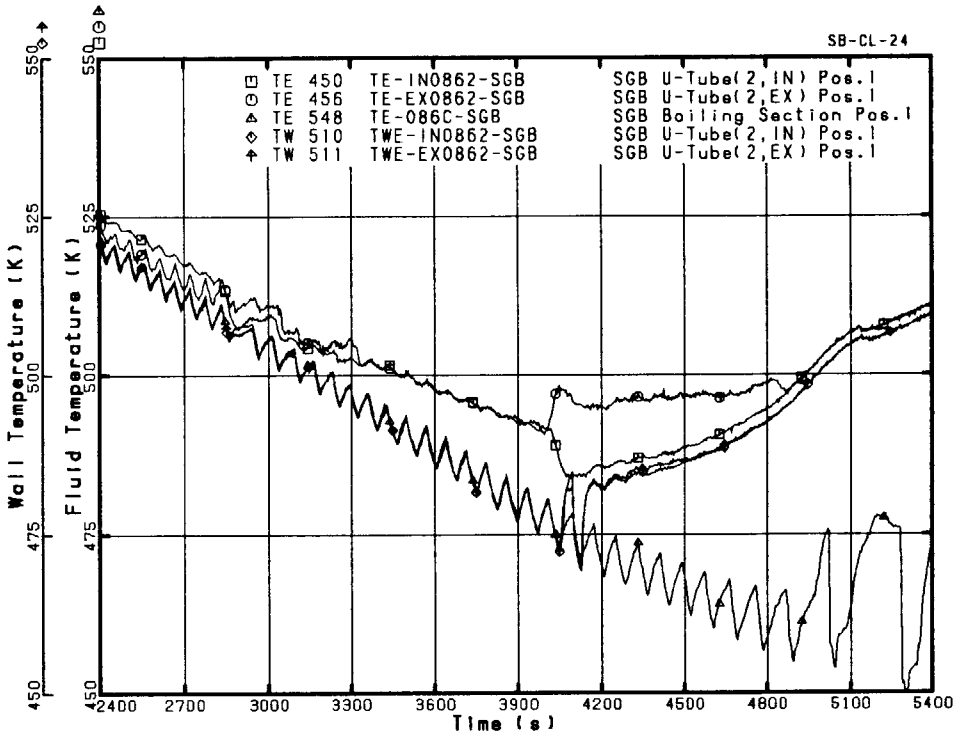

Fig. 4. 4. 9 Temperature distribution across SG-B U-tube No. 2 at Pos. 1

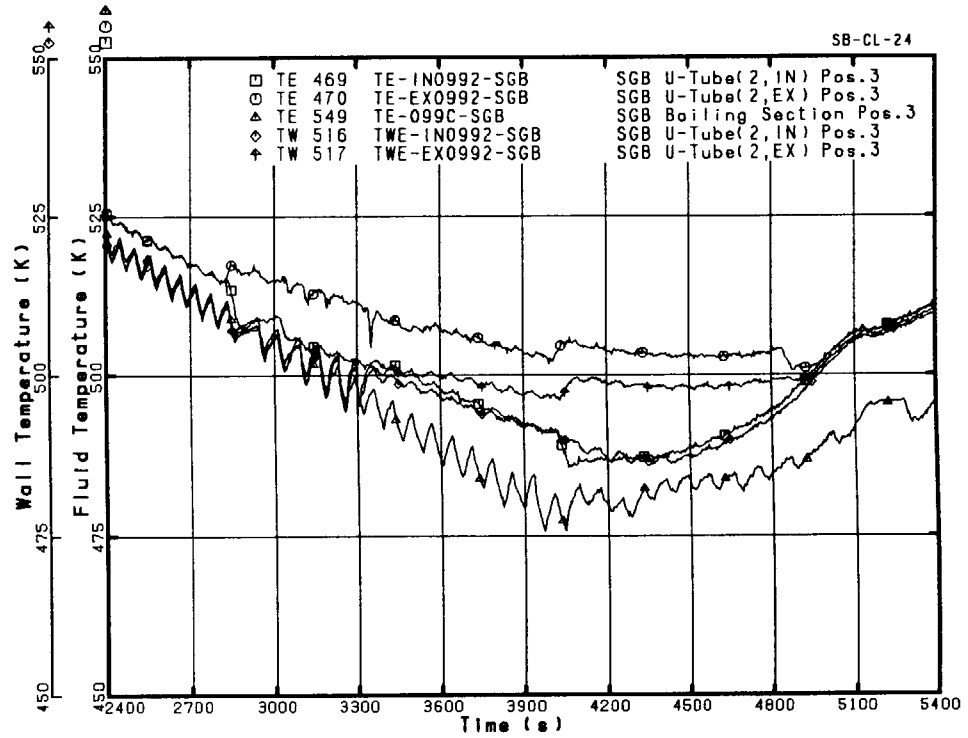

Fig. 4. 4. 10 Temperature distribution across SG-B U-tube No. 2 at Pos. 3

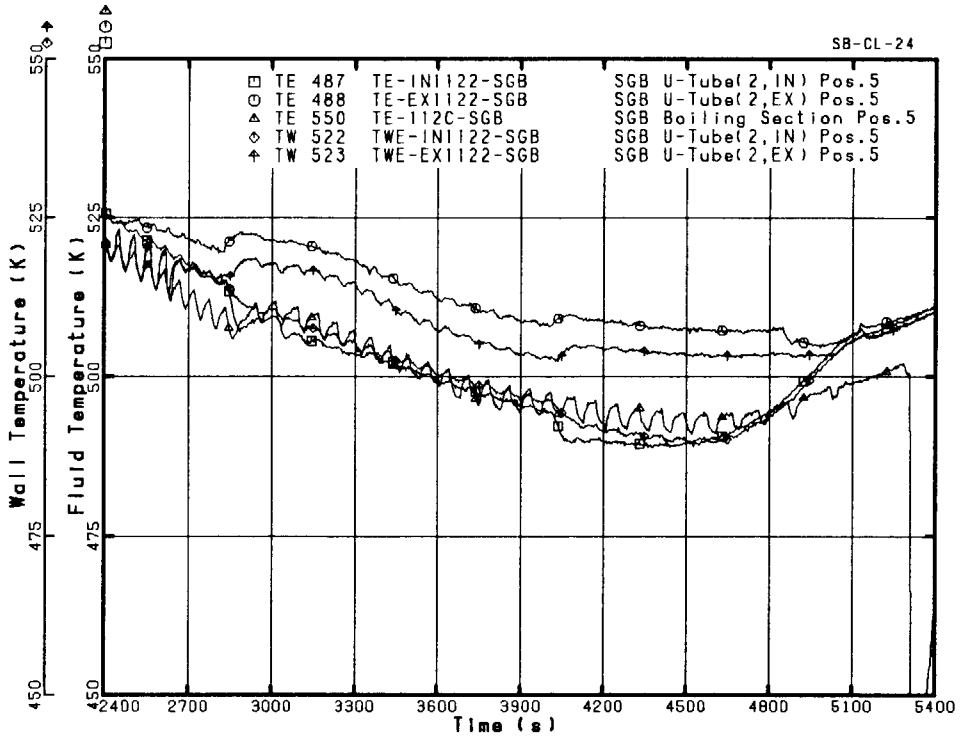

Fig. 4. 4. 11 Temperature distribution across SG-B U-tube No. 2 at Pos. 5

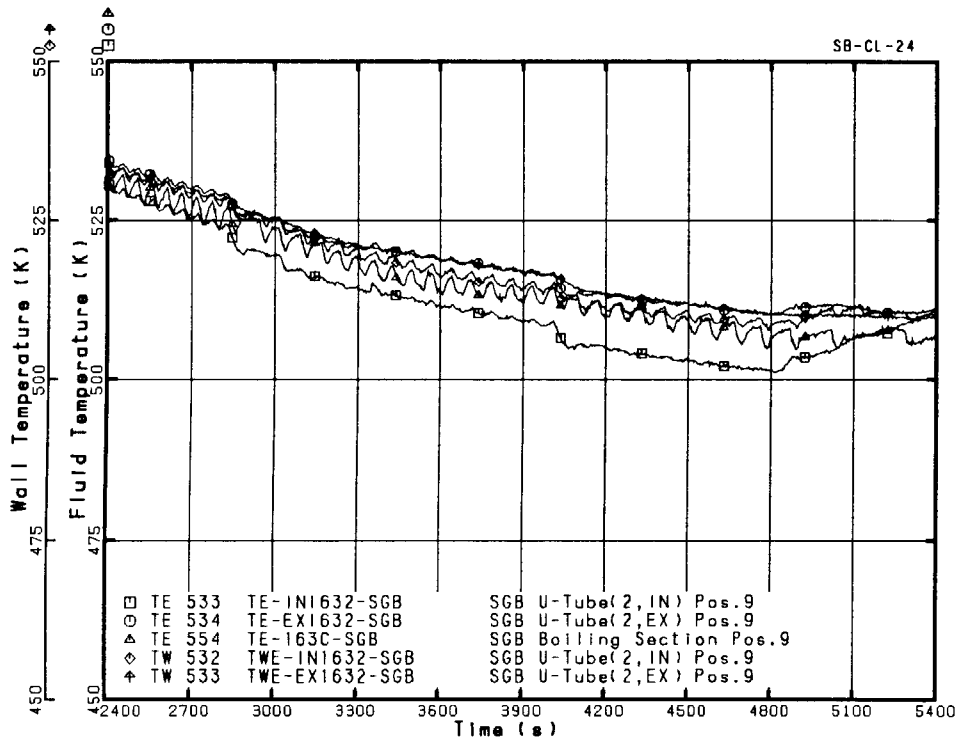

Fig. 4. 4. 12 Temperature distribution across SG-B U-tube No. 2 at Pos. 9

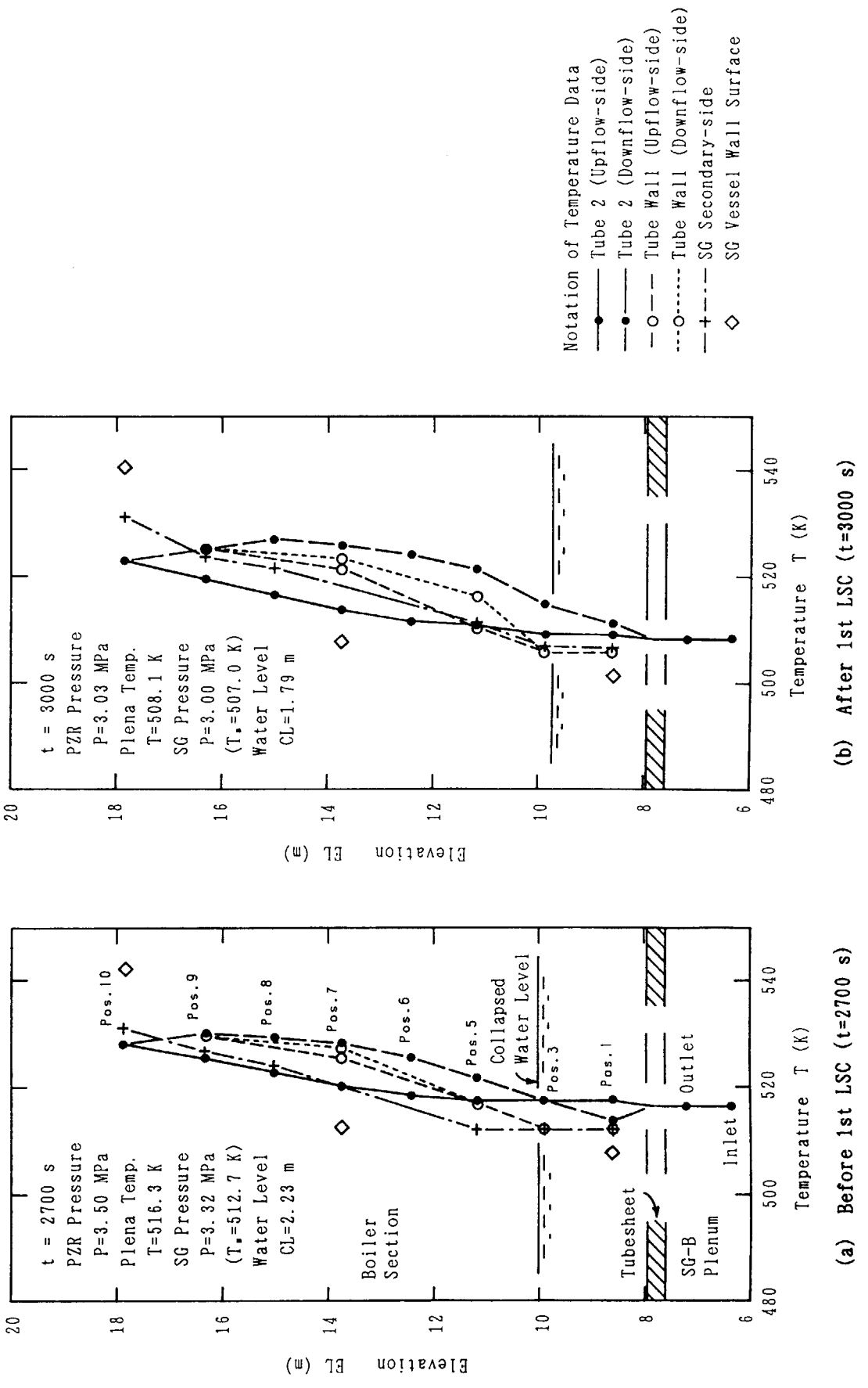

(a) Before 1st LSC (t=2700 s)

(b) After 1st LSC (t=3000 s)

Fig. 4. 4. 13 Representative fluid temperatures in SG-B U-tube before and after 1st LSC

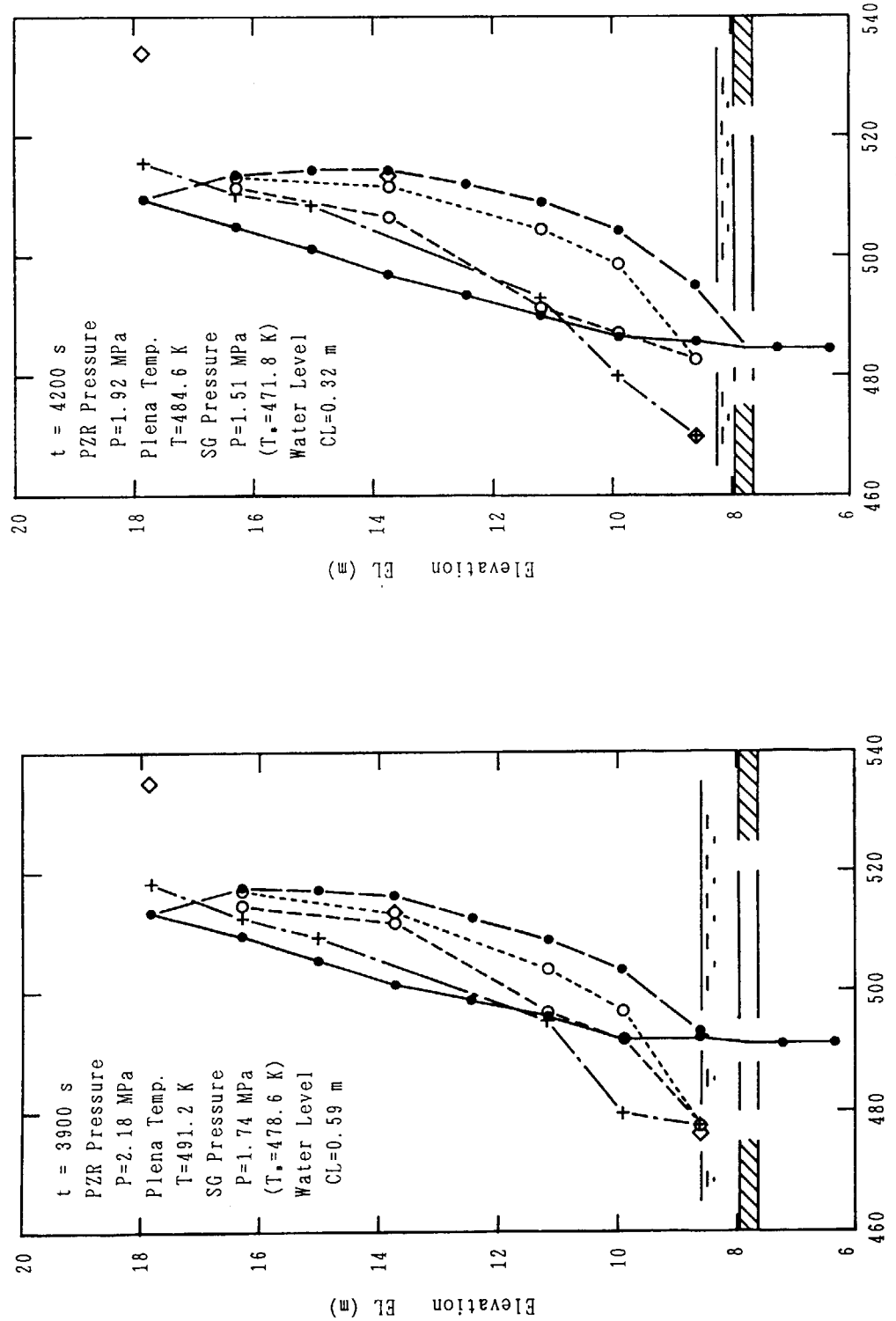

(a) Before 2nd LSC (t=3900 s)

(b) After 2nd LSC (t=4200 s)

Fig. 4. 4. 14 Representative fluid temperatures in SG-B U-tube before and after 2nd LSC

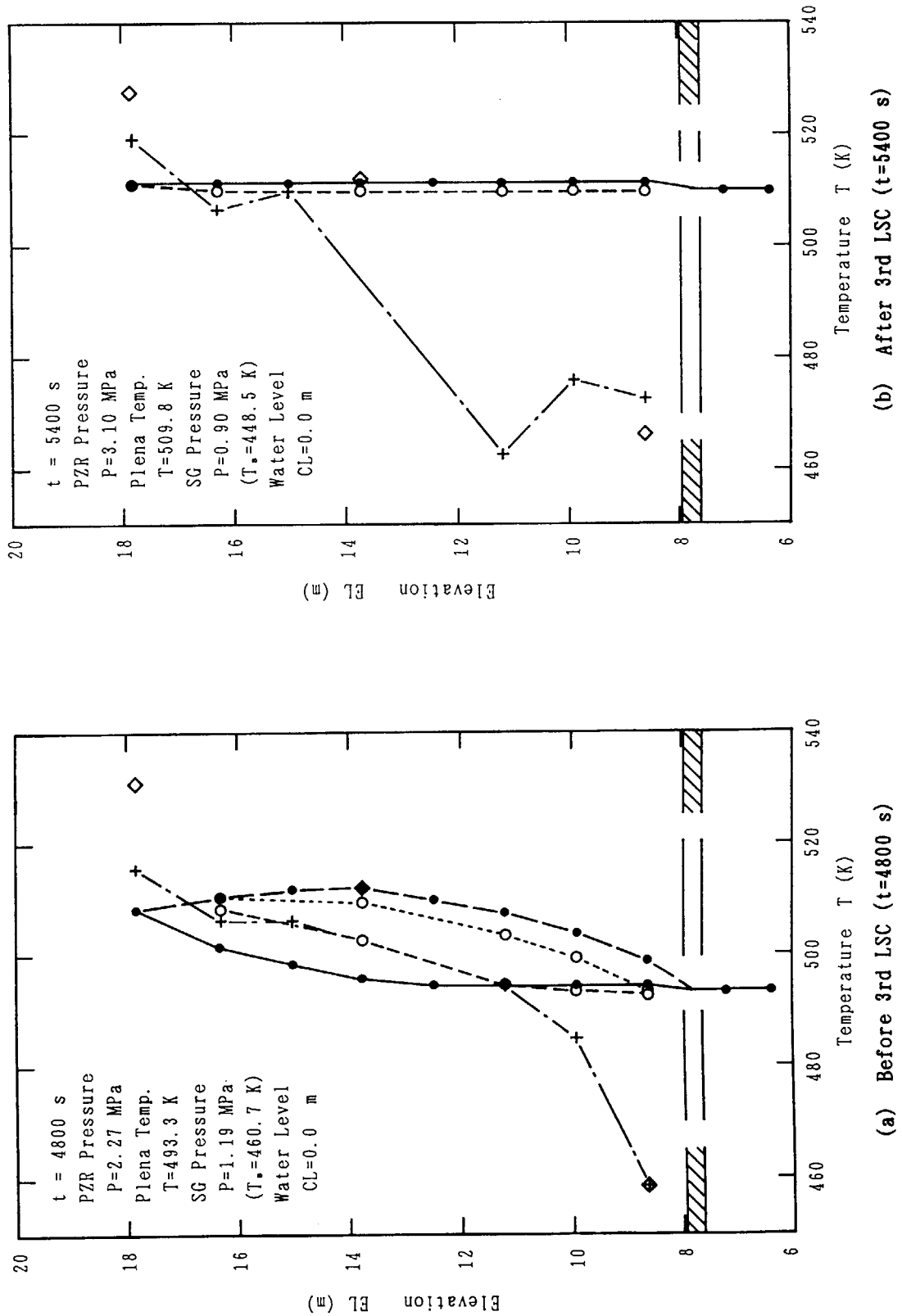

(a) Before 3rd LSC (t=4800 s)

(b) After 3rd LSC (t=5400 s)

Fig. 4.4.15 Representative fluid temperatures in SG-B U-tube before and after 3rd LSC

5. Concluding Remarks

An SBLOCA experiment, SB-CL-24, was conducted at the LSTF with the specified boundary conditions simulating a 0.5% break area at the CL-B horizontal line and an intentional secondary depressurization action under the failure assumptions on both HPI system and auxiliary feedwater system. The following are concluded with respect to the general thermohydraulic phenomena in this experiment, typical responses of the accident indication systems during inadequate core cooling (ICC) conditions, and mass and energy balances for the primary and secondary systems.

(1) General Thermohydraulic Phenomena in Experiment SB-CL-24

This SBLOCA experiment is characterized by four phases, i.e., ① an initial blowdown transient (0 - 600 s) after the break, ② a long cooldown transient (600 - 4163 s) promoted by the secondary depressurization action and typical fluid behaviors related to the repeated loopseal clearings (LSCs) and AIS actuation, ③ a primary pressurization phase (4163 -6568 s) with the boil-off core heatup phenomena, and ④ a rapid depressurization phase (6568 - 7844 s) initiated by the PORV open action to lead the LPI actuation and the final core quench.

In a long-term cooldown transient and the following pressurization phase, the LSC occurred in three times with the temporary core level depression and the ICC occurrence. After the primary cooldown action became inadequate due to loss of the secondary coolant, the primary pressure started to increase and the core was significantly uncovered (5929 - 7675 s). By additional primary depressurization actions to open the PORV and the safety valve at the pressurizer, the LPI was actuated to result in the core quench. The core power was controlled after 7109 s to limit the heater rod temperature excursion within 923 K.

(2) Effects of Secondary Depressurization Action

The secondary depressurization action was effective to lead the AIS actuaion (4.5 MPa) at 2210 s but was not sufficient to result in the LPI actuation at 1.29 MPa due to empty of the SG secondary as stated above. Although the SG-RV cyclic opening was continued to depressurize the secondary system throughout the test, the primary pressure started to increase at 4163 s when the secondary water level decreased to 0.4 m above the bottom in two SGs. Steam in the primary system was condensed in the SG U-tubes and flowed down to two ways, i.e., one is the hot leg sides toward the upper core, and the other one is the SG outlet plena toward the loopseal regions.

The SG-RV cyclic opening actions caused the primary pressure oscillations and therefore significantly oscillated the AIS injection flows (see Figs. 4.1.21 and 4.1.22). Namely, the AIS injection flow rate decreased to zero whenever the primary pressure increased. The oscillations of the AIS injection flow rates caused oscillating steam condensation in two cold legs. These caused oscillations not only in the local primary water levels but also in the core void fraction. After the primary pressurization started, these oscillating behaviors almost diminished.

(3) Repeated Loopseal Clearings with Temporary Core Heatup

Repeated LSCs occurred in the loopseal-B, while no LSC occurred in the loopseal-A except for a minor water level depression in each LSC process.

(a) The First LSC and Reformation Process

The first LSC process started after the AIS actuation started, which condensed steam in the cold legs and resulted in water-filled condition at the CL-B break location, since steam accumulated in the hot primary regions caused the manometric water level depression both at the loopseal downflow-sides and the core. This process ended when the accumulated steam completely cleared the water in the loopseal-B region and dischrged from the break at 2831 s. Thereafter, the first loopseal reformation process started by accumulating both condensed water from the SG-B U-tube outlets and fall-back AIS water from the CL-B. The water accumulation progressed in two stages, i.e., the first one is a gradual water level increase (2855 - 3240 s) up to half of the loopseal horizontal pipe in which steam flowed above the water level, and the second one is a rapid water refill (3240 - 3352 s) caused by a break of the counter current flow limitation (CCFL) in the upflow-side of the loopseal-B region or at the primary pump-B (see Fig. 4.3.14 (a)). The primary coolant distribution largely changed from the first stage (Fig. 4.3.10) to the final condition of the second stage (Fig. 4.3.11) by this rapid refill process.

(b) The Second LSC and Reformation Process

The second LSC process started after the first reformation process completed, and then manometric water level depression occurred like as the first LSC process. After the second LSC occurred at 4009 s, the second reformation process started in three stages, i.e., a gradual water accumulation (4042 - 4377 s) like as the first stage of the first reformation process, a faster water accumulation (4377 - 4820 s) only at the upflow-side, and a rapid water refill (4820 - 4890 s) like as the second stage of the first reformation process. The second stage was mainly caused by the condensed water fall-back from the SG-B outlets (AIS was terminated at 4086 s) and by a higher steam flow rate which sup-

ported the two-phase fluid in the upflow-side (up to a maximum collapsed water level of 1.54 m, see Fig. 4.3.14 (b)). The higher steam flow rate in the second reformation process can be ascribed to the decreased steam condensation rate at both SGs compared to the first reformation process. As the primary mass continued to decrease in the second reformation process, the upflow-side water level at the end of the third stage was lower than that at the end of the first reformation process.

(c) The Third LSC Process

The third LSC process started just after the second reformation completed, and the loopseal-B water was cleared by steam discharge at 5122 s. After the third LSC, no loopseal was reformed in the loopseal-B region due to lack of the primary mass inventory but the boil-off heatup process started in the core.

(d) Temporary Core Heatups during Three LSC Processes

It was clarified that three LSCs occurred at similar primary mass inventory ratios of $M^*(=M_R/M_0)$ = 0.33 to 0.30 which corresponded to water levels as shown in Figs. 4.3.2 and 4.3.3. The core collapsed water level was depressed to approximately EL 2.0 m (above the core bottom elevation) and the core heatup was temporarily detected in a lmited range of one third core region (a maximum temperature increase was $\Delta T \leqq 26$ K) during the first and second LSC processes in which a local cooling effect was observed in the hot leg side bundles as a result of fall-back condensed water from both SGs. The core heatup in the third LSC process, however, was detected in most of the rod bundles in one third of the upper core region with higher temperature increases ($\Delta T \leqq 78$ K) as a result of less mixture level swelling in the core under the primary pressurization condition compared to the first and second LSC processes.

(4) Less Mass Accumulation by AIS Injection

The AIS injected water of 2229 kg which corresponded to 41% of the initial primary mass, into two cold legs between 2110 s and 4086 s. A study of primary mass balance showed less mass accumulation in the primary system by this AIS actuation, i.e., most of the injected AIS water flowed out of the break location and therefore primary mass inventory did not recover to an initial mass level at the AIS actuation time of 2110 s.

(5) Boil-off Core Heatup Process

The upper plenum water level started to decrease at the primary mass ratio of $M^*= M_R/M_0$ = 0.30 prior to the core heatup initiation at M^*= 0.27 in the boil-off process. The core heatup started at 5929 s (1843 s after the AIS termination) and completely diminished at 7675 s (304 s after the LPI actuation). The heatup range covered more than 50% of total

core (see Fig. 4. 1. 44) and a maximum rod temperature turned to decrease after the primary depressurization was conducted by opening the PORV and SV recording a maximum rod temperature of 921 K at 7167 s. The core power was controlled from 100% to 10% of the standard decay power between 7109 and 7166 s to limit the rod temperature increases.

In the upper core region, local cooling effects due to the fall-back condensed water were also observed during this boil-off process and a maximum heatup delay time of 690 s was detected at the hot leg side core (Pos. 9). The mixture level responses detected by the conduction probes (CPs) agreed well with the rod heatup front and also with the rod quench front. The mixture levels were slightly higher than the collapsed water level in the core (see Fig. 4. 1. 44).

(6) Detection of Core Heatups by Temperature Measurements

The temperature measurements at the core exit, in the upper plenum and the hot legs were investigated in relation to the core heatup phenomena on the view point of ICC detection both in the repeated LSC processes and the boil-off process.

(a) CET (Core Exit Thermocouple) Measurement

Twenty of CETs were installed at the upper core plate outlet in the LSTF. The CET data in this experiment showed no heatup during the repeated LSC processes despite the temporary core heatups existed as shown above. These CET responses are common during a LSC process in a SBLOCA condition with the secondary depressurization action.

On the other hand, CET responses during the boil-off process showed good correspondences to the core heatup phenomena with detection delay times and degraded heatup temperatures. An average detection delay time was obtained for this experiment as approximately 300 s compared to the upper core heatups (at Pos. 9 and Pos. 8). An average temperature increase of the CET data was rather proportional to an average temperature increase of the core top region (Pos. 9) as shown in Fig. 4. 2. 13. Thus, it is valuable to use the CETs to detect the ICC condition except for the LSC phenomena.

(b) Upper Plenum Temperature Measurement

Fluid temperatures in the upper plenum were measured at six locations (three vertical elevations at the outer parts of two control rod guide tubes). In the repeated LSC processes, the top part T/Cs were affected by hot metal walls such as the upper core support plate since the top region was filled with stagnant steam, and did not correspond to the core heatup behaviors. On the other hand, the middle and lower T/Cs in the upper plenum showed saturated conditions, and thus no correspondence to the core heatups during the

LSC processes was confirmed.

During the boil-off core heatup process, all the upper plenum temperatures showed better correspondences to the core heatup behaviors compared to the CET responses. Namely, the detection delay times were approximately 100 s earlier than the average CET responses and the temperature increasing rates were higher than those of the CETs. These indicate less influences of the fall-back water on the upper plenum temperature measurements in comparison with the CET measurements and therefore the upper plenum temperature measurements are available for an alternative core heatup detection measurement.

(c) Hot Leg Temperature Measurements

The hot leg temperatures showed no heatup during the repeated LSC processes like as the CETs. In the boil-off core heatup process, the hot leg temperatures showed rather complicated behaviors and less correspondences to the core heatup behaviors due to effects of the secondary depressurization actions and the primary depressurization actions. Therefore, the hot leg temperature measurements are less effective than the CETs and the upper plenum temperatures with respect to the core heatup detection.

(7) Mass and energy balance at two SGs during repeated LSC processes

The discharged steam mass from the cyclicly opened RV at each SG agreed well to the mass decrease in each secondary system which was calculated by cumulating the regional masses within a discrepancy of ± 26 kg. Thus, the secondary mass balance was well held for the repeated LSC processes. An energy balance was also investigated for the secondary system and the following are derived. Namely, the steam discharge from the RV was a controlling factor on the secondary energy balance. The primary-to-secondary transfered energy was approximately 37 to 56% of the discharged steam energy as long as the secondary water level existed. After the seconadry water level became almost zero, the primary-to-secondary transfered energy significantly decreased. Steam condensation heat transfer rate at the SG U-tubes before each LSC time was higher than that after the LSC. The condensed water at the U-tube inlet-side flowed down to the hot legs and contributed to cool the partial core region, while the condensed water at the U-tube outlet-side flowed down to the loopseal regions and contributed to repeat the LSC phenomena.

Acknowledgment

The authors are grateful to Mr. H. OHSAKI, T. OHWADA, M. OGAWA, A. OHWADA in Safety Facility Engineering Services Division and Mr. T. NISHIKIZAWA in Office of Operational Safety Administration for their technical supports, and to Mr. Y. SHIMANE, Ms. K. TOYODA and Ms. T. KUROSAWA for their contribution to data reduction and reporting.

References

(1) The ROSA-IV Group, "ROSA-IV Large Scale Test Facility (LSTF) System Description for Second Simulated Fuel Assembly", JAERI-M 90-176, Oct. 1990.

(2) The ROSA-IV Group, "Supplemental Description of ROSA-IV/LSTF with No. 1 Simulated Fuel-rod Assembly", JAERI-M 89-113, Sept. 1989.

(3) M. FUJII, et. al., "ROSA-IV/LSTF Experimental Data Reduction and Management Software System (Version 1)", JAERI-M 85-121, Sept. 1985.

(4) K. TASAKA, et. al., "The results of 0.5% Small Break LOCA in ROSA-IV LSTF Break Location Parameter Test Series", Proc. 15th Water Reactor Safety Inf. Mtg., NUREG/CP-0091, Vol. 4 (1987).

(5) K. TASAKA, et. al., "The Effects of Break Location on PWR Small Break LOCA", Nucl. Eng. Des., 122 (1990)

(6) M. SUZUKI, "Break Location Effects on PWR Small Break LOCA Phenomena -- Inadequate Core Cooling in Lower Plenum Break Test at LSTF --", JAERI-M 88-271, Jan. 1989.

(7) H. KUMAMARU, et. al., "ROSA-IV/LSTF 5% Cold Leg Break LOCA Experiment, RUN SB-CL-18, Data Report", JAERI-M 89-027, Mar. 1989.

(8) Y. KUKITA, et. al., "Data Report for ROSA-IV LSTF 5% Cold Leg Break LOCA Experiment RUN SB-CL-08", JAERI-M 89-220, Jan. 1990.

(9) Y. KUKITA, et. al., "Data Report for ROSA-IV LSTF 5% Hot Leg Break Experiment RUN SB-HL-01", JAERI-M 89-225, Jan. 1990.

(10) Y. KUKITA, et. al., "Data Report for ROSA-IV LSTF 10% Hot Leg Break Experiment RUN SB-HL-02", JAERI-M 90-039, Mar. 1990.

(11) Y. KUKITA, et. al., "Data Report for ROSA-IV LSTF 10% Hot Leg Break Experiment RUN SB-HL-04", JAERI-M 91-040, Mar. 1991.

(12) M. SUZUKI, "Characteristic Responses of Core Exit Thermocouples during Inadequate Core Cooling in Small Break LOCA Experiments Conducted at Large-Scale Test Facility (LSTF) of ROSA-IV Program", Proceedings of the 2nd ASME·JSME Joint Conference on Nuclear Engineering (1993).

(13) M. SUZUKI, et. al., "Quick Look Report for ROSA/AP600 Phase-II No. 5 Experiment, AP-FW-01 (Cooperative Research)", JAERI Internal Report (1998).

(14) R. A. SHAW, et. al., "A Description of the Instrumentation Used during ROSA/AP600 Experiments in LSTF", JAERI Internal Report (1995).

Appendix A Instrumentation Locations for Experiment SB-CL-24

Instrumentation locations for most of the measurements (see Table 2.2-2) are presented below in Figs. A.1 through A.16. Precise description of the measurement system is shown in Reference [1].

List of Figures

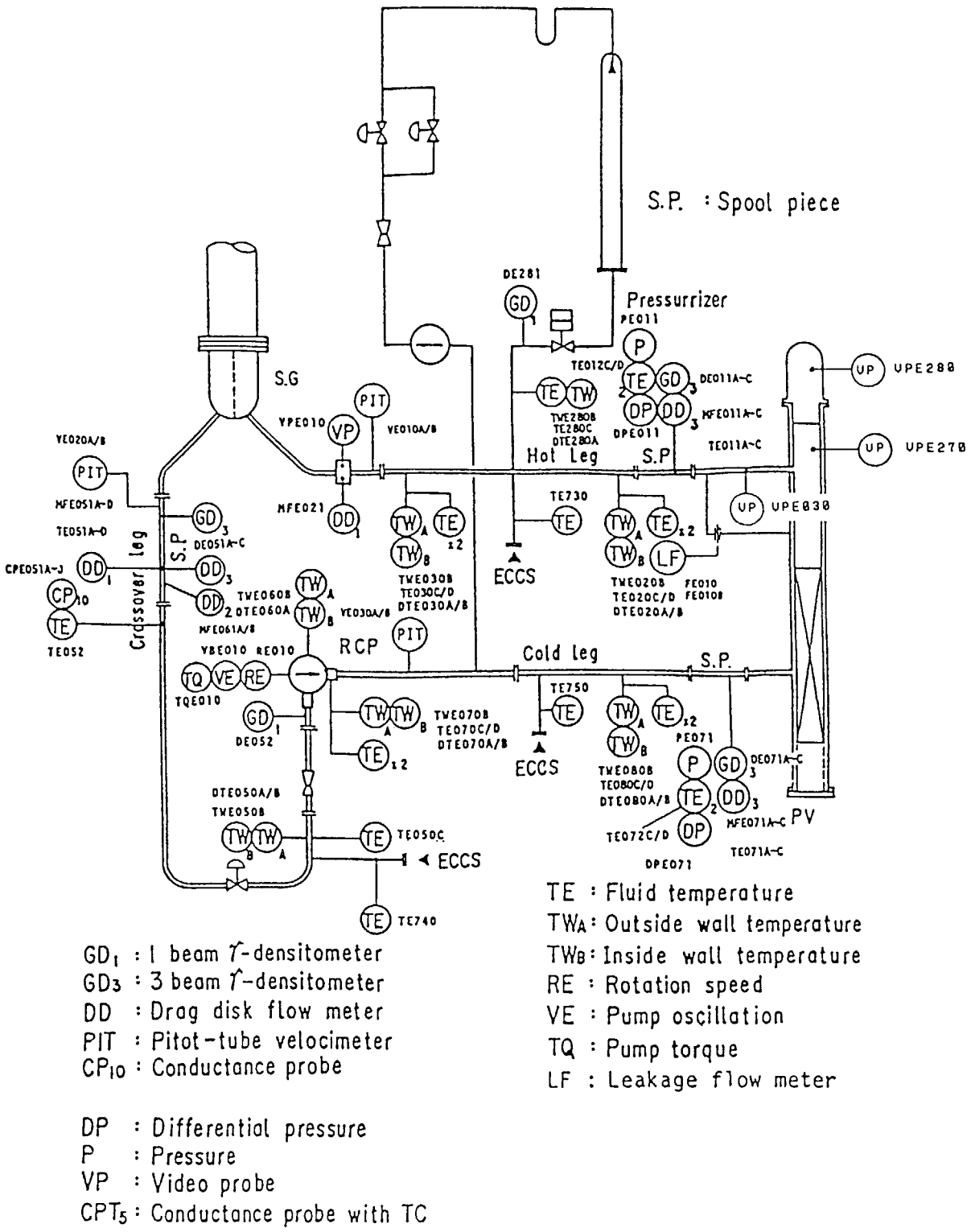

Fig. A. 1 Primary loop-A instruments for measurements of pressure, temperature, fluid density and others

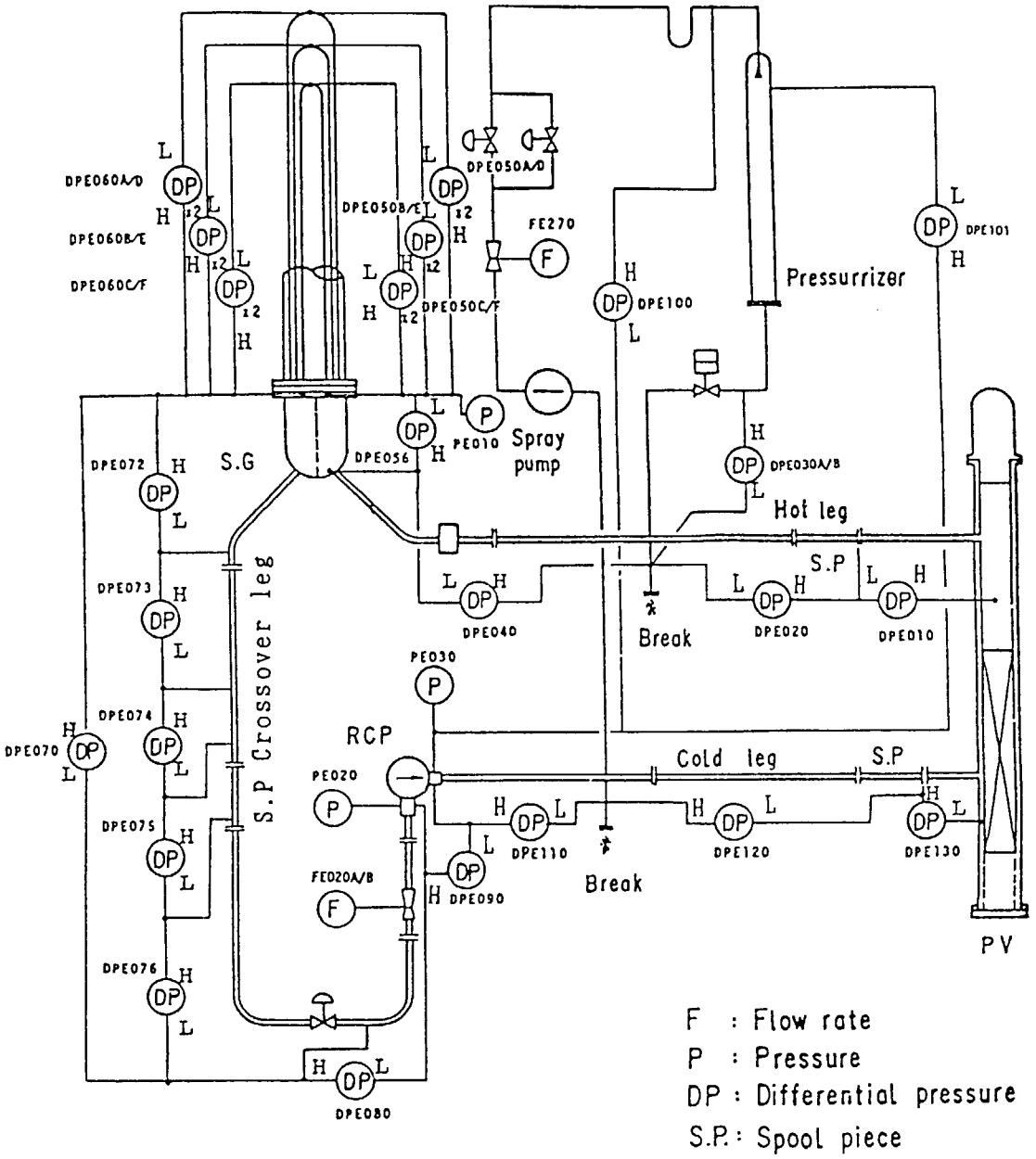

Fig. A. 2 Primary loop-A instruments for measurements of DP and flow-rate

VP : Video probe
GD_3 : 3 beams γ – densitometer
DD : Drag disk flow meter
CP_{10} : Conductance probe

DP : Differential pressure
P : Pressure
CPT_5 : Conductance probe with TC
TE : Fluid temperature
TW_A : Outside wall temperature
TW_B : Inside wall temperature
RE : Rotation speed
VE : Pump oscillation
TQ : Pump torque
LF : Leakage flow meter

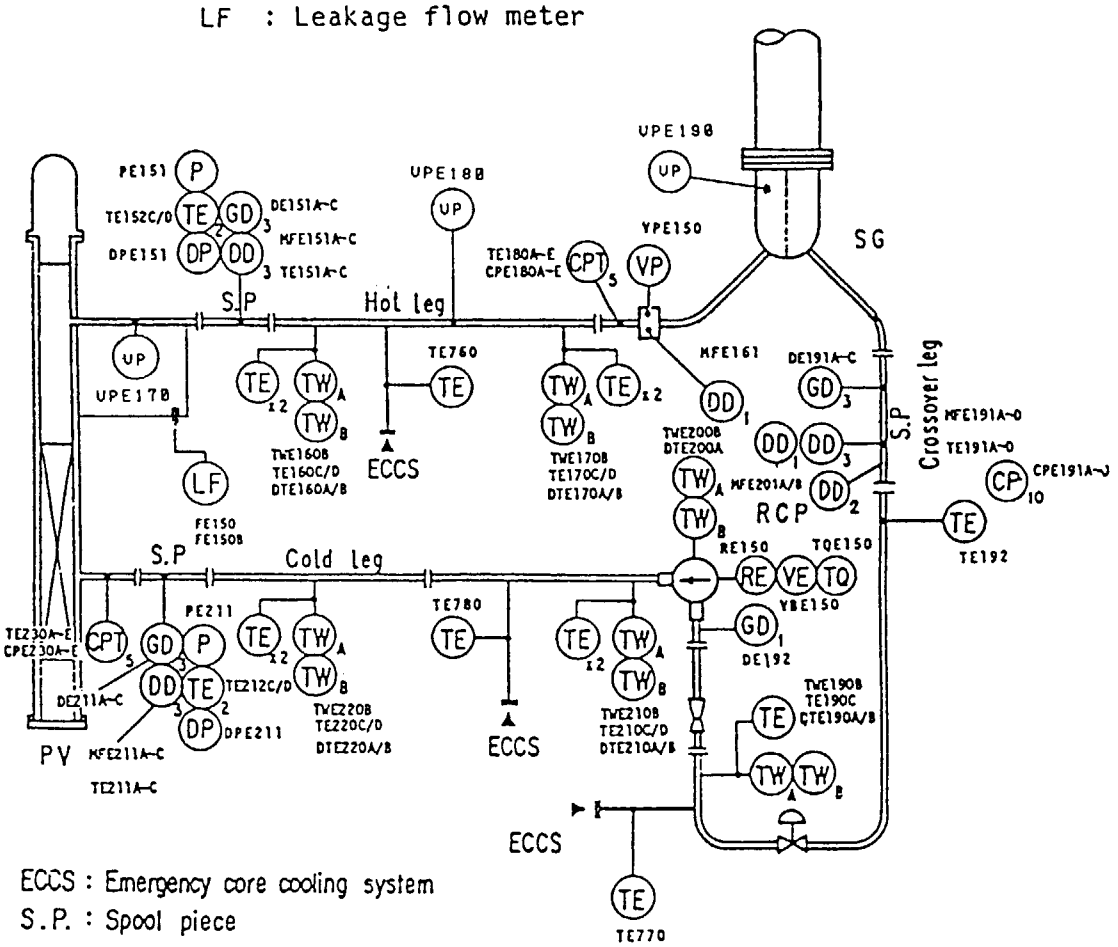

Fig. A. 3 Primary loop-B instruments for measurements of pressure, temperature, fluid density and others

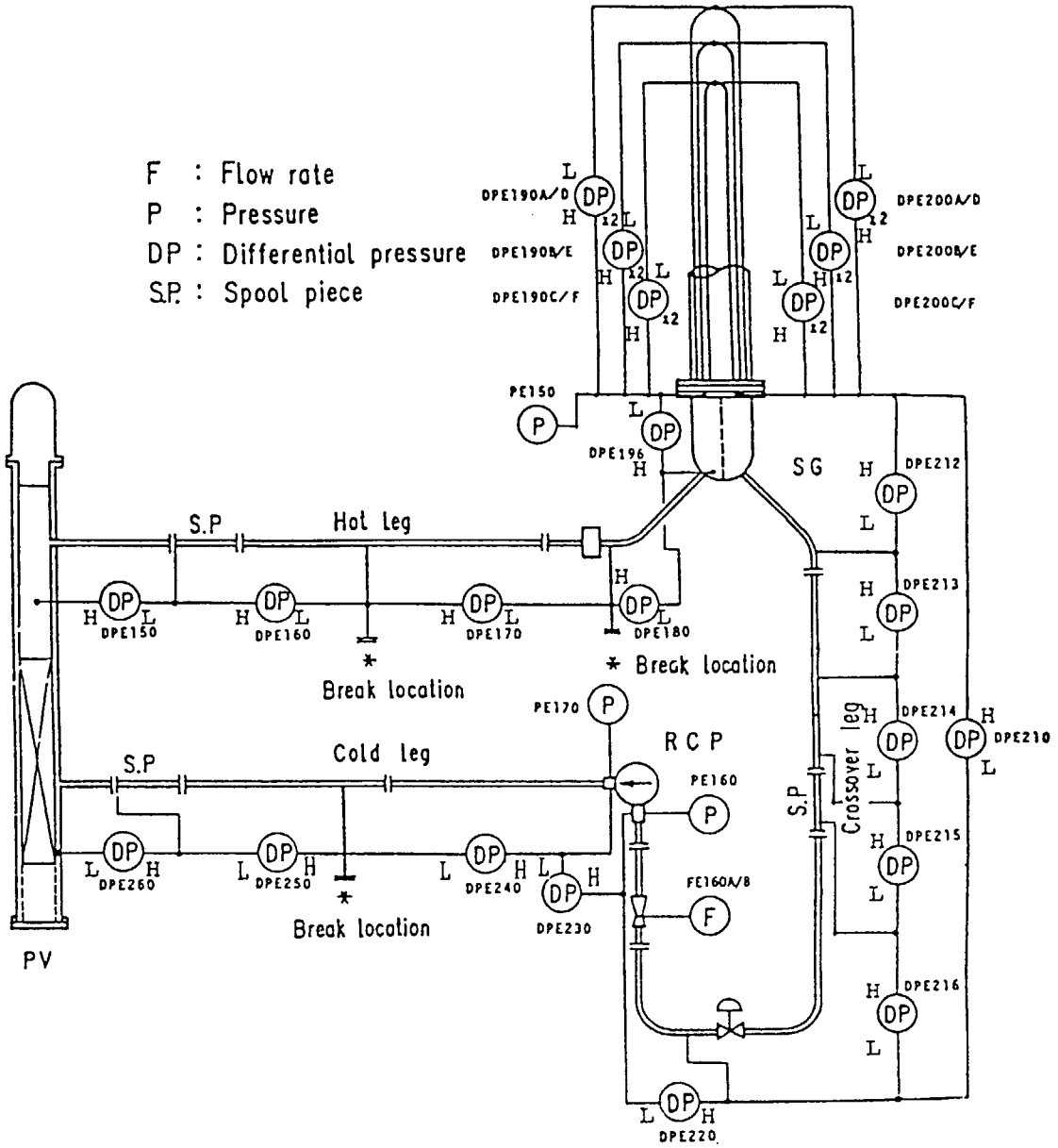

Fig. A. 4 Primary loop-B instruments for measurements of DP and flow-rate

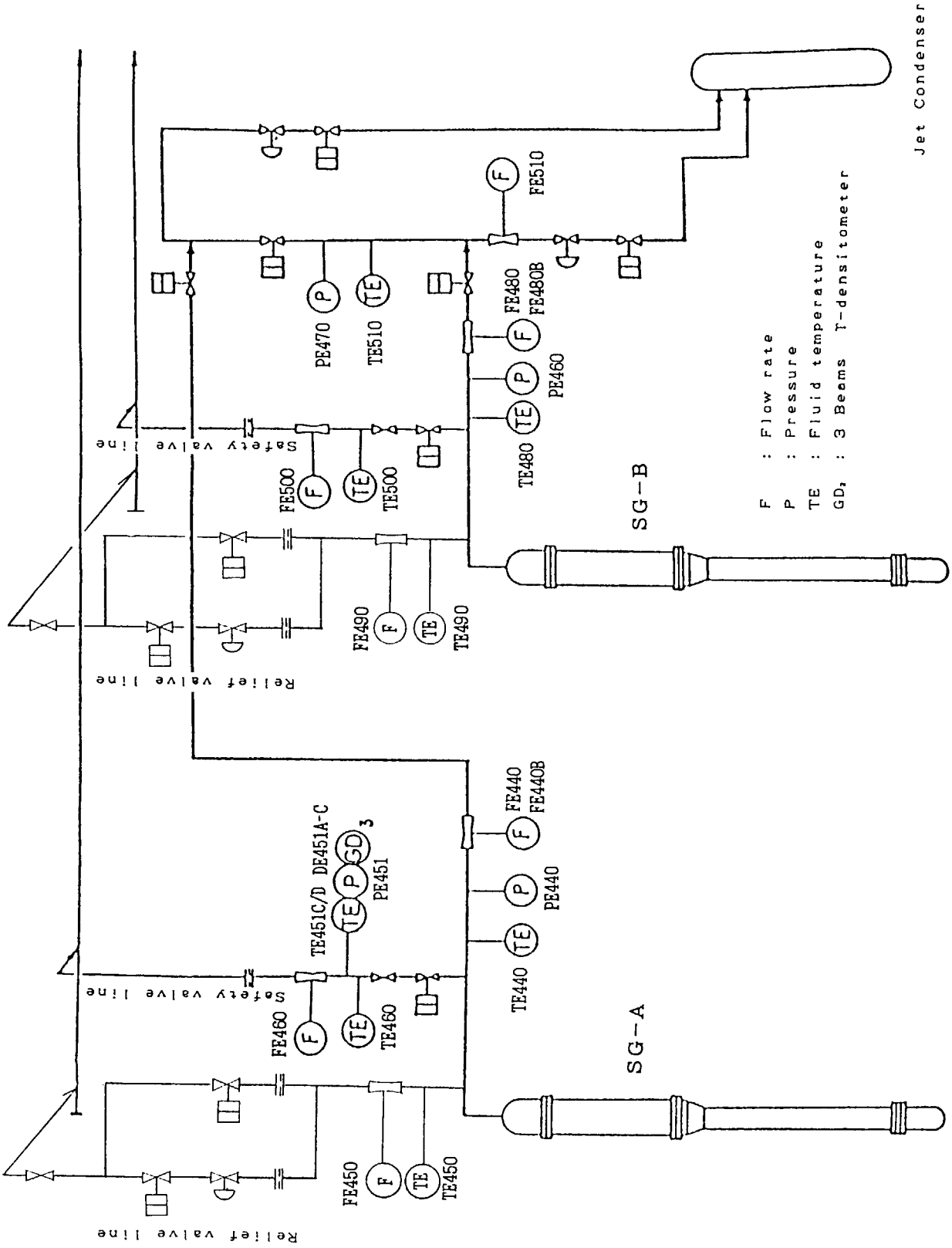

Fig. A.5 Instruments in main steam lines, relief valve lines and safety valve lines

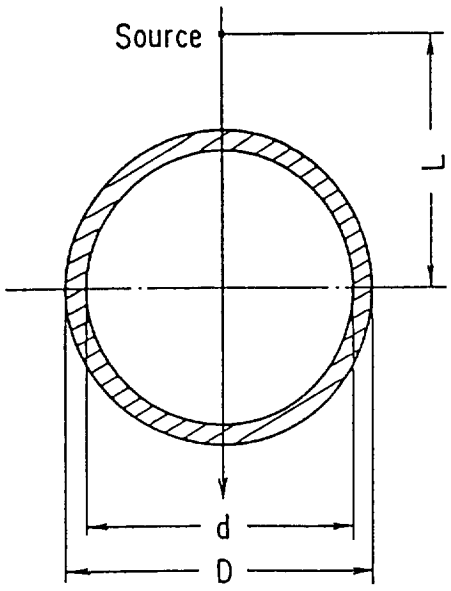

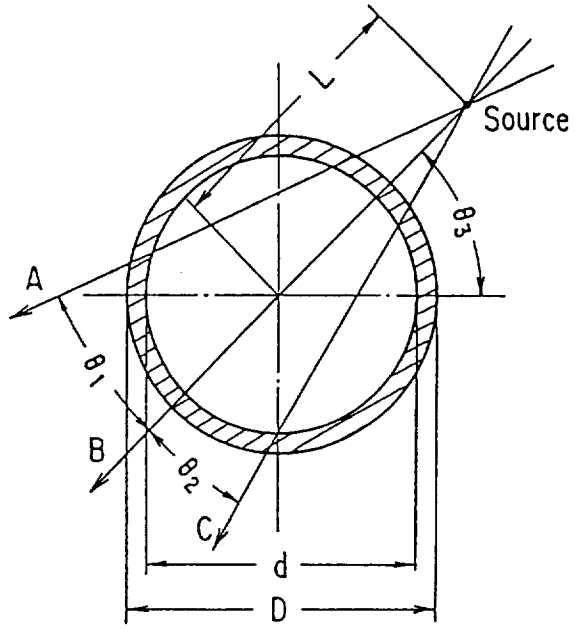

Single-Beam Densitometer

ID No.	D (mm)	d (mm)	L (mm)	Pipe Name/Direction
DE 19	240.2	168.2	305.0	Loopseal A/Vertical
〃 20	〃	〃	〃	Loopseal B/ 〃
〃 21	89.1	66.9	155.0	PR Surge L. 〃
〃 22	48.6	34.4	145.0	PORV L./Horiz.
〃 23	60.5	43.1	150.0	PR SV L./ 〃
〃 24	〃	〃	〃	PR Vent L./ 〃
〃 25	114.3	97.1	170.0	SG-A DC/Vertical
〃 26	〃	〃		SG-D DC/ 〃

Three-Beam Densitometer

ID No.	D (mm)	d (mm)	L (mm)	θ_1 (Degree)	θ_2 (Degree)	Pipe Direction/θ_3
DE 1～3	295.0	207.0	212.9	22.10	14.35	HLA, Horiz./45.0
〃 7～9	〃	〃	〃	〃	〃	CLA, 〃 / 〃
〃 10～12	〃	〃	〃	〃	〃	HLB, 〃 / 〃
〃 16～18	〃	〃	〃	〃	〃	CLB, 〃 / 〃
DE 4～6	240.2	168.2	240.0	15.9	11.2	LSA, Vertical/—
〃 13～15	〃	〃	〃	〃	〃	LSB, 〃 /—
〃 27～29	216.3	190.9	240.0	18.1	12.3	SGA, Horiz./
〃 30～32	114.3	87.3	180.0	10.3	8.3	Break Unit, ——
〃 33～35	〃	〃	〃	〃	〃	〃 〃 , ——

Fig. A. 6 Measurements by single- and three-beam gamma densitometers

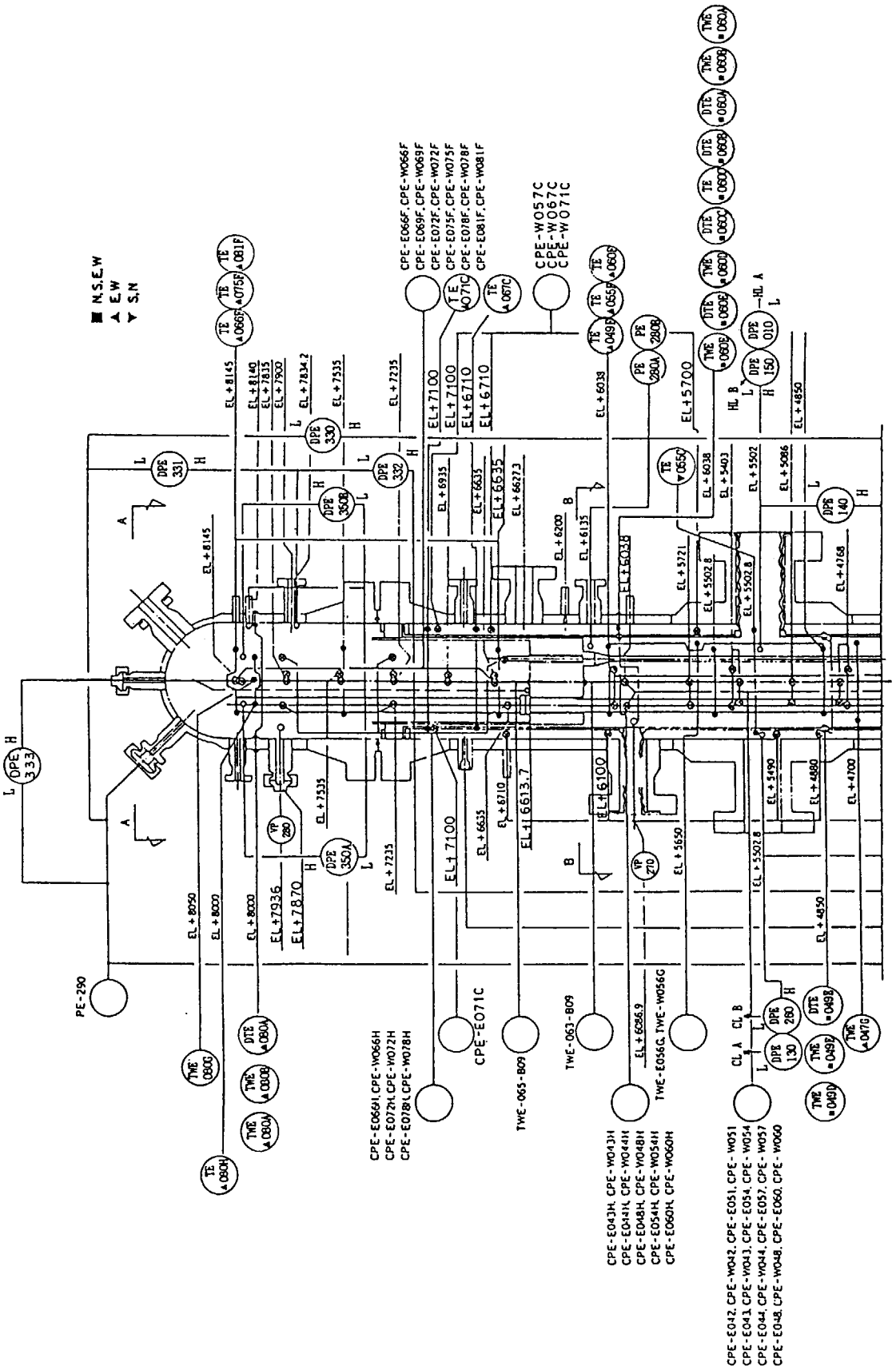

Fig. A. 7 Vertical locations of upper pressure vessel instruments (except for core)

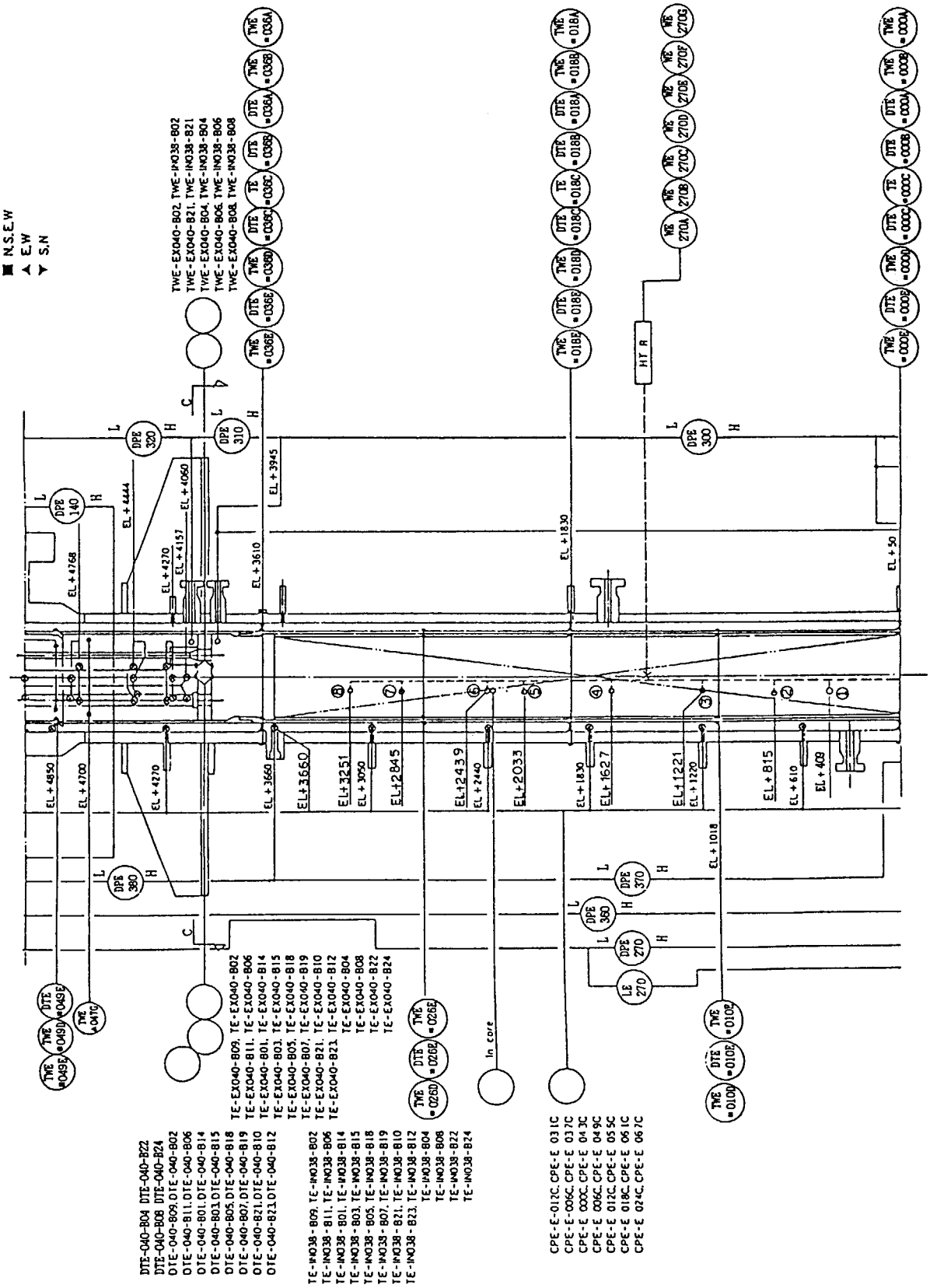

Fig. A. 8 Vertical locations of middle pressure vessel instruments (except for core)

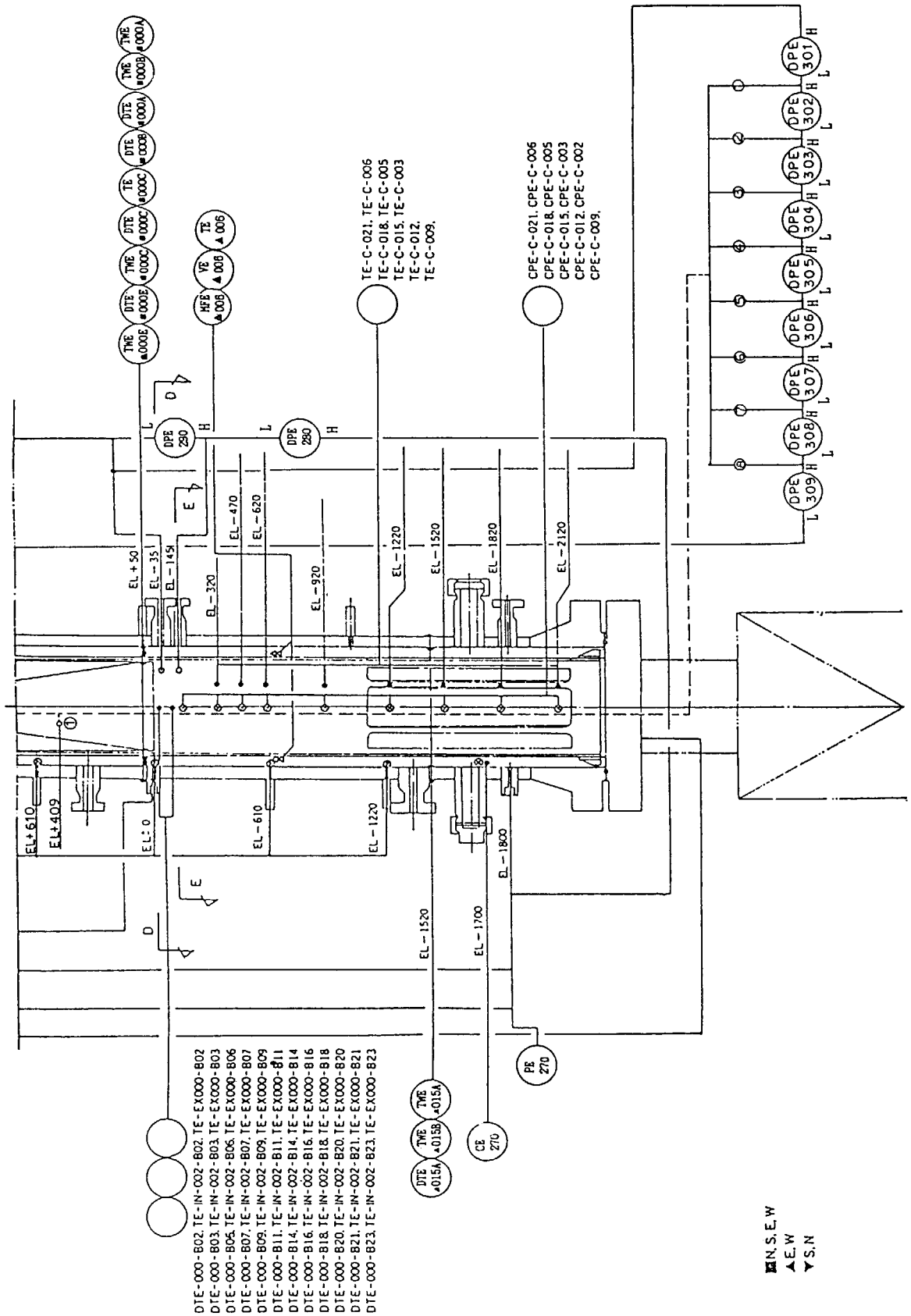

Fig. A. 9 Vertical locations of lower pressure vessel instruments (except for core)

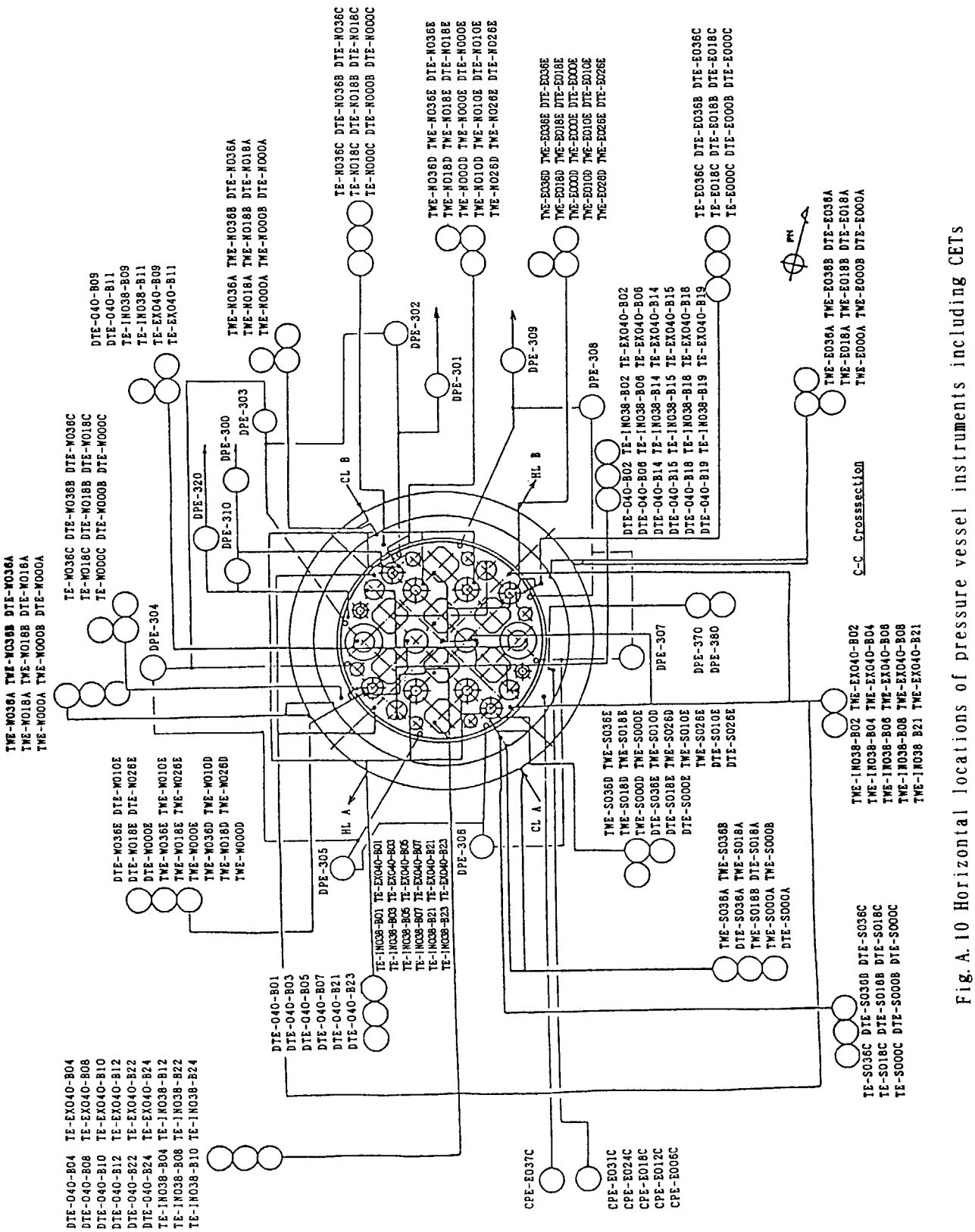

Fig. A. 10 Horizontal locations of pressure vessel instruments including CETs

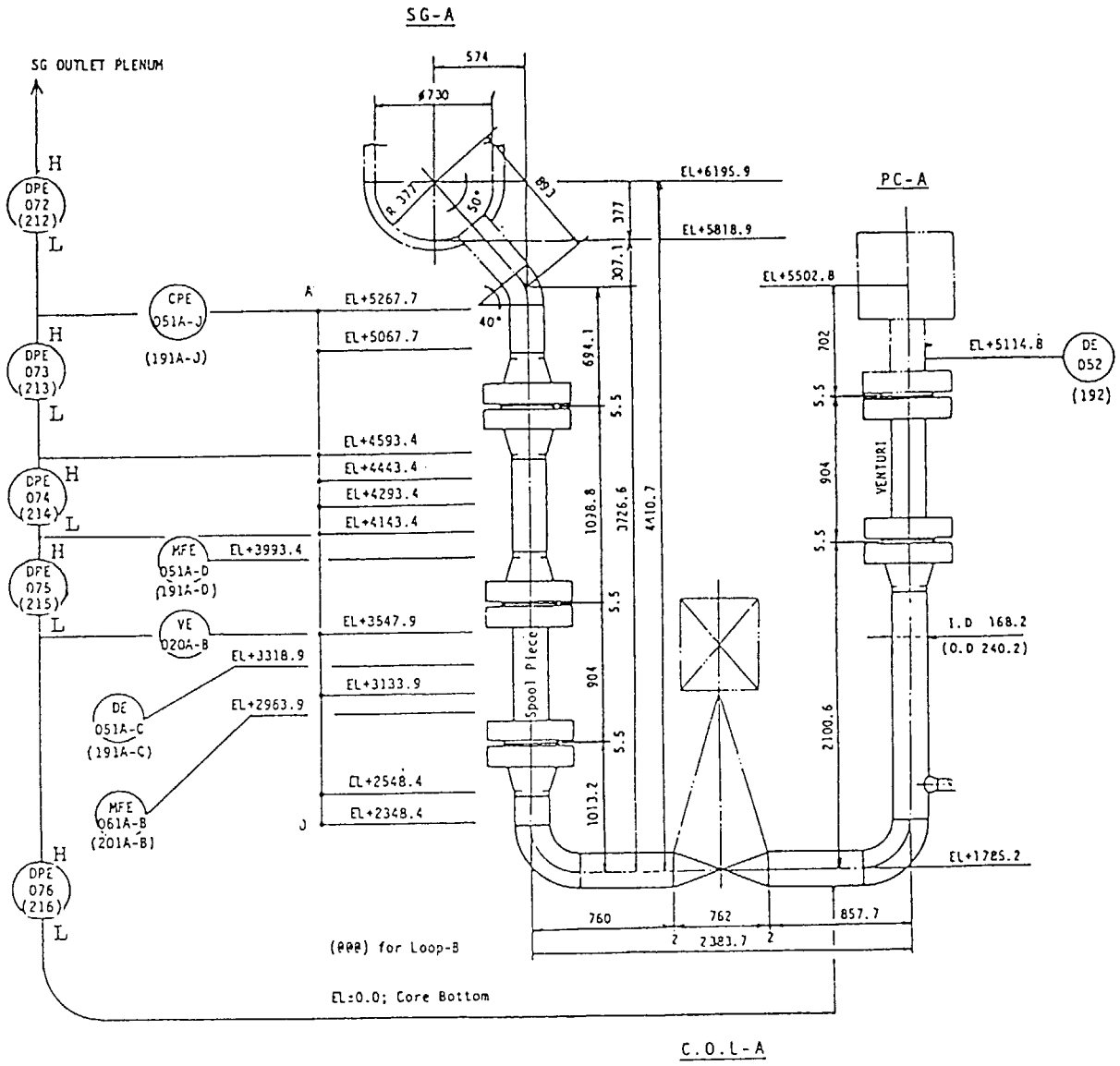

Fig. A. 11 Locations of selected instruments at cross-over legs A and B

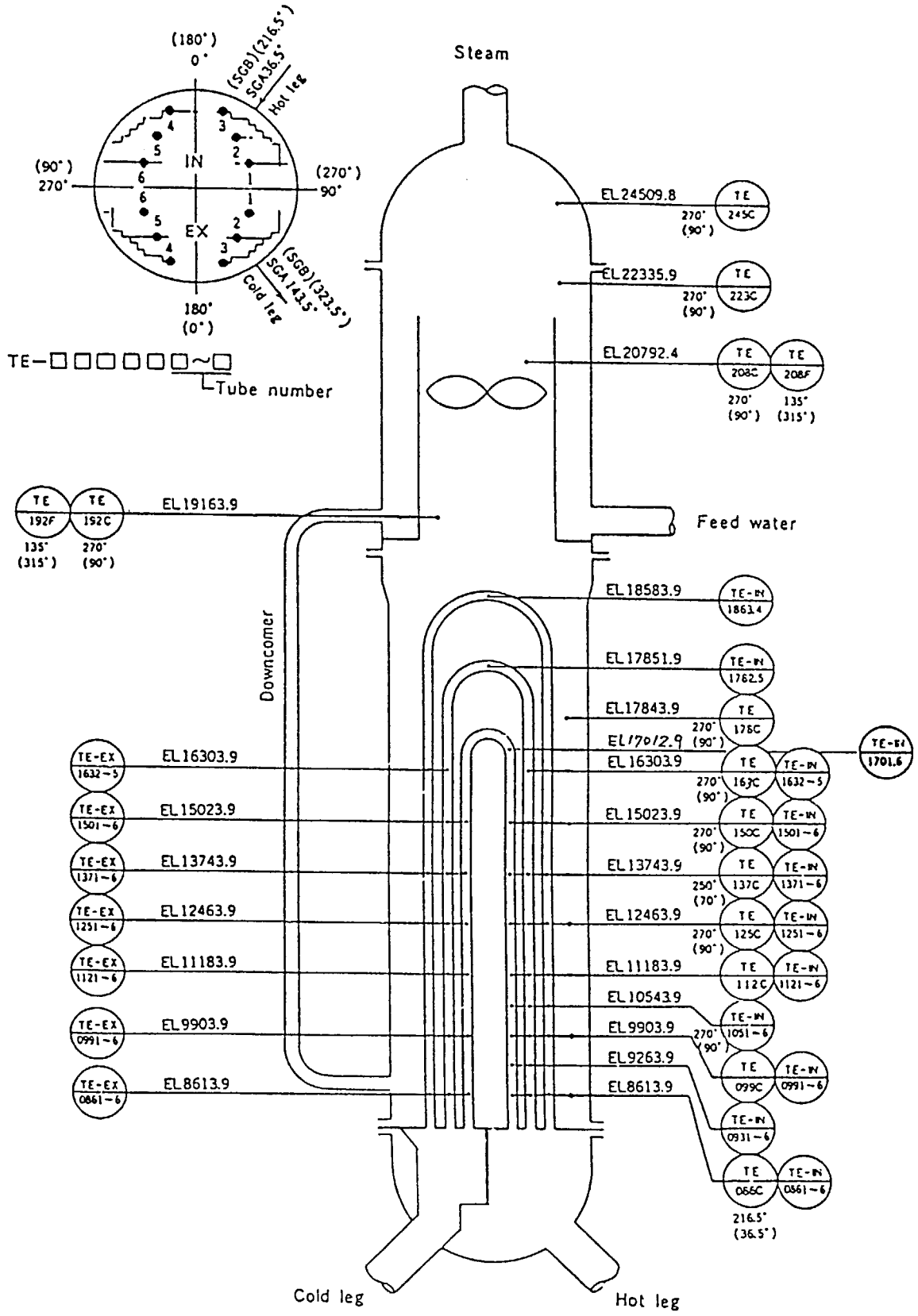

Fig. A. 12 Locations of temperature measurements for SG-A and SG-B (I)

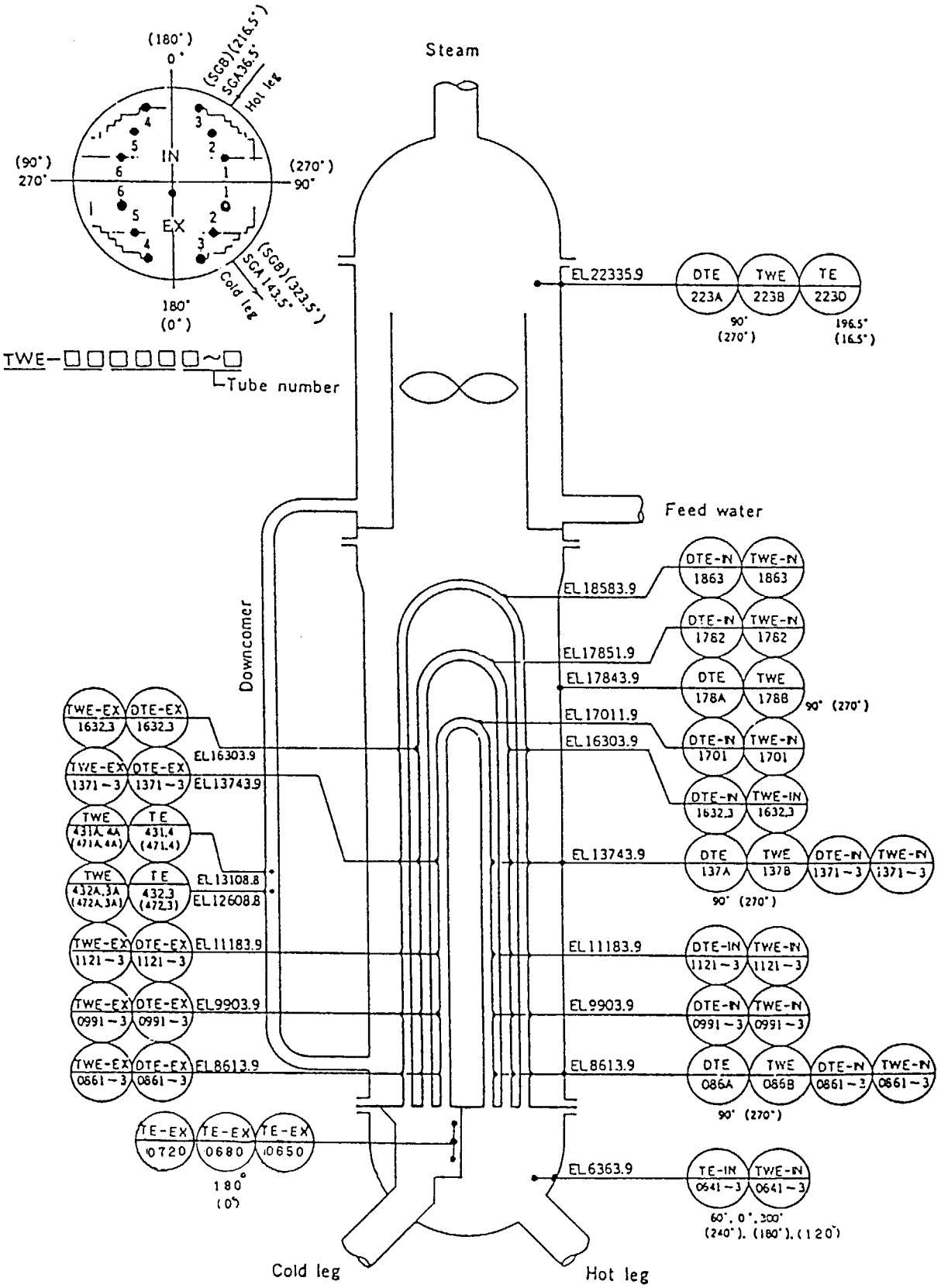

Fig. A. 13 Locations of temperature measurements for SG-A and SG-B (II)

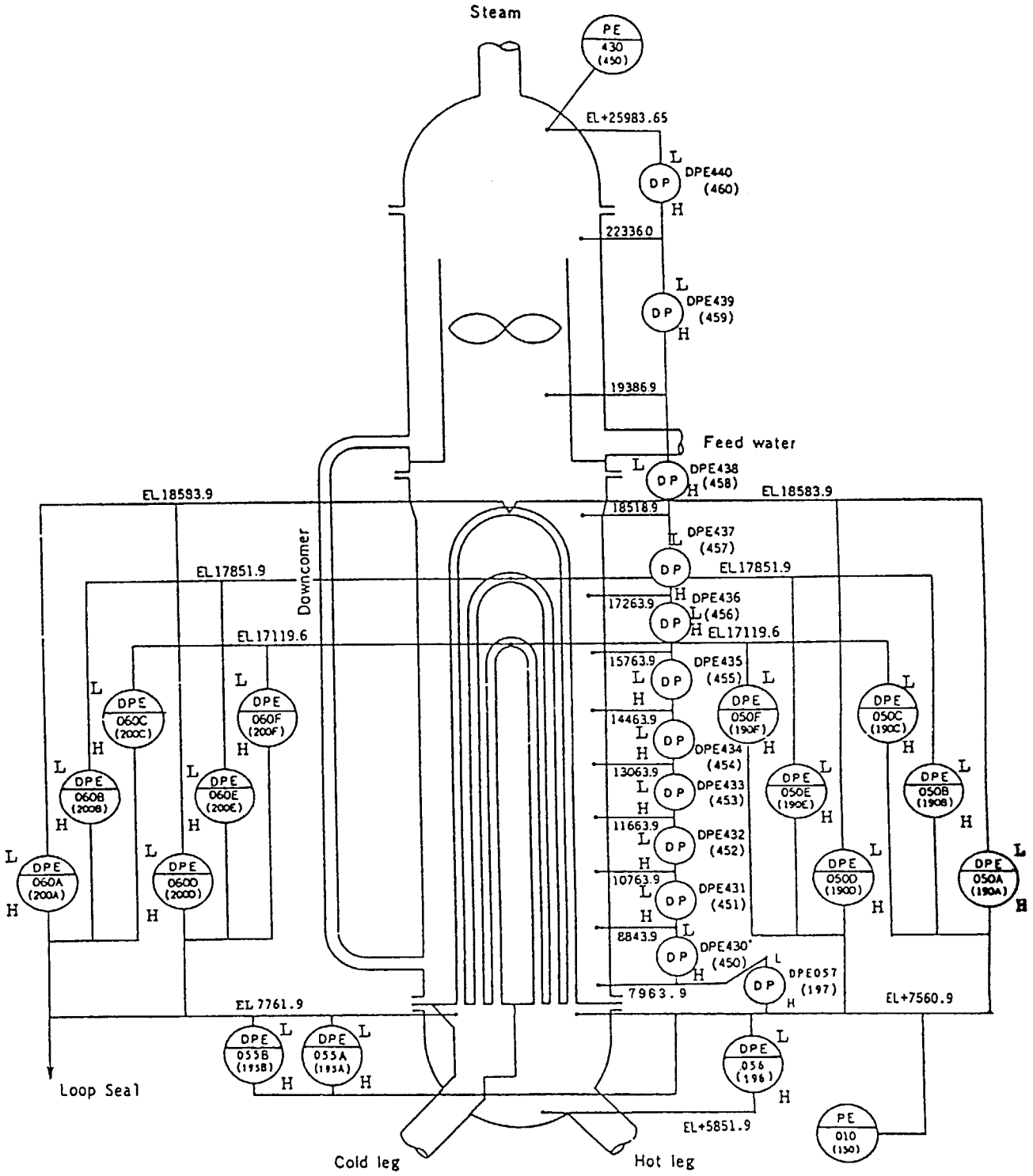

Fig. A. 14 Locations of DP measurements for SG-A and SG-B

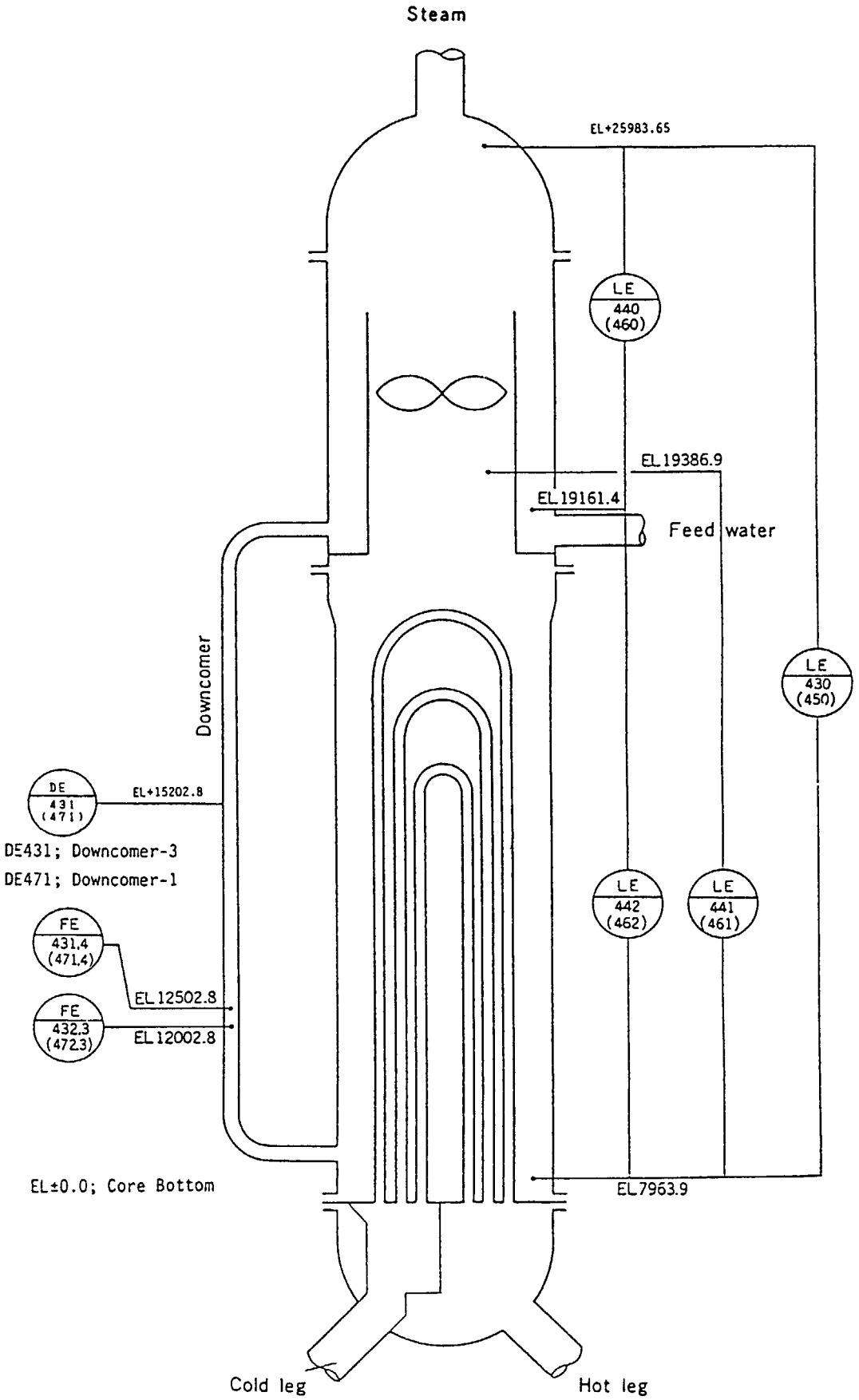

Fig. A. 15 Locations of level and flowrate measurements for SG-A and SG-B

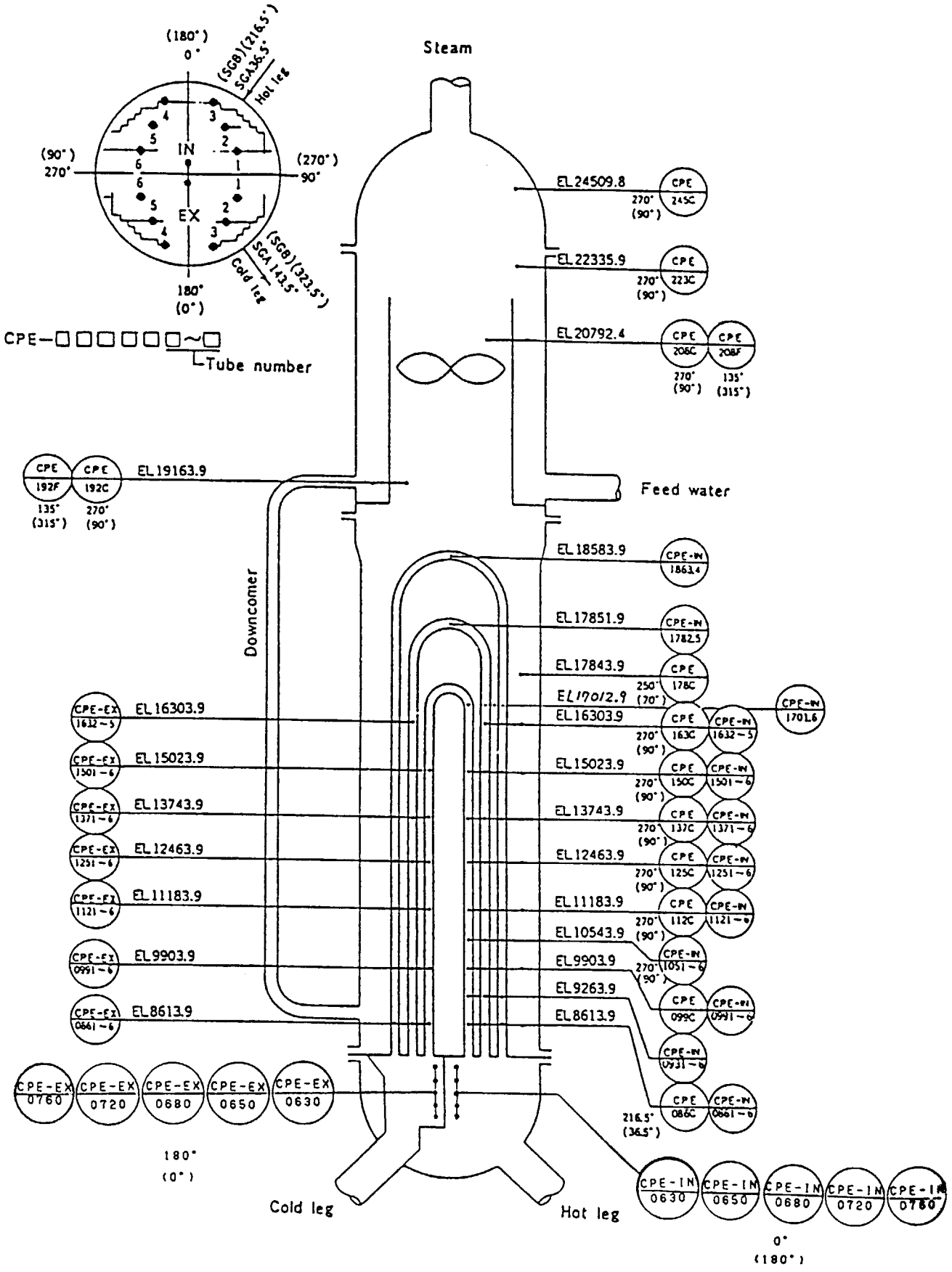

Fig. A. 16 Locations of CP measurements for SG-A and SG-B

This is a blank page.

国際単位系 (SI) と換算表

表 1　SI基本単位および補助単位

量	名称	記号
長さ	メートル	m
質量	キログラム	kg
時間	秒	s
電流	アンペア	A
熱力学温度	ケルビン	K
物質量	モル	mol
光度	カンデラ	cd
平面角	ラジアン	rad
立体角	ステラジアン	sr

表 2　SIと併用される単位

名称	記号
分，時，日	min，h，d
度，分，秒	°，′，″
リットル	l，L
トン	t
電子ボルト	eV
原子質量単位	u

1 eV = 1.60218 × 10^{-19} J

1 u = 1.66054 × 10^{-27} kg

表 5　SI接頭語

倍数	接頭語	記号
10^{18}	エクサ	E
10^{15}	ペタ	P
10^{12}	テラ	T
10^{9}	ギガ	G
10^{6}	メガ	M
10^{3}	キロ	k
10^{2}	ヘクト	h
10^{1}	デカ	da
10^{-1}	デシ	d
10^{-2}	センチ	c
10^{-3}	ミリ	m
10^{-6}	マイクロ	μ
10^{-9}	ナノ	n
10^{-12}	ピコ	p
10^{-15}	フェムト	f
10^{-18}	アト	a

表 3　固有の名称をもつSI組立単位

量	名称	記号	他のSI単位による表現
周波数	ヘルツ	Hz	s^{-1}
力	ニュートン	N	$m \cdot kg/s^2$
圧力，応力	パスカル	Pa	N/m^2
エネルギー，仕事，熱量	ジュール	J	N·m
仕率，放射束	ワット	W	J/s
電気量，電荷	クーロン	C	A·s
電位，電圧，起電力	ボルト	V	W/A
静電容量	ファラド	F	C/V
電気抵抗	オーム	Ω	V/A
コンダクタンス	ジーメンス	S	A/V
磁束	ウェーバ	Wb	V·s
磁束密度	テスラ	T	Wb/m^2
インダクタンス	ヘンリー	H	Wb/A
セルシウス温度	セルシウス度	℃	
光束	ルーメン	lm	cd·sr
照度	ルクス	lx	lm/m^2
放射能	ベクレル	Bq	s^{-1}
吸収線量	グレイ	Gy	J/kg
線量当量	シーベルト	Sv	J/kg

表 4　SIと共に暫定的に維持される単位

名称	記号
オングストローム	Å
バーン	b
バール	bar
ガル	Gal
キュリー	Ci
レントゲン	R
ラド	rad
レム	rem

1 Å = 0.1 nm = 10^{-10} m

1 b = 100 fm^2 = 10^{-28} m^2

1 bar = 0.1 MPa = 10^5 Pa

1 Gal = 1 cm/s^2 = 10^{-2} m/s^2

1 Ci = 3.7 × 10^{10} Bq

1 R = 2.58 × 10^{-4} C/kg

1 rad = 1 cGy = 10^{-2} Gy

1 rem = 1 cSv = 10^{-2} Sv

（注）

1. 表1－5は「国際単位系」第5版，国際度量衡局 1985年刊行による。ただし，1 eVおよび1 uの値はCODATAの1986年推奨値によった。
2. 表4には海里，ノット，アール，ヘクタールも含まれているが日常の単位なのでここでは省略した。
3. barは，JISでは流体の圧力を表わす場合に限り表2のカテゴリーに分類されている。
4. EC閣僚理事会指令ではbar，barnおよび「血圧の単位」mmHgを表2のカテゴリーに入れている。

換算表

力	N(=10^5 dyn)	kgf	lbf
	1	0.101972	0.224809
	9.80665	1	2.20462
	4.44822	0.453592	1

粘度　1 Pa·s(N·s/m^2) = 10 P(ポアズ)(g/(cm·s))

動粘度　1 m^2/s = 10^4 St(ストークス)(cm^2/s)

圧力	MPa(=10 bar)	kgf/cm^2	atm	mmHg(Torr)	lbf/in^2(psi)
	1	10.1972	9.86923	7.50062 × 10^3	145.038
	0.0980665	1	0.967841	735.559	14.2233
	0.101325	1.03323	1	760	14.6959
	1.33322 × 10^{-4}	1.35951 × 10^{-3}	1.31579 × 10^{-3}	1	1.93368 × 10^{-2}
	6.89476 × 10^{-3}	7.03070 × 10^{-2}	6.80460 × 10^{-2}	51.7149	1

エネルギー・仕事・熱量	J(=10^7 erg)	kgf·m	kW·h	cal(計量法)	Btu	ft·lbf	eV
	1	0.101972	2.77778 × 10^{-7}	0.238889	9.47813 × 10^{-4}	0.737562	6.24150 × 10^{18}
	9.80665	1	2.72407 × 10^{-6}	2.34270	9.29487 × 10^{-3}	7.23301	6.12082 × 10^{19}
	3.6 × 10^6	3.67098 × 10^5	1	8.59999 × 10^5	3412.13	2.65522 × 10^6	2.24694 × 10^{25}
	4.18605	0.426858	1.16279 × 10^{-6}	1	3.96759 × 10^{-3}	3.08747	2.61272 × 10^{19}
	1055.06	107.586	2.93072 × 10^{-4}	252.042	1	778.172	6.58515 × 10^{21}
	1.35582	0.138255	3.76616 × 10^{-7}	0.323890	1.28506 × 10^{-3}	1	8.46233 × 10^{18}
	1.60218 × 10^{-19}	1.63377 × 10^{-20}	4.45050 × 10^{-26}	3.82743 × 10^{-20}	1.51857 × 10^{-22}	1.18171 × 10^{-19}	1

1 cal = 4.18605 J(計量法)

= 4.184 J　(熱化学)

= 4.1855 J (15 °C)

= 4.1868 J(国際蒸気表)

仕事率　1 PS(仏馬力)

= 75 kgf·m/s

= 735.499 W

放射能	Bq	Ci
	1	2.70270 × 10^{-11}
	3.7 × 10^{10}	1

吸収線量	Gy	rad
	1	100
	0.01	1

照射線量	C/kg	R
	1	3876
	2.58 × 10^{-4}	1

線量当量	Sv	rem
	1	100
	0.01	1

(86年12月26日現在)

ROSA/LSTF EXPERIMENT REPORT FOR RUN SB-CL-24 REPEATED CORE HEATUP PHENOMENA DURING 0.5% COLD LEG BREAK LOCA